Palaeogeographic Development and Economic Potential of the Coal-Bearing Palaeocene Todalen Member, Spitsbergen

Christopher John Marshall,

MSc, BSc(hons)

Thesis submitted to

the University of Nottingham

for the degree of

Doctor of Philosophy

December 2013

UNIS

The University of Nottingham

UNITED KINGDOM · CHINA · MALAYSIA

Store Norske

– MINING IN THE HIGH NORTH

Abstract

Palaeocene high-latitude coals from the Todalen Mbr. Central Tertiary Basin, Svalbard present an opportunity to understand the processes which controlled Arctic peat formation. Coals from this region have produced sub-economic quantities of bitumen during the 1920's. Previous palaeogeographic models show significant variation between studies favouring deltaic and tidal wetland conditions. In addition, coal geochemistry studies have been limited to characterisation with little integration with palaeogeographic studies.

This study utilises a large database of drill-logs to create cross sections and coal isopach maps to examine the spatial relation between seam thickness and palaeotopography. Palaeotopography is defined by mapping a 'valley indicator'; the Grønfjorden bed, a fluvial conglomerate representing the first Palaeocene sedimentation. In addition, organic petrology organic and inorganic geochemistry were applied to samples from two mine sections and two boreholes to examine how coal quality and oil potential changed both within and between seams.

The cross sections and isopach maps reveal that landscape had a significant but diminishing control upon peat accumulation. Thickest peats consistently formed at the break-in slope whilst topographic lows acted as areas of preferential channel formation

and conduits for clastic sedimentation. Evolution of the landscape control had a significant control upon groundwater supply. As landscape control decreased the coals moved from isolated, raised bogs (Svea Seam) to laterally expansive minerotrophic fens (Svarteper and Askeladden Seams).

Evidence of increasing marine influence and higher groundwater input was also observed from the Svea Seams to the Askeladden seam. In the Svea Nord and Longyear seam, supply of lithophile elements (Al, Ti, Na, K) is shown to be controlled by dust supply controlled by orbital cyclicity. By the Svarteper/Askeladden period lithophile element concentrations are controlled by clastic supply. Ca, Mg and Fe appear to be derived from groundwater. Sulfur concentration primarily reflects the supply of marine sulfur.

Upper Todalen coals (Longyear, Svarteper and Askeladden) have significantly more oil potential than the Svea Seams with estimated retorting yields of 170-190kg/ton vs. 50kg/ton respectively. The Longyear seam exhibits relatively high HI values (ca. 300-400 mg/g TOC) consistent with a mixed Type II/III kerogen source. Greatest oil potential is shown to be favoured by formation within a fen environment, with high bacterial degradation (>100µg/g TOC hopanes), marine influence (>0.5wt% sulfur, Fe/S <0.9) and the unique temperate high lattitude Palaeocene climate of Svalbard, leading to preservation of hydrogen rich organic matter via organo-sulfur bond formation.

Acknowledgements

I would like to gratefully acknowledge the financial support of the Natural Environmental Research Council (NERC), the University of Nottingham Graduate School BESTS Scholarship and the Midlands Energy Graduate School Travel Prize. I would like to thank Store Norske Spitsbergen Kulkompani (SNSK) for their enthusiastic and constant support during my time on Svalbard without which this project would not be possible. I would also like to thank Prof. Snorre Olaussen and UNIS for both their logistical and financial support during my studies.

Particular thanks are owed to my principal supervisor Dr. David Large whose door was always open and who enthusiastically guided and supported me throughout the PhD process. Special thanks are also owed to Dr. Will Meredith and Dr. Clement Uguna who guided me patiently through the experimental process and Prof. Colin E. Snape who always provided a new perspective on things.

I would like to thank Prof. Trevor. Drage, Mr David Clift, Dr. Baruch Spiro and Mr Alv Orheim for their analytical and theoretical assistance during my PhD studies. Also many thanks to Dr. Gary Nichols for constructive comments given during an interesting viva discussion.

Many thanks are owed to the SNSK geologists; Malte, Bjarki, Bernt and Morten for making my time on Svalbard as productive and enjoyable as possible, as well as for creating the first vitrinite reflectance joke in history. In addition, I would like to thank the SNSK assistant geologists/Icelandic Mafia for making my time on Svalbard unforgettable, especially Anna Stella (whose logs are without compare), Gauti, Minney, Anna Mjöll, Hanne, Tomas, Christine and Marit Ann. Also thanks to Maggie who acted as a safety valve when things got just too quiet in L3. Thanks to the Wild Swimmers, Andy, Pip, Zoe, Atkins and my housemates Katie, Vicky and Saif.

Most importantly, thank you to my family; Nick for his bright and cheery disposition, Andy for his patience and self-control, Dad for his hard work and encouragement and finally my Mum (Angie) without whom none of this would have been possible.

"To a naturalist nothing is indifferent; the humble moss that creeps upon the stone is equally interesting as the lofty pine which so beautifully adorns the valley or the mountain: but to a naturalist who is reading in the face of the rocks the annals of a former world, the mossy covering which obstructs his view, and renders indistinguishable the different species of stone, is no less than a serious subject of regret." James Hutton

For Stan Martin, who taught me to; "*Sail away from the safe harbour. Catch the trade winds in your sails. Explore. Dream. Discover"*

Table of Contents

Abstract ..... **II**

Acknowledgements ..... **IV**

Table of Contents ..... **VII**

Table of Figures ..... **XIII**

List of Tables ..... **XXV**

Chapter 1 - Introduction **1**

1.1 – Context 1

1.2 – Aims and Objectives 9

Chapter 2 – Sampling and Analytical Methodology **13**

2.1 – Sampling methods and localities 13

2.2 – Sample Preparation 17

2.3 – Analytical Methodology 19

2.3.1 – Organic Petrology 19

2.3.1.1 – Sample Preparation 19

2.3.1.2 – Coal Maceral Analysis and Vitrinite Reflectance 20

2.3.1.3 – Tissue Preservation and Gelification Index 20

2.3.1.4 – SEM EDAX analysis 21

2.3.2 – Organic Geochemistry 21

2.3.2.1 – Soxhlet and Accelerated Solvent Extraction 21

2.3.2.2 – Rock Eval Pyrolysis 22

2.3.2.3 – Hydrous Pyrolysis 22

2.3.2.4 – Nitrogen Pyrolysis 23
2.3.2.5 – Gas Chromotography – Mass Spectrometry (GC-MS) 24
2.3.2.6 – Biomarker Biochemistry 24
2.3.2.7 – ^{13}C Nuclear Magnetic Resonance Spectrometry (NMR) 27
2.3.3 – Inorganic Geochemistry 28
2.3.3.1 – ICP-AES Analysis 28
2.3.3.1.1 – Data Quality 28
2.3.2 – Carbon and Sulfur Coulometry 29
2.3.3 – Ash Measurement 31
2.3.4 –Miscellaneous Techniques 32
2.3.4.1 –Spectral Analysis and Fourier Analysis 32
3.1 – Conclusions 33
Chapter 3 – Structural and Palaeogeographic Controls Upon Coal Thickness Within the Todalen Member 34
3.1 – Introduction 34
3.2 – Geological Background 34
3.2.1 –Regional Tectonic Development of Svalbard 35
3.2.2 – Structural Framework of the Central Tertiary Basin 39
3.2.3 –Tertiary infill of the Central Tertiary Basin 46
3.2.4 –Previous Palaeogeographic Reconstructions 48
3.3 – Sequence Stratigraphy and Hydrological Landscapes 52
3.3.1 –The Sequence Stratigraphic Approach to Peatland 52
3.3.2 –The Hydrological Landscape Approach 55
3.3.3 – Applying the Hydrological Landscape Approach to Coal 59
3.4 – Sampling Methodology 61
3.5 – Defining the Cretaceous-Tertiary Peneplain 65
3.5.1 – The Grønfjorden Bed 65
3.5.2 – The Grønfjorden Bed Valley Complex 66
3.5.3 – Structural Controls upon Peneplain Topography 70

3.6 – Development of Coal Forming Environments 71
3.6.1 – The Svea Seams 71
3.6.1.1 – Svea Coal Thickness and Underlying Topography 72
3.6.1.2 – Bentonite and the Svea Seam 76
3.6.1.3 – Hydrological Development of the Svea Seams 79
3.6.2 –The Longyear Coastal Peatland 80
3.6.2.1 – The effect of landscape upon Longyear coal thickness 80
3.6.1.2 – Peatland Response to Relative Sea Level Change 83
3.6.1.3 – Local Scale Reconstruction of the Longyear Peatland 89
3.6.1.4 – Palaeogeographic development of the Longyear Seam 92
3.6.3 – The Svarteper and Askeladden Seams 93
3.7 – Long Term Structural Controls on Coal Formation in the C.T.B 97
3.8 – Conclusions 101
Chapter 4 – Economic and Source Rock Potential of the Svalbard Coals 103
4.1 – Introduction 103
4.1.1 – Oil Prone Coals 104
4.1.1.1 – Liptinite Rich vs. Vitrinite Rich Perhydrous Coals 105
4.1.1.2 – Oil Prone Coals within the Svalbard Region 107
4.2 – Approach 108
4.3 – Oil Content of the Longyear Coal 110
4.3.1 – Oil Content of the Other Svalbard Coals 113
4.3.2 –Quantifying Oil Potential from HI 115
4.3.3 – Prospective Geological Yield Estimates 119
4.3.4 – Retorting Yield Estimates 123
4.3.5 – Resource Estimate for the Eastern C.T.B 126
4.4 – Maturity of the Svalbard Coals 126
4.4.1 – Vitrinite Reflectance 128

4.4.2 – Aromaticity of the Svea and Longyear Coals 128
4.4.3 – Organic Maturity Parameters 132
4.4.4 – Implications for Local and Regional Erosion Models 136
4.5 – Origins of the Oil Potential of the Longyear seam 137
4.5.1 – Provenance of Extracted Hydrocarbons from Longyear Seam 137
4.5.2 – Peatland Environment and Oil Potential 142
4.5.3 – Microbial Processing and Oil Potential 145
4.5.4 – Sulfur and Oil Potential 149
4.6 – Conclusions 151
Chapter 5 – Development of the Svea Seams – Palaeo-environment and Coal Quality 152
5.1 – Introduction 152
5.2 – The Svea Seams 153
5.3 – Persistence of the Svea Peatland 155
5.3.1 – Estimation of Deposition Period from Coal TOC 156
5.4 – Coal Quality Issues in the Svea Seam 158
5.4.1 – Inorganic Composition of the Svea Nord Coal 161
5.4.2 – Composition of Local Clastic Sediments – Svea Nord 167
5.4.3 – Inorganic Composition of 'Fan Type' Breinosa Svea 169
5.5 – Controls upon Coal Quality within the 'Valley' Svea Nord Seam..172
5.5.1 – Hydrological Controls upon Coal Quality 173
5.5.1.1 – Coal Macerals and the Hydrology of Svea Nord Peatland 173
5.5.1.2 – Hydrological Development of Lower Svea Nord Coal 174
5.5.1.3 – Hydrological Development of Upper Svea Nord Coal 178
5.5.1.4 – Effect of Peatland Hydrology upon the Inorganic Composition of the Svea Nord Seam 184
5.5.1.5 – Phosphorus and Peatland Fires 189

5.5.2 – Dust Deposition and the Lithophile Elements 191

5.5.3 – Marine Supply of Sulfur to the Peatland 197

5.6 – Palaeo-environmental Development of the Svea Seams 202

5.7 – Conclusions 206

Chapter 6 – The Palaeo-envrionmental Evolution of the Longyear Seam and its Effect upon Coal Quality 209

6.1 – Introduction.....209

6.2 – The Longyear Seam 210

6.3 – Period of Deposition of the Longyear Seam.....213

6.3.1 – Carbon Accumulation Rates.....213

6.3.2 – Orbital Cycling 215

6.4 – Controls upon Coal Quality within the Longyear Seam 218

6.5 – Controls on Major and Minor Elemental Composition of the Longyear Seam 220

6.5.1 – Determining Controls upon the Major and Minor Elemental Composition of the Longyear seam.....223

6.5.2 –Groundwater Controls upon the Longyear Seam 227

6.5.2.1 –Coal Macerals and the Hydrological Development of the Longyear Seam.....228

6.5.2.2–Groundwater Influence and the Ca-group elements.....239

6.5.3 – Climatic Controls on Atmospheric Dust supply 244

6.5.3.1 – Peatland Fires and the Arctic Palaeocene Climate.....249

6.5.3.2 – Provenance of Dust Supply to the Longyear Seam.....255

6.5.4 –Marine Controls upon the Longyear seam.....262

6.5.3 – Clastic Sediment Supply at Lunckefjellet.....267

6.6 – Plant Communities Forming the Longyear Seam.....269

6.6.1 –Organic Biomarkers 269

6.7 – Bacterial Communities within the Longyear Seam 272

6.7.1 – Size and Composition of Bacterial Communities 278

6.7.2 – Implications for Carbon Cycling during the Palaeocene 282
6.8 – Palaeo-Environmental Development of the Longyear Seam 287
6.9 – Conclusions 294
Chapter 7 – Development of the Svarteper and Askeladden Seams – Palaeo-environment, Coal Quality and Future Potential 297
7.1 – Introduction.....297
7.2 – The Svarteper and Askeladden Seams 298
7.3 – Coal Quality within the Svarteper and Askeladden Seams 299
7.4 – Palaeo-environmental Development of the Svarteper Seam 305
7.4.1 – Hydrological Controls upon the Svarteper Seam 308
7.4.2 – Controls upon inorganic species within the Svarteper Seam.312
7.5 – The Askeladden Seam.....317
7.6 – Conclusions 319
Chapter 8 – Conclusions and Future Work 322
8.1 – Palaeo-Environmental Development of the Todalen Member.....322
8.1.1 – Hydrological Landscape Approach 330
8.3 – Oil Potential.....333
8.4 – Future Work.....335
References.....340

For Appendices see attached disc

Table of Figures

Figure Caption	Page
Fig. 1.1 – Map of the island of Spitsbergen showing the extent of late Mezozoic – Cenozoic sediments and the location of major settlements referred to in this study	**2**
Fig. 1.2 – Map of the island of Spitsbergen showing the mines and settlements of the NW Central Tertiary Basin	**3**
Fig. 2.1 – Map of the NE Central Tertiary Basin with current and prospective mine deposits. Sample Locations used in this study are also shown.	**14**
Fig. 2.2 – Map of the Svea Nord Mine showing the sample location at DT6/9. *Courtesy Bjarki Friis (SNSK)*	**15**
Fig. 2.3 – Map of Mine 7 (Adventdalen) showing the section location. *Courtesy Bjarki Friis (SNSK)*	**16**
Fig. 3.1 – Tectono-stratigraphic development of Svalbard showing the key tectonic events in the formation of modern day Svalbard (*From Harland,* 1997)	**36**
Fig. 3.2 – N-S section of the NE Central Tertiary Basin (A) *After Luthje,2008), (B) After Nottvedt, 1985.* Note that one section appears to show the Van Mijenfjorden Faultblock clearly and in the other it is not present.	**41**
Fig. 3.3 – (Top) Structural features within the Northern Central Tertiary Basin showing a number of swells and troughs (After Sokholov et al., 1968). (Bottom) A	**43**

geophysical W-E section across Van Mijenfjorden showing undulations in Triassic sediments (Eiken, 1985). (D/E =Permo-Triassic Sediments)

Fig. 3.4 – East-West Cross Sections from (Top Left to Bottom) Eiken, 1985, Livsic, 1974, Nottvedt et al., 1988 and Sokolov et al., 1968 showing the various levels of detail within sections from this region **44**

Fig. 3.5 – The Palaeogene Succession of the Central Tertiary Basin, Spitsbergen (From Steel et al., 1985) **47**

Fig. 3.6 Palaeo-environmental Reconstruction of the Todalen Member from (A) Worsley et al., (1986), (B) Nøttvedt, 1982, (C) Lüthje, 2008 showing interpretations from tidal flat to deltaic conditions **49**

Fig. 3.7 – Palaeo-environmental reconstruction of Nagy, (2005) from W. Central Tertiary Basin, possibly showing the earliest phase of coal deposition **50**

Fig. 3.8 – The coal geometry and thickness predictive model of Bohacs and Suter, (1997). 1= Late high-stand- Early Lowstand. Falling base lavels promotes progradation and subaerial erosion 2= Middle Lowstand Conditions (Rising Sea Levels and groundwater tables lead to medium thickness continuous coals. 3 =Late Lowstand-Early Transgressive coals. Thick isolated coals due to rising water table. 4 = Transgressive. High accommodation increases cause shoreline to move landward leading to restricted mire conditions due to increasing clastic sedimentation and rapidly increasing water table. 5 = Early Highstand – Reduction in rate of sealevel and groundwater rise allows establishment of thick isolated peatlands. 6 = Stable Groundwater results in thinner, more continuous seams. **53**

Fig. 3.9 – Fundamental Landscape Units showing areas of groundwater discharge within a valley, hummocky landscape and coastal plain setting (After Winter, 2000) **56**

Fig. 3.10 – (Left) Distribution of the Gronfjorden Bed in the Eastern Basin (Red = Datapoints). Note the pattern of valleys and ridges picked out by the conglomerate. (Right) Proposed extension of the trough and swell system identified by Sokholov et al. (1968) to the Billefjorden Faultzone. Note the approximately similar wavelength to pre-existing structures. **68**

Fig. 3.11 – (Left) Reconstruction of the Gronfjorden valleys presuming the valley system identified extends to the previously identified swells and troughs. (Right) Similar braided river system from Alaska (http://pages.uoregon.edu/millerm/braided.html) **69**

Fig. 3.12 – (Left) Coal Isopach Map of the Svea Seams overlaid over the inferred Grønfjorden Valleys and highs (Right) Schematic diagram of 'Valley' and 'Fan' Type Svea Seams. Note all seams are adjacent to inferred ridges. Position of a bentonite layer also shows that the Svea Seam retreated northward in response to rising sea levels. (Inferred seam from former mine) **73**

Fig. 3.13 – (Top) 3D reconstruction of the Svea Nord Deposit showing position within the Grønfjorden valley and localised hydrology. (Middle) Modern analogue for 'Fan type' Svea in Adventdalen. (Bottom) Peat infilling valleys in China possibly analogous to 'Valley Type' Svea Seams. **74**

Fig. 3.14 – Bentonite Isopach map showing the redistribution of the Bentonite layer into the Grønfjorden Valleys soon after deposition **78**

Fig. 3.15- Coal Isopach map for the Longyear seam overlaid with mean Sulfur content and inferred Gronfjorden highs. Note the position of many of the current and prospective mines adjacent to the ridges indicating a possible hydrological landscape control. Sulfur picks out a number of high sulfur areas of coal penetrating the peatland possibly representing tidal channels or estuaries. **81**

Fig. 3.16. Model of the effect of base level rises on the Longyear using coal thickness as an indicator of duration of peat accumulation from maximum extent to termination of the peatland. Note the area of non-peat deposition adjacent to Lunckefjellet, followed by bay formation and peat accumulation shifting northward. Yellow indicates limit to tertiarysedimentation. **85**

Fig. 3.17. Map showing the position of any splits within the Longyear coal, with most originating from the coast and overlying the Gronfjorden depressions and gulleys (Lunckefjellet). **87**

Fig. 3.18. Palaeo-environmental development of the Longyear seam, A and E based on lithology maps as defined in Section 3.4. B-D based on coal isopach maps and response to sea level shown in Fig. 3.16 **88**

Fig. 3.19 - Palaeo-environmental Development of **91**

Lunckefjellet Area (Top-left) Maximum extent showing area of low coal thickness deposition to W of Lunckefjellet possible representing coastal lake/lagoonal deposits (Bottom Left) Lunckefjellet after sea level rise showing formation of tidal inlets and estuaries adjacent to the site. These are also shown by coal sulfur contents showing position relative to these is a major control on coal quality. (Right) Schematic Sections across Lunckefjellet showing maximum thickness at the break in slope and preferential channel formation in topographic lows.

Fig. 3.20 Coal Isopach map for the Svarteper seam showing peat deposition to have shifted to the North and East of the basin with high marine influence likely due to the limited extent of the coastal plain **94**

Fig. 3.21 Coal Isopach map for the Askeladden seam showing that peat deposition is limited to the northernmost part of the basin as relative sea levels increase further **95**

Fig. 3.22 – Cross Section across Lunckefjellet (NW-SE) with datum as the Todalen/Endalen Mbr. Boundary. This appears to show the Cretaceous Pene-plain beneath Lunckefjellet. The depressions shown also appear to be areas of preferential conglomerate/channel deposition and also the origin of the splits within later seams. The Svea seam, bentonite and Askeladden seams also appear to be only present overlying the topographic lows in this location **98**

Fig. 3.23 NW-SE Cross Section across Breinosa showing the underlying Cretaceous Pene-plain. Note that these underlying topographic lows appear to be areas of preferential split formation and channel formation. At the edge of the highs, the thickest coals occur as areas of hydrological stability **99**

Fig. 4.1 – Map of the island of Spitsbergen showing the mines and settlements of the NW Central Tertiary Basin and sample locality and type. **109**

Fig. 4.2 – Comparison of (A) Soxhlet Solvent Extraction (B) Accelerated Solvent Extraction (C) Rock Eval (S1) (D) Coal Hydrogencontent (%) as a means of measuring the current hydrocarbon content of the Longyear coal. Note the similarity between yields from the Soxhlet and ASE techniques. Orthohydrous/Perhydrous definition *after Wilkins and George, 2002)* **111**

Fig. 4.3 – Comparison of the Rock Eval Hydrogen Index (HI) parameter within the Lower Svea Nord Seam (A) and **116**

the Longyear Seam in Mine 7 (B). Oil prone-Gas prone *after Wilkins and George, 2002).* Note that the entire Longyear seam is shown to have some oil potential

Fig. 4.4 – (A) Adapted Van Krevelen diagram (*after Meyers and Terranes, 2001)* using the Rock Eval HI and OI parameters. The Svalbard coals show values consistent with a mixture of Type I/II material and Type III material. (B) HI vs Ro diagram showing comparing the HI with coals from the Danish N. Sea, Greenland (After, Petersen, 2005). This shows the very high oil potential of the Longyear, Svarteper and Askeladden seams. **118**

Fig. 4.5 Comparison of the Rock Eval (S2) parameter with hydrous pyrolysis yields as a means of measuring future oil yields within the Longyear Seam. Maximum geological oil yields are derived from the addition of Soxhlet and hydrous pyrolysis yield. Note the similarity between the two techniques. **120**

Fig. 4.6 – Composition of the oil yielded from nitrogen retortion compared to global crude oils (adapted from Lundegard and Knott, 2001) showing the retortion products composition within the range of natural crude oils **125**

Fig. 4.7 - Variation in rank (R0) within the Longyear seam in Mine 7, Adventdalen. Examination of the distribution of vitrinite reflectance values measured shows a shift to lower values, bi-modal distribution upseam. **130**

Fig. 4.8 Aromaticity of the Svalbard Coals (A) LYR and (B) SVB. Note the large difference between the seam indicating an apparent maturity equivalent to that of R0 0.5% and 0.78% respectively (Carr and Williamson, 1990). This cannot be the case as the Longyear is not a lignite, therefore the Longyear is enriched with non-coaly aliphatics. **132**

Fig. 4.9. Variation in hopane and *n*-alkane maturity parameters up-seam within the Longyear seam. Note little variation in maturity up-seam indicating no maturity gap. **134**

Fig. 4.10 Typical mass chromatogram from the Longyear coal at 117cm above seam base. (A) Total ion chromatogram. Note the high hopane concentrations. (B) *m/z* 71 chromatogram showing *n*-alkane distribution, peak concentrations at around *n*C23 (C) *m/z* 191 chromatogram showing hopane distribution (D) *m/z* 218 chromatogram showing sterane distribution **138**

Fig. 4.10 Typical mass chromatogram from the Longyear coal at 117cm above seam base. (A) Total ion chromatogram. Note the high hopane concentrations. (B) *m/z* 71 chromatogram showing *n*-alkane distribution, peak concentrations at around *n*C23 (C) *m/z* 191 chromatogram showing hopane distribution (D) *m/z* 218 chromatogram showing sterane distribution **141**

Fig. 4.12 (A). Tissue preservation index (TPI) vs. Gelification index (GI) (after Casareo et al., 1996) of the Svalbard Coals. Note that the coals with most oil potential are characterised by low TPI, high GI values. **143**

Fig. 4.13 Comparison of Soxhlet yield (%) with total coal sulfur and Fe/S ration within the Longyear seam. Note the rapid increase in sulfur concentration and shift from iron enriched to sulfur enriched conditions after 80cm above seam base. **145**

Fig. 5.1 – Map of the distribution of Svea Seams across the Central Tertiary Basin in Relation to the inferred 'structural highs' indicated in Chapter 3. Note that all the seams are adjacent to the ridge. Approximate location of seam is also given relative to the bentontite bed described in Chapter 3 showing that the seams were not formed concurrently. Sample locations are also given. Inferred seam from derived from historic mining in the area **154**

Fig. 5.2 Long Term Carbon accumulation rates (LORCA) g/m/yr vs Latitude showing the linear decrease in LORCA rates from the equator to the poles (From Large et al., 2011) **157**

Fig. 5.3 – Correlation Matrix comparing the major and minor elemental composition of the Lower Svea Nord Seam at DT6/9 **165**

Fig. 5.4 – Correlation Matrix comparing the major and minor elemental composition of the Upper Svea Nord Seam at DT6/9 **166**

Fig 5.5 –Distribution of Al, Ca, Fe and S within the Breinosa Svea at BH5/2009. Note the similar distributions of each element **172**

Fig. 5.6 – Vitrinite, Liptinite and Inertinite profiles up seam within the lower Svea Nord Seam. Note that vitrinite increases upseam, liptinite decreases and inertinite exhibits a more cyclic distribution **179**

Fig. 5.7 – TPI, GI (*after Casareo et al., 2006)* and observed mineral matter profile within the Lower Svea Nord Seam. Note the drying events within the lower TPI profile and the increasingly wet conditions as indicated by higher GI values at the top of the seam **180**

Fig. 5.8 – Vitrinite, inertinite and liptinite profile up-seam within the upper Svea Nord Seam showing increasing vitrinite, stable inertinite and decreasing liptinite up-seam. **182**

Fig. 5.9 – TPI, GI (*after Casareo et al., 2006)* and observed mineral matter profile within the Upper Svea Nord Seam. Note the wetter conditions and fewer drying events within the upper seam compared to the lower seam **183**

Fig. 5.10 – Log Cu/Ti, Log Al/Ti profile from the Lower Svea Nord Seam, Note the 'saw tooth' profile at 110cm and 160cm indicating acidification and leaching of the peatland **186**

Fig. 5.11 – Log Fe/Ti, Log K/Ti, Log Mg/Ti profile from the Lower Svea Nord Seam, Note the 'saw tooth' profile at 110cm and 160cm indicating acidification and leaching of **187**

the peatland
Fig. 5.12 – Log Ti and inertinite profile from the Lower Svea Nord Seam. Note peak Ti occurs slightly after peak inertinite **188**
Fig. 5.13 – Log P and inertinite profile from the Lower Seam, Note P is concentrated within the more inertinite rich bottom of the seam **190**
Fig. 5.14 – Major element profiles normalised to Ti in the Upper Svea Nord Seam. Note the lithophiles show values close to mean continental crust (*Rudnick and Gao,2003)* whereas Fe and Ca are relatively enriched. **192**
Fig. 5.15 – Log Cu/Ti and inertinite profile from the Lower Svea Nord seam showing values consistent with mean continental dust (MCD; Lawrence and Neff, 2009) except during peak inertinite where local clastic sediment is deposited **195**
Fig. 5.16 – Log Cu/Ti and inertinite profile from the Upper Svea Nord seam showing values consistent with mean continental dust (MCD; Lawrence and Neff, 2009) this alternated between more Cu rich and more
typical MCD values on cyclic basis (40cm cycles) consistent with precession (Chapter 6) **196**

Fig. 5.17 – Log Fe, Log S and Log Fe/S ratio in the Lower Svea Nord Seam showing constant S concentrations up-seam, variable Fe and a Fe enriched peatland system with little free sulfur, indicating low oil potential (Chapter 4) **198**

Fig. 5.18 – Log Fe, Log S and Log Fe/S ratio in the Lower Svea Nord Seam showing gradually increasing S concentrations up-seam, variable Fe and a S enriched peatland system with free sulfur, indicating higher oil potential (Chapter 4) **199**

Fig. 5.19 Palaeo-environmental development of the Svea Nord Peatland from initiation to termination (A) Initiation of the peatland (B) Conditions within the Lower seam and split development (C) The upper Svea Nord Seam (D) Termination of the Svea Nord Seam **203**

Fig.5.20 – Summary diagram of the major controls upon coal quality within the Svea Nord Sea, (A) and Breinosa Svea (B). Note that the 'fan type' peat deposits can still be seen in Adventdalen today (*source M. Jochmann)* **206**

Figure 6.1 – Sample locality map of the NE Central Tertiary Basin with locations of currently operational and prospective mines. Blue dashed line – Maximum extent of the Longyear seam
(Chapter 3) **211**

Figure 6.2 – (Top) - Al profile of the Longyear seam at Mine 7 as a time series shows a series of apparent cycles. (Bottom) Power spectrum of the Al concentration of the Longyear seam. Expected Precession component calculated from number of 21kyr cycles expected/m at Tropical and Boreal LORCA rates. Shows that the cycles are consistent with a precessional control on Al and indicating estimates from LORCA rates are generally accurate **216**

Fig. 6.3 – Correlation matrix of major and minor elemental composition of the Longyear Seam at Mine 7. **225**

Fig. 6.4 – Correlation matrix of major elemental composition of the Longyear Seam at Lunckefjellet **226**

Fig. 6.5 – Vitrinite, Detrovitrinite, Inertinite and Liptinite profile upseam within the Longyear Seam at Mine 7. Note the transition at 80cm between raised bog-fen conditions causing elevated detrovitrinite and lower more stable inertinite. **231**

Fig. 6.6 – Inertinite, GI and TPI profile from the Longyear seam at Mine 7 showing the transition to wet conditions and increasingly degraded organic matter (reducing conditions) **232**

Fig. 6.7 – Vitrinite, Detrovitrinite, Inertinite and Liptinite profile upseam in the Longyear at Mine 7 showing a shift to wetter conditions ~ 259.7m depth **236**

Fig. 6.8 – % Observed Mineral Matter, GI and TPI profile for the Longyear seam at Lunckefjellet showing a transition at ~259.7 followed by an increase in observed mineral matter **237**

Fig. 6.9 – Fe, Mg, Ca and TIC profile upseam in the Longyear at Mine 7 showing concentration in fusinite rich areas, indicates deposition within higher porosity areas, post deposition **241**

Fig. 6.10 – Ca/Mg ratio within the Longyear seam at Mine 7 showing compositions broadly in the range of coastal and continental rainfall (Weiss et al., 2002 and references therein **242**

Fig. 6.11 – (Top) Modern trend in Long Term Carbon Accumulation rates with Latitude (Large et al., 2011) showing decreasing LORCA towards the poles (Bottom) The trend used to predict mass loss during coalification plotted on a van Krevelen diagram and compared to the USGS Coals (Bragg et al., 1998) and the results of artificial **246**

coalification (Mursito et al., 2010).

Fig. 6.12 – Predicted recent mineral dust deposition rates (Mahowald et al., 2006) **247**

Fig. 6.13 – Measured vs. predicted Ti concentrations within Cenozoic coals (Large et al., 2011). Close agreement indicates that the techniques should be valid **248**

Fig. 6.14 – Lithophile elements (Al, K, Na, Ti) profiles upseam in the Longyear at Mine 7. High values indicate dustier periods/ drier periods **250**

Fig. 6.15 – Al and fusinite profile showing fires during locally wetter periods, this indicates that although peatland hydrology made large fires possible the causes of the fires may be external for example ignition by lightning. When hydrology was more stable the peatland was harder to burn and so the fire cycles seen were not as prominent **252**

Fig. 6.16 – Palaeogeographic/climatological model of the Arctic region in the Palaeocene (After Scotese, 2002) showing conditions during globally cooler periods and during periods more intense hydrological cycling. **254**

Fig. 6.17 – Al/Ti, Fe/Ti, Ca/Ti, K/Ti, Na/Ti ratio profiles upseam in the Longyear at Mine 7 showing that Al is consistentwith Mean Continental Crust Values (MCC) but that Fe and Ca are enriched probably due to groundwater supply. **256**

Fig. 6.18 – Al/Ti, Fe/Ti, Na/K and Ash content of the Longyear Seam at Lunckefjellet **257**

Fig. 6.19 – Na/K profile of the Longyear Seam at Mine 7 showing increased clastic input at the base of the seam **258**

Fig. 6.20 Al and Cu/Ti profile of the Longyear at Mine 7 showing that in drier periods, dust was locally derived and in wetter periods less dust was delivered but from and a more copper enriched distal source. **260**

Fig. 6.21 – Modelled effect of sea salt sulphate deposition at low,medium and high latitude and a measured transect inland from an inferred tidal channel shows close correlation. Using this model the Longyear terminated at 1km from the coast in mine 7 and 0.5km in Lunckefjellet **263**

Fig. 6.22 (Top) S and Fe/S profile for the Longyear at Lunckefjellet (Bottom) S and Fe/S profile for the Longyear at Mine 7. Pyrite line from atomic ratio of Fe/S in pyrite **265**

Fig. 6.23 – Al, K, Na, Ti profile showing increasing clastic deposition towards the top of the Longyear seam at Lunckefjellet **268**

Fig. 6.24 - (Top) Macrofossils from the Palaeogene of Svalbard (Source Denk et al., 1999) Bottom- Possible *Acer Arctica* fossil from a split in the Longyear seam in BH14/2011 **270**

Fig. 6.25 – m/z 123 mass chromatograms showing the tricylic diterpanes showing a dominance of isopimarane and 4ß-(H)-19-norisopimaranes in the Longyear seam at Mine 7 **271**

Fig. 6.26 - m/z 191 and m/z 205 mass chromatograms identifying the main hopanes,2-methyl hopanes and 3-methyl hopanes (identified from Farrimond et al., 2004) **275**

Fig. 6.27 – Log hopane/sterane concentration (µg/g TOC) and hopane concentration (mg/g extract) showing the distribution and percentage hopanes upseam in the Longyear at Mine 7 **279**

Fig. 6.28 – Ratio of 3-Methyl hopanes to total hopanes and 2-methyl-hopanes to total hopanes and concentration of 2-methyl hopanes and 3-methyl hopanes upseam within the Longyears seam at mine 7. **280**

Fig. 6.29 – Relationship between water table depth and methane flux (after Bubier et al., 2003) showing greatest methane flux at the shallowest water table depth. **285**

Fig. 6.30 – Palaeo-environmental reconstruction of the initiation of the Longyear seam and conditions within the Lower Longyear seam **289**

Fig. 6.31 – Palaeo-environmental reconstruction of the conditions at the raised bog-fen transition and during the upper Longyear seam **291**

6.32 – Palaeogeographic reconstruction of the conditions present immediately after the termination of the Longyear seam. **293**

Fig. 6.33- Summary diagram of the major controls on coal quality within the Longyear seam at Mine 7 and Lunckefjellet before and after the raised-bog – fen transition **295**

Fig. 7.1 – Vertical maceral profile for the Lunckefjellet and Breinosa Svarteper (A) Inertinite (%) (B) Liptinite (%) (C) Detrovitrinite (%) *Blue Box – split* **309**

Fig. 7.2 – Vertical maceral profile for the Lunckefjellet and Breinosa cores (A) Mineral Matter (%) (B) GI (Gelification Index; see chapter 2) (C) TPI (Tissue Preservation Index; see chapter 2) *Blue Box – split* **311**

Fig. 7.3 – Geochemical Parameters from BH15-2011 (Lunckefjellet) *Top Row (left-right) – Ca/Mg (Water Compositions Berner and Berner, 1997) , Fe/S , Na/K Bottom Row – Al/Ti, Fe/Ti, Ca/K (MCC values Rudnick and Gao, 2003)* **314**

Fig. 7.4 – Geochemical Parameters from BH5-2009 (Breinosa) Svarteper Seam *Top Row (left-right) – Ca/Mg (Water Compositions Berner and Berner, 1997) , Fe/S , Na/K Bottom Row – Al/Ti, Fe/Ti, Cu/Ti (MCC values Rudnick and Gao, 2003)* **315**

Fig. 7.5 – Geochemical Parameters from BH5-2009 (Breinosa) Askeladden Seam *Top Row (left-right) – Ca/Mg (Water Compositions Berner and Berner, 1997) , Fe/S , Na/K Bottom Row – Al/Ti, Fe/Ti, Cu/Ti (MCC values Rudnick and Gao, 2003)* **318**

Fig. 7.6 – Summary diagram showing the main sources of Ash and sulphur from the Svarteper and Askeladden Seams alongside a demonstration of increasing marine influence from the deposition of the Longyear seam to the Svarteper/Askeladden area. The primary controls are S from seawater, Ash from marine and fluval flooding events and Fe/Ca from groundwater. Highest quality and thickest coal would be expected in the Bassen area for both seams due to its relatively sheltered position at the NE edge of the coastal plain. N.B the rapid northeasterly retreat of peatland from the Longyear to Svarteper Askeladden period represent the final infilling of the underlying palaeotopography **320**

Fig. 8.1 – (Left) Reconstruction of the Gronfjorden valleys presuming the valley system identified extends to the previously identified swells and troughs. (Right) Similar braided river system from Alaska (http://pages.uoregon.edu/millerm/braided.html) **323**

Fig. 8.2 Palaeo-environmental development of the Svea Nord Peatland from initiation to termination (A) Initiation of the peatland (B) Conditions within the Lower seam and split development (C) The upper Svea Nord Seam (D) Termination of the Svea Nord Seam **325**

Fig. 8.3. Palaeo-environmental development of the Longyear seam, A and E based on lithology maps as defined in Section 3.4. B-D based on coal isopach maps and **327**

response to sea level shown in in Fig. 3.16

Fig. 8.4 – Summary diagram showing the main sources of Ash and sulphur from the Svarteper and Askeladden Seam alongside a demonstration of increasing marine influence from the deposition of the Longyear seam to the Svarteper/Askeladden area. The primary controls are S from seawater, Ash from marine and fluvial flooding events and Fe/Ca from groundwater. Highest quality and thickest coal would be expected in the Bassen area for both seams due to its relatively sheltered position at the NE edge of the coastal plain. N.B the rapid north-easterly retreat of peatland from the Longyear to Svarteper Askeladden period represent the final infilling of the underlying palaeotopography

List of Tables

Table 2.1 – Standard and Reproducibility data for ICP-AES analysis **29**

Table 4.1 – Characterisation of the oil potential of the Longyear coal using Soxhlet Solvent Extraction, Accelerated Solvent Extraction and Hydrous Pyrolysis **113**

Table 4.2 – Oil Yields from the other Central Tertiary Basin coals usingAccelerated Solvent Extraction (ASE) **115**

Table 4.3 – Rock Eval Pyrolysis results for the Svea Nord (SVN), Breinosa Svea (SVB), Longyear (LYR), Svarteper (SVART) and Askeladden Seam (ASK) **117**

Table 4.4 –Comparison of the hydrous pyrolysis and Rock Eval yields from the Longyear Seam with published oil shale data (Lewan, 2006) and other coals (Uguna et al., 2012a;b) on a TOC and rock basis **122**

Table 4.5 – Yields from nitrogen retortion of bulk samples of the Svea Nord, Longyear, Svarteper and Askeladden Seams **125**

Table 4.6 – Vitrinite Reflectance (R_o), *n*-alkane, hopane, sterane and aromatic biomarker parameters within the Central Tertiary Basin Coals [a] after Cassani et al., 1998 [b] after Radke and Welte, 1983 **129**

Table 4.7 – Concentrations of hopanes up-seam within the Longyear Seam at Mine 7 on an extract and TOC basis **148**

Table 5.1 – Typical Coal Quality Analyses from the Svea Nord seam and Breinosa Svea seam (SNSK data) **160**

Table 5.2 – Major and minor whole coal elemental composition of the Lower Svea Nord Seam at DT6/9 **163**

Table 5.3 – Major and minor whole coal elemental **164**

composition of the Upper Svea Nord Seam at DT6/9

Table 5.4 – Major and minor elemental composition and elemental ratios from the Svea Nord Split at DT6/9 **168**

Table 5.5 – Major and minor elemental composition of the Breinosa Svea at BH9/2009 **170**

Table 5.6 – Coal Maceral composition of the Lower Svea Nord Seam at DT6/9 **175**

Table 5.7 – Coal Maceral composition of the Upper Svea Nord Seam at DT6/9 **176**

Table 6.1 – Coal Quality (Ash, Sulfur, Calorific Value and Free Swelling Index (FSI) from Longyear Seam Coals at Breinosa (Mine 7) and Lunckefjellet areas
(Source SNSK) **219**

Table 6.2 – Major and minor elemental composition of the Longyear Seam at Mine 7. B.D = Below detection **221**

Table 6.3 – Major Elemental composition of the Longyear Seam at Lunckefjellet **222**

Table 6.4 – Maceral compositon of the Longyear seam at Mine 7 showing a dominance of
vitrinite macerals **230**

Table 6.5 – Maceral composition of the Longyear seam at Lunckefjellet showing the dominance of vitrinite group macerals in these coals **234**

Table 6.6 – Predicted dust contribution for peatland (assumed dust deposition 1g/m/yr) and the actual composition of the Longyear seam, note the close correlation of Ti, Cu and Pb (the most immobile lithophile element with that predicted). K is low
due to its mobility within peats **248**

Table 6.7 – Comparison of the hopane and methyl-hopane content of the Longyear coal with other coals and source rocks (from Farrimond et al., 2004) **276**

Table 6.8 – Hopane concentration and hopane ratios at increasing height above seam base (cm) **283**

Table 7.1 – SNSK Core Data from BH5/2009 (Breinosa Region) and BH15/2011 (Lunckefjellet Region) for the **300**

Svarteper and Askeladden Seams

Table 7.2 – Major and Minor elemental composition of the Svarteper and Askeladden Seams from BH5/2009 (Breinosa) **301**

Table 7.3 - Major elemental composition (oxide wt%) of the Svarteper Seam at BH15/2011 (Lunckefjellet) **302**

Table 7.4 – Correlation Matrix between major and minor elements within the Svarteper and Askeladden Seams, BH5/2009 **304**

Table 7.5 – Maceral Composition of the Svarteper seams at BH5/2009 (Breinosa) andBH15/2011 (Lunckefjellet), Point Count (500counts, 50x lens) *TPI = Tissue Preservation Index, GI = Gelification Index, V/I = Vitrinite/Inertinite (see Chapter 2 for calculations)* **306**

Table 7.6 – Maceral Composition of the Askeladden seam at BH5/2009 (Breinosa), Point Count (500 counts, 50x lens) *TPI = Tissue Preservation Index, GI = Gelification Index, V/I =Vitrinite/Inertinite (see Chapter 2 for calculations)* **307**

Chapter 1

INTRODUCTION

The purpose of this study is to investigate the economic potential and understand the peatland processes which characterise high latitude peatland formation.

1.1 Context

Modern high latitude peat formation is limited (Gorham, 1991) and therefore peatland character and dynamics at high latitude during periods of global warmth such as the Palaeocene are little understood. Peat accumulation and preservation occurs where the peat production exceeds decay. This in part controlled by the hydrodynamics of the peatland (Belyea and Bird, 2006).

Coal mining has taken place upon Svalbard since the early 20th Century with current mines operational in Adventdalen (Mine 7), Svea Nord and Barentsburg. A new mine is also in construction at Lunckefjellet (Fig.1.1;1.2). Currently, only the Palaeocene coal-bearing Todalen Member is exploited but in the past both Cretaceous coals (Advent City) and Carboniferous coals (Pyramiden) have also been mined (Harland et al., 1997)

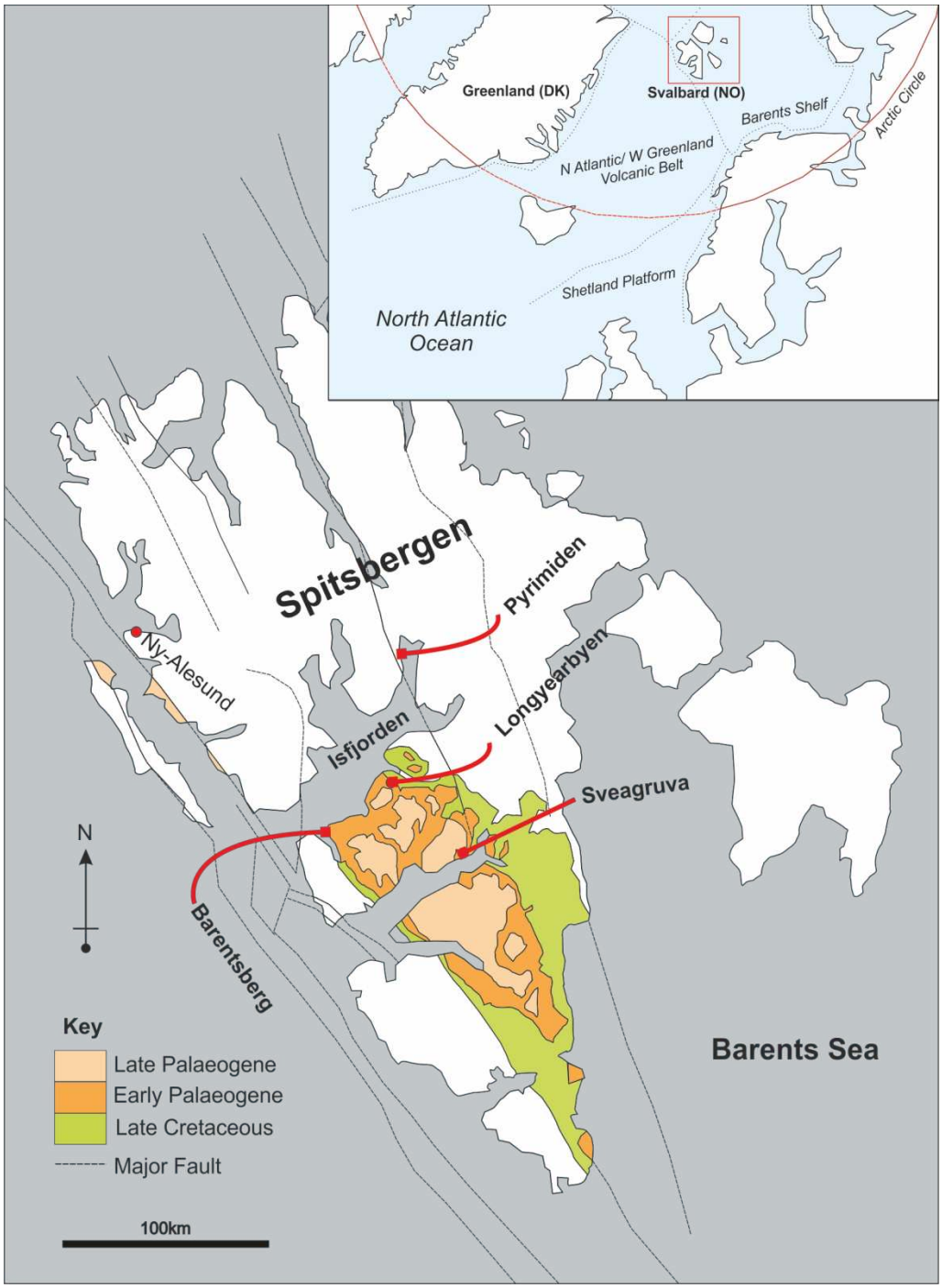

Fig. 1.1 – Map of the island of Spitsbergen showing the extent of late Mezozoic – Cenozoic sediments and the location of major settlements referred to in this study

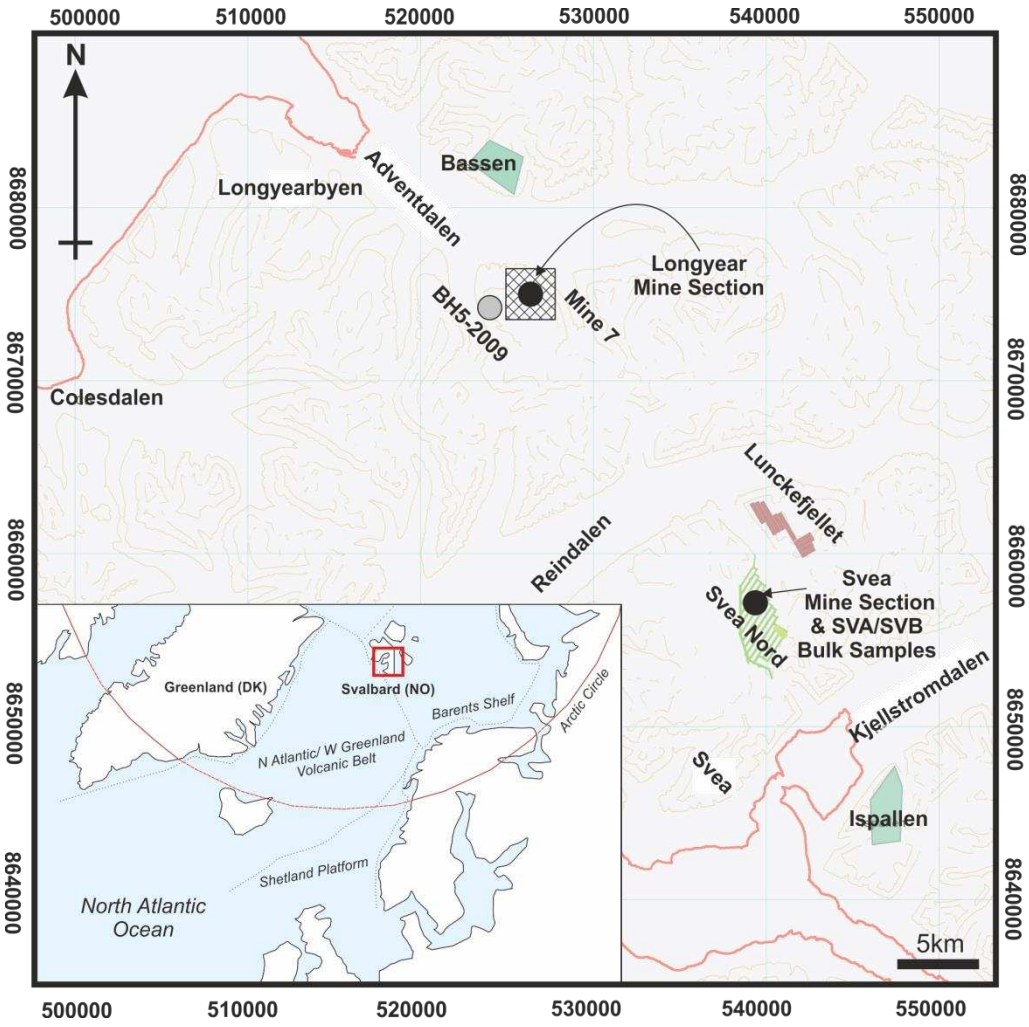

Fig. 1.2 – Map of the island of Spitsbergen showing the mines and settlements of the NW Central Tertiary Basin

Todalen Member coals have been extensively studied from a palaeogeographic viewpoint (Dalland and Steel, 1981; Worsley et al., 1986; Nøttvedt, 1985; Jochmann, 2004; Nagy, 2005; Lüthje, 2008; Aspøy, 2011). Many of these studies are in the form of PhD and master's theses on specific areas of interest such as Ispallen (Jochmann, 2004) and Lunckefjellet (Aspøy, 2011), etc., however non-schematic palaeogeographic reconstructions of the entire eastern coalfield has been limited to more recent studies (Lüthje, 2008).

Previous palaeogeographic interpretations of the Todalen Member have been surprisingly diverse with some authors supporting a deltaic origin (Dalland and Steel, 1981; Worsley et al., 1986) and others a tidal coastal wetland (Lüthje, 2008; Aspøy, 2011). Even amongst authors who share the same general view regarding depositional environment significant differences remain regarding the interpretations of the relative importance and position of estuaries and tidal channels (Lüthje, 2008; Aspøy, 2011). This uncertainty even applies to the number of coal seams within the Todalen member with most authors citing five seams, the Svea, Todalen, Longyear, Svarteper and Askeladden (Harland et al., 1997; Dallmann, 1999; Orheim et al., 2007). However, a cross-section by Lüthje (2008) appears to indicate more than 20 seams.

The Todalen member lies unconformably above the Carolinefjellet formation representing a hiatus of ~40Myr. The resulting peneplain

has been shown previously to exert a significant control upon the location of the lowermost Svea seam; however the effect upon later more laterally extensive seams is unknown.

Sequence stratigraphic models of coal deposition are based on the balance of peat accumulation and accommodation rate rise (Bohacs and Suter, 1997). This has proven useful at predicting when large scale coal formation occurs, but appear to have difficulty predicting where the coal formation will be sustained and produce the thickest peats (Bohacs and Suter, 1997 and references therein). This is possibly due to the assumption that accommodation rate in paralic settings is almost entirely due to base level changes (Sea-level; Bohacs and Suter, 1997), ignoring the effects of underlying topography and changes in hydrological supply.

Hydrological landscape theory (Winter, 1992; 2000; 2001) represents a new approach to understanding and predicting the distribution of the thickest coals. It states that peat thickness in modern peatlands should be driven by the stability of hydrological supply, itself a function of the interaction between structure, climate and landscape. Unlike sequence stratigraphic approaches it considers even minor landscape features to have a role in controlling peat thickness around them.

Hydrological stability is often found in areas of regional groundwater supply and at areas of groundwater discharge such as

the break in slope. These areas should continue to be areas of consistent hydrological stability even during base level falls, allowing thick peats to continue accumulating much longer than predicted by the Bohacs and Suter, (1997) model. By contrast depressions within the coastal plain would be expected to act as conduits for channel formation favouring lower quality and thickness coal deposits (Bohacs and Suter, 1997 and references therein).

Consequently, it is thought necessary to re-examine the palaeo-geography of the Central Tertiary Basin with more emphasis on the information regarding palaeo-extent and hydrology contained within the coals. In order to do this coal isopach mapping at a variety of scale will be compared with a palaeo-topographic indicator; the fluvial conglomerate known as the Grønfjorden bed which should only present within the valleys of the Cretaceous pene-plain. This should then show how the landscape controls upon peat formation evolved over the history of the Todalen member.

Two types of oil prone coal exist (Macgregor, 1994), one formed at high latitude (Fleet and Scott, 1994 Killops et al. 1994; Sandison et al. 2002; Petersen, 2005; Vu et al. 2009) and the other in equatorial regions (Macgregor, 1994; Van Koeverden et al, 2010; Van Koeverden et al., 2011; Bojeson-Koefoed et al., 2012) both of which can be found upon Svalbard in the Norwegian Arctic.

Lower Carboniferous coals previously mined at Pyramiden, Svalbard (Abdullah et al. 1988, Nøttvedt et al. 1993, Harland et al. 1997, Tangedal, 2011) and found more widely within the Barents Region (Moi, 2008, Van Koeverden et al. 2011, Bojeson-Koefoed et al., 2012) are representative of the better studied 'equatorial' type oil-prone coal. Lower Palaeogene coal from the Central Tertiary Basin (CTB), Svalbard represents the less well studied high latitude type (Harland et al. 1997, Orheim et al. 2007).

Oil-prone coals are economically important as oil source rocks and have been the subject of numerous publications over the past twenty years (e.g. Fleet and Scott, 1994; Diessel and Gammidge, 1998; Sandison et al., 2002; Wilkins and George, 2002; Sykes and Johansen, 2006; Vu et al., 2009). Although coals from the Taranaki Basin, New Zealand (Killops et al., 1998) and from the Danish North Sea (Petersen, 2005) have been broadly characterised, oil-prone coals from within the high Arctic have only been described anecdotally (Macgregor, 1994).

This makes the coals of the Central Tertiary Basin, invaluable for understanding the processes and conditions required for oil prone coal formation in the high Arctic and in particular whether the warm Palaeogene climate was a contributing factor (Macgregor, 1994). In addition, with a coal resource of in excess of 3000 MT (Orheim et al., 1986), the coals of the Central Tertiary Basin may

represent a previously unknown unconventional hydrocarbon province.

Consequently this study will attempt to confirm the previous findings of Hoel (1925) and Orheim et al., (2007) through a number of solvent extraction techniques to examine the present, future and economic oil potential of the coals. In addition organic biomarker and maturity analyses are applied to investigate the controls upon oil potential during this period of global warmth.

Bulk coal quality data has been widely collected by the mining company Store Norske Spitsbergen kulkompani (SNSK). In addition, published work by Orheim et al., (2007), Ćmiel and Fabiańska, (2003) and Lewinska-Preis et al., (2009) has primarily been focussed upon coal characterisation (organic/inorganic geochemistry, organic petrography) and therefore only bulk samples were examined. Unfortunately, this does not provide sufficient resolution to both identify the main controls upon inorganic species within the coals and to examine how these controls changed over time.

As a result, previous work has struggled to integrate coal chemistry (Ćmiel and Fabiańska, 2003; Orheim et al., 2007; Lewinska-Preis et al., 2009) with palaeo-geography, which is partially due to the more schematic nature of many reconstructions (Dalland and Steel, 1981; Worsley et al., 1986).

This study attempts to resolve this by using two high resolution (~2.5cm sampling density) sections from the Svea Nord and Mine 7 mines alongside 2 boreholes from Lunckefjellet and Breinosa (BH15/2011 and BH5/2009) to examine how the controls upon coal quality changed both within each seam and over the period of Todalen coal formation. When integrated with the palaeogeographic models of each peatland, this should allow detailed correlation between both long term and short-term basinal processes and coal distribution, quality and oil potential.

1.2 Aims and Objectives

The main aim of this thesis was to develop understanding with regard to the response of high latitude peatland to changes in underlying topographic/structural controls, rising relative sea level and palaeo-hydrology and its effect upon oil potential and coal quality.

The approach was to develop a palaeogeographic and palaeo-environmental model of peat accumulation throughout the duration of the Early to Mid-Palaeocene Todalen member. Various organic petrographic, inorganic and organic geochemical palaeo-hydrological and palaeo-environmental proxies were then applied and interpreted within the context of the palaeogeographic model created. The thesis is structured as follows;

1. Chapter 2 presents a summary of the sampling methodologies and analytical methodologies used during within later chapters. Also reviewed are the measures used to measure the precision and accuracy of the data collected. The objective of this chapter was to provide background on the techniques used and demonstrate the reliability of the results.
2. Chapter 3 examines previous depositional models from the Todalen member coals before developing and demonstrating a method for using coal isopach maps to understand the palaeogeographic development of the Todalen peatlands. The objective of this chapter was to (A) Understand and evaluate previous depositional models from this period and (B) Develop more high resolution models suitable for predicting the effect of rising sea levels, potential sources of coal contaminants and oil potential.
3. Chapter 4 examines the amount and causes of oil potential within the Todalen coals. The objectives of this chapter are to (A) quantify the present, future and economic oil yields from the Todalen coals, (B) Improve upon previous coal maturity models (C) Discuss possible mechanisms for the formation of high latitude oil-prone coals.
4. Chapter 5 integrates inorganic geochemical and organic petrographic data with palaeogeographic models of the Svea Nord and Breinosa Svea seams. The objectives of this chapter

are to highlight any dominant controls upon the inorganic composition of the coals and develop a palaeo-environmental model for the development of the Svea Nord and Breinosa Seams

5. Chapter 6 integrates inorganic and organic geochemical proxies and organic petrographic data with the palaeogeographic models of the Longyear seam at Mine 7 and Lunckefjellet (Chapter 3). The objectives of this chapter were to (A) indicate an approximate duration of Longyear peat formation (B) highlight any dominant controls upon the inorganic composition of the coals (C) explore the possible climatic impacts of high latitude peatlands (D) Develop a palaeo-environmental model for the development of the Longyear seam.
6. Chapter 7 integrates inorganic and organic geochemical proxies and organic petrographic data from the Svarteper and Askeladden seams with the palaeo-environmental models produced in Chapter 3. The objectives of this chapter were to understand why coal quality issues were most pronounced in these seams and develop a palaeo-environmental model for the development of these seams.
7. Chapter 8 presents the overall conclusions and future work. The objective of this chapter was to combine the environmental and palaeogeographic data to show how controls upon peatland distribution and type developed over the duration of Todalen member deposition, the effect of this upon coal quality and oil

potential and discuss how this approach can be applied to other peatlands.

Chapter 2

SAMPLE AND ANALYTICAL METHODOLOGY

2.1. Sampling methods and localities

Three bulk coal samples were provided, two Svea Nord mine (Courtesy SNSK) and one from the Longyear seam mine 7 (Statoil/SNSK; Fig. 2.1).

Svea coal was sampled from a section within the centre of the Svea Nord Mine (DT6-9; Fig. 2.1; 2.2) in April 2011. Great care was taken to preserve both the orientation and position of the base and top of each coal sampled whilst avoiding areas of faulting. Care was also taken to remove areas of calcite paste (Used for fire proofing) prior to sampling). Samples were then wrapped in paper with the sample identification and orientation written a number of times on the covering to ensure preservation. This was then wrapped within a plastic sample bag which was marked again with the sample name, orientation and sample interval. Where sampling was not possible directly above the previous sample, areas of similar stratigraphic positioning (as identified by vitrain/durain banding) were collected.

In addition a 1.5m Longyear coal section from Mine 7 (Gruve 7) mine in Adventdalen (Fig. 2.1) was sampled at the location marked on Fig. 2.3. Sampling followed the same scheme as in the Svea

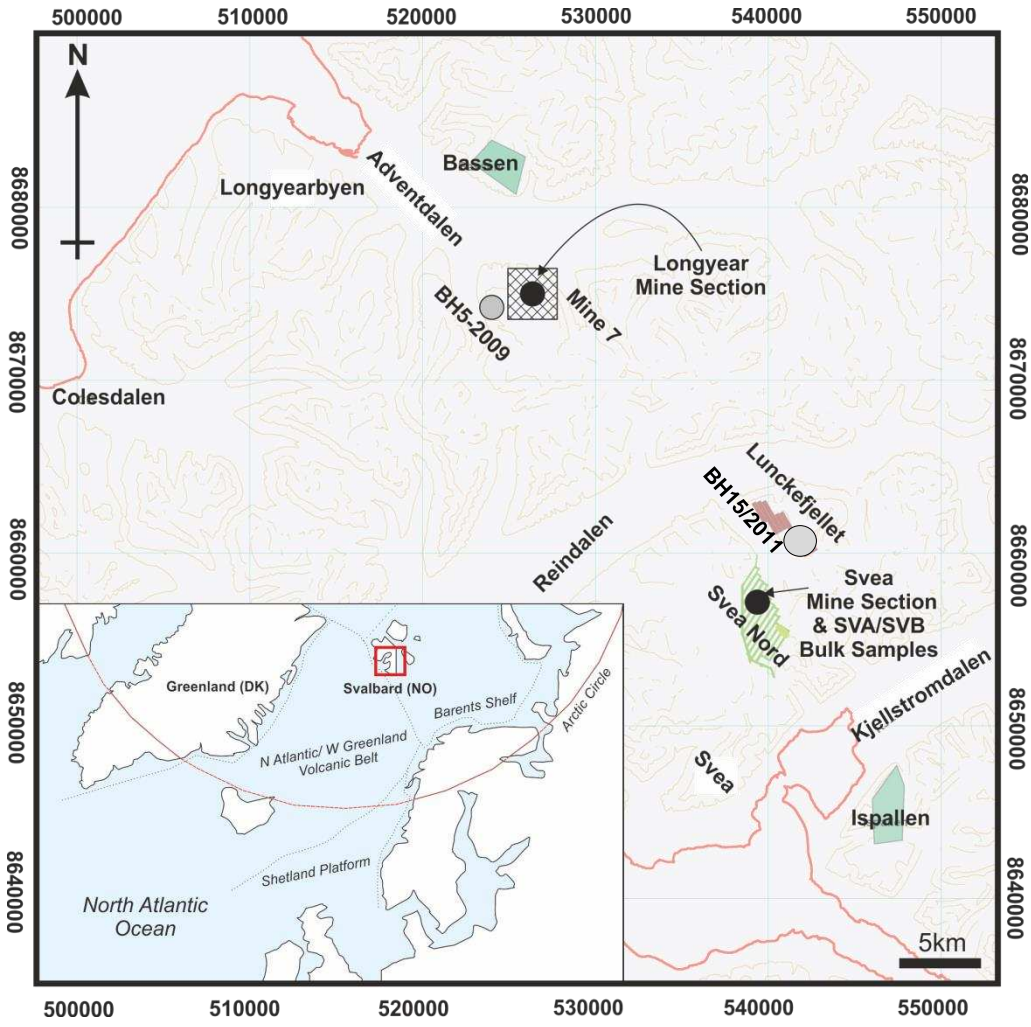

Fig. 2.1 – Map of the NE Central Tertiary Basin with current and prospective mine deposits. Sample Locations used in this study are also shown. Black Circle = Mine Section, Grey Circle = Borehole samples.

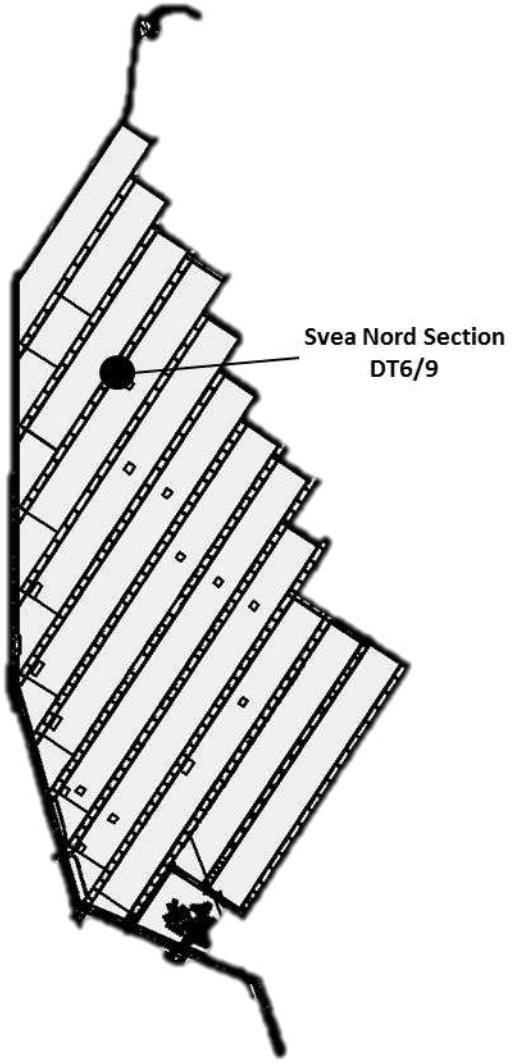

Fig. 2.2 – Map of the Svea Nord Mine showing the sample location at DT6/9. *Courtesy Bjarki Friis (SNSK)*

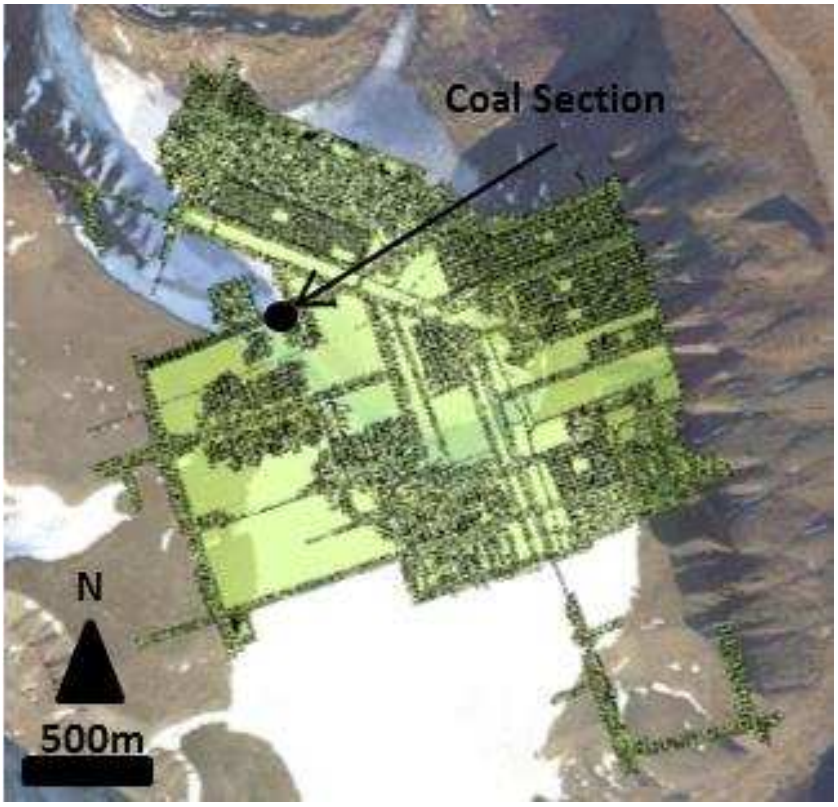

Fig. 2.3 – Map of Mine 7 (Adventdalen) showing the section location. ***Courtesy Bjarki Friis (SNSK)***

Nord mine with the exception of the precautions regarding fireproofing paste as this was not present.

Coal samples from two cores were also sampled with one from the Breinosa region and the other from Lunckefjellet region (Fig. 2.1). The Breinosa region core (BH5/2009) contained coal samples from the Breinosa Svea (See Chapter 3), Todalen, Svarteper and Askeladden Seams. Samples were pre-prepared, homogenised and crushed by SNSK AS at sample intervals between 20cm and 30cm. The Lunckefjellet Core (BH15/2011) contained samples from the Longyear and Svarteper seams and was sampled directly from core at higher resolution (10cm) as whole coal samples. Core Samples were packed as described previously with the exception of labelling orientation as the coals were fragmented and subject to limited movement during transportation from the drill site.

Surface coals from Barentsburg and Pyrimiden were also collected to compare with those found previously

2.2 – Sample Preparation

The Svea Nord and Mine sections were initially washed in water to remove any contamination on their surface, air dried, then sub-sampled by cutting using a diamond tipped bench mounted circular saw. The Svea samples showed significant contamination from the fireproofing material (calcite paste) up to 5cm into the coal and as a consequence these were removed where possible during sub-

sampling. The samples were then washed in water again and left to dry before being wrapped in foil and placed in a plastic sampling bag labelled with the code NCM2010 – xx (sample number) with samples 10000-10199 from Svea Nord, 10200-10299 from Longyear Mine 7 and 10300+ coals sampled from core. Coals sampled from BH5/2009 and BH15/2011 were also washed prior to crushing

Coals were then coarse crushed in a metal pestle and mortar. The pestle and mortar was cleaned using industrial methylated spirits (IMS) after each use to prevent cross contamination. The coarse crushed material was then separated by cone and quarter into coal to be retained, used for coal petrology and to be fine crushed (<100μm).

Samples for coal petrography were hand crushed within a plastic bag and the coal sieved to a particle size of <1mm and >200μm. A new bag was used each time and the sieve cleaned using IMS to prevent cross contamination. The fine crushed samples were placed in a Agate TEMA mill for 5 minutes until a fine powder was produced. Samples with higher clastic content and sediments took longer (~10mins/sample). Another difficulty was observed in the top of the Longyear seam as the samples became sticky when ground and the TEMA mill stained by a brown substance. This made cleaning difficult; however this was solved by running quartz sand in the mill between runs. This was followed by cleaning in water and IMS before the mill was dried to prevent the coal from sticking.

The fine (<100μm) was then placed in glass bottles, labelled and dried within an oven at 80°C overnight.

2.3 – Analytical Methodology

The following section deals with the techniques and data quality measures used to examine the geochemistry and organic petrology of the coals sampled.

2.3.1 – Organic petrology

2.3.1.1 – Sample Preparation

The 0.2-1mm particle fraction separated previously from the coals was poured into moulds and mixed with a small amount of Epofix ® resin and stirred, this was then placed within an Epovac ® vacuum chamber in order to remove any trapped air bubbles for 45mins and topped up to approximately 75% of the mould and left to air dry overnight. The sample was etched with the sample number and the coal surface ground to remove irregularities and then polished initially with increasing grade diamond based polishing fluids and finally by colloidal silica. The surface of each sample was then examined under a microscope for any surface defects/polishing artefacts and if present the process repeated.

2.3.1.2 – Coal Maceral Analysis and Vitrinite Reflectance

Maceral composition and vitrinite reflectance was determined using polished blocks (particle size, 0.2mm-1mm) by point-counting (500 points) according to the classification scheme (ICCP, 1994a, 1994b) and BSI standards. The microscope was fitted with a 50x oil immersion objective and 10x oculars, 12V 100W quartz halogen lamp and 100W HBO high pressure mercury lamp.

Vitrinite reflectance (R_o) measurements were taken using an attached photomultiplier (100 points) and calibrated in oil using a 1.24 R_o 564nm glass prisma standard and blank black plastic oil filled depression standard according to BSI standards. In addition a number of photomicrographs of the coals within both white and blue light were produced from selected samples and these can be seen in Appendix I.

2.3.1.3 Tissue Preservation and Gelification Index

Maceral indices such as gelification index (GI) and Tissue Preservation Index (TPI) provide information regarding the wetness/dryness and humification/tree density respectively (Diessel, 1986, Casareo, 1996). Due to the virtual absence of macrinite GI is defined by (1) and TPI by (2) within the Svalbard coals;

$$(1) GI = \frac{Vitrinite}{Inertinite}$$

$$(2) TPI = \frac{Telovitrinite + fusinite + semifusinite}{Detrovitrinite + inertodetrinite}$$

2.3.1.4 – SEM EDAX analysis

SEM-EDAX analysis was carried out on selected samples of the Svea and Longyear seams in order to examine the inorganic constituents of the coals. The polished blocks were carbon coated prior to examination. EDAX was used to identify the mineral species within the coals which in the Svea were Ca-phosphates such as crandallite and apatite and in the Longyear were Fe-Ca-Carbonates such as ankerite, siderite and calcite. Pyrite was also ubiquitous within all samples measured. The photomicrographs of these can be seen in Appendix II.

2.3.2 – Organic Geochemistry

2.3.2.1 – Soxhlet and Accelerated Solvent Extraction

Free hydrocarbons were Soxhlet extracted from selected Longyear coal samples using in a pre-extracted cellulose tube in a 93:7 DCM:methanol mix for a period of 7-14 days by an MSc student (Ikechukwu Mokogwu; Mokogwu, 2011). This was then evaporated and transferred to a pre-weighed vial.

Duplicate Longyear samples were also extracted by Accelerated Solvent Extraction (ASE). Whilst ASE yields were slightly lower

than Soxhlet, due to less efficient asphaltene extraction, up-seam trends were reproduced (Fig. 4.2). Consequently, the more rapid ASE method was used on samples of Svea Nord and Breinosa Svea, Svarteper and Askeladden seam from BH5/2009.

The extracts were then separated into aliphatic, aromatic and polar components by silica/alumina adsorption column chromatography (I Mokogwu, 5 Soxhlet samples). This was achieved through progressively changing the solvent mix in the reservoir form 15ml n-hexane (aliphatics), 15ml n-hexane/DCM (9:6v/v; aromatics) and 15ml DCM/methanol (7.5:7.5v/v; polar).

2.3.2.2 – Rock Eval Pyrolysis

Twenty-six 1g fine coal samples from the Longyear seam, Breinosa Svea, Svea Nord, Svarteper and Askeladden seams were sent away for Rock Eval Pyrolysis 6 analysis. The results compared well with those achieved by Uguna et al., (2012a) for the Longyear seam.

2.3.2.3 – Hydrous Pyrolysis

One gram of pre-extracted coal from six samples of Longyear seam was subjected to hydrous pyrolysis at 350°C for 24 hours in a Parr 4740 series hastalloy cylindrical pressure vessel filled with 15ml of distilled water and connected to 690bar rated pressure gauge by I Mokogwu. Samples (~1g) from the Longyear, Svea, Svarteper and Askeladden seams were subjected to nitrogen pyrolysis in order to simulate retortion using an adapted hydropyrolysis rig (described in

Meredith et al., 2003). Interpretation of these results can be seen within Mokogwu, (2011) and this study.

2.3.2.4 – Nitrogen Pyrolysis

Samples (~1g) from the Longyear, Svea, Svarteper and Askeladden seams were subjected to nitrogen pyrolysis in order to simulate retortion using an adapted hydropyrolysis rig (described in Meredith et al., 2003) by Dr Will Meredith and a MSc student Yukun Wang (Wang, 2011).

Briefly, the vacuum-dried coal sample (0.25 g) was mixed with sand (1:20 w/w) in a tube reactor in order to avoid the swelling of the coal. The samples were heated resistively from ambient temperature to 250°C at 300°C min^{-1} then to 520°C at 8°C min^{-1} where it was held for 2 mins. The experiments were carried out under a nitrogen pressure of 2 bar, with a nitrogen flow of 1 L/min, measured at ambient temperature and pressure, to ensure that the generated volatile components were quickly swept out of the reactor. The volatized oil was then collected in a dry-ice cooled silica trap, and recovered in DCM for subsequent fractionation and analysis. New interpretation of these results in relation to the coals economic potential is offered in this study.

2.3.2.5 – Gas Chromotography-Mass Spectrometry (GC-MS)

Gas chromatography mass spectrometry (GC-MS) analysis of both the aromatic and aliphatic fractions (2mg/1ml DCM) were performed on a Varian 1200 Quadropole Mass Spectrometer (ionising energy 70 eV, source temperature 280°C, transfer line 300°C; Varian Corporation, Lake Forest, CA, USA), coupled with a CP3800 GC. Separation was achieved on a VF-1MS-low bleed 100% dimethylpolysiloxane column (30m length, 0.25mm ID and .25µm film thickness with a helium carrier gas (100kPa) and oven temperature increasing from 50°C (2 minutes) to 300°C at a rate of 4°C/min, before being held at temperature for 20.5 mins.

Full Scan and Selective Ion Recording (SIR) modes were used to examine mass range 50-450m/z with ion of particular interest including m/z 71 (*n*-alkanes), m/z 123.2 (diterpinoids), m/z 191 (hopanes), m/z 205 (Methyl-hopanes) and m/z 218 (steranes).

Peaks were identified from relative retention times, elution patterns, fragmentation patterns and comparison with published mass-spectra (Bechtel, 2002a; 2002b; 2003; 2004; 2005; Peters et al., 2005 and references therein)

2.3.2.6 – Biomarker Biochemistry

The origins and biochemical precursors of some of the biomarkers examined is discussed within this section.

m/z 71 - n-Alkanes

The n-alkanes are straight chain aliphatic compounds, found with cell membranes and responsible for controlling the passage of solutes and water in and out of the cell. Terrestrial plants contain significant quantities of C_{27}, C_{29} and C_{31} *n*-alkanes within epicuticular waxes (Eglington and Hamilton, 1967), leading to a dominance of long chain length n-alkanes within organic matter of terrestrial origin. Cuticular waxes of chain length, C_{21}, C_{23}, C_{25} are considered indicative of formation within submerged vascular plants (Ficken et al., 2000) and n-alkanes < C_{20} of algae and micro-organisms (Cranwell et al., 1987). The *n*-alkanes are relatively resistant to biodegradation and therefore can be highly specific in identifying the source of organic matter. However, the relative distribution of the *n*-alkanes can be affected by maturity (Peters et al., 2005)

m/z 123 – Diterpenoids

Diterpenoids are primarily derived from gymnosperm resin and are generally found in a plant defense role either through sealing wounds or discouraging animal attack (Killops and Killops, 1993). Trycyclic diterpanes can therefore be used as an indicator of gymnosperm input to the peatland relative to angiosperms. However, the generally poorer preservation/biodegradation resistance of angiosperm biomarkers relative to gymnosperm

markers may mean that this ratio may over represent the gymnosperm community.

m/z 191 – Triterpanoids

The hopanes are pentacyclic triterpanoids comprising six isoprene units found primarily within the cell membranes of oxic bacteria. Hopanes have also been found within the cell-membranes of the obligate anaerobe *Geobacter* (Härtner et al. 2005). Hopanes are highly sensitive to maturity through the conversion of the more immature βα C_{29}/C_{30} moretanes to the αβ (hopane) form. These ratios reach equilibrium within the early oil window in many source rocks (Peters and Moldowan, 2005).

m/z 205 – Methyl-hopanes

Methantrophic and acetic acid bacteria biosynthesize a range of 3ß-methyl-hopanes. The 3-methyl hopanes have primarily been linked to Type I methanotrophs (Farrimond et al., 2004). 2-methyl hopanes have been associated with cyanobacteria (Farrimond et al., 2004). Ratios between the methyl-hopanes and total hopanes have been shown to be of use in oil correlation studies and within mixed oils (Farrimond et al., 2004).

m/z 218 - Steranes

The steranes from part of the steroid group of compunds, derived from the cell membranes of eukaryotes, predominantly those of

higher plants and algae (Huang and Meinshein, 1979). Sterane compositions within higher land plants are typically dominated by C_{29} steranes whereas C_{27}/C_{28} steranes are thought characteristic of marine sediments. (Jiamo et al., 1990). The steranes can be found in a number of configurations whose relative abundance is largely controlled by thermal maturity (Moldowan et al., 1991). This makes them of interest in assessing the maturity of source rocks.

2.3.2.7 – ^{13}C NMR

High resolution solid state 50 MHz ^{13}C NMR analysis of the LYR and SVA coal samples were carried out in a BrukerAvance 200 spectrometer using the cross polarisation (CP) sequence in conjunction with magic angle spinning (MAS). For CP-MAS analysis, the acquisition time was 0.05 s, the relaxation delay was 1.5 s and the contact time was 1 ms. The samples were packed tight into a cylindrical (7 mm o.d.) zirconia rotor with a cap made of a homopolymer of chlorotrifluoroethene (Kel-F) and spun at the magic angle (54.7356°) with a spinning rate of approximately 5 kHz. Tetrakis (trimethylsilyl) silane (TKS) was added to the samples as an internal standard. The number of scans was 2500 and the free induction decays (FIDs) were processed using a line broadening factor of 50 Hz.

2.33 – Inorganic Geochemistry

All the samples collected were randomised using a random number generator and allocated a new sample number to avoid sampling bias and to reduce carry-over. Each sample was dried in an oven over night at 80°C before 1g of each sample was placed within a pressure vessel. Samples were digested using a nitric, hydrochloric, hydrofluoric and boric acid mixture using a CEM MARS5 sealed vessel microwave digestion system (after Laban and Atkins, 1999) followed by measurement of major and trace element determination by ICP-AES Perkin-Elmer Optima 3300DV emission spectrometer. Accuracy was checked using SARM-19 coal reference material. Any samples showing more than 10% deviation from each other were re-analysed until the required precision was achieved.

2.3.3.1 – Data Quality

Repeat Standard Deviation values and SARM-19 reference material data (measured and reported), can be seen in Table 2.1.

These show that reported SARM-19 standards were generally reproduced with the exception of Al which is consistently around 6000ppm lower than reported. This is thought to be a product of the high ash nature of the SARM-19 coal with the buffering capacity of the acids used exceeded during digestion. This leads to Al precipitating within the digestion vessel and consequently being under-represented within the measured samples.

	Standard SARM-19 (ppm)					Samples	Mean STDEV between
	Measured	SDEV	Actual	Min	Max	Mean	sample repeats (ppm)
Al	35235	3724.4	42600	41598	43133	2754	49
Ca	9229	786	9934	9791	10070	14083	418
Fe	12984	1614	12256	12116	12326	6039	381
K	2000	168	1992.4	1992.4	2075	384	8.6
Mg	1086	100	1206.1	1206	1326	2114	105
Mn	170	8	157	143	168	19	1.6
Na	1998	89	2151	2077	2299	1290	254
P	125	22	130	108	135	414	37
S	13950	811	14900	14200	15500	5707	285
Ti	1997	92	2040	1942	2134	399	18
Ba	265	8.35	304	295	318	202	4
Cr	49	3.5	50	47	58	16	0.19
Cu	11.84	1.36	13	11	14	6	0.205
Li	45	2.2	37	-	-	10	0.003
Ni	17	4.14	16	13	20	5	0.36
Rb	9.65	2.2	9	8	10	6	1.6
Sc	4.79	1.5	7.6	7	8.3	11	0.9
Sr	104	5.83	126	125	141	447	5.49
U	56	18	5	3	6	142	4.81
V	32	0.66	35	33	37	17	1.56
Zr	276	6	351	336	361	14	0.34

Table 2.1 – Standard and Reproducibility data for ICP-AES analysis

However, Al concentrations measured within the coal samples from the Central Tertiary Basin fit within the limits described by Orheim et al., (2007) showing that this effect does not appear to be present within low-ash coals. Consequently, Al data within the coals themselves are considered suitable for further examination, but future work would require a less ash rich standard than SARM-19.

Another difficulty was observed within the Ca content of the Lower Svea seam where values were significantly elevated. This is thought to represent residual contamination from a calcite rich fire-proofing paste used in the Svea Nord mine and therefore is considered unsuitable for further investigation.

2.3.3.2 – Carbon and Sulfur Coulometry/ Elemental Analysis

The hydrogen content of the coal sample was determined using a Thermo-Electron Flash EA 1112 Elemental Analysed. Briefly a furnace is heated to 900°C, the sample introduced alongside a small amount of oxygen to aid combustion. A helium carrier gas (140L/min) carries the combustion products through to a reducing stage before passing then into a Gas Chromotography Column for separation. These are then compared to a standard reference material (2.5 Bis [5-tert-butyl-benzoxazol-2-yl] thiophene). The samples were analysed alongside blanks and SARM-19 ref material to compare inter-analysis precision and contamination. Samples were also analysed in duplicate and any samples deviating by >5%

were reanalysed until values could be reproduced. The resulting data was recalculated on a dry ash free basis (d.a.f)

Total Organic Carbon was determined using carbon Coulometry to determine Total Inorganic Carbon (TIC) and Total Carbon (TC). Total carbon was determined using a furnace at temperature 950°C and oxygen atmosphere. The combustion gases were passed through a barium chromate catalyst/scrubber and other combustion products removed. The remaining CO_2 was passed through the coulometric cell and the reading taken.

Total Inorganic carbon was determined by acidification of the coal by hydrochloric acid, the acid was heated (70°C) and the inorganic carbon dioxide passed to the coulometric cell as for Total Carbon. TOC was calculated by difference (TOC=TC-TIC). Values were tested using calcite with recovery rates of between 97-101% considered normal. Samples were measured in duplicate with any samples showing deviation of >5% retested until the desired precision was achieved.

2.3.3.3 – Ash Measurement

Ash content was measured within a high temperature muffle furnace (800°C) overnight. Samples were pre-dried at 60°C in an oven before both the crucible and 1g of coal were weighed. Samples were analysed in duplicate to assess any cross contamination and test the precision of the technique. A coal reference material was

also added (SARM-19) and blanks to test both the inter-sample precision. The oven was allowed to heat up to 800°C and maintained for 6 hours before being turned off and allowed to cool overnight. The ash was measured with any samples showing 5% difference in values reprocessed until the desired level of precision was achieved.

2.4 – Misc Techniques

2.4.1 – Spectral Analysis and Fourier analysis

Singular spectral analysis (SSA) is used to extract information from short and noisy time series to understand the underlying dynamics (whether known or partially unknown) that generated the series (Yiou et al., 1996). This allows trend, oscillitary components and noise within the series to be ascertained (Allen and Smith, 1996). However to analyse the precise spectral component this technique needs to be combined with other techniques such as the multi-taper method (MTM).

The MTM allows signal reconstruction through Fourier analysis and spectral estimation. However this technique works best with series where the signal to noise ratio is high (Ghil et al., 2002). This SSA-MTM toolkit has previously been the basis for understanding the contributions of selected Milankovitch cycles within the peatland record (Large et al., 2004; Briggs, 2007).

Spectral analysis of the Longyear coal seam was carried out on the Al record as it showed the clearest cyclicity of the lithophile elements. Height above seam base was treated as time and a cubic spline fitted to the data and interpolated at 5cm intervals. The Al record was prefiltered by SSA to enhance signal separation and signal identification (Ghil et al., 2002) comprising the identification and extraction of the underlying trend within the series and signal/separation of the detrended dataset. Noise was identified and subtracted from the data by examining the slope-break from an eigenvalue spectrum.

The filtered spectrum was then subjected to SSA to identify any oscillatory components. This was achieved through Fast Fourier Transform Criteria. The resulting precise spectral component was then subjected to further MRM and plotted on a power spectrum diagram and confidence limits applied. Any values greater than 95% confidence were considered suitable for further examination and compared with the constraints derived from LORCA rates.

2.5 - Conclusions

This section gives the sample locations, sample preparation and methodologies used to produce the data and conclusions within later chapters. It also gives the measures used to ensure data quality. The analytical data collected in this study is therefore considered of suitable quality to be investigated further.

Chapter 3

STRUCTURAL AND PALAEOGEOGRAPHIC CONTROLS UPON COAL THICKNESS WITHIN THE TODALEN MEMBER

3.1 Introduction

The objective of this chapter is to investigate how the interplay of structural and palaeo-topographic features and consequently palaeo-hydrology controlled the distribution and thickness of the economic coal seams within the Todalen Member.

Previous sequence stratigraphic studies (Nøttvedt, 1982, Worsley et al., 1986, Nagy, 2005, Lüthje, 2008, Aspøy, 2011) identified the key depositional environments found during the earliest Palaeogene on Svalbard, however have produced only schematic palaeogeographic maps without both the temporal and spatial resolution to understand variations in coal quality and thickness. Structural controls upon coal formation have not been previously considered.

Adopting the hydrological landscape approach (Winter et al. 1992; 2001; 2002; previously applied solely to peatland) for use in coal seams, presents the opportunity to both verify previous depositional models and constrain at high resolution, the palaeo-topographic highs and lows which formed the initial basinal framework for coal formation during the Palaeocene. The distribution of the Grønfjorden fluvial conglomerates is used to delineate the palaoetopographic/structural controls within the basin. Coal isopach

maps are then overlain in order to examine how the influence of this underlying control evolved over the period of Todalen Member deposition

The Central Tertiary Basin coals also has significant economic potential, with two seams currently mined economically (Longyear and Svea) and the Longyear, Svarteper and Askeladden Seams significantly oil-prone. (Marshall et al. 2012). Consequently a detailed understanding of not only coal thickness and distribution but also coal quality is required to target the highest quality reserves in the future. Changes in coal quality are primarily caused by the degree of marine influence, particularly sulphur.

3.2 Geological Background

3.2.1 Regional Tectonic Development of Svalbard

To understand the depositional and structural setting of the Central Tertiary Basin coals we first need to consider how the Svalbard archipelago and underlying structural trends were formed. Svalbard, situated upon the north-western edge of the Barents Shelf has experienced a number of large scale tectonic episodes during its genesis (Fig. 3.1).

It began as a number of pieces of the Laurentian margin situated along the northern margin of Greenland adjacent to Ellesmere Island (Nøttvedt et al. 1988, McCann, 2000, Gee and Teben'kov,

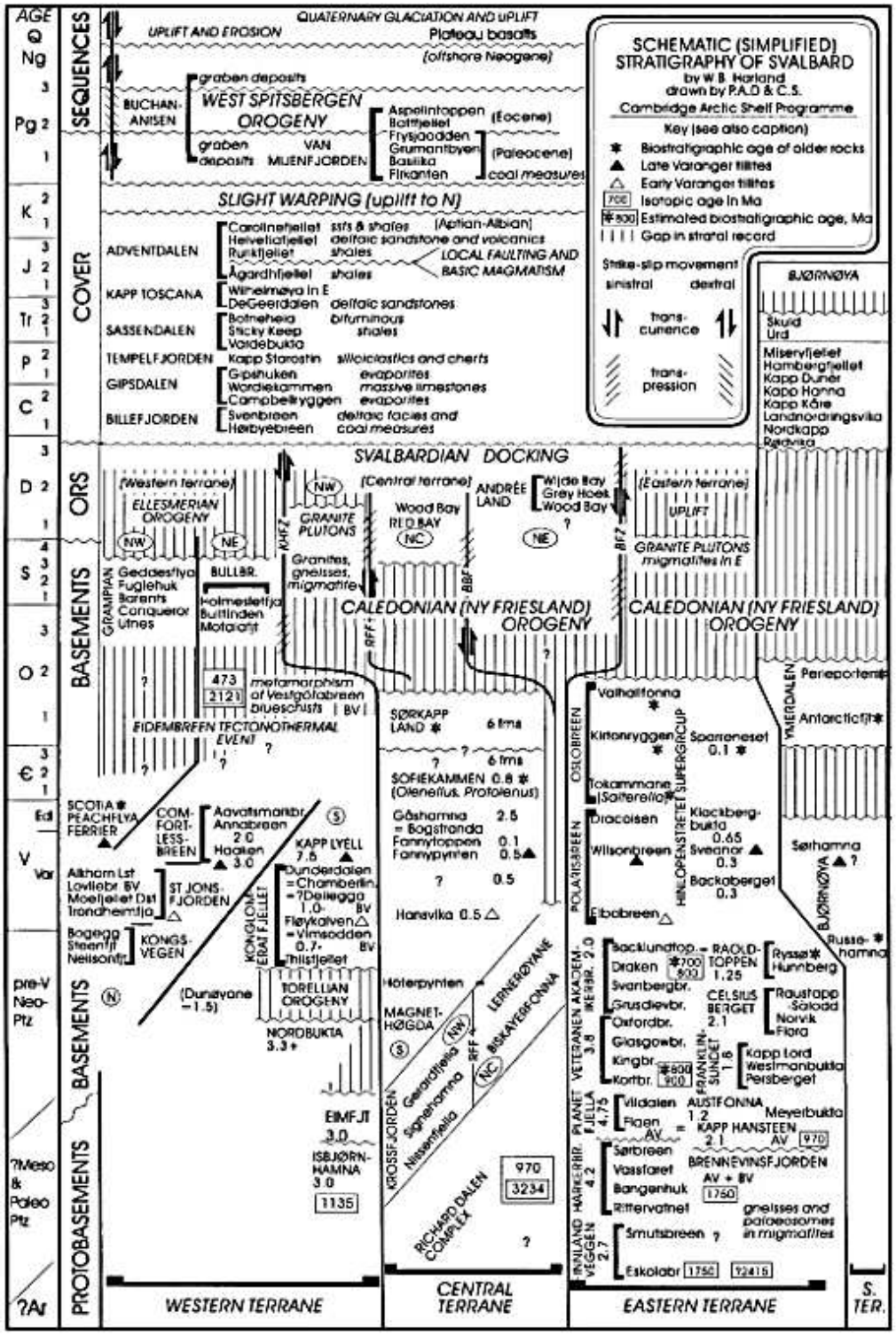

Fig. 3.1 – Tectono-stratigraphic development of Svalbard showing the key tectonic events in the formation of modern day Svalbard (*From Harland,* 1997)

2004). Models for the eventual docking of these fragments differ (Harland et al., 1997; Gee and Teben'kov, 2004; Breivik et al., 2005). However, most authors (Harland et al., 1997; Gee and Teben'kov, 2004) agree that it had completed by the mid to late Devonian.

By the mid Devonian, the main phase of Caledonian phase compression had ended on Svalbard with uplift followed by erosion (Harland et al. 1997). This erosion led to the concurrent formation of old red sandstone deposits within the Caledonides, including Spitsbergen (Harland et al., 1997, Friend et al., 2000) forming the basement of the Central Tertiary Basin. From the mid-Devonian to Mid Carboniferous, sinistral transverse fault movements lead to the northward movement of Svalbard, away from Greenland (Harland, 1997).

This was accompanied by minor compression within the Svalbard region, resulting in Svalbardian folding (Harland, 1997). This period of faulting and compression resulted in the stable positioning of Svalbard to the NE of Greenland until the mid-Cretaceous (Harland, 1997).

The Billefjordan fault zone forms the eastern boundary to the Central Tertiary Basin. It is a long-lived and often reactivated structure, which is thought to have played a significant role in the geological evolution of Svalbard. Interpreted by Breivik et al. 2005 as part of a Caledonian suture or thrust belt, formed during the

closure of the Iapetus, its roots are thought to extend back to the Pre-Cambrian (Breivik et al., 2005).

Evidence of the opening of the Atlantic to the south began prior to the Tertiary; however compression associated with the northward movement of Greenland leading to the West Spitsbergen orogeny which forms the western edge of the Central Tertiary Basin. Manby and Lyberis, (2000) indicate that this had commenced by the Late-Cretaceous (91Ma) and was well established by the mid-Palaeocene (59Ma).

Uplift from this event lead to a late Cretaceous hiatus lasting until the mid-Palaeocene (Blythe and Kleinspehn, 1998) leading to erosion and incision of the Aptian Carrolinefjellet shales to form an uplifted pene-plain. Deposition resumed during the mid-Palaoecene, initially by the fluvial Gronfjorden conglomerate (Otha et al., 1992; Dallmann, 1999) and followed by the coal bearing coastal plain sediments of the Firkanten Formation. This was followed by dextral movement along the de Geer line in the late Palaeocene/Early Eocene, leading to separation of Spitsbergen from Greenland (Harland, 1997).

The formation of North Atlantic mid-oceanic ridge system continued this process of separation, along the Hornsund fault zone until at least the early Oligocene (Smith, 2000). This was accompanied by the formation of the Vestbakken Volcanic Province to the South of Spitsbergen (Smith, 2000).

3.2.2 – Structural Framework of the Central Tertiary Basin

Central Spitsbergen has been present as a stable structural block since the late Devonian (McWhae, 1952, Harland, 1997, Gee and Teben'kov, 2004); however the structural trends defining this block may have much older origins (e.g. Billefjorden Fault Zone, Hornsund Fault Zone; Breivik et al. 2011; Skilbrei, 1991; Livšic, 1974).

During the Palaeocene, the Central Tertiary Basin was bound to the east by the Billefjorden fault zone, however the relative timing and role of the West Spitsbergen Orogen is disputed. Older basinal models (Steel et al., 1981; Steel et al., 1985) indicate that basin formation occurred prior to the onset of fold and thrust belt initiation in the Eocene. Steel et al. (1985) infers a transtensional (pull-apart basin) regime during the Paleocene period of coal formation, followed by a Late Palaoecene-Early Eocene transtensional regime associated with nearby deformation.

However, Bruhn and Steel (2003) and Lüthje (2008), state that the Central Tertiary Basin was formed in the Palaeocene as a flexural depression associated with the West Spitsbergen fold and thrust belt. Bruhn and Steel (2003) cites the presence of compressional structural features within both Palaeocene and Eocene strata alongside a lack of extensional features to support this.

The model also indicates that the accompanying foreland bulge (Bruhn and Steel, 2003) may have been sufficiently uplifted to

provide a sediment source during the earliest Palaeocene deposition. However, the importance of the foreland bulge as a sediment source is disputed by Lüthje, (2008), citing insufficient evidence of significant uplift to the East and favouring a more northerly sediment provenance.

The Central Tertiary basin is asymmetrical, dipping more steeply on the western flank compared to the eastern flank (Harland et al., 1997). The basin plunges to the SSE (Sokolov et al., 1968, Livšic, 1974, Nøttvedt et al., 1988) leading to progressively thicker Palaeogene deposits to the south. Nøttvedt (1985), building on work by Steel et al. (1981), infers that the basin is sub-divided by a number of E-W trending normal faults, most notably to the south of Van Mijenfjorden and an as yet unidentified northern fault block.

This apparently uplifted block is observed within an N-S section by Nøttvedt (1985) through the uplift of the KT unconformity and a distinct thinning of the coal bearing Todalen Member (Fig. 3.2). It is intriguing that a number of modern drainage and fjord systems have the same E-W alignment and the persistence of this trend may indicate a probable structural control active from the Tertiary to the present day.

Lüthje (2008) in another N-S section across the basin from Adventdalen to the south of Van Mijenfjorden (Fig. 3.2), however does not report this feature. This may be through the use of

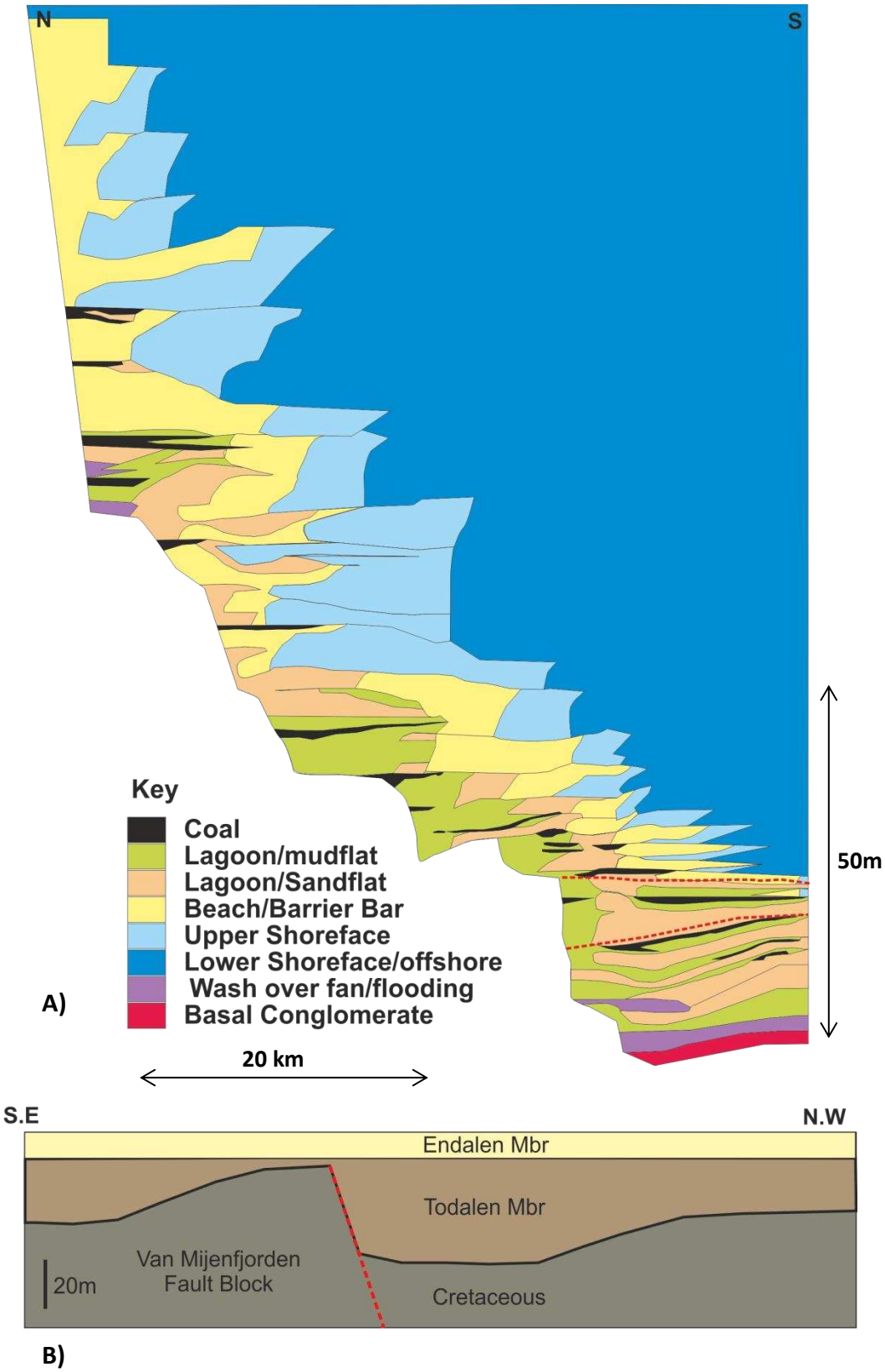

Fig. 3.2 – N-S section of the NE Central Tertiary Basin (A) *After Luthje, 2008), (B) After Nottvedt, 1985.* Note that one section appears to show the Van Mijenfjorden Fault block clearly and in the other it is not present. Location of sections seen in Fig. 3.3

different scales and datum used by each investigation or that the Lüthje (2008) section terminated to the north of the inferred fault zone. Additional evidence for uplift at the time of coal formation within the proposed van Mijenfjordan fault zone is a coal gap to the south of Ispallen, and a thinning of the Todalen Member, consistent with a structural high (Nøttvedt, 1985).

Structural studies in the basin have mainly investigated The intense deformation of the West Spitsbergen Orogen and large-scale fault zones such as the Billefjordan fault zone have been been the subject of numerous publications (Manby and Lyberis, 2000, Breivik et al. 2011, Skilbrei, 1991, Livšic, 1974).

Published information regarding smaller scale structural deformation features within the Central Tertiary Basin is more limited. This is due in part to the difficulty in accessing suitable outcrop due to scree and glaciation within Tertiary formations and the burial depth of much earlier structures. Consequently knowledge of the internal basin structure is limited to what can be determined from coastal sections (Sokolov et al., 1968, Livšic, 1974, Eiken, 1985, Nøttvedt et al., 1988 and Harland, 1997), and mine plans. This shows the basin to be composed of a number of trending NNW-SSE swells and troughs (Fig. 3.3).

These swells and troughs define a number of sub basins within the basin (Sokolov et al., 1968; Nøttvedt et al., 1998; Harland et al.,

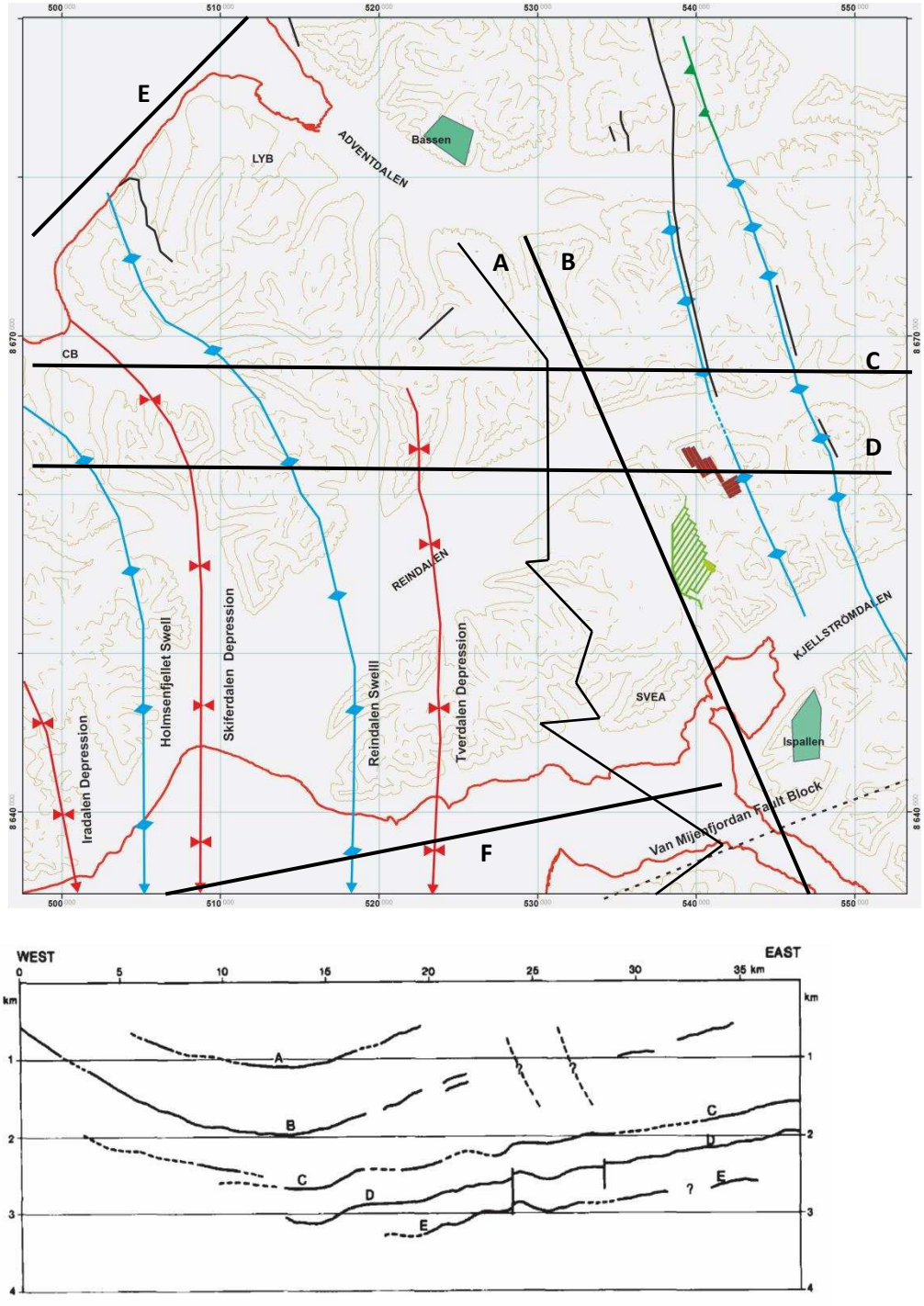

Fig. 3.3 – (Top) Structural features within the Northern Central Tertiary Basin showing a number of swells and troughs (After Sokholov et al., 1968) and a geophysical W-E section across Van Mijenfjorden showing undulations in Triassic sediments (Eiken, 1985) indicating more swells and troughs to the east of those indicated (D/E =Permo-Triassic Sediments) Black lines indicate section lines from adjacent figures (A= Lüthje, 2008 B = Nøttvedt, 1985 C= Nøttvedt et al., (1988) D = Sokholov et al., (1968), E = Livšic, 1974, F = Eiken, 1994)

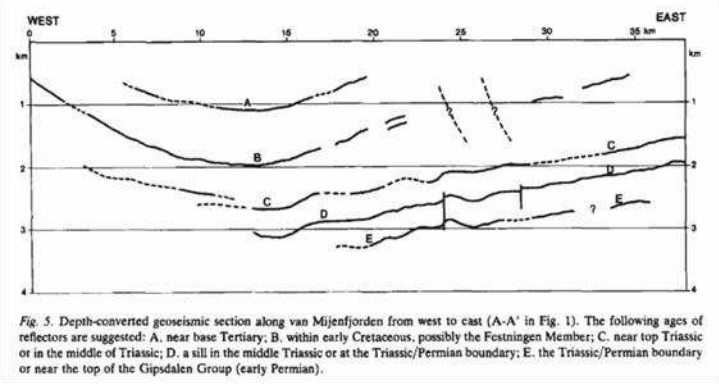

Fig. 5. Depth-converted geoseismic section along van Mijenfjorden from west to east (A-A' in Fig. 1). The following ages of reflectors are suggested: A. near base Tertiary; B. within early Cretaceous, possibly the Festningen Member; C. near top Triassic or in the middle of Triassic; D. a sill in the middle Triassic or at the Triassic/Permian boundary; E. the Triassic/Permian boundary or near the top of the Gipsdalen Group (early Permian).

Eiken, 1985

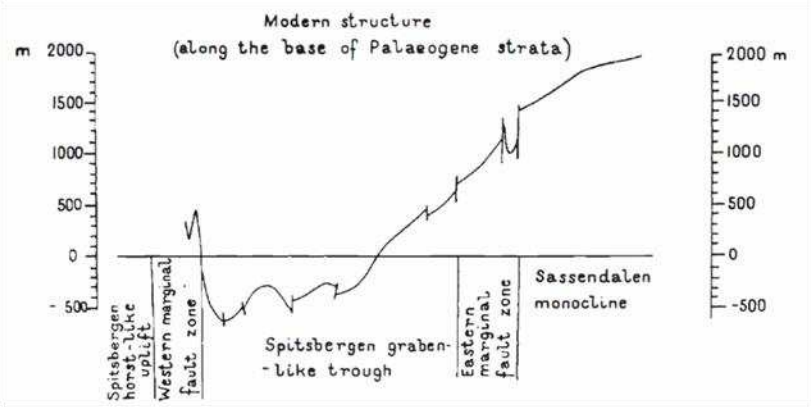

Livšic, 1974

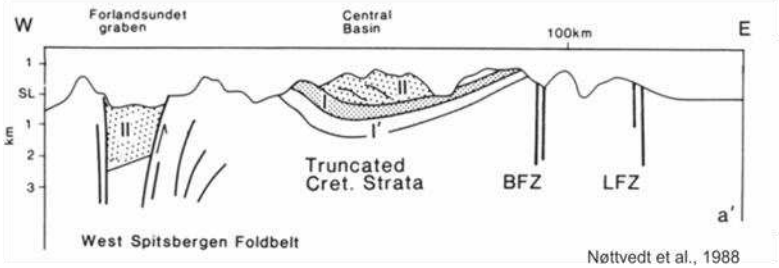

Nøttvedt et al., 1988

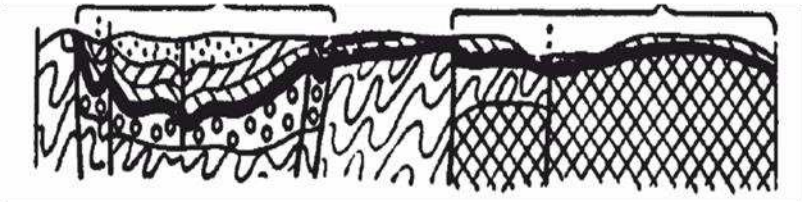

Sokolov et al. 1968

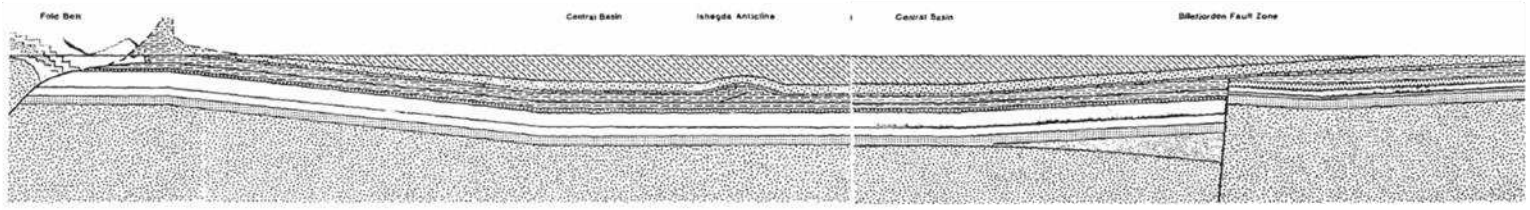

Sokolov et al. 1968

Fig. 3.4 – East-West Cross Sections from (Top Left to Bottom) Eiken, 1985, Livsic, 1974, Nottvedt et al., 1988 and Sokolov et al., 1968 showing the various levels of detail within sections from this region. Section line seen in Fig. 3.3

1997). However, the structure of these differs from study to study. Livšic, (1974) for example indicates that the swells and troughs are fault bounded forming a number of small scale graben structures. Whereas Sokolov et al., (1968), Nøttvedt et al., (1988) and Harland, (1997) interpret these as folding structures.

Evidence of older structural controls upon the positioning of these features is difficult to assign due to limited published data. The E-W section (Fig. 3.4), by Livšic, (1974), shows that the long-lived Billefjordan fault zone was a persistent structural and topographic high throughout the Palaeocene. This provides a raised hinterland for clastic sediment supply to the basin and bounds the area of coal deposition on the eastern basin margin. Livšic, (1974) also indicates a number of graben like features within the Triassic fill of the basin. These features seem to be along a similar trend to the previously discussed depressions and swells, possibly indicating these were are inter-related long lived structural lineaments/trends

Evidence of the longevity of structural control in the basin is on a seismic section across Van Mijenfjorden (Eiken, 1985) where normal faulting of basal Permo-triassic sediments is reproduced as minor folding in later sediments (Fig. 3.3). It is proposed that possible reactivation and subtle representation of these older faults within the Cretaceous peneplain landscape that may exert a significant control upon coal extent and thickness within the Tertiary.

3.2.3 – Tertiary infill of the Central Tertiary Basin

The Van Mijenfjordan Group comprises the remaining Tertiary infill of the Central Tertiary Basin resting unconformably upon the Lower Cretaceous Carolinefjellet formation. The group is made up of a number of formations, namely the Palaeocene Firkanten, Basilika, Grumantbyen, Frysjaodden, Hollandardalen formations and the Eocene Battfjellet and Aspelintoppen formations each representing major transgressive/regressive cycles. The PETM boundary has recently been located at the upper Hollandardalen/Frysjaodden boundary (Dypvik et al. 2011). The lateral and vertical relationships can be seen in Fig. 3.5.

This study is focussed upon the Firkanten Formation which is divided into three Members; the Todalen, Endalen and Kolthofberget of which the Todalen Member contains the majority of economic coal seams upon Svalbard. These represent coastal plain, shoreface and offshore environments respectively during the earliest period of Tertiary sedimentation (Dallmann, 1999).

The coal bearing Todalen Member is preceded in some areas by the Grønfjordan bed, a fluvial conglomerate infilling depressions within the Cretaceous peneplain (Dallmann, 1999). The Todalen Member contains five main seams, named the Svea Todalen, Longyear, Svarteper and Askeladden (Harland et al. 1997, Orheim et al. 2007).

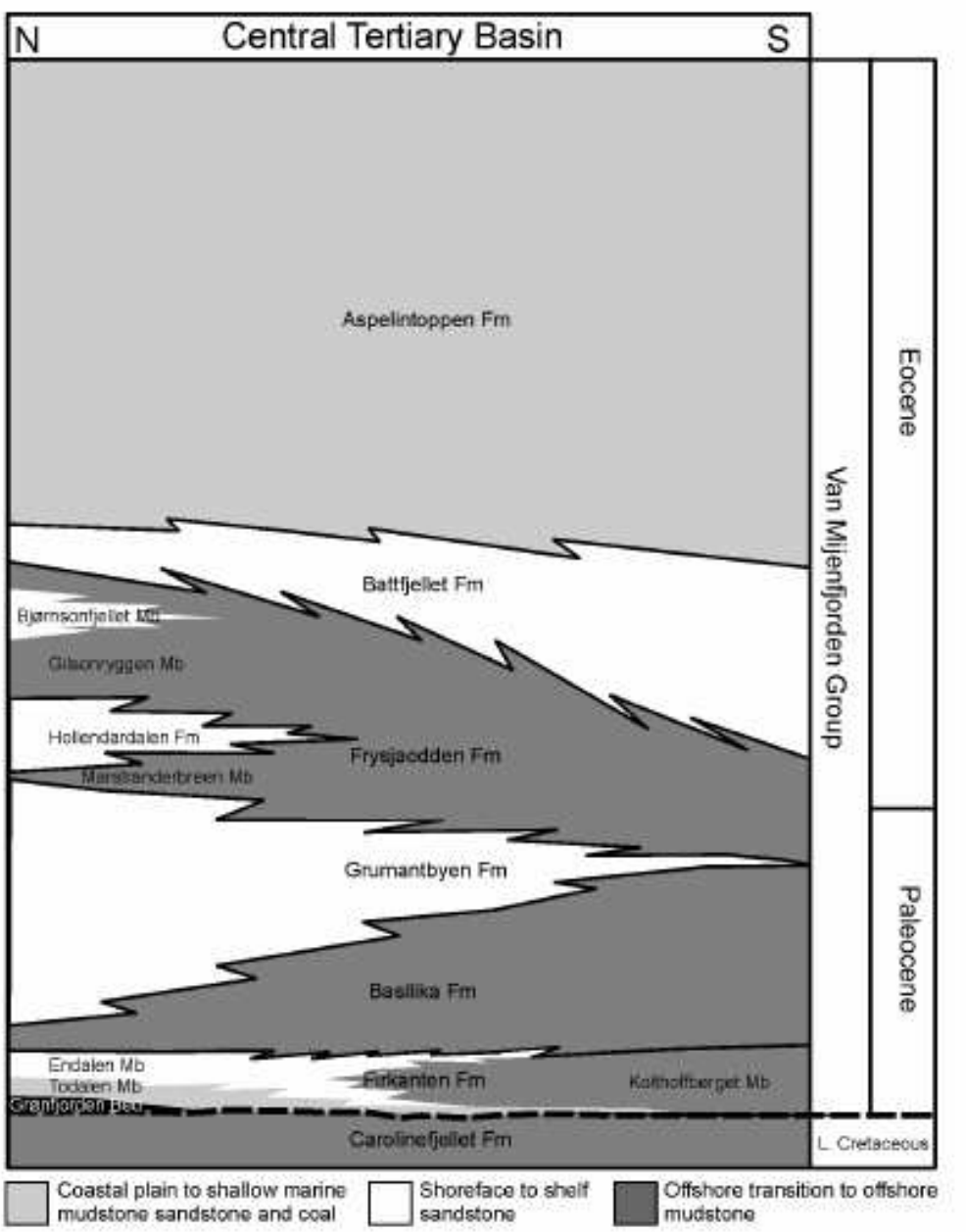

Fig. 3.5 – The Palaeogene Succession of the Central Tertiary Basin, Spitsbergen (From Luthje, 2008, adapted from Steel et al., 1985)

3.2.4 – Previous Palaeogeographic Reconstructions

Before formulating a new palaeogeographic interpretation of the Todalen Member, it is necessary to consider existing interpretations. There have been a number of attempts to reconstruct the palaeo-geography and environment of the coal-bearing Todalen Member from a sequence stratigraphic viewpoint (Steel and Dalland, 1978; Steel, 1981; Steel and Worsley, 1984; Nøttvedt, 1985; Worsley, 1986, Jochmann, 2004; Nagy, 2005; Lüthje, 2008). The reconstructions can be divided into two main groups (Fig. 3.6), promoting either a deltaic (Steel, 1981; Steel and Worsley; 1984, Worsley, 1986) or tidal/estuarine/coastal plain (Steel and Dalland, 1978; Jochmann, 2004; Lüthje, 2008; Aspøy, 2011) origin of the Todalen Member

Deltaic interpretations of the Todalen Member show a fluvial tidal and wave dominated delta system building from the E-NE (Steel, 1981, Steel and Worsley, 1984). Mud and siltstones were thought to represent inter-distributary bay and coastal plain deposits with lack of marine indicators cited as evidence (Steel, 1981, Steel and Worsley, 1984).

Coastal Plain interpretations show a linear coastal plain punctuated by tidal channels and estuaries with occasional coastal lake sediments (Lüthje, 2008). Inland tidal flats give way forming the peatlands which form the basis of the Longyear, Svarteper and Askeladden Seams (Lüthje, 2008).

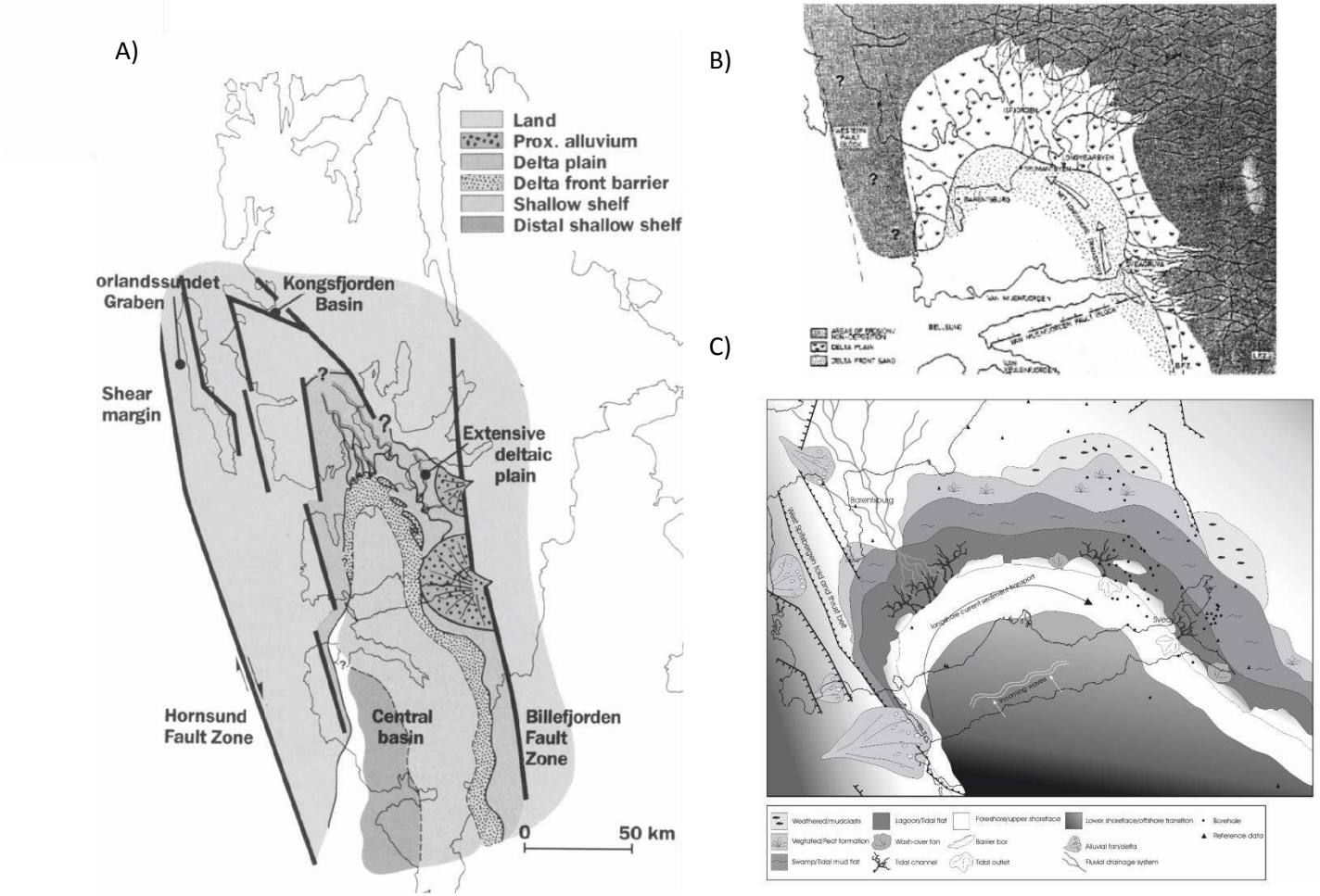

Fig. 3.6 Palaeo-environmental Reconstruction of the Todalen Member from (A) Worsley et al., (1986), (B) Nøttvedt, 1982, (C) Lüthje, 2008 showing interpretations from tidal flat to deltaic conditions

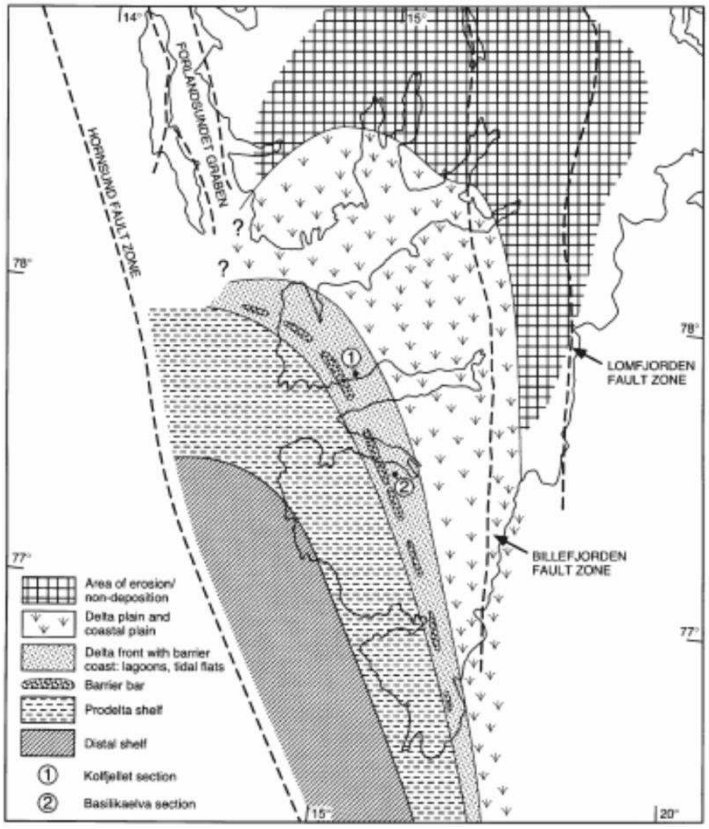

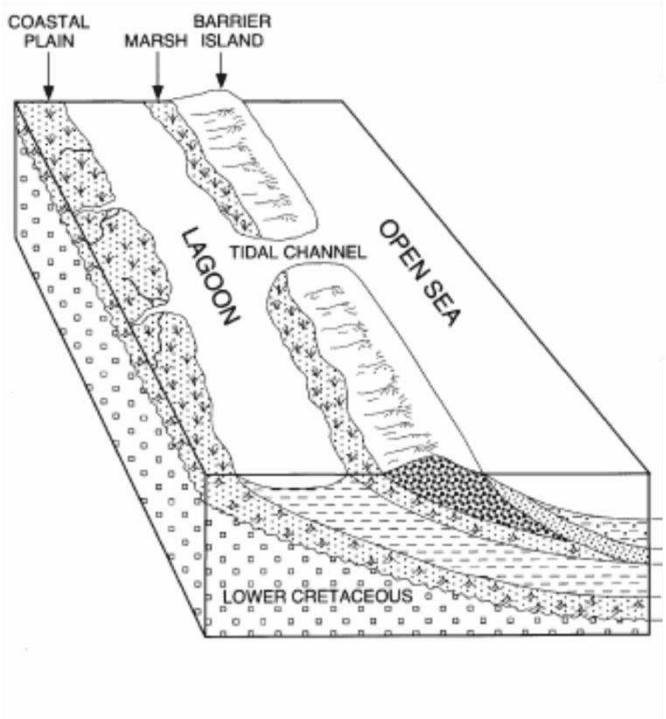

Fig. 3.7 – Palaeo-environmental reconstruction of Nagy, (2005) from W. Central Tertiary Basin, possibly showing the earliest phase of coal deposition

The reconstruction of Nagy (2005) appears to represent the earliest stage of coal development as the coal forming coastal plain extends much further westwards than other studies. These areas are characterised by much thinner Todalen Member and are followed rapidly by offshore marine sediments (Fig. 3.7).

The relationship between the coal seams of the Western and Eastern sides of the basin is not well known. Many of the reconstructions indicate that the Barentsburg and Colesdalen coal fields are a northern continuation of the more extensive eastern coalfield (Steel and Dalland, 1978; Steel, 1981; Steel and Worsley, 1984; Nøttvedt, 1985; Worsley, 1986; Nagy, 2005; Lüthje, 2008). However, there are only three coal seams present to the West, with a different naming system and characteristics (the Nidzny, Verkny and Sputnik). Eastern seams to the south of Grønfjorden and Barentsburg are inferred to be associated with fan deposits from the newly forming West Spitsbergen Fold and Thrust Belt (Worsley, 1986).

Nagy, (2005) presents an alternative reconstruction, suggesting that these coal seams represent a west facing barrier coastal plain deposit. This representation may indicate that these deposits represent the earliest coal forming environments within Tertiary Svalbard, with conglomerates being fed to the coastline by the Grønfjorden valley system.

Previous sequence stratigraphic studies and depositional models (Steel and Dalland, 1978, Steel, 1981, Steel and Worsley, 1984 Nøttvedt, 1985, Worsley, 1986, Nagy et al. 2005, Lüthje, 2008), do not explain the considerable small scale variations in coal thickness, distribution and quality. This is partially due to the fact that the models produced have interpreted coal seams within a clastic sedimentological context, with the coals interpreted as maximum flooding surface.

The difficulty of this approach is that by ignoring the coal, an opportunity to understand the interaction between persistent topographic/structural features and peatland hydrology, making prediction of where the thickest deposits of peat (and therefore coal) were located very difficult.

3.3 – Sequence Stratigraphy and Hydrological Landscapes

The accumulation and preservation of peat requires conditions suitable for the preservation of organic matter namely clastic sediment starvation alongside a relatively impermeable substrate and water supply sufficient to maintain and expand the peatland (Yu et al. 2001).

3.3.1 – The Sequence Stratigraphic Approach to Peatland

The sequence stratigraphic approach to coal seam distribution is based around the balance of accommodation rate rise and peat accumulation (Bohacs and Suter, 1997). Accomodation rate is

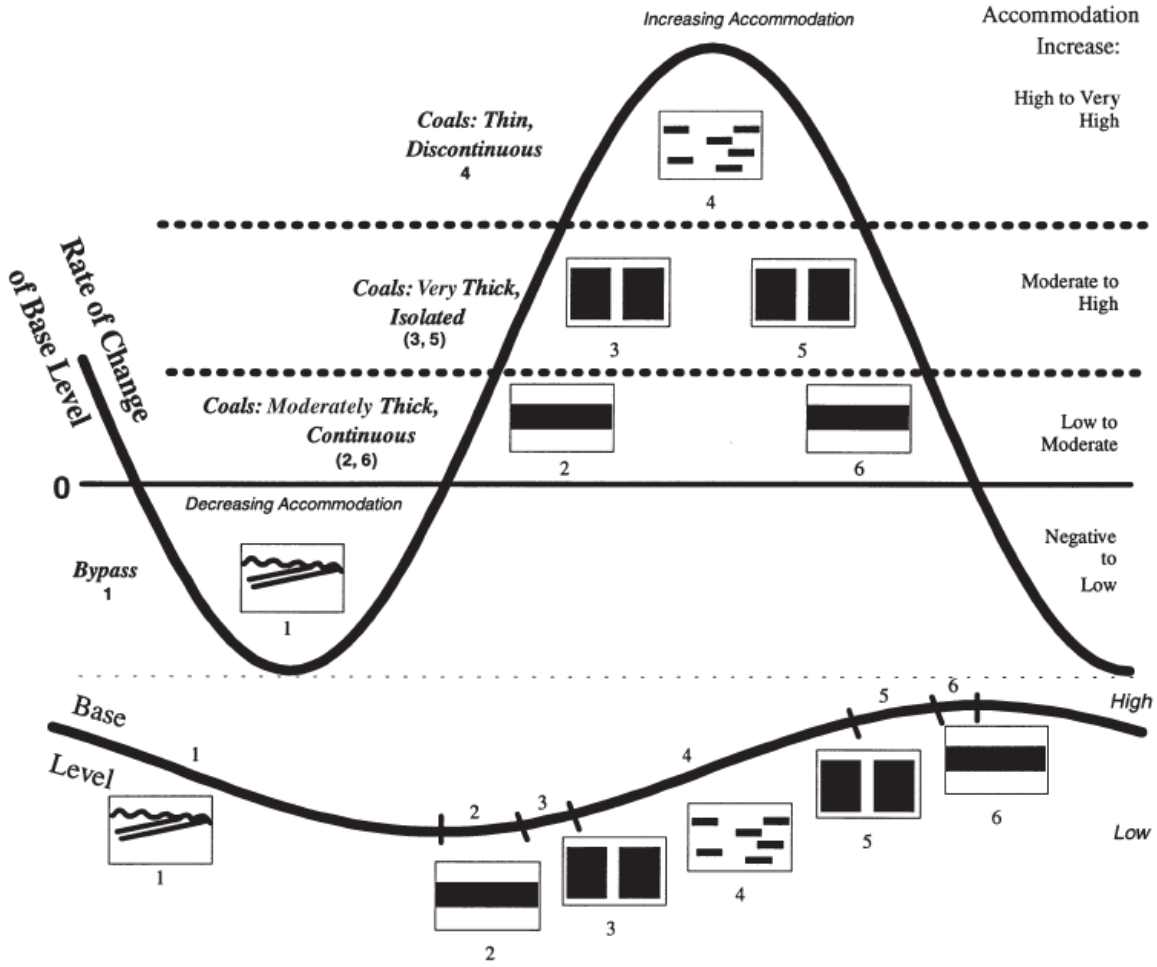

Fig. 3.8 – The coal geometry and thickness predictive model of Bohacs and Suter, (1997). 1= Late high-stand- Early Lowstand. Falling base lavels promotes progradation and subaerial erosion 2= Middle Lowstand Conditions (Rising Sea Levels and groundwater tables lead to medium thickness continuous coals. 3 = Late Lowstand-Early Transgressive coals. Thick isolated coals due to rising water table. 4 = Transgressive. High accommodation increases cause shoreline to move landward leading to restricted mire conditions due to increasing clastic sedimentation and rapidly increasing water table. 5 = Early Highstand – Reduction in rate of sealevel and groundwater rise allows establishment of thick isolated peatlands. 6 = Stable Groundwater results in thinner, more continuous seams.

defined as the rate of subsidence + base level change (Bohacs and Suter, 1997) with base level in the case of peatlands defined specifically as the level of the water table (Diessel, 1992).

In many cases, basinal subsidence is relatively constant over the lifetime of a peatland and therefore changes in base level are considered more important in paralic settings (Bohacs and Suter, 1997). Where there is a balance between accommodation creation and peat accumulation, Bohacs and Suter (1997) predict the thickest seams (Fig.3.8). Medium-thick continuous seams are favoured by a slightly higher peat accumulation rates and thick discontinuous seams reflect higher accommodation rate creation. Where peat accumulation or accommodation creation dominates, peat formation is considered unlikely.

This approach has been shown to be useful for predicting when coal will occur and the type of coal seams to expect within paralic settings (Bohacs and Suter, 1997). However, this approach works best within relatively idealised conditions such as a flat coastal plain, where accommodation rate is controlled primarily by sea level and where topography is dismissed as unimportant (Bohacs and Suter, 1997).

Coastal plain systems are generally more complex than this with the thickest coal deposits apparently distributed erratically. This implies additional controls upon the location of peatlands other than

sea level as if this was the case coal thickness would be homogenous parallel to the coast. Bohacs and Suter (1997) acknowledge that this complexity means that local conditions need to be considered alongside sequence stratigraphic interpretations. Therefore in order to identify additional local controls and the location of the thickest deposits another approach is required

3.3.2 – The hydrological landscape approach

The hydrologic landscape approach Winter (1992; 2000; 2001) is based on the concept that peat and peatlands are made up primarily of water and consequently will develop only in areas where water is close to or immediately below the surface (Winter, 2000). This hydrological control is itself a function of climatic, topographic and underlying lithological and structural basinal controls (Winter, 2001 etc).

Therefore a hydrological landscape may be defined by the interaction of atmospheric, surface and groundwater within a set of simplified geomorphological units which incorporate the region of interest (Winter, 1992, 2000, 2001). This approach means that although hydrology-wetland interactions can be complex at local scales, when viewed as a part of the complete hydrological system, their response to changing forcing factors can be identified and predicted.

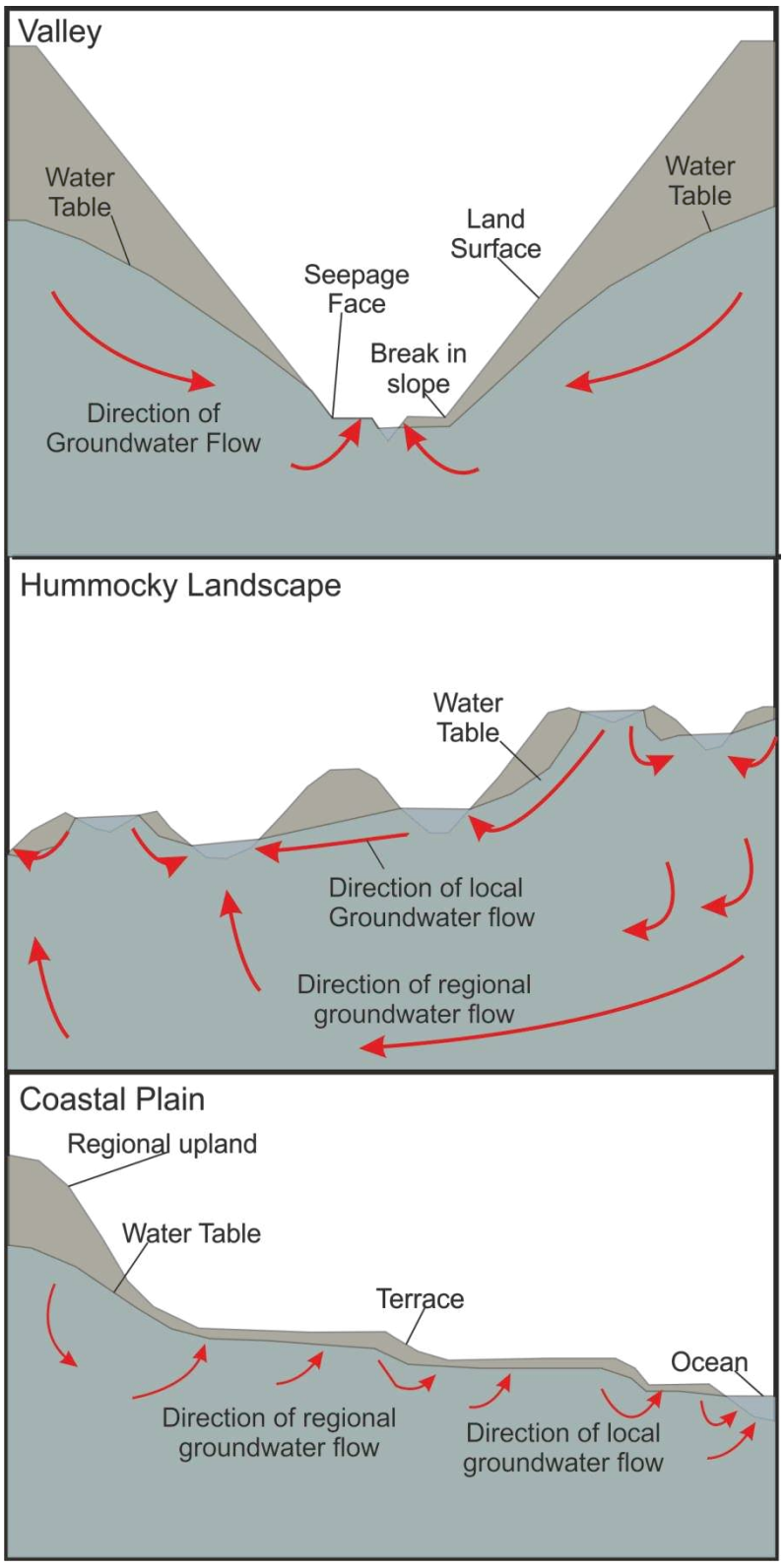

Fig. 3.9 – Fundamental Landscape Units showing areas of groundwater discharge within a valley, hummocky landscape and coastal plain setting (After Winter, 2000)

The hydrological landscape can be broken down into a number of fundamental landscape units (Fig. 3.9; Winter 1992; 2000; 2001). These can be found at a range of scales with a number of small scale landscape features grouping together to form a larger scale landscape unit. This approach therefore allows landscape to be observed at any scale allowing high resolution prediction of thick peat deposits. It also allows the cumulative effects of small landscape features on local hydrology to be incorporated within larger scale models without the assumptions used in sequence stratigraphic models.

Most peatlands require some form of groundwater input as without saturated substrates wetlands can't persist (Raid and Wood, 1976). Consequently peatland is most likely to initiate in areas of groundwater discharge, often located at the break in slope between topographic highs and lows (Winter, 2000; 2001). These will often be structurally controlled or reflect persistent underlying topographic features which can be predicted.

The hydrological stability at these locations makes them ideal for sustained peat formation and as refuges during base level rises leading to the sporadic distribution of coals within these conditions (Bohacs and Suter, 1997). During relative sea level falls new breaks in slope may be revealed shifting the focus of peat formation

seaward; however these areas of hydrological stability should remain positions of preferential peat formation.

The concept of water balance is also important within the hydrological landscapes model, with peat acting as a form of hydrological storage. Once established, rather than being passive within the landscape, peatland can alter local hydrology, slowing flow rates, shifting the water balance towards a high input low output regime allowing the peatland to be sustained and to expand into flatter areas.

During low input periods depending on the structural integrity of the peatland the peatland may remain raised and become desiccated, eventually fostering palaeosol development or if structurally weak (fen) rise and fall with the water table.

During rapid base level increases, lower gradient areas are expected to be more vulnerable. In addition to the risk of inundation, the rapid rise in hydrological input would be accompanied by a reduction in hydrological output, triggering flooding of the peat surface and the onset of clastic sedimentation.

At the break in slope, steeper gradients would maintain hydrological output and therefore hydrological balance. In addition topography generated from preferential peat formation at the break in slope makes peats at these locations less vulnerable to changes in base level. This would lead to peat formation to be sustained long after

the rest of the peatland had terminated and reinforcing the link between the break in slope and thick peat deposits.

3.3.3 – Applying the hydrological landscape approach to coal

The use of this technique with regard to coal deposits has not been previously considered, however by understanding basin dynamics and the hydrologic response to changing forcing factors in the landscape it should be possible to predict the pattern, occurrence and growth of thick peat deposits within the geological record.

Landscape evolution is an expression of the dynamics of sedimentary basins and is driven by the combined forcing effects of tectonism, accommodation availability, erosion, transport and deposition. Therefore, consideration of coal seams from a hydrological landscape perspective may indicate whether specific tectonic regimes can result in widespread peatland formation, subsequent carbon burial and long term crustal carbon storage. Conversely using the hydrologic landscape concept the distribution of coal seams may be used to understand regional palaeo-hydrology.

Due to the large variations in peat compaction (Nadon, 1998) it is difficult to estimate the thickness of peats from coal thickness. As a consequence, coal thickness is thought to represent the period of deposition, with more hydrologically stable areas thicker and vice versa. Consequently the thickest peats within the peatland would

be expected to be adjacent to topographic highs with splitting originating upslope and from depressions.

An ideal setting in which to test these ideas is the coal-bearing Palaeocene Todalen Member of the Central Tertiary Basin (CTB), Spitsbergen. Section 3.2.2 shows that a number of minor structural lineaments trending N-S have been identified (Fig.3.3; Sokolov et al., 1968; Nøttvedt, 1985; Harland et al., 1997) occurring parallel to the basin axis. However there is a conspicuous gap in the line of domes and depressions encompassing the eastern coalfield. Local topography has been widely cited as controlling early coal formation within the Todalen Member (Jochmann, 2004; Luthje, 2008), however whether this was structurally controlled is currently unknown.

The basal Palaeocene is characterised by a sporadic fluvial conglomerate known as the Grønfjorden bed which provides a good valley/depression indicator, allowing the initial landscape of the Todalen Member to be characterised and any structural control identified. This then allows any variations in coal thickness, split origins, high conglomerate density areas to be related to initial landscape conditions.

The Todalen Member represents the gradual retreat of a coastal plain with increasing marine influence upwards therefore this will also show how the relative importance of structural and eustatic

controls changed the distribution, thickness and character of the Svalbard coals over geological time.

3.4 – Sampling Methodology

The logs of 96 boreholes sampled and logged between 2002 and 2012 by Store Norske Spitsbergen Kulkompanie AS (SNSK) were analysed. As a potential palaeo-topographic indicator the thickness of the Grønfjorden bed was measured from the logs. Absence of Grønfjorden bed was classified as topographic highs and the thickest Grønfjorden bed as valley bottom sediments. This was thought suitable as fluvial channels are often preferentially located within existing topographic and structural depressions within the landscape. The thickness and distribution of a commonly found bentonite layer was also logged to examine the effect of topography upon its distribution and to examine its use as a possible marker bed.

The thickness of coal (without splits) was also recorded for the Svea, Longyear, Svarteper and Askeladden seams. In addition the composition of the sediments immediately above and below the Longyear seam were recorded and assigned a number based on particle size to aid mapping. The classification is as follows 1=mudstone, 2=siltstone, 3=Fine Sand, 4=Medium Sand, 5=Coarse Sand, 6=Conglomerate. This was then used to reconstruct the

environment immediately prior and following the deposition of the Longyear seam (Chapter 6).

The datasets were then plotted using the Surfer 7 © software using the kriging method. This method was chosen as it is unbiased; the estimation achieved honours the observed values and is considered by Cressie (1993) to be a good interpolation method when used in spatially dependent data.

However as with any interpolation method, kriging is dependent on the quality of the data, and distance from data points, meaning areas with low sampling density are likely to be less accurate than those with higher sampling densities. There also may be better non-linear techniques available in other programs. However, examination of the other methods within the Surfer 7 © program produced visually poorer interpolation compared to the kriging method and consequently this method was selected

The Grønfjorden thickness map was overlain over a contour map encompassing the areas of Svea, Longyearbyen and Colesdalen any linear features within the topographic highs and lows identified marked and compared to those from the central basin (Fig.3.3).

The coal thickness maps (Appendix I) were then overlain over the inferred palaeo-topographic maps in order to examine the effect of landscape on each seams distribution. As boreholes are located preferentially within high coal thickness areas, low thickness areas

are covered by much lower borehole densities. As a consequence interpolation within these areas is of poorer quality. Consequently, coals with less than 40cm thickness were removed from the palaeogeographic maps. This then restricts the interpolation to areas of good borehole coverage.

This is thought appropriate as although there is thin coal in these regions, as evidenced from the SNSK sedimentological logs, it is thought these coals are of little temporal significance (<21kyr; Chapter 6) within the context of the thick seam areas and are characterised only by their hydrological instability. The ability to study whether this instability was influenced by landscape or sea level is not lost and therefore seams of less than 40cm were removed from the map.

To examine the effect of sea level upon the Longyear seam, 10cm coal thickness was progressively removed from the coal isopach map. This assumes that areas of high thickness represent greater stability and vice versa. An areas vulnerability and resilience to sea level rise was then compared to the topographic map produced from the Grønfjorden Bed.

In order to investigate the effects of local landscape upon Longyear coal thickness at higher resolutions, boreholes were restricted to those close to Lunckefjellet. This is a good area to test this technique as due to the development of a new mine in the area, an

extensive drilling program has produced high borehole density within this region.

In addition two whole Todalen Member sections from Lunckefjellet were created to examine how the landscape controls upon coal formation changed over the lifetime of the Todalen Member and whether any persistent topographic lows provided a focus for channel formation in later strata. The Todalen-Endalen boundary (defined as the first massive sandstone after the Svarteper/Askeladden seam, Dallman, 1999) was used as the datum, allowing the underlying topography to be shown and because at least locally the transition is thought to have occurred relatively synchronously as seen by the similar lithologies and proximity to the upper coals seams in Fig. 3.22;3.23.

The sections produced were correlated on a lithological basis guided primarily by grain size indicators. As the purpose of these sections is primarily to examine the position of the thickest coals, the direction of splitting and channel deposits, a more detailed facies based profile is thought to be not required. In addition as the main palaeo-environmental facies within the Todalen are generally linked to grain size (Lüthje, 2008), a simplified palaeo-environmental interpretation can be made using the following descriptions;

- Coastal Plain Sediments – Mud-Silt deposits with high organic content, minor tidal influence upon floodplain, and

colonisation by rootlets, usually adjacent to/underlying peatlands. Thin coals seams

- Tidal flats and lagoons – heterolithic silts to fine sandstones tidal influenced sediments, small scale channel formation – thin conglomerates, occasional herringbone cross stratification and mud drapes.
- Foreshore and Shoreface – highly bioturbated well sorted sandstones containing most notably *Ophiamorpha nodosa*, *Thalssinoides* and *Terebellina* trace fossils.

3.5 Defining the Cretaceous-Tertiary Peneplain

It is important to define the palaeo-topography of the Cretaceous pene-plain as it forms the initial topographic starting point for subsequent peatland formation.

3.5.1 – The Grønfjorden bed

Variations in the palaeo-topography of the Cretaceous pene-plain landscape have been inferred to exert significant controls upon the early coal forming environments within the Todalen Member, particularly during the formation of the Svea seam (Jochmann, 2004, Lüthje, 2008). However, the palaeo-geographic context of this inferred landscape of palaeo-topographic highs and lows has previously been limited in geographical area and lacking a palaeo-topographic indicator bed.

The Grønfjorden bed, a conglomerate found sporadically within the eastern basin and further developed in the western basin may represent such a marker bed. Described by Nagy (2005), Otha et al., (1992), Dallmann (1999) and Luthje (2008, in the west) as fluvial in origin, it represents the first deposition of Palaeocene sediments within the basin. Composed of imbricated rounded pebbles, with a diameter up to 8cm using the Hjulstrøm curve indicates flow rates in excess of $0.8ms^{-1}$ rising to a least $1.2ms^{-1}$ in the hinterland (to erode such material). The fits well with previous comparisons of the Grønfjorden bed to braided river systems (Otha et al. 1992, Nagy. 2005).

The presence of clay lenses, high organic content and root colonisation of the upper bed (Nagy, 2005) supports this. It is therefore postulated that the Grønfjorden bed represents a clear depression indicator, with the thickest conglomerates found in palaeotopographic lows (possibly valleys) and no conglomerates over topographic highs. To test this hypothesis, the total thickness or absence of the Gronfjorden bed was measured and plotted (Fig. 3.10) using the Store-Norske boreholes and methodology detailed in section 3.4.

3.5.2 – The Grønfjorden Bed Valley complex

The distribution of the Grønfjorden bed (Fig. 3.10) appears to reveal a depression, possibly a side valley situated to close to the current

Svea Nord Mine. These topographic lows are subdivided by three linear linear ridges, parallel to the regional NNW-SSE structural trend and to the Billefjorden fault zone. The detail of the plot in areas of high borehole density (such as close to Lunckefjellet) appears to show details of incision of the high in the form of small gulleys. The highs are also often accompanied by local accumulations of thicker conglomerates immediately adjacent to the high which are interpreted as debris fan deposits (intra-formational, angular, poorly sorted conglomerates) possibly associated with gulleys.

The plot also indicates a high to the south-west of Ispallen, which may provide evidence for the Van Mijenfjorden fault zone (Nøttvedt, 1985) and supports the conclusion of a blocking high to the south of Ispallen (Jochmann, 2004). The topographic highs are also parallel to and in the case of the easternmost ridge incorporate the Billefjorden fault zone indicating this was an important feature and natural limit to peat deposition to the East.

The provenance of the Gronfjorden bed sediments is predominantly metamorphic, dominated by quartzite pebbles (Nagy 2005) indicating a source region in the metamorphic terranes of N Spitsbergen. There is also evidence of erosion of more local sediment providing fine grained sediments from underlying Cretaceous formations as mud clasts (Nagy, 2005, Lüthje, 2008).

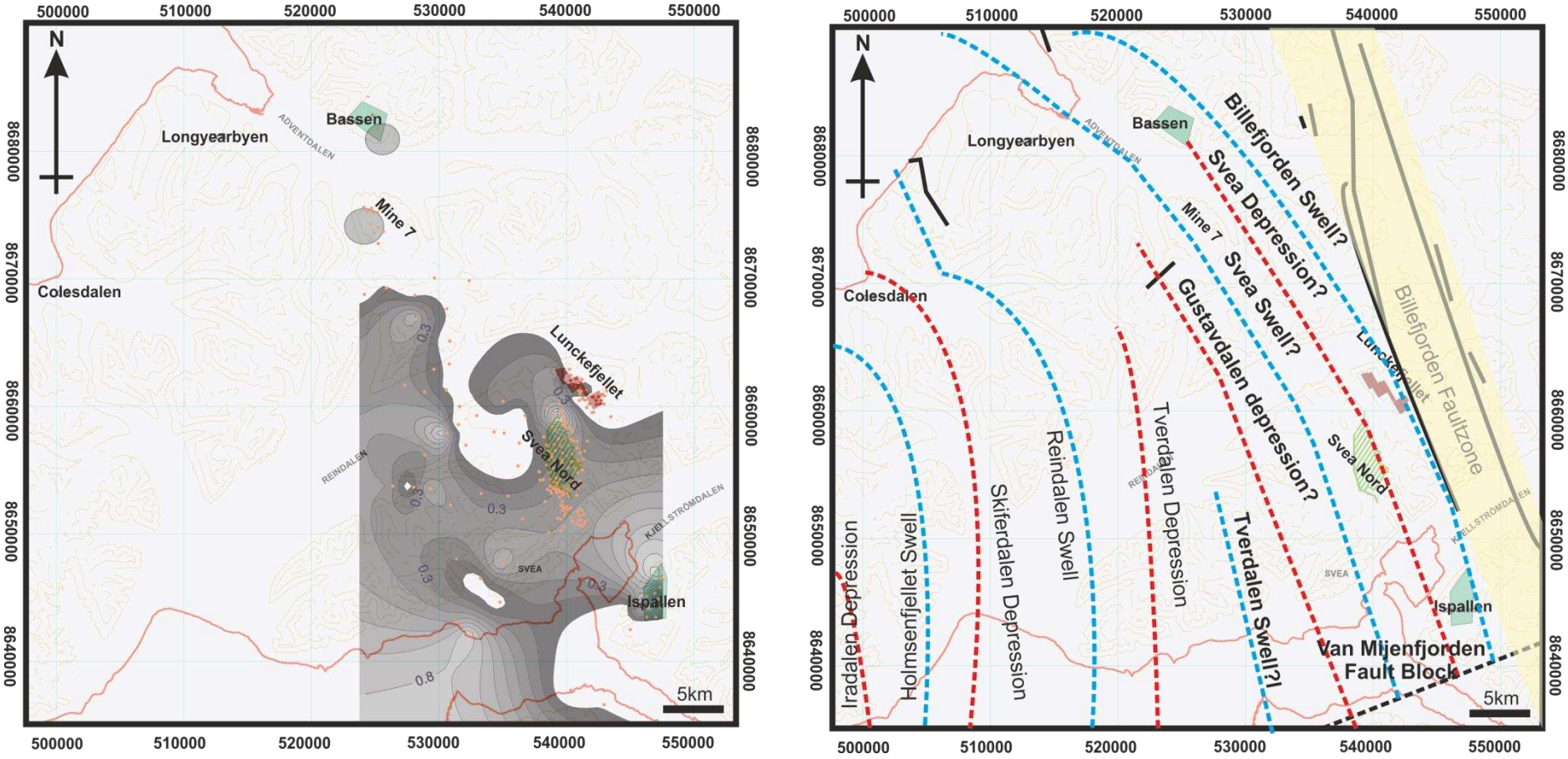

Fig. 3.10 – (Left) Distribution of the Gronfjorden Bed in the Eastern Basin (Red = Datapoints). Note the pattern of valleys and ridges picked out by the conglomerate. (Right) Proposed extension of the trough and swell system identified by Sokholov et al. (1968) to the Billefjorden Faultzone (denoted by ?). Note the approximately similar wavelength to pre-existing structures. Red dots represent sample sites, areas of low sample density are subject to edge effects and plotting errors

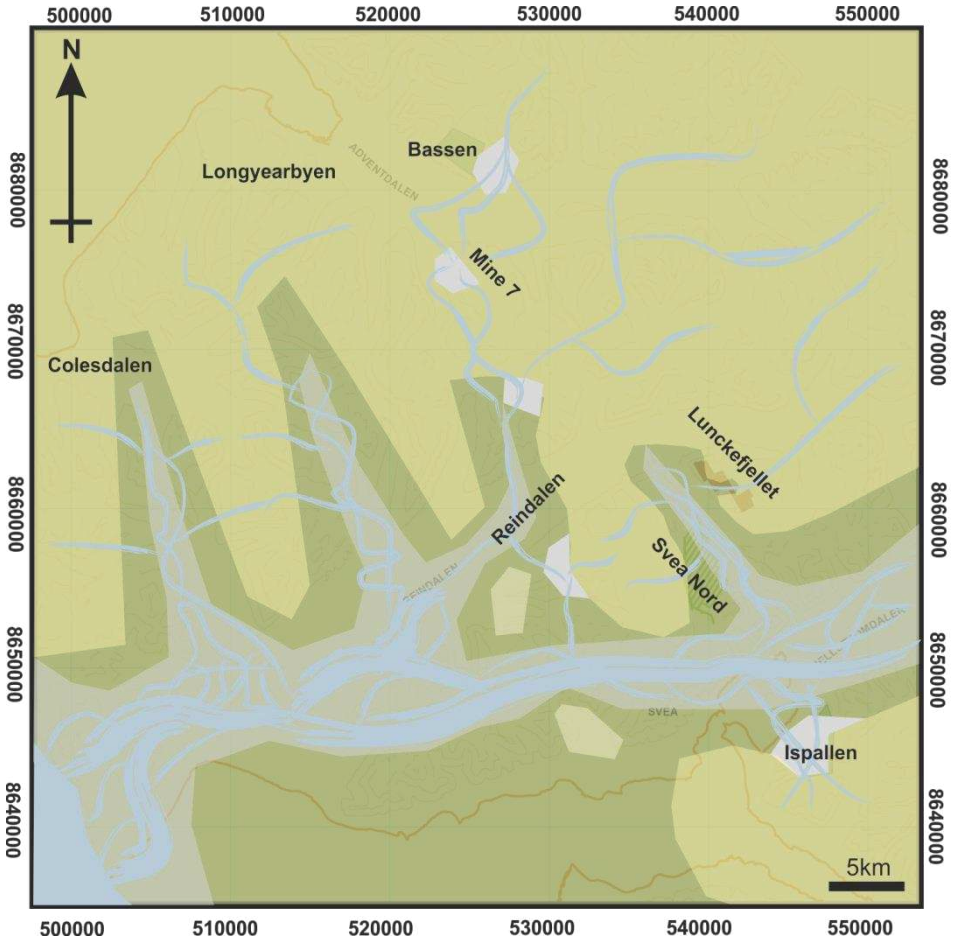

Fig. 3.11 –Possible Reconstruction of the Gronfjorden valleys assuming the valley system identified extends to the previously identified swells and troughs to the deposits described by Nagy (2005)

The braided river and side valley system presented in the reconstruction (Fig. 3.11) forms a snapshot of a much larger fluvial system within the early Palaeocene. This fluvial system appears to flow in a southwesterly direction overall, intersected by a number of extensive N-S side valley systems (two of these can be seen in the reconstruction in Fig. 3.11). This system would be expected to outflow to the West. The thicker deposits of Grønfjorden bed to the southwest (Nagy 2005) could therefore be linked to coastal reworking of the fluvial deposits. Fitting with the idea of an early coastal plain located further to the West (Nagy 2005).

These NNW-SSE side valley systems are presumably subject to the same controls as the series of swells and troughs described earlier in this chapter which appear to reflect structural features within the basin basement (Fig. 3.3).

3.5.3 – Structural controls upon pene-plain topography

The patchy nature of the Tverdalen swell (Fig. 3.10) may be evidence of a number of domal structures similar to those reported by Livšic, (1974), Nottvedt et al. (1988), Harland, (1997) forming the Reindalen swell. The Svea and Billefjorden ridges appear to be more continuous features with the Billefjorden ridge (adjacent to Lunckefjellet) ostensibly associated with the uplifted block of the Billefjordan fault zone.

When plotted on the structural map (Fig. 3.10), the line of the ridge and valley system indicates a continuation of the swell and trough system deeper within the basin. The presence of these NNW-SSE ridges is not entirely unexpected as the previously described swells and troughs exhibit a characteristic wavelength, however there is a conspicuous gap between the Tverdalen depression and Billefjorden fault zone. These have not been observed in previous studies; however this may be due to the increasingly gentle nature of folding away from the main area of thrusting as seen in other foreland type basins (DeCelles and Giles, 1996). Alternatively the small scale of the structures could reflect merely the surface draping over more deeply buried structures, such as the Triassic graben structures shown by Livšic, (1974) and Eiken (1986).

These structural lineaments would have controlled the location of the valley systems which in turn would have enhanced the hydrological landscape via erosion, thus providing the environment for the formation of the first Todalen peatlands.

3.6 Development of coal forming environments

3.6.1 – Svea Seams

The Svea Seam, the earliest of those found within the eastern coalfield, occurs sporadically across the eastern basin. Basin-wide studies regarding the distribution of the Svea have been limited (Jochmann, 2004; Orheim et al., 2007) with the focus of

many studies (Steel and Dalland, 1978; Steel, 1981; Steel and Worsley, 1984; Nøttvedt, 1985; Worsley, 1986, Lüthje, 2008) examining the later Longyear seam.

The Svea peatlands as recorded previously by Jochmann, (2004) and Lüthje, (2008) are present as a number of isolated independent peatlands which are lensoidal in shape, reaching peak thicknesses of up to 4.5m. This lensoidal shape compares well with that of an ombrotrophic raised bog type peatland, where water supply is highly localised and mainly precipitation fed, with the thickest deposits centrally located.

3.6.1.1 – Svea coal thickness and underlying topography

The Svea peatlands were overlain over the outline of the Grønfjorden ridge and valley systems (Fig.3.12). From the map it can be seen that the Svea peat bodies formed adjacent to the topographic highs and side valleys identified on the Grønfjorden reconstruction, at the break in slope. This is as predicted by the hydrological landscape model. The groundwater supply appears to be very localised making these peatlands likely to be highly vulnerable to oxidation in periods of low precipitation.

The Svea peatlands can be divided into two formation styles; the 'valley infill' and 'fan' types. The thickest deposits are found with

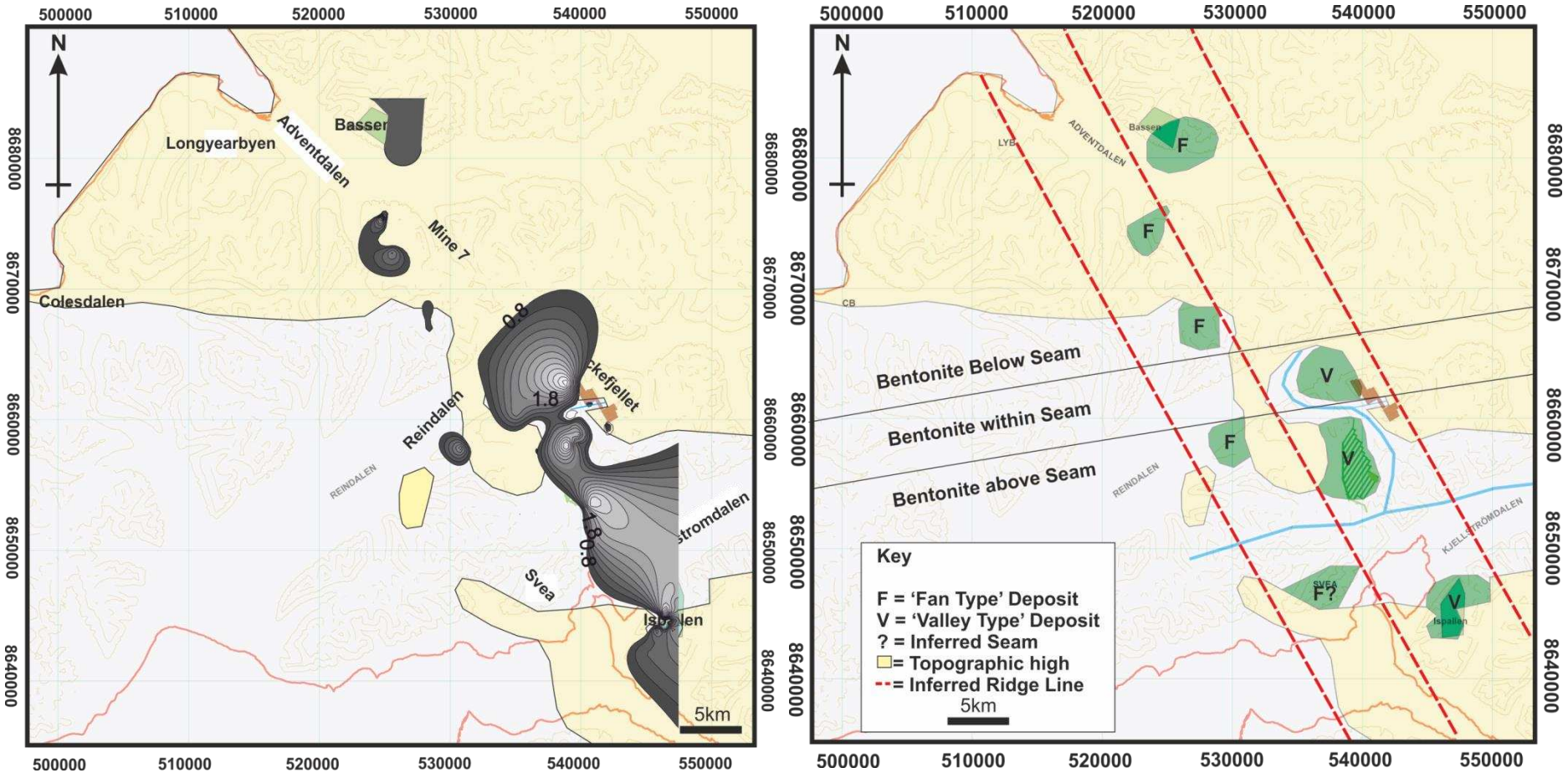

Fig. 3.12 – (Left) Coal Isopach Map of the Svea Seams overlaid over the inferred Grønfjorden Valleys and highs (Right) Schmeatic diagram of 'Valley' and 'Fan' Type Svea Seams. Note all seams are adjacent to inferred ridges. Position of a bentonite layer also shows that the Svea Seam retreated northward in response to rising sea levels. (Inferred seam from former mine)and is clearly diachronous

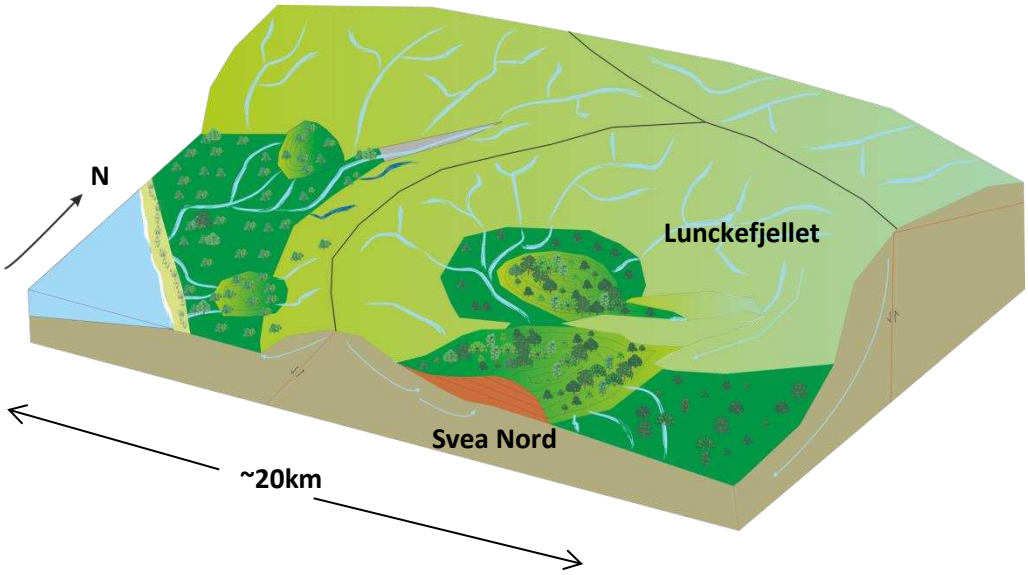

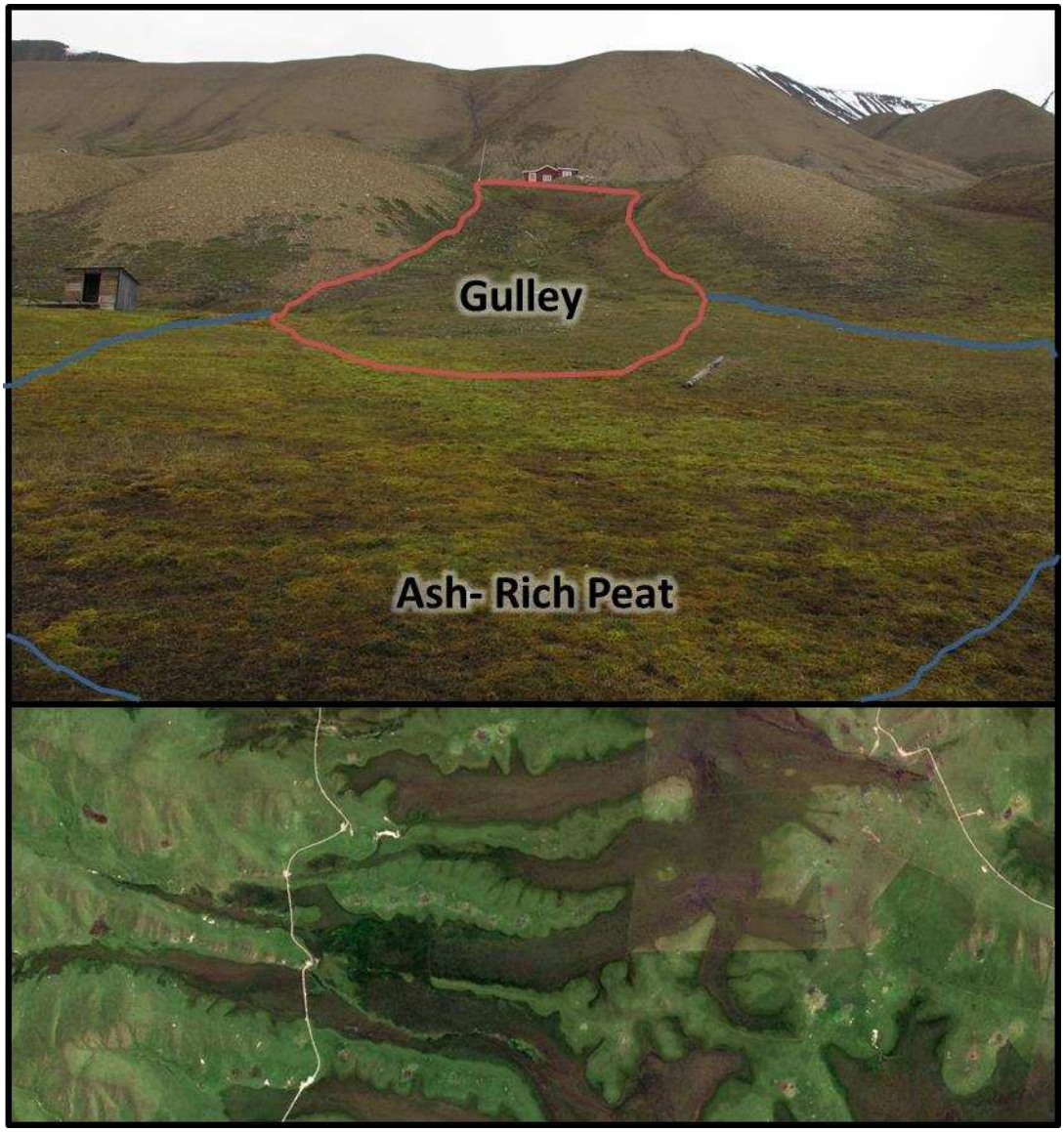

Fig. 3.13 – (Top) 3D reconstruction of the Svea Nord Deposit showing position within the Grønfjorden valley and localised hydrology. (Middle) Modern analogue for 'Fan type' Svea in Adventdalen. (Bottom) Peat infilling valleys in China possibly analogous to 'Valley Type' Svea Seams.

the ‘valley infill’ type, where peatlands are constrained by a relatively narrow valley sides and groundwater supply is sourced from multiple directions.

This type of peatland deposition can be seen today in China (Fig. 3.12) where peatlands infill and migrate down valleys. This is perhaps not surprising as the moisture content of peat soils is very high (Kuntze, 1972).

The thinner ‘fan’ type deposits are situated over the former Grønfjorden debris fans (Fig. 3.10), where hydrological supply was most stable, fed by the pre-existing gulley system. The thinner nature of this type of Svea seam is probably due to a smaller more localised, groundwater water catchment and susceptibility to surface flow down the gulley during intense precipitation events. This would make the ‘fan type’ peatlands vulnerable to clastic sedimentations.

In addition, the fan deposits are generally more low lying and closer to the coastal plain and as result comparatively unprotected against coastal inundation when compared to the more sheltered ‘valley infill’ type deposits. Similar process producing fan type peatland formation can be seen today at the base of Hijortfjellet, with a gulley and debris fan system supporting a lens of peat at the break in slope (Fig 3.13). This would form an ash rich and small relatively thin coal deposit which is what is seen in the isopach map (Fig.3.12; Table 5.1)

The thick Svea deposits in Ispallen appear to be a combination of both fan and valley type deposit, forming in a short side valley with a debris fan at the juncture with the main E-W drainage (Fig.3.10;3.12).

3.6.1.2 Bentonite and the Svea Seam

A major problem with the nomenclature of the Svea seam is that it implies that it is made up of a single seam. However, the geographic separation of the seams shown in Fig. 3.12 makes this unlikely. Consequently, it is very difficult to predict coal quality across the basin (from lens to lens) as this is determined by local and temporal factors specific to each lens during formation although generally the peat-forming conditions found within valley type deposits appear to be superior compared to those found within fans.

The presence of a single layer of bentonitic clay, within the lower todalen Member demonstrates this. Thought to represent a volcanic ash layer from a single event, the bentonite layer appears above the Svea Seam to the South, within the Svea Seam in the Lunckefjellet region and below the Svea in Adventdalen. This indicates that over time the Svea seam migrated north-eastward probably due to the effect of rising sea-level. This migration upstream over the early deposition of the Todalen Member supports the hypothesis that seams found to the southwest of the basin could represent the earliest peat deposition within the basin.

A plot of bentonite thickness across the basin (Fig. 3.14) shows that although the bentonite must have been reworked from the highs into the valleys soon after deposition it represents a single event and a datum. Thus this further proves the temporal diversity of individual Svea seams within the Central Tertiary Basin with the northern Svea seams younger than those in the south. In consequence, to avoid future confusion a new naming system is proposed, where the name of the nearest landmark to the thickest part of the seam in each lens is appended to the current Svea name with the exception of the Svea Nord lens for example the Lunckefjellet Svea, Breinosa Svea, Bassen Svea etc.

Further study of this bentonite layer may provide a radiometric date for the formation of the Svea seams, as currently the only known date within the basin is the PETM boundary (Dypvik et al., 2011) and the Tertiary in Svalbard is notoriously difficult to date using palynology. This would help improve previous subsidence and accumulation rates and help to improve knowledge of basin history during the Palaeocene. Also bentonitic clays have been used previously as maturity parameters. Analysis of this would provide an independent maturity measure as previous studies in the basin (Manum and Throndsen, 1978) have focused primarily on vitrinite reflectance.

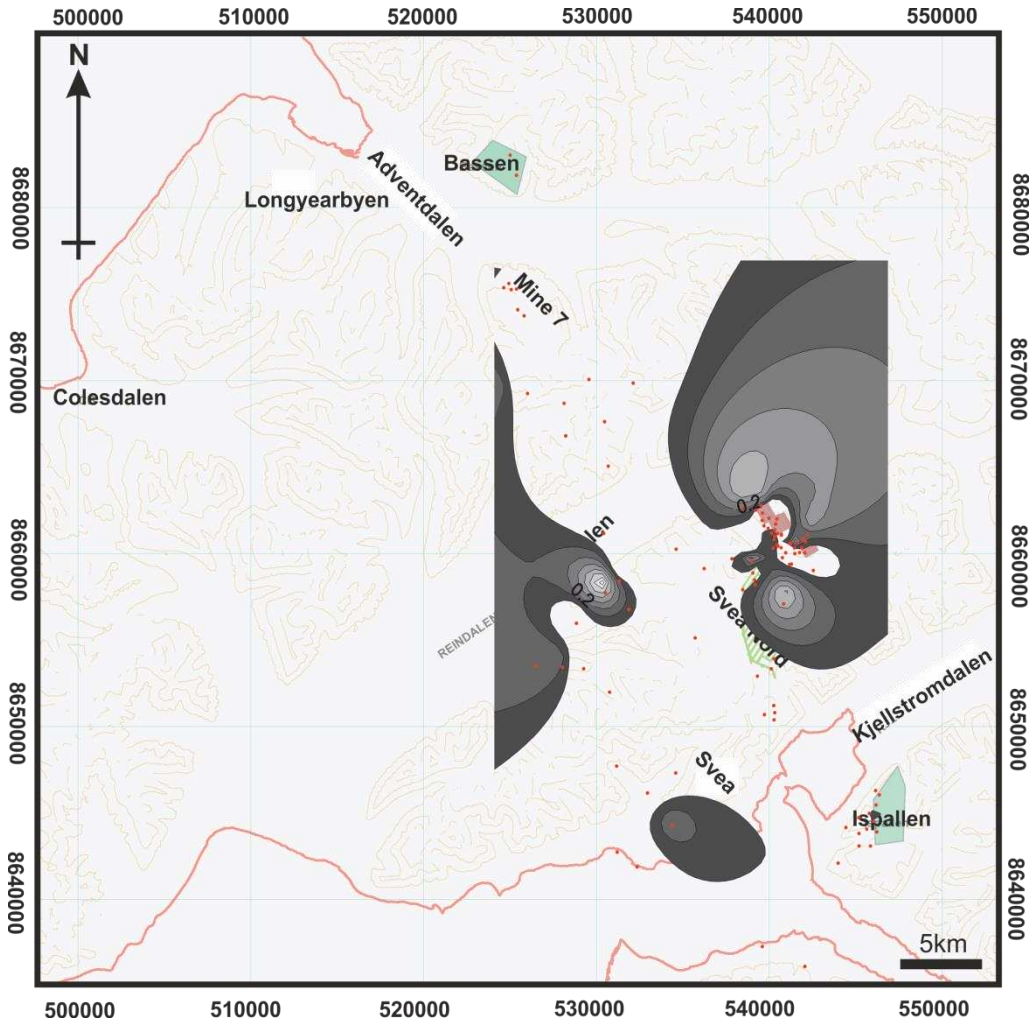

Fig. 3.14 – Bentonite Isopach map showing the redistribution of the Bentonite layer into the Grønfjorden Valleys soon after deposition

3.6.1.3 – Hydrological Development of the Svea Seams

The palaeo-environmental reconstruction of the Svea seams (Fig.3.11) shows their distribution and thickness is heavily dependent upon the local catchment. It also shows that the positions of optimum hydrological stability were structurally controlled, and that these areas remained stable for long period of time. The position of optimum peatlands reacted to changes in regional changes, moving North-eastward as sea levels rose.

Smaller peatlands were more transient, situated adjacent to point sources of groundwater discharge, generally at the bottom of gulleys and overlying former debris fans. The hydrological supply to these peatlands was less stable as a result leading to poorer quality coal deposits.

The Svea Seams show that the hydrological landscape model is useful for understanding why thick coal seams are situated where they are and identifying possible palaeo-environmental sources of inorganic contamination. In addition the close relationship between the distribution and thickness of the Svea seam and the Grønfjorden bed (Fig. 3.12) makes it an ideal target for exploration. Knowledge of the position of palaeo-topography would also help target the thickest coal deposits situated within valleys at the break in slope between topographic highs and lows. These ridges should be easily predicted as it appears they are structurally controlled.

3.6.2 – The Longyear Coastal Peatland

The Longyear peatland forms the basis for the majority of the previous reconstructions (Steel and Dalland, 1978; Steel, 1981; Steel and Worsley, 1984; Nøttvedt, 1985; Worsley, 1986; Lüthje, 2008; Aspøy, 2011). The reconstructions of the Longyear seam fits well with the transgressive system indicated by Luthje, 2008, with lowlying areas of zero coal deposition filled with lagoonal sediments (Jochmann, 2004). The distribution of the coal seams and the similarity between the Endalen Member and that of a barrier coastline indicates that this is unlikely to be a deltaic environment. This section will examine the distribution of the thickest Longyear coals seams and their relationship with the underlying structural highs and lows observed from the Grønfjorden bed. It will also examine how the existing landscape reacted to increasing sea levels and how this could affect coal quality up-seam on both a local (Lunckefjellet) and regional basis.

3.6.1.1 – The effect of landscape upon Longyear coal thickness

The coal isopach map of the Longyear seam (Fig. 3.15) shows that the thickest coal seams are located to the N and NE of the basin with thickest deposits around the Bassen/Operafjellet region in excess of 2.5m. Coal thickness within the currently mined Mine 7 is generally in excess of 1.5m and in the new Lunckefjellet mine the

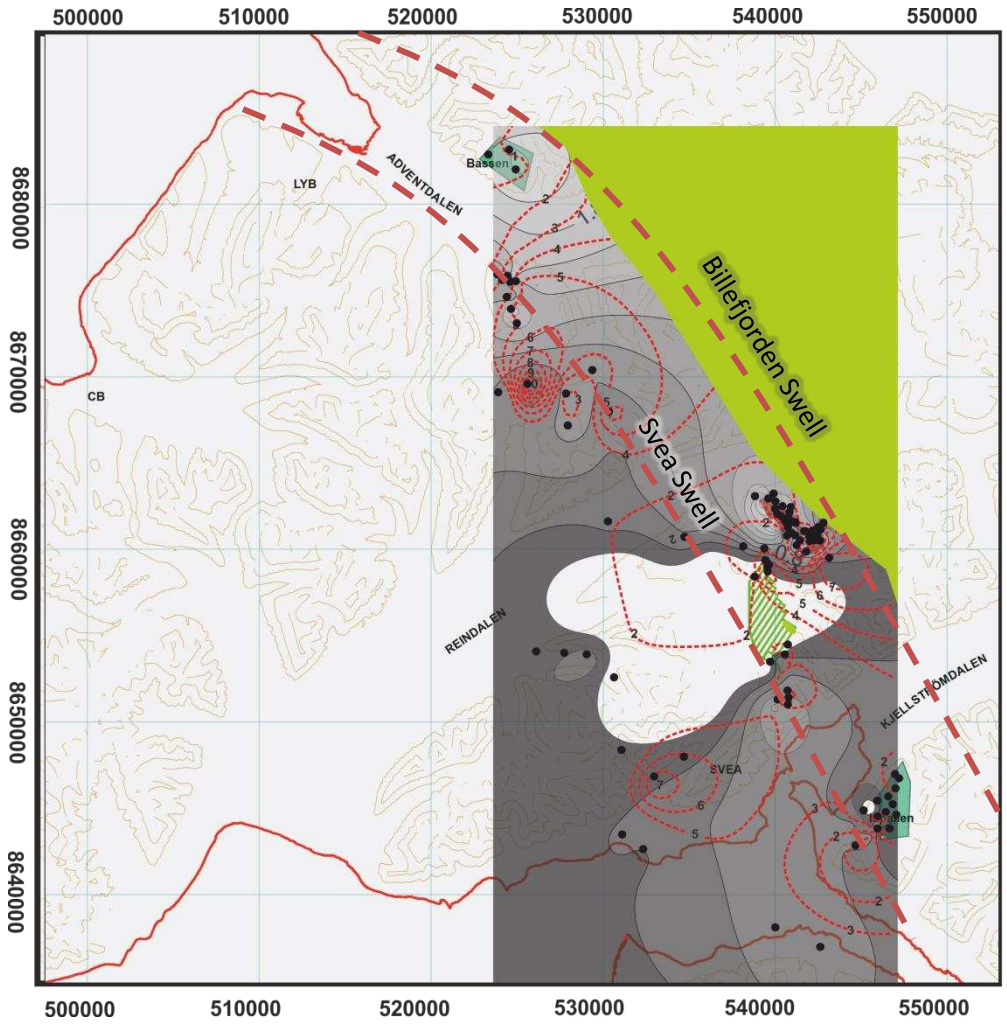

Fig. 3.15- Coal Isopach map for the Longyear seam overlaid with mean Sulfur content and inferred Grønfjorden highs. Note the position of many of the current and prospective mines adjacent to the ridges indicating a possible hydrological landscape control. Sulfur picks out a number of high sulfur areas of coal penetrating the peatland possibly representing tidal channels or estuaries.

Red contours represent sulfur contours (SNSK data) and black, coal isopach lines

coal seam is up to 2.15m thickness. Unlike the Svea seam, the Longyear seam overlying the Svea Nord Mine and Ispallen regions is relatively thin (<1m) indicating that the landscape control on peat accumulation changed between seams.

The Longyear seam is more laterally extensive than the Svea seam, indicating a more regional control on hydrology compared to the Svea, however there are numerous small scale changes in thickness across the basin which indicate that coal thickness is controlled by more than base level changes.

The series of ridges and troughs identified from the Grønfjorden bed appear to still have a control upon coal thickness with the Lunckefjellet mines lying adjacent to the Billefjordan ridge (Fig. 3.15). The Tverdalen ridge appears to have relatively little control upon peat accumulation during this period however it may have played a role in controlling the position of sandbanks/shoals during this period, which requires further investigation.

The Svea Nord swell appears to mark the limit of peat accumulation in the southwest and only contains thin peat deposits. There is a conspicuous area of no coal formation in some areas of the Svea Nord trough which is in-filled by tidal/coastal lake sediments indicating this was a persistent low which made it vulnerable to inundation during base level rises.

Due to the southerly tilting of the basin the Longyear peatland was able to expand further westward in the north. Consequently the Svea Nord Swell appears to be responsible for the higher coal thicknesses at both Mine 7 and Bassen. Either side of this swell depressions lead to thinner coals and preferential channel formation. These depressions can be identified by the higher S coal contents to the E and W of Breinosa/Mine 7. It is presumed that this pattern of swells and depressions would have played a part in the distribution of thickest coals in Mines 1-6 in Adventdalen, however due to the lack of data, this could not be ascertained.

Consequently, although the Tverdalen and Svea Nord ridges and troughs appear to be of lesser importance to Longyear seam in the SE of the basin, in the north of the basin they appear to have a significant control on coal thickness in the North. The Billefjorden ridge system allowed a thin coastal plain of thick coal to form during the formation of the Longyear seam, but appears to have provided a natural limit to coal formation to the east.

3.6.1.2 Peatland Response to Relative Sea Level Change

Coal isopach mapping can also be used to help understand how the peatland reacted to changes in relative sea level. By changing the minimum thickness shown in the plot, the maximum and minimum extent of the peatland can be shown over time. This also helps to highlight the areas of maximum stability and consequently the

break in slope. The thinnest areas of coal are taken to represent the least hydrological stability and the thickest the most stable, defining semi-permanent breaks in slope.

Used in series, this can give a simplified model of peatland expansion and regression. This can then be used to predict what the primary controls upon coal quality might be at a particular time period. Thus, allowing identification of areas of the seam (both vertically and horizontally) where coal quality may be an issue.

When this technique was applied to the Longyear seam, the following plots were created (Fig. 3.16). The sequence begins at the maximum extent of peatland formation, around the period of lowest relative sea level. To simulate the effect of rising sea levels, the minimum coal thickness shown on the plot was raised by 0.2m for each time segment.

It is thought that prior to maximum extent the peatland expanded rapidly to fill the newly exposed floodplain as hydrological supply rapidly migrated westward. This is a similar response to decreasing sea-level as that seen in more recent peatlands, described previously (Miguez-Macho and Fan, 2009).

The isopach map (Fig. 3.16) indicate that as relative sea level rose, the peatland retreated eastwards. Initially the remnant of the Grønfjorden highs allowed the formation of 'ridges' of thicker

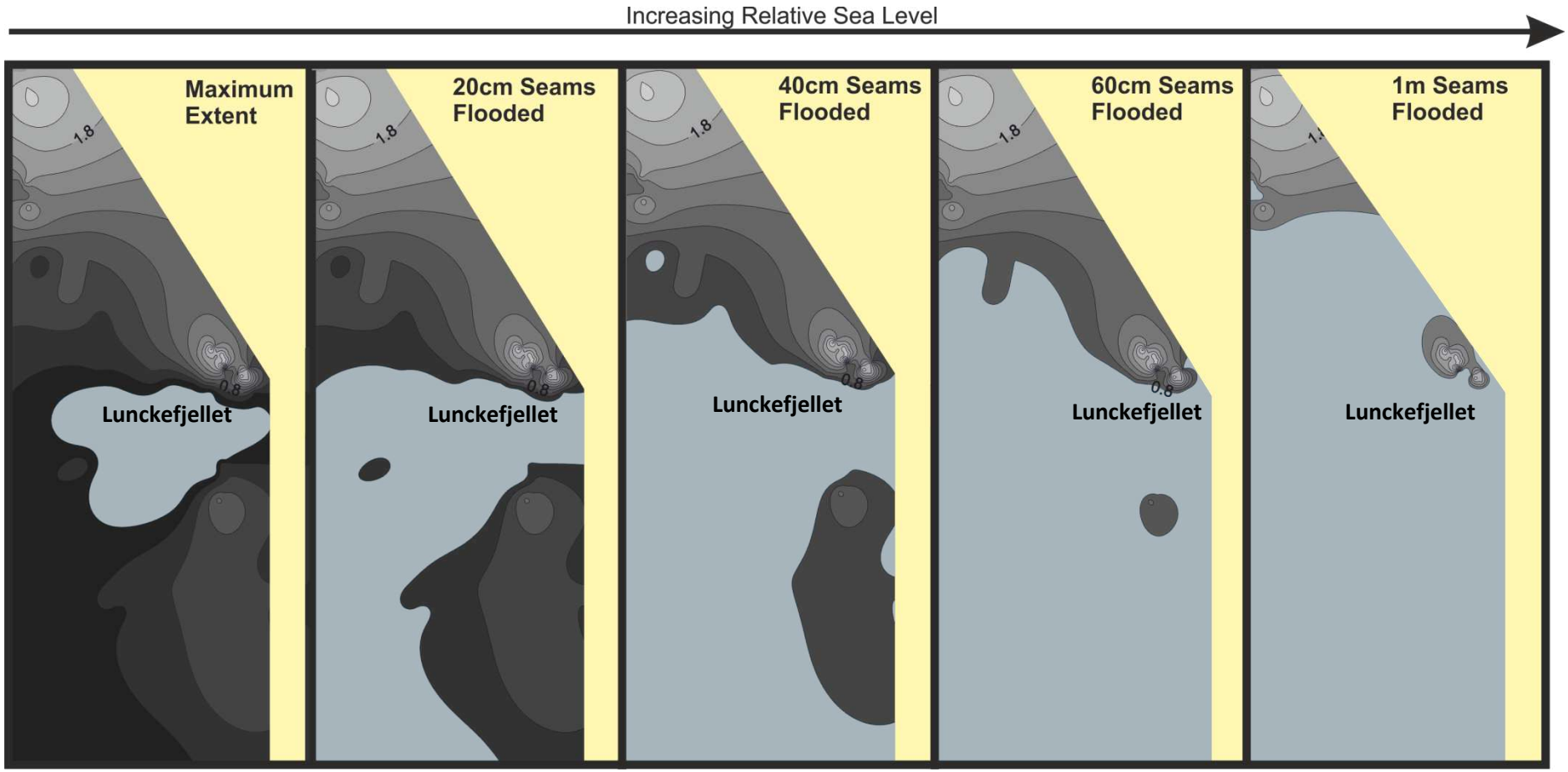

Fig. 3.16. Model of the effect of base level rises on the Longyear using coal thickness as an indicator of duration of peat accumulation from maximum extent to termination of the peatland. Note the area of non-peat deposition adjacent to Lunckefjellet, followed by bay formation and peat accumulation shifting northward. Yellow indicates limit to tertiary sedimentation.

peatland protecting the more inland areas from marine influence. The area to the west of Lunckefjellet contains an area of zero coal deposition which is likely to represent a storm supplied lagoonal deposit or coastal lake deposit (Appendix I). This depression is likely structurally controlled as it lies directly above the 'Svea Nord' valley system.

Later as sea levels continued to rise the high points of the ridges were cut off from the mainland forming peat islands, possibly supplied by groundwater upwelling driven by the higher ground to the N and E. The lagoonal deposits were inundated and formed two bays (Fig.3.18). This is represented within the coals as splits which appear to extend along areas of low ground. This can be seen in the split plot seen in Fig. 3.17. Eventually, this structural control was overtopped and peatland retreated to the longstanding structural highs at the edge of the basin, around Lunckefjellet and Bassen. A reconstruction of this can be seen in Fig. 3.18

The effect upon coal quality of the Longyear peatland's response to changes in relative base level can now be predicted using the detailed palaeogeographic reconstruction created. It would be expected that the western part of the basin would be most vulnerable to marine influence, leading to higher sulphur contents and ash supply due to supply from sea spray and vulnerability to inundation. This also limits the thickness of these coals. It is also

likely that the character of the peatland would change as groundwater would be forced closer to the surface, in consequence of

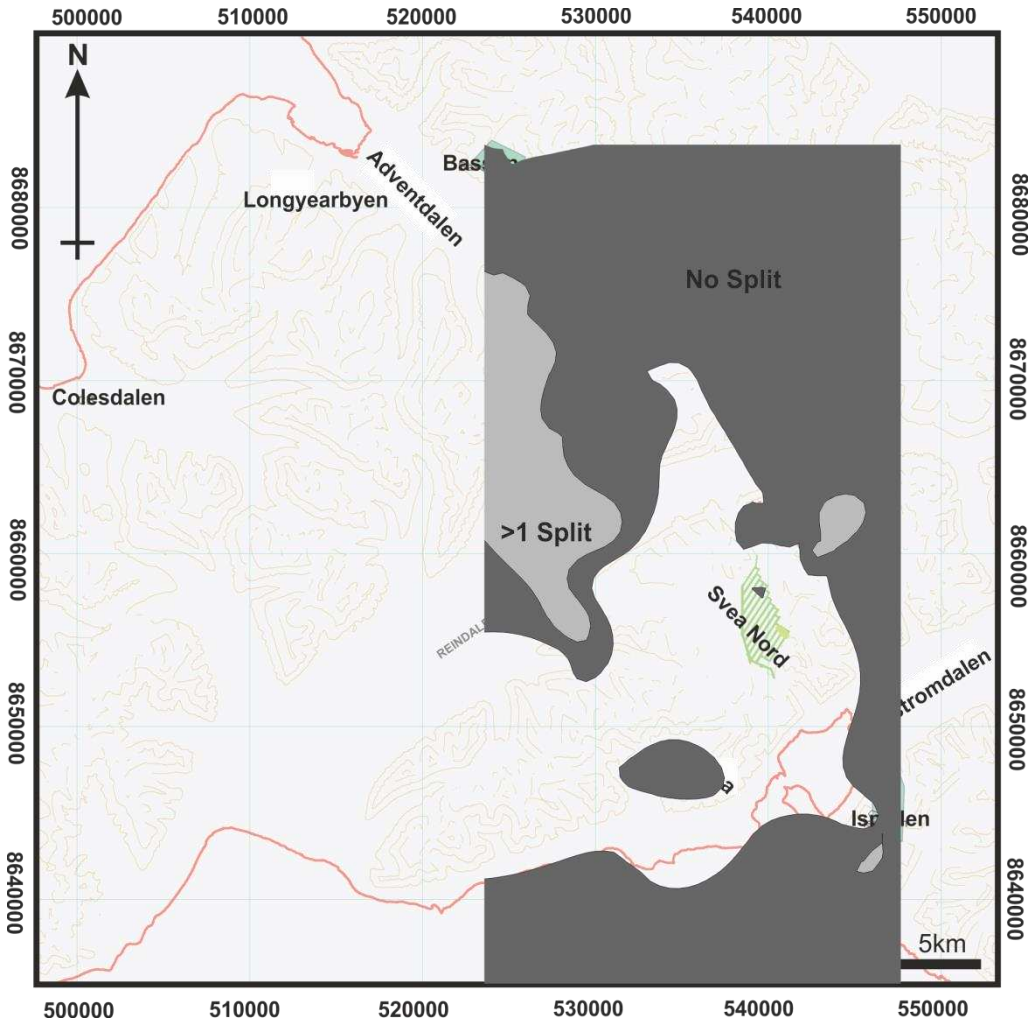

Fig. 3.17. Map showing the position of any splits within the Longyear coal, with most originating from the coast and overlying the Gronfjorden depressions and gulleys (Lunckefjellet).

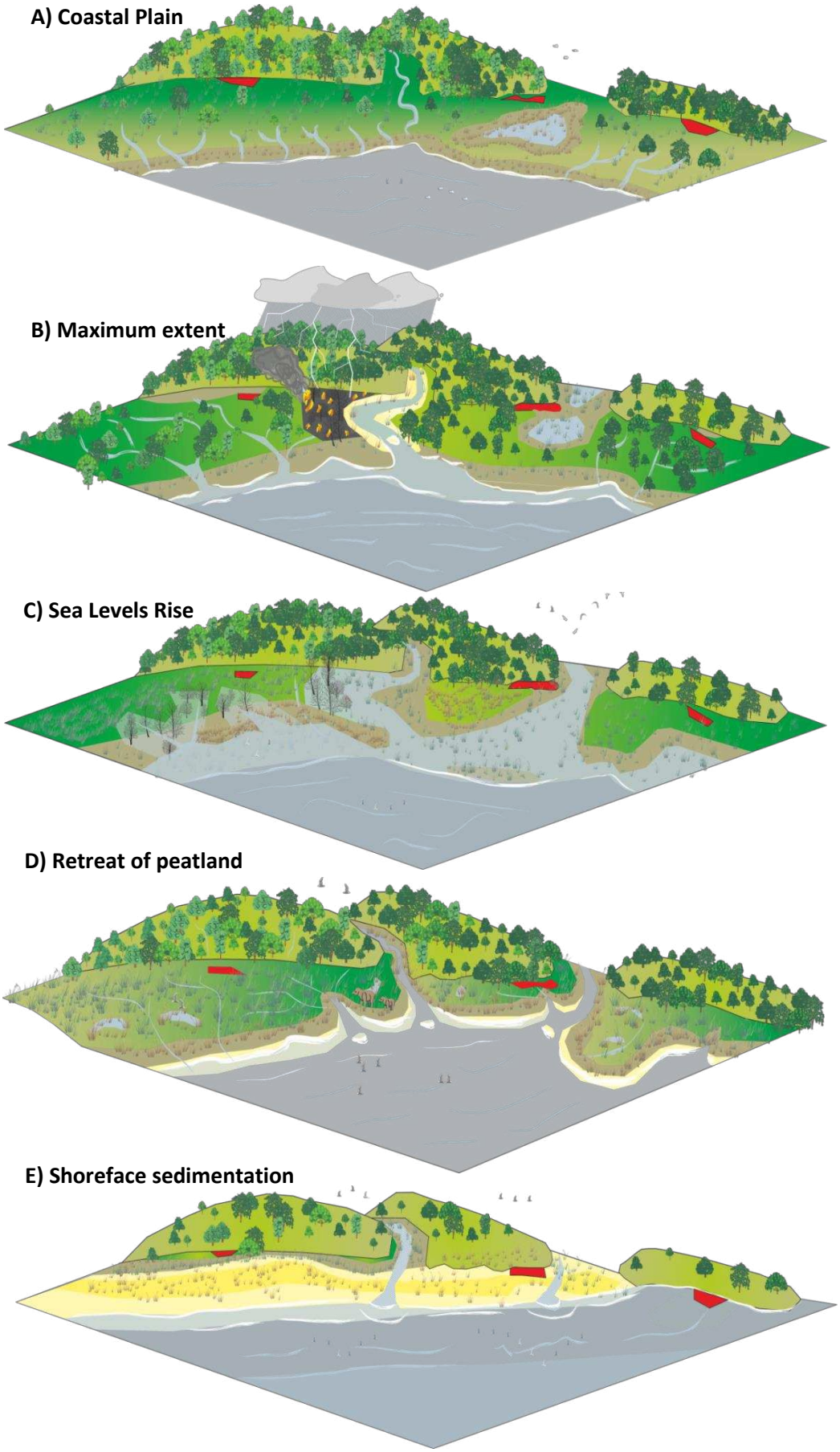

Fig. 3.18. Palaeo-environmental development of the Longyear seam, A and E based on lithology maps and logs as defined in Section 3.4. B-D based on coal isopach maps, sedimentological logs, response to sea level shown in Fig. 3.16 and coal geochemistry seen in Chapter 6. Red areas represent mine sites

rising sea levels. This would lead to a possible transition from more raised bog conditions to fen conditions as observed in previous hydrological landscape studies (Amon et al., 2002).

Evidence of marine influence would be expected to appear later and later towards the interior of the peatland with the associated coal quality issues decreasing to a minimum at the basin edge at Lunckefjellet and Bassen. However, any low-lying conduits for marine incursions such as estuaries or former river channels adjacent to the inland peatland would be expected to lead to localised splitting and enhance or increased coal sulphur contents adjacent to channels. The effect of these smaller scale features will be examined in the next section.

3.6.1.3 – Local Scale Reconstruction of the Longyear Peatland

In areas of high sampling density it is possible to look in high resolution at smaller scale controls on the location and quality of coal deposits. Using the area of the proposed mine at Lunckefjellet where high density sampling has been carried out in preparation for mining, a coal isopach map was prepared. This was then used to produce a palaeogeographic map of peatland extent at low and high relative sea level (Fig. 3.19). In addition historic whole seam sulphur contents were overlaid as an indicator of marine influence.

The coal isopach maps (Fig. 3.17) shows that coal thickness is greatest towards the centre of the Lunckefjellet deposit and rapidly

thins westward over the Svea Nord mine. In the centre and southern edge of the deposit coal thickness also rapidly decreases. In addition the coal in these locations is split (Fig.3.22) this indicates that these areas were vulnerable to clastic sedimentation, probably indicating channels. There is an area of no coal deposition in the area to the SW of Lunckefjellet. This may represent lagoonal/coastal lake deposition, as described by Lüthje, (2008)

The palaeogeographic reconstruction of the Longyear seam at low relative sea level (Fig. 3.19) indicates that the peatland in the Lunckefjellet region built out from the high ground to the east, expanding into a slight depression (overlying the Svea valley). In the centre of the depression peatland formation was prevented by a lagoonal deposit or coastal lake deposit. As sea levels began to rise (Fig.3.19) the depression was quickly infilled by marine deposits and peat formation retreated rapidly to the break-in slope. This can also be seen within the whole Todalen Member cross section from Lunckefjellet (Fig. 3.22).

Peat formation remained stable in the Lunckefjellet area for a prolonged length of time; however the peatland is punctuated by a number of areas of thinner peat, indicating either depressions or highs. The areas of low coal thickness are preferentially filled with conglomerates and appear to be a focus for split formation (Fig. 3.22; 23) indicating that these are depressions and channels. The conglomerates indicate that these were probably tidal channel or

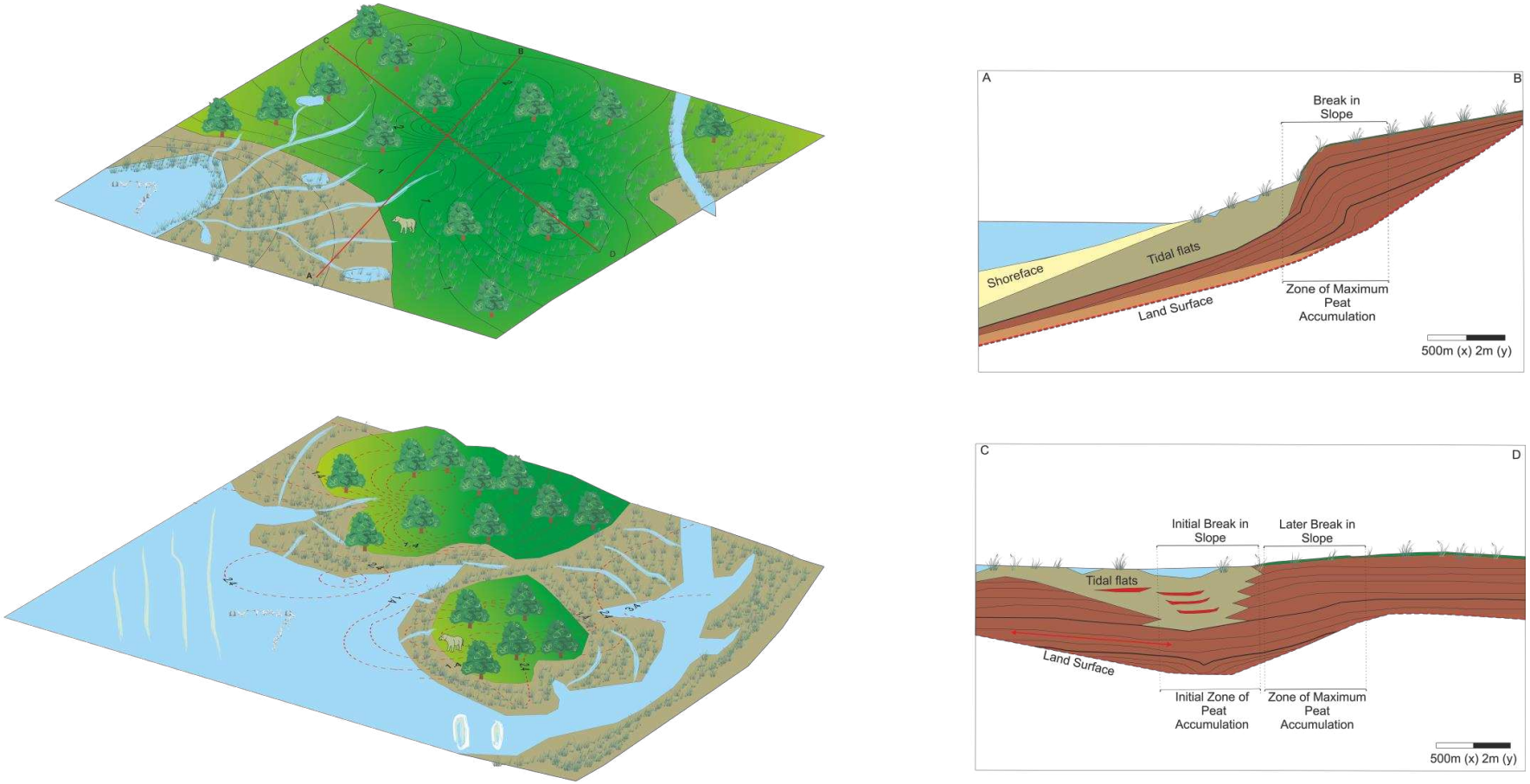

Fig. 3.19 - Palaeo-environmental Development of Lunckefjellet Area (Top-left) Maximum extent showing area of low coal thickness deposition to W of Lunckefjellet possible representing coastal lake/lagoonal deposits (Bottom Left) Lunckefjellet after sea level rise showing formation of tidal inlets and estuaries adjacent to the site. These are also shown by coal sulfur contents showing position relative to these is a major control on coal quality. (Right) Schematic Sections across Lunckefjellet showing maximum thickness at the break in slope and preferential channel formation in topographic lows.

coastal channel deposits, which fits with previous interpretations of the coastline (Lüthje, 2008). The inlets are also defined by higher sulphur contents, consistent with a tidal channel environment and marine influence. The channels shown by the sulfur and coal isopach map (Fig.3.19) and shown within the cross-section (Fig.3.22) fit closely with previously reported channels and mouthbars (Aspøy, 2011).

3.6.1.4 – Palaeo-geographic development of the Longyear seam

The use of coal isopach mapping and a hydrological landscape approach confirms many of the features described by Jochmann (2004) Lüthje (2008), Aspøy (2011) regarding the Longyear peatland, namely a continuous tidal dominated plain with coastal lakes with channels and coastal inlets (Fig.3.18).

Unlike previous models, this technique provides a high resolution map of the distribution of the peatland and its relationship to the underlying landscape. Consequently it allowed the following conclusions to be made;

- Even minor landscape features controlled how different areas of peatland were affected by base-level rises leading to distribution of high thickness coal to be very complex
- However, the thickest deposits of the Longyear seam are found adjacent to topographic highs which are controlled by

underlying structural features. These acted as both areas of initiation and refuge for peat during periods of rising base levels.

- Persistent topographic lows acted as conduits for both fluvial and tidal channels. As a consequence splits within the coal seam can be seen to originate from these areas.
- Sulfur deposition is controlled by proximity to these channels with sulfur concentrations greatest adjacent to the channels and rapidly decreasing inland (Fig.3.19).
- Relatively minor features such as underlying gulleys can be seen to have an effect on coal thickness and coal quality/splitting.

3.6.3 – The Svarteper and Askeladden Seams

The Svarteper and Askeladden seams represent the last period of coal formation within the basin. They are separated by only 1-2m in some areas making them difficult to distinguish. The reconstruction by Nøttvedt, (1985) shows the Askeladden to be a northern delta sequence and the thickest deposits do seem to be focussed around Adventdalen. The coal isopach map (Fig. 3.20) for the Svarteper period shows that a period of bay formation with inundation of areas that in the earlier Longyear seam were stable and protected from sea level rise for a much longer period. Highest coal thickness is still found alongside the Billefjordan high however by this time the Svea Nord and Tverdalen swells appear to be very minor features

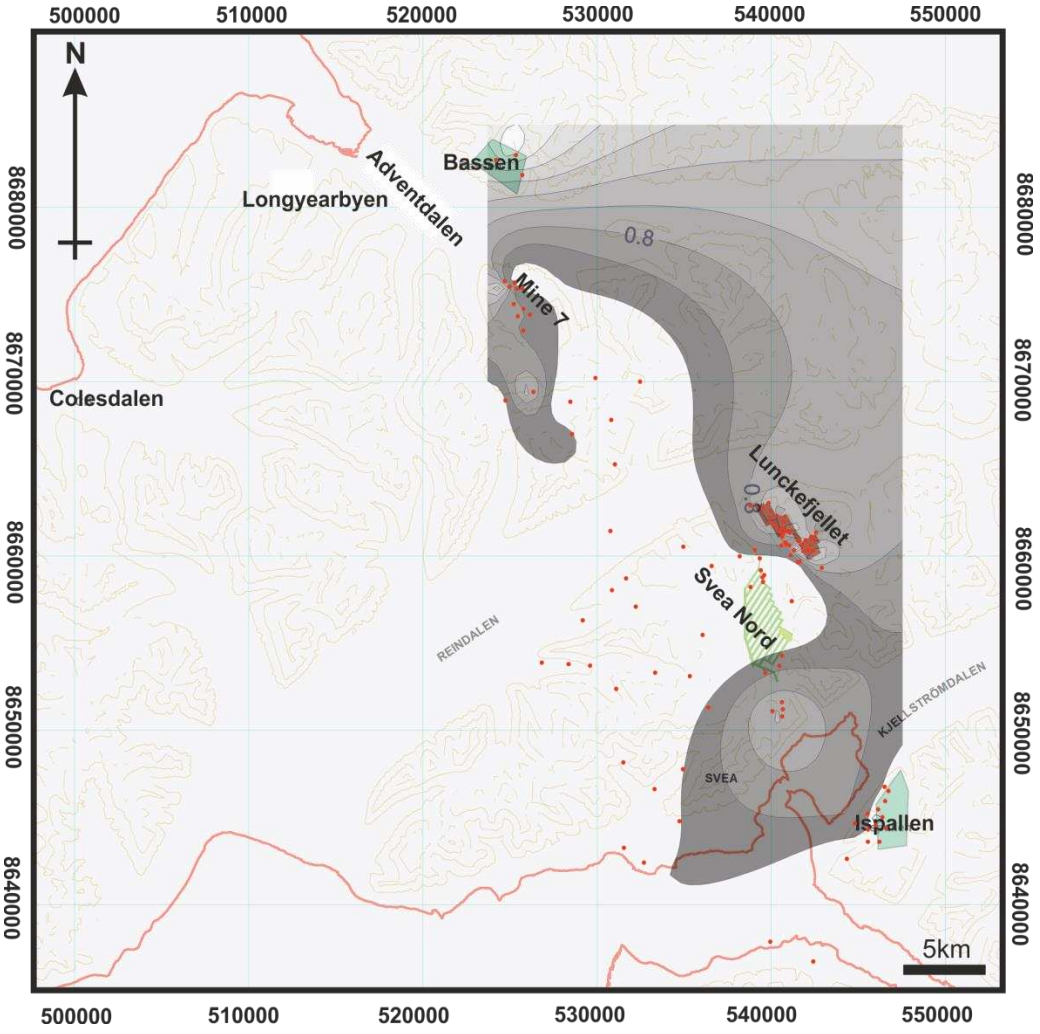

Fig. 3.20 Coal Isopach map for the Svarteper seam showing peat deposition to have shifted to the North and East of the basin with high marine influence likely due to the limited extent of the coastal plain

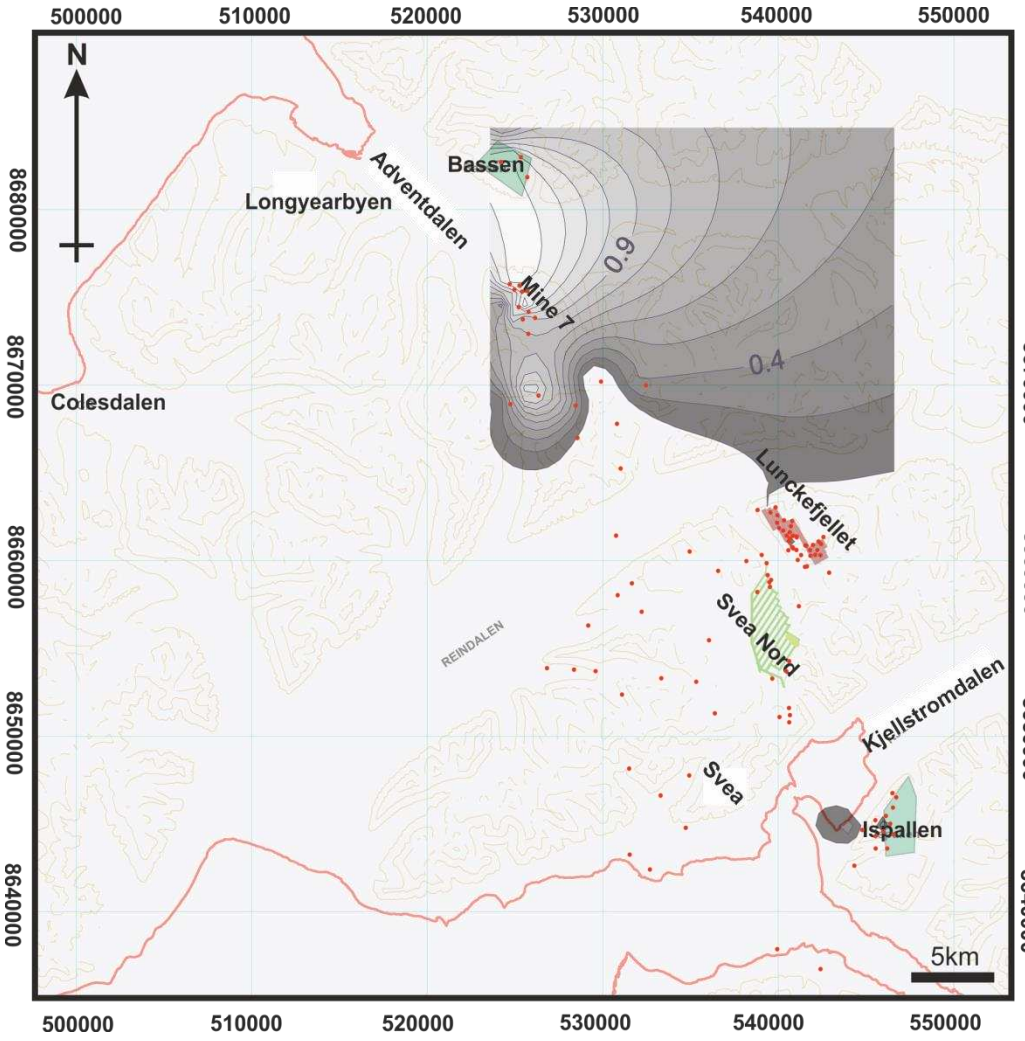

Fig. 3.21 Coal Isopach map for the Askeladden seam showing that peat deposition is limited to the northernmost part of the basin as relative sea levels increase further

in the south. This is shown by the lack of coal deposition in these areas and the presence of only marine facies material during this period. This means that the entire peatland was more vulnerable to marine influence and inundation, leading to greater vulnerability to high sulphur as described by Orheim et al. (2007).

By the Askeladden seam (Fig. 3.21) coal formation was entirely limited to the extreme North and North West of the basin around the Adventdalen area. This shows that by this time the infill of the Cretaceous pene-plain was almost complete. The erratic thickness and poor quality of the Askeladden Seam (Orheim et al., 2007) likely reflects an increasingly constrained coastal plain with a steep slope to the north unsuitable for peat accumulation and the sea to the south (Fig.3.21).

The Askeladden may well represent a late period of progradation from the North as suggested by Nøttvedt (1986), however this was relatively short-lived leading to predominantly marine deposition until the deposition of the Aspelintoppen formation in the Eocene. Consequently once the Askeladden seam terminated, the conditions to the north were unfavourable to large scale peat accumulation in most areas. The exception to this is an Endalen Member coal seam observed at Bassen, emphasising the long-term hydrological stability at this location.

3.7 – Long term structural controls on coal formation in the Central Tertiary Basin

Isopach mapping of the Todalen coal seams has shown that underlying structural and topographic trends represented a significant but diminishing control upon the distribution of thick coal within the Central Tertiary Basin.

This can also be seen within the Breinosa and Lunckefjellet regions in cross sections through the Todalen Member (Fig.3.22; 3.23). At both locations, the Svea is present within depressions within the underlying Cretaceous pene-plain. These depressions also form the focus for channel formation throughout the deposition of the Todalen Member within both coastal plain and shore-face conditions. Coal overlying these depressions repeatedly contains the thickest splits further indicating that these features acted as an important and persistent control on channel and clastic sedimentation throughout the Todalen Member.

The thickest coal deposits in the Longyear, Svarteper and Askeladden seams all overly the break in slope of the Cretaceous peneplain (Fig.3.22;3.23). In general the coal seams thin over topographic highs and lows. This is as predicted by the hydrological landscapes model (Winter, 1992; 2000; 2001) with the thickest coals located adjacent to the most stable hydrological supply.

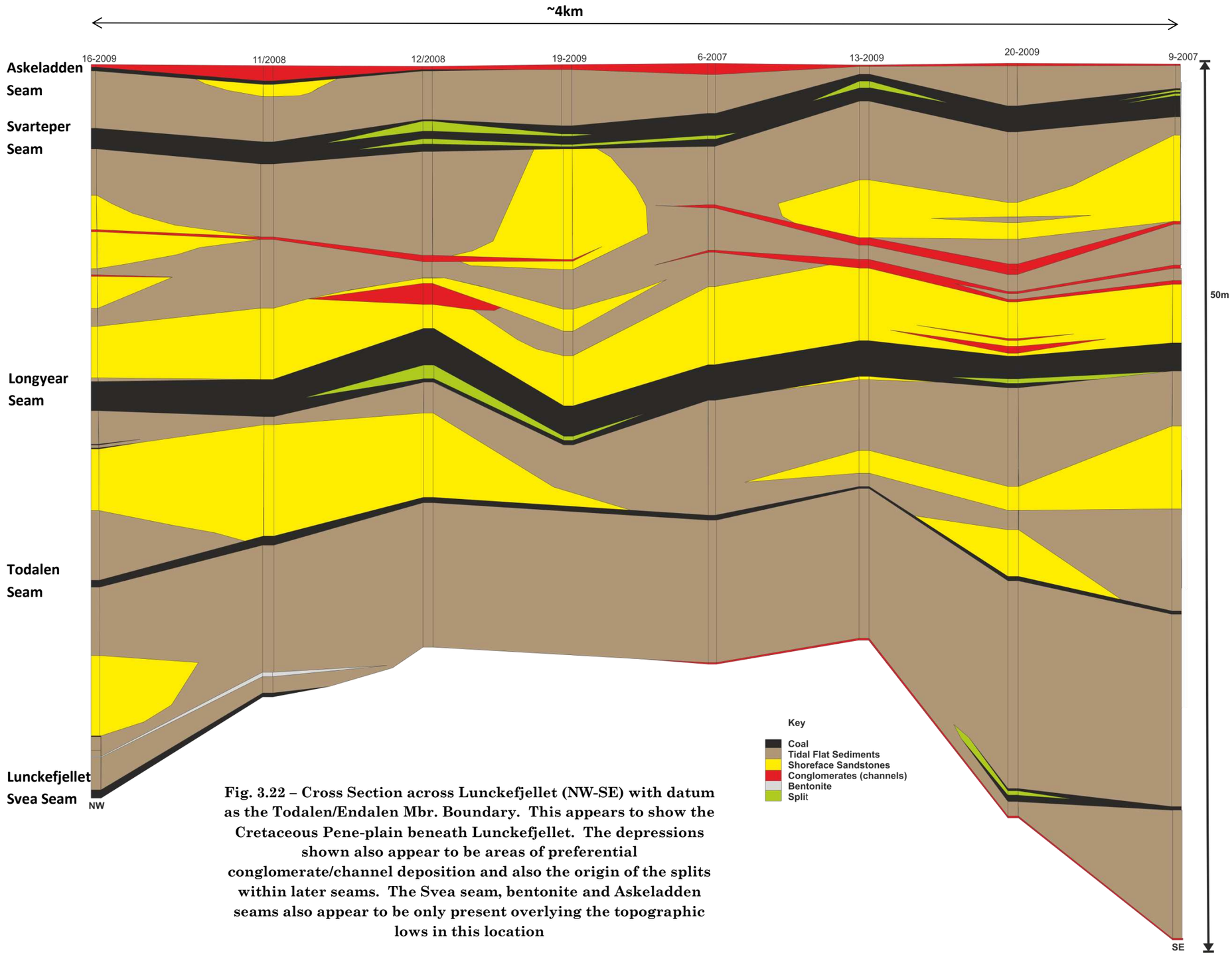

Fig. 3.22 – Cross Section across Lunckefjellet (NW-SE) with datum as the Todalen/Endalen Mbr. Boundary. This appears to show the Cretaceous Pene-plain beneath Lunckefjellet. The depressions shown also appear to be areas of preferential conglomerate/channel deposition and also the origin of the splits within later seams. The Svea seam, bentonite and Askeladden seams also appear to be only present overlying the topographic lows in this location

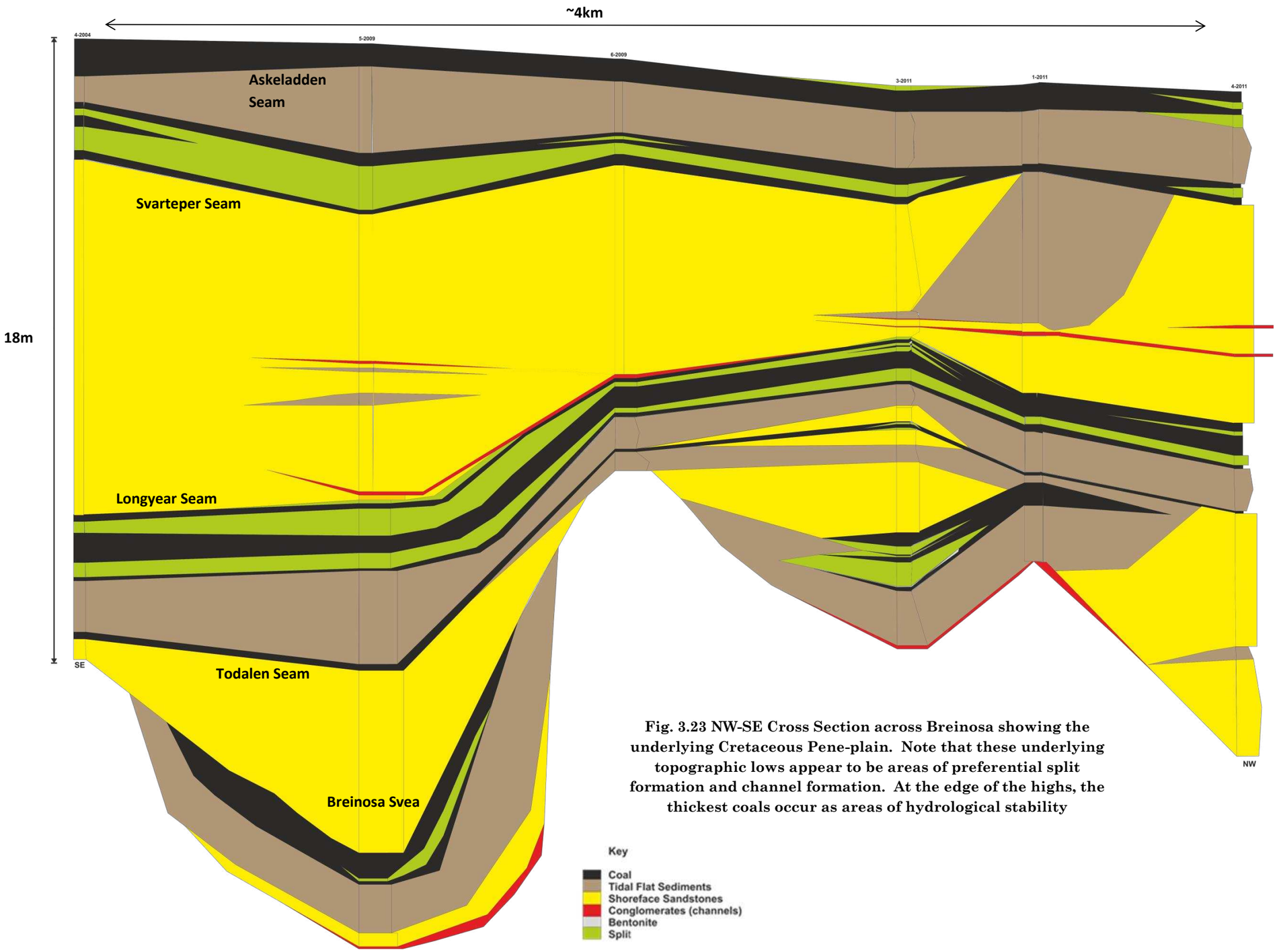

Fig. 3.23 NW-SE Cross Section across Breinosa showing the underlying Cretaceous Pene-plain. Note that these underlying topographic lows appear to be areas of preferential split formation and channel formation. At the edge of the highs, the thickest coals occur as areas of hydrological stability

The repeated formation of thick coals within different seams adjacent to the Tverdalen, Svea Nord and Billefjorden highs shows that they provided areas of hydrological stability for the duration of the formation of the Todalen Member.

The swells and troughs are not present within previous structural maps of the Central Tertiary Basin (Sokholov, 1968; Harland, 1997) indicating that these must be relatively minor features. However, they appear to have a significant control upon coal thickness. The same can also be said of the depressions identified from the Grønfjorden bed in the case of coal quality with lowest coal quality in the Lunckefjellet and Breinosa regions adjacent to persistent depressions.

As discussed previously (Section 3.53) these ridges and troughs appear to follow the regional trend (NNW-SSE) indicating they are structurally controlled. These ridges also appear to overly Triassic half-graben structures (Eiken,1986) indicating a basement control upon the Carolinefjellet valleys and subsequent coal thickness. The small-scale topographic highs and lows which make up the ridges and troughs may therefore represent either draping over previous structures or the reactivation of underlying structures during the early stages of the formation of the West Spitsbergen Orogeny. However, additional work is required to examine this further.

3.8 Conclusions

The use of coal isopach mapping alongside a palaeo-topography indicator such as the Grønfjorden Bed has proven effective for examining the landscape controls upon the Todalen Member. It has also allowed the examination the role of landscape on peat accumulation during base level rises. The technique also has allowed both low and high resolution reconstruction of the Longyear peatland allowing both the general and mine specific controls upon coal thickness and quality to be identified.

In addition;

- A number of structurally controlled topographic swells and depressions are highlighted by the position of the Grønfjorden bed. These appear to be controlled by underlying structure which was present or reactivated in response to the W. Spitsbergen Orogeny.
- Coal isopach maps have proven useful in showing the palaeogeographic controls upon coal thickness and the potential role of persistent topographic lows as a conduit for clastic sedimentation.
- The importance of the topographic control lessens over time with the Svea seam most affected and the Askeladden seam the least affected coinciding with increased marine influence within the basin, due to relative sea level rises.

- At high base levels underlying topography still has a key role in determining the position of the thickest coals. These are consistently found adjacent to topographic highs.

Chapter 4

ECONOMIC AND SOURCE ROCK POTENTIAL OF THE SVALBARD COALS

4.1 Introduction

The objective of this chapter is to characterise the maturity of the Svalbard coals and further investigate the observations of Orheim et al. 2007 regarding their oil potential. Coals are generally regarded as Type III Kerogens and gas prone, however a significant minority (particularly those formed in equatorial mangroves) are oil prone and provide a major contribution to world oil reserves. The discovery of oil prone coals formed at high latitude could therefore provide additional targets for exploration particularly in frontier regions such as the Arctic basin, Beaufort-Mackenzie and N.E Greenland.

Previous research has identified the equatorial Carboniferous Coals from the Pyramiden area of Svalbard as significantly oil prone, with high liptinite contents leading to the coal resembling a type II kerogen (Bojeson and Koefoed, 2009). Comparable high latitude oil prone coals are globally rarer; however the coals of the Taranaki basin (Sandison et al. 2004, Killops, 1994) may form the closest resemblance to those of Svalbard, forming at a similar palaeo-climatic position and geological period.

This chapter will attempt to classify the Svalbard coals in relation to their similarity to the equatorial type or 'Taranaki' type of oil prone coals, assess the maturity of the coal and characterise the amount and character of oils yielded. Possible economic implications of the research will also be investigated.

4.2 Oil Prone Coals

Two types of oil prone coal exist (Macgregor, 1994), one formed at high latitude (Sandison et al. 2002, Vu et al. 2009, Killops et al. 1994) and the other in equatorial regions (Van Koeverden et al, 2010, Van Koeverden et al., 2011, Bojeson-Koefoed et al., 2012, Macgregor, 1994) both of which can be found upon Svalbard in the Norwegian Arctic.

Oil-coals are economically important as oil source rocks and have been the subject of numerous publications over the past twenty years (e.g. Diessel and Gammidge, 1998; Sandison et al., 2002; Wilkins and George, 2002, Sykes and Johansen, 2006, Vu et al., 2009). Coals are generally defined perhydrous at >5.6wt% and orthohydrous at 4-5wt% H (Diessel, 1992) with a general trend of concurrent increase of H and S content (Petersen and Nytoft, 2006). Two main groups of oil prone macerals have been identified: liptinite and perhydrous vitrinite (Wilkins and George, 2002). Liptinites are derived from amongst others plant waxes and resins (spores, pollen, algae) and form the basis for 'equatorial type' coal oil potential.

The oil proneness of perhydrous vitrinite is more problematic with oil potential attributed to the destruction of liptinite during petroleum generation (Shanmugam, 1985), dispersed sub-microscopic lipids (Liu and Taylor, 1991) and the oil proneness of detro-vitrinites (Killops et al. 1994). In the case of the 'high latitude' type New Zealand Taranaki oil prone coals; the latter suggestion appears most appropriate, explained by microbial processing of organic source material followed by preservation by organo-sulfur molecule (OSM) formation (Killops et al. 1994; Diessel and Gammidge, 1998; Sandison et al., 2002).

4.2.1 Liptinite rich vs. Vitrinite rich perhydrous coals

Oil-prone coals consequently can be divided into two main types: liptinite rich & vitrinite rich (liptinite poor). The Gippsland Basin, Australia is a good example of a liptinite dominated oil prone coal. The Latrobe Formation of the Gippsland Basin is hydrogen rich (Hydrogen Index >300), liptinite and vitrinite rich with liptinite dominated by cutinite and resinite (Shanmugam, 1985). The coals are thought to have been formed in a lower coastal plain setting behind a wave-dominated linear shoreline. The oil generative potential of the coals appears to be related to distance from the palaeo-coastline with decreasing hydrogen index (HI) away from the coast and the huge brown coal deposits of Victoria (Peters et al, 2005).

The coals are postulated to have formed within an ombrotrophic raised mire at a time of high rainfall, high groundwater levels and cold climate (Shanmugam, 1985). The biomarkers reflect a gymnosperm dominated input of organic matter with significant amounts of tricyclic diterpanes (pimarane, phylloclodane). High hopanes/sterane ratios indicate that microbial degradation played an important part in the formation of the oil prone coals. This is thought to have liberated hydrogen rich material through the decay of lignin and cellulose. The oils generated are low in sulphur and contain a terrestrial Pr/Ph signature.

The New Zealand Buller Coalfield represents the Vitrinite rich/liptinite poor type of oil prone coal. The coals formed in the Eocene, in similar conditions to the more famous Taranaki basin oil prone coals (Norgate et al, 1997). The coals are Vitrinite dominated (~90%) with lesser liptinite (2-5%) and low inertinite content (funginite dominated; Norgate et al, 1997). The coals are orthohydrous –perhydrous (200-300) and were formed in a lower coastal plain setting. The climate during deposition is thought to have been sub-tropical and the coals show evidence of some marine influence.

The coals contain high levels of organic sulphur which has been associated with perhydrous coal formation. Unfortunately, the sulphur in some areas is thought to be secondary, an artefact of post depositional percolation of marine groundwater through overlying

sediments (Norgate et al, 1997). Secondary sulphur enrichment (although stored as organic sulphur) is thought not to play a significant role in perhydrous coal formation (Newman, 1991). The Buller coals do show evidence of high bacterial activity, which appears to be a common feature in the formation of both types of oil (even the spore dominated liptinite coals) prone coals.

The main features of the New Zealand Tertiary coals and of the 'perhydrous vitrinite' type oil prone coals in general can be defined by dominance of perhydrous vitrinites (Diessel and Gammidge, 1998), formation in a coastal setting with high organic sulfur content (Sandison et al., 2002) and high bacterial component (Rathbone and Davis, 2001)

4.2.2 – Oil Prone Coals within the Svalbard Region

Lower Carboniferous coals previously mined at Pyramiden, Svalbard (Abdullah et al. 1988, Nøttvedt et al. 1993, Harland et al. 1997, Tangedal, 2011) and found more widely within the Barents Region (Moi, 2008, Van Koeverden et al. 2011, Bojeson-Koefoed et al., 2012) are representative of the better studied 'equatorial' type oil-prone coal. Lower Palaeogene coal from the Central Tertiary Basin (CTB), Svalbard represents the less well studied high latitude type (Harland et al. 1997, Orheim et al. 2007). The oil potential of the Palaeocene coals on Svalbard has previously been limited to descriptions of expulsion of oil from polished sections (Orheim et al.,

2007) and reports of significant retortion yields in the geographically separate Tertiary sub-basin of the Kings Bay, Kongsfjorden Region (Hoel, 1925). The factors and conditions required to produce this type of oil prone coal are not well understood, in particular whether the warm Palaeogene climate was a contributing factor (Macgregor, 1994).

4.2.3 Approach

Coal was sampled (Fig. 4.1) from the Svea, Todalen, Longyear, Svarteper and Askeladden seams both in bulk and at high resolution from mine sections in Svea Nord and Mine 7 and from borehole BH5-2009, Breinosa region. The samples were then subjected to Soxhlet Solvent Extraction, Accelerated Solvent Extraction (ASE), Rock Eval Pyrolysis, element Analysis in order to examine the current oil potential of the coals (Methods in Chapter 2). The residues were then subjected to hydrous pyrolysis to determine maximum hydrocarbon yields (Chapter 2). Bulk retortion yields were simulated using nitrogen pyrolysis on an adapted hydropyrolysis rig (Chapter 2).

The maturity of the coals was determined using vitrinite reflectance (R_0), ^{13}C NMR, various organic maturity parameters (Chapter 2). This was used to determine the position of the coals within the oil window and to infer details regarding the burial history of the coals.

Organic Biomarker analysis, organic petrography including TPI and GI indices and Fe S Chemistry (Chapter 2) were used to examine the

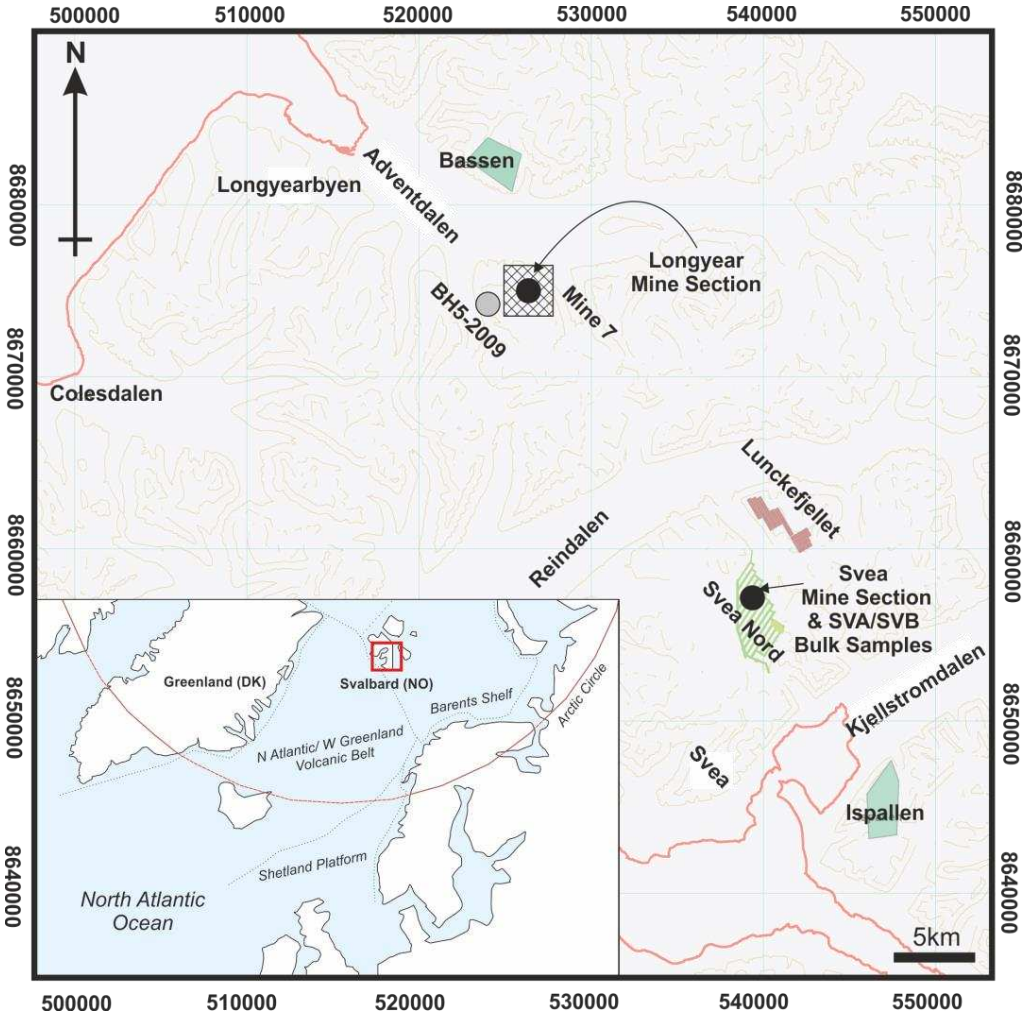

Fig. 4.1 – Map of the island of Spitsbergen showing the mines and settlements of the NW Central Tertiary Basin and sample locality and type.

effects of palaeo-environment upon oil potential over the life of the Longyear peatland.

4.3 Oil Content of the Longyear Coal

Soxhlet Solvent Extraction, ASE and Rock Eval (S_1) yields were measured and compared in samples of the Longyear coal to assess their free hydrocarbon content (Fig. 4.2 and Table. 1). In addition, the hydrogen content (% coal) was measured as it is considered an indicator of oil potential (Diessel, 1992, Wilkins and George, 2002). Each method of measuring hydrocarbon yield displays a similar trend, with lower yields at seam base, a transition around 80cm above seam base and elevated yields above (Fig. 4.2).

Each method varies greatly at the top of the seam. The coal in this area appears visually different from the rest of the seam in hand specimen, displaying conchoidal fracture and a bitumen like appearance. It is ash rich (>50%) and highly heterogenous under the microscope. It is this continued variability, after extensive processing which is deemed responsible for the observed bitumen yield variation. The Rock Eval S_1 parameter produces significantly reduced free hydrocarbon yields compared to the ASE and Soxhlet techniques although the values still indicate oil potential (S_1 >1mg/g rock; Tissot and Welte, 1994). This is probably due to the absence of the less volatile asphaltene fraction and its measurement as part of the Rock Eval S_2 parameter.

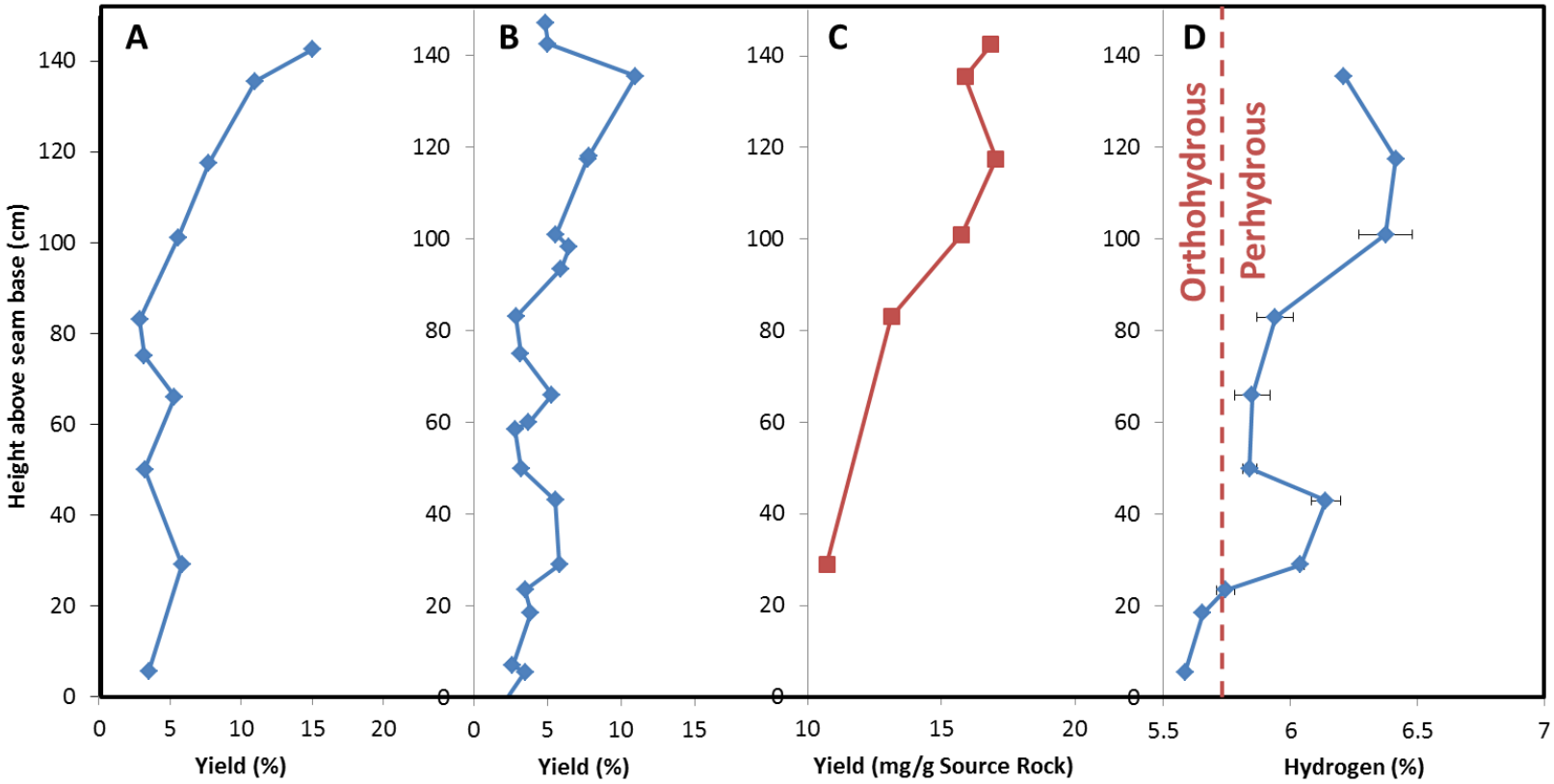

Fig. 4.2 – Comparison of (A) Soxhlet Solvent Extraction (B) Accelerated Solvent Extraction (C) Rock Eval (S_1) (D) Coal Hydrogen content (%) as a means of measuring the current hydrocarbon content of the Longyear coal. Note the similarity between yields from the Soxhlet and ASE techniques. Orthohydrous/Perhydrous definition *after Wilkins and George, 2002.* Selected repeated samples show a mean deviation from values shown of (A) 0.2% (B) 0.2% (C)2mg/g Source Rock

Seam	**LYR**	**LYR**	**LYR**	**LYR**	**LYR**	**LYR**	**LYR**	**LYR**	**LYR**	**LYR**
Seam Height (cm)	**5.5**	**7**	**18.5**	**23.5**	**29**	**43**	**50**	**58.5**	**60**	**66**
TOC (wt%)	80.1	80.5	81.2	81.5	82.5	82.1	82.3	82.9	83	82.5
Mean H (wt %)	5.58	-	5.65	5.72	6.03	6.1	5.82	-	-	5.8
ASE (mg/g Coal)	28.1	26.3	38.6	34.9	51.3	55.5	28.0	27.9	37.4	44.3
Soxhlet (mg/g Coal)	35.02	-	-	-	58.39	-	32.08	-	-	53.20
Hydrous pyrolysis (mg/g Coal)	195.4	-	-	-	332.1	-	-	-	-	259.5
Seam	**LYR**	**LYR**	**LYR**	**LYR**	**LYR**	**LYR**	**LYR**	**LYR**	**LYR**	**LYR**
Seam Height (cm)	**75**	**83**	**93.5**	**98.3**	**101**	**117.5**	**118**	**135.5**	**143**	**147**
TOC (wt%)	82.3	82	81.2	80.4	80.5	80.5	80.6	80.5	78	76.1
H (wt %)	-	5.99	-	-	6.3	-	6.41	6.21	-	-
ASE (mg/g Coal)	27.7	21.2	59.3	64.7	55.7	72.2	78.1	98.8	50.4	48.7
Soxhlet (mg/g Coal)	31.75	28.77	-	-	55.67	77.32	-	110.04	-	50.37
Hydrous pyrolysis (mg/g Coal)	-	253	-	-	-	292.1	-	268.7	-	-

Table 4.1 – Characterisation of the oil potential of the Longyear coal using Soxhlet Solvent Extraction, Accelerated Solvent Extraction and Hydrous Pyrolysis (TOC (wt%) and H (wt%) mean values derived from repeats)

Examination of the hydrogen content of the Longyear coal shows that much of the seam can be termed perhydrous (>5.7% H), with only the basal 20cm termed orthohydrous (5>H%<5.7) as defined by Diessel, (1992), Wilkins and George, (2002). The perhydrous nature of coal is strongly associated with oil potential. This link is supported by the free hydrocarbon yields measured in the Longyear seam where trends in hydrogen content correlate closely with those of free hydrocarbon content.

4.3.1 Oil Content of the other Svalbard Coals

The free hydrocarbon yields of both the Svea Nord and Breinosa Svea Seams are lower than seen in the lower Longyear Seam (<6 wt%; Table. 4.2). Samples adjacent to seam base or coal partings produce the highest yields (~6 wt%), perhaps representing a change in peatland character during these periods. Rock Eval S_1 pyrolysis yields are also reduced compared to the Longyear Seam. The lower oil potential of the Svea Coals is consistent with a very different formation environment to the Longyear (Section 6.8). This is supported by the sporadic distribution of the Svea seam compared to the more laterally expansive Longyear seam.

The Svarteper and Askeladden Seams by contrast exhibit similar free hydrocarbon yields to that of the upper Longyear Seam (>5 wt%). Some areas of the Svarteper and Askeladden Seams are often very ash rich (>50%) which limits oil potential. Rock Eval S_1 yields

Seam	Height above seam base (cm)	TOC (wt%)	ASE Yield (mg/g coal)
Breinosa Svea	124.5	81.4	39.7
Breinosa Svea	99.5	81.7	44.8
Breinosa Svea	74.5	82.6	53.5
Breinosa Svea	31	81.9	17.5
Breinosa Svea	7	82	25.4
Svea Nord	244.5	83	6.4
Svea Nord	167.5	82.4	48.1
Svea Nord	110.5	81.9	19.6
Svea Nord	63	81.5	39.1
Svea Nord	36.75	80.9	65.7
Svarteper	114.5	76.1	82.1
Svarteper	93.5	80.1	105
Svarteper	72.5	78.3	91.2
Svarteper	50	72.1	51
Svarteper	26.5	72.7	44.6
Svarteper	7.5	78.1	96.8
Askeladden	77.5	76.1	73.2
Askeladden	55	78.5	65.3
Askeladden	33	76.3	86.9
Askeladden	11	73.2	71.9

Table 4.2 – Oil Yields from the other Central Tertiary Basin coals using Accelerated Solvent Extraction (ASE)

are within the range of those measured in the Longyear seam (14-18mg/g coal). These similarities are unsurprising as the Svarteper and Askeladden peatlands occupy similar positions on the coastal plain to the Longyear peatland.

4.3.2 Kerogen type

A method for indicating kerogen type and consequently oil potential, is the Hydrogen Index (HI) parameter derived from Rock Eval pyrolysis ((S_2 * 100)/TOC). A HI value of >150 is generally considered indicative of oil potential (Petersen, 2005).

The Longyear coal samples (Fig. 4.3, Table. 4.3) show HI values ranging from 300 at seam base to 394 at seam top. This indicates that the Longyear seam represents a mixture of Type II and Type III kerogen. By contrast the HI of the lower Svea seam (Fig. 4.3, Table. 4.4.3) only exceeds 270 at the base of the seam before rapidly decreasing to values of around 200 consistent with predominantly Type III kerogen.

Using the adapted Van Kerevelen diagram, (HI vs. OI, Fig. 4.4) the Svalbard coals have higher HI values than would be expected from a Type III kerogen, this indicates that the coals are enriched with oil prone paraffinic material (as suggested by Killops et al., 1998). This indicates that the Longyear, Svarteper and Askeladden seams have significant oil potential.

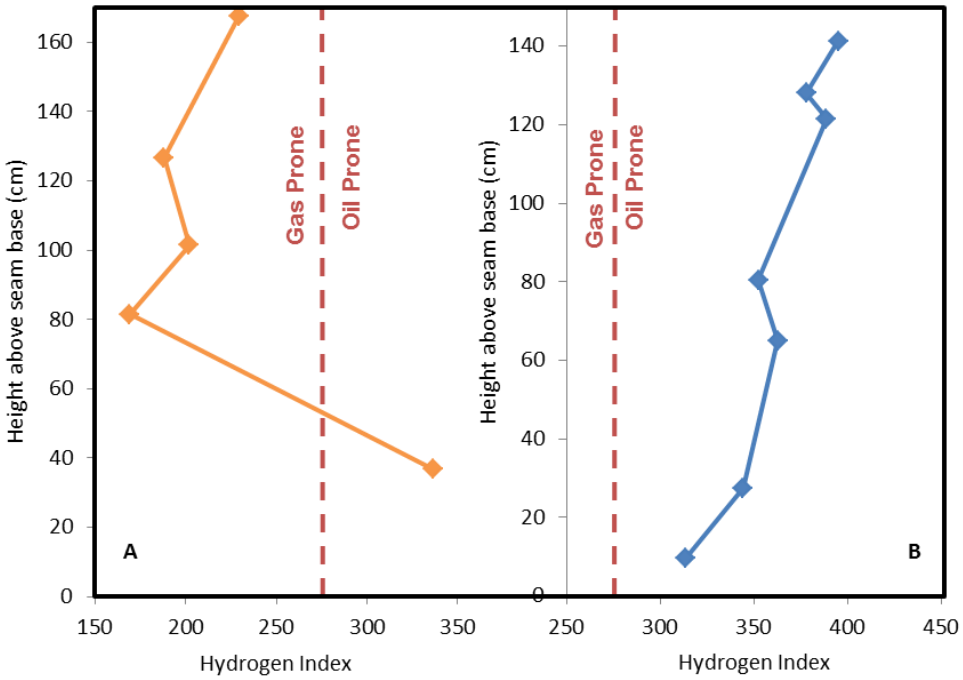

Fig. 4.3 – Comparison of the Rock Eval Hydrogen Index (HI) parameter within the Lower Svea Nord Seam (A) and the Longyear Seam in Mine 7 (B). Oil prone-Gas prone *after Wilkins and George, 2002).* Note that the entire Longyear seam is shown to have some oil potential

Seam	LYR	LYR	LYR	LYR	LYR	LYR	LYR	SVB	SVN
Height in seam (cm)	7	29	66	83	117.5	135.5	142.5	49.5	7
TOC (wt%)	80.1	82.5	82.5	82	80.5	80.5	78.2	82	82
S1 (mg/g coal)	12.07	10.71	13.1	15.8	17.03	15.88	16.84	10.59	15
S2 (mg/g coal)	238.3	261.5	275	268	295.31	287.26	300.05	204.69	256
S3 (mg/g coal)	2.26	2.07	1.83	2.53	2.59	2.12	3.54	2.51	5.5
Tmax (°C)	441	446	446	441	437	434	433	447	444
HI	296	317	334	326	366.84	356.84	383.7	250	311
OI	0.948	0.792	0.66	0.95	0.877	0.738	1.1798	3	6.7
PI	0.05	0.039	0.05	0.06	0.0545	0.0524	0.0531	0.05	0.1
S2/S3	105.4	126.3	151	106	114.02	135.5	84.76	81.55	47
Seam	**SVN**	**SVN**	**SVN**	**SVN**	**SVART**	**SVART**	**SVART**	**ASK**	**ASK**
Height in seam (cm)	**81.5**	**101.5**	**127**	**83**	**26.5**	**50**	**93.5**	**33**	**78**
TOC (wt%)	82.5	82.9	81.2	81.4	74.00	72	80	76	76
S1 (mg/g coal)	8.29	7.49	6.43	25.7	17.42	9.67	25.77	16.86	15
S2 (mg/g coal)	128.6	153.5	143	174	257.44	121.74	265.47	228.16	176
S3 (mg/g coal)	2.62	1.76	1.61	1.67	2.33	0.68	1.67	2.2	2
Tmax (°C)	442	447	448	443	437	441	452	446	437
HI	155.9	185.2	176	214	348	169	332	300.211	232
OI	3.176	2.123	1.98	2.05	3	1	2	2.89474	2.6
PI	0.061	0.047	0.04	0.13	0.06	0.07	0.09	0.06881	0.1
S2/S3	49.08	87.22	88.8	104	110.28	179.03	158.96	103.709	89

Table 4.3 – Rock Eval Pyrolysis results for the Svea Nord (SVN), Breinosa Svea (SVB), Longyear (LYR), Svarteper (SVART) and Askeladden Seam (ASK)

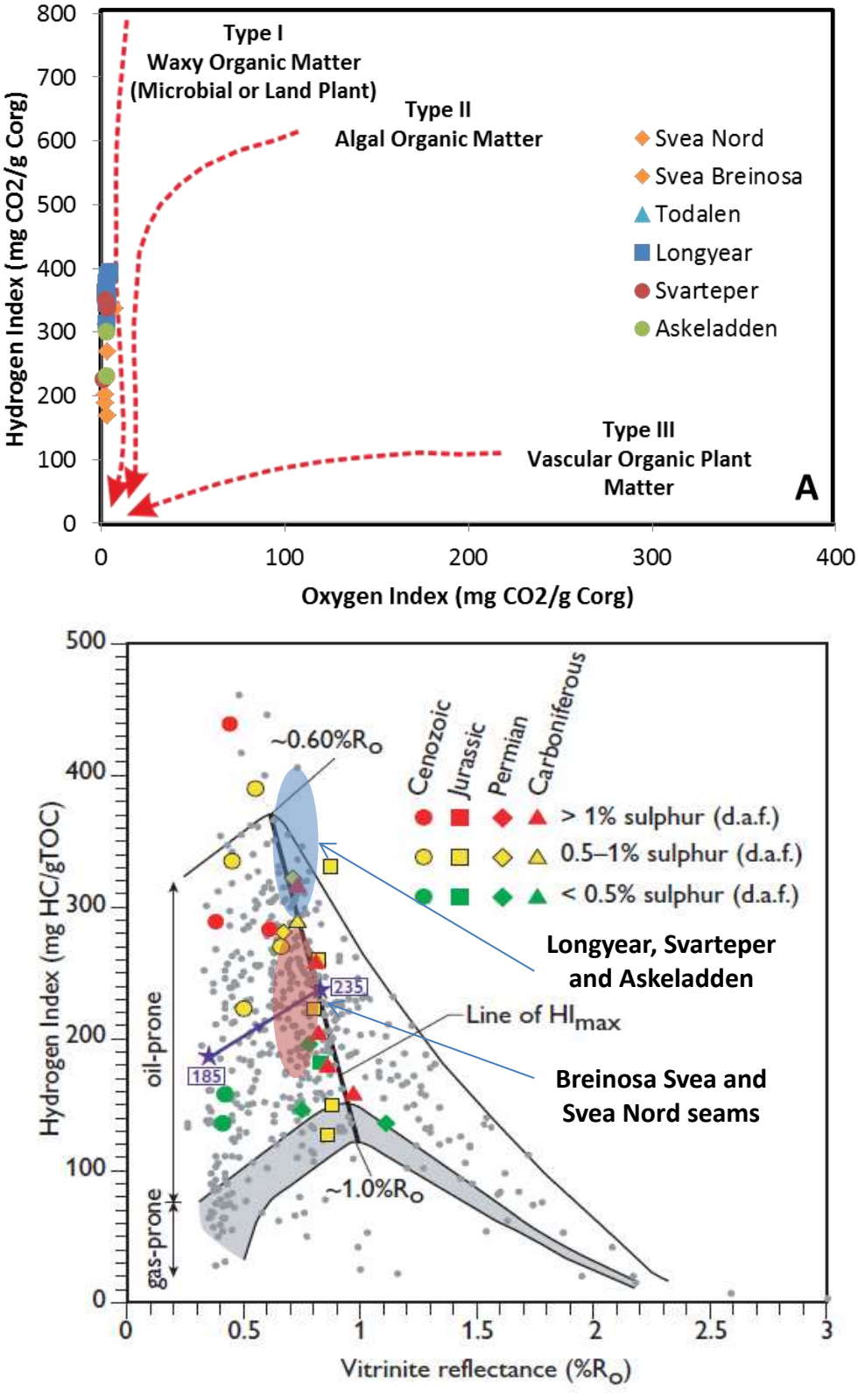

Fig. 4.4 – (A) Adapted Van Krevelen diagram (*after Meyers and Terranes, 2001)* using the Rock Eval HI and OI parameters. The Svalbard coals show values consistent with a mixture of Type I/II material and Type III material. (B) HI vs R_o diagram showing comparing the HI with coals from the Danish N. Sea, Greenland (After, Petersen, 2005). This shows the very high oil potential of the Longyear, Svarteper and Askeladden seams.

The HI vs. R_o diagram (Petersen, 2005) shows that all the Svalbard coals are oil-prone to a certain extent but the Longyear, Svarteper and Askeladden seams are comparable to the most oil prone coals studied. The HI_{max} line is caused by additional oil potential from the reorganisation of the coal structure at ~0.6% R_o (Petersen,2002). The maturity of the Longyear, Svarteper and Askeladden seams 0.78% Ro) shows that the coal had reached this stage before being uplifted and therefore the HI values seen are close to the maximum possible for these coals. There is also a general trend of more sulfur rich coals (Petersen, 2005) exhibiting higher HI values. This trend can also be seen within the Longyear seam (fig. 4.13).

The HI data therefore confirms the oil potential of the upper Todalen coals and indicates total geological yields from the coal could be comparable with the best of the oil-prone coals found in the region.

4.3.3 Prospective Geological Yield Estimates from the Svalbard Coals

Hydrous Pyrolysis yields (on Soxhlet extracted residues) and the Rock Eval S_2 parameter were used to predict prospective source rock potential from the Longyear coal. Rock Eval S_2 was applied to the remaining coals for comparison purposes.

The Longyear seam is shown (Fig. 4.5, Table. 4.1; 4.3) to produce broadly comparable yields from both of the above methods

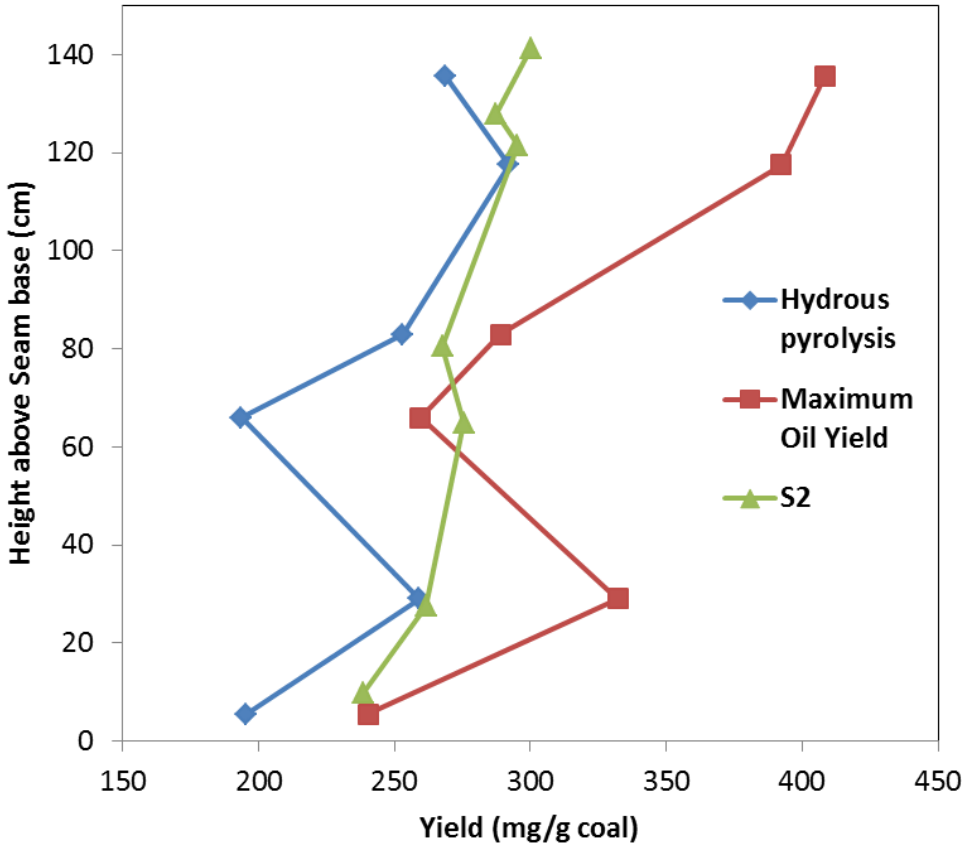

Fig. 4.5 Comparison of the Rock Eval (S_2) parameter with hydrous pyrolysis yields as a means of measuring future oil yields within the Longyear Seam. Maximum geological oil yields are derived from the addition of Soxhlet and hydrous pyrolysis yield. Note the similarity between the two techniques.

(>250mg/g coal) which is consistent with previous studies (Lewan, 2006). Both methods show a general trend of increasing yields up-seam. However, hydrous pyrolysis yields are much more variable compared to Rock Eval (S_2) yields and follow trends closely reflecting those seen in free hydrocarbon yields. This may be due to larger free hydrocarbon yields from Soxhlet solvent extraction compared to the S_1 parameter (80-150mg/g vs. 10-15mg/g). These excess hydrocarbons are then included as part of the S_2 peak leading to increased yields and lower variability compared to hydrous pyrolysis. Nevertheless, these results show that the Longyear coal would have significant further oil generative potential upon future burial.

Comparison of Rock Eval S_2 yields from the Longyear seam and the remaining Svalbard coals (Table. 4.3) shows similar trends to those seen in free hydrocarbon yields. The Svea seam has relatively low further oil potential with oil yields (<170mg/g coal). The Svarteper and Askeladden seams by contrast are again more similar to the Longyear seam and generally produce higher yields (>200mg/g). Lower yields in the Svarteper and Askeladden seams are due to higher ash content.

The production index (PI = $S_1/(S_1+S_2)$) is another measure of future oil potential. Values <0.1 indicate an immature source rock and values >0.4, a mature source rock (Maky and Ramadan, 2008). The Svalbard coals all have values approaching 0.1 (Table. 4.3),

Source Rock	TOC	Hydrous Pyrolysis		Rock Eval Pyrolysis (S2)	
	(Wt%)	mg/g rock	mg/g TOC	mg/g rock	mg/g TOC
Longyear Coal (This Study)	80	244	321	275	362
Longyear Coal (Uguna et al. 2012a)	79	273	348	273	214
Longannet Coal (Uguna et al. 2012a)	70	87	124	101	144
Oil Shales (Lewan 2006)					
Green River	25	148	1167	54	217
Timahdit	9	25	518	5	53
Gharab (Israel)	16	70	886	18	111
Ghareb (Jordan)	21	112	1073	33	158
Blackstone	54	109	404	176	325
Irati (US)	11	48	875	9	80
Glen Davis Torbanite	56	90	323	292	521
Phosphoria Retort	29	45	317	39	134
Pumpherston	29	65	453	42	146
New Albany Shale	15	35	475	12	82
Kukersite	45	276	1236	198	439
Alum Shale	12	4	69	7	57
Kimmeridge Shale (Uguna et al. 2012b)	25.5	178	614	174	682

Table 4.4 –Comparison of the hydrous pyrolysis and Rock Eval yields from the Longyear Seam with published oil shale data (Lewan, 2006) and other coals (Uguna et al., 2012a;b) on a TOC and rock basis

suggesting the coals were exhumed during the early oil window and therefore have yet to produce the majority of their hydrocarbons.

When compared to the Longannet coal (Uguna et al., 2012a) and oil shales/source rocks (Lewan, 2006, Uguna et al., 2012b), the Longyear seams economic potential is confirmed (Table. 4.4). Both hydrous pyrolysis and Rock Eval techniques show that on an economic basis (mg/g rock) the Longyear seam produces yields similar to the best performing oil shale (Ordovician Kukersite, Estonia, Lewan, 2006) deposits (246mg/g coal vs. 276mg/g shale respectively).

However, on a mg/g TOC basis, the Longyear coal is amongst the lowest performing of the oil source rocks compared. This indicates that although the coals contain significant TOC, the carbon is less reactive than the lower TOC oil shale.

4.3.4 Retortion yield estimates

Tertiary coals from the Kings Bay region were reported Hoel, (1925) to have been successfully retorted by low temperature distillation at small scale during the 1920's, producing average yields of 180-214 kg/ton. The Kings Bay and Central Tertiary Basin coals, now geographically separate are thought to be have been formed synchronously Harland et al., 1976. This historic precedent and sub-mature nature of the CTB coals point towards bulk retortion (in-

situ or ex-situ) as being the best method of realising the CTB coals' economic potential.

Retortion yields were simulated using nitrogen pyrolysis upon bulk CTB Coal samples (Table. 4.5). Whilst the Svea seam produces low yields (<50mg/g coal) from retortion, the Longyear, Svarteper and Askeladden seams show yields between 175-195mg/g coal similar to yields reported by Hoel, 1925 from Kings Bay (180-210 mg/g coal). This indicates that the retortion yields seen in Adventdalen from the upper CTB coals may be a basin wide feature, which would represent a significant oil resource In addition the oil produced was seen to be partially cracked during the retortion process, with the resulting free hydrocarbons comparable to other global crude oils (Fig. 4.6)

A useable sub-coke was also produced, which could either be used to power the retortion process or be sold locally for power generation. In the case of the Kings Bay coals (Hoel, 1925) this was considered to be around 66% of the input material with an additional 73 L/kg coal gas. Another advantage of the retortion process would be to reduce the sulfur content of the coals through the thermal decomposition conversion of pyrite (FeS_2) to pyrrhotite ($Fe_{(1-x)}S_{(x \text{ is } 0-0.17)}$) (Lambert et al., 1998) by between 30-50%. This would mean areas previously considered uneconomic to mine (S% >2%) would become available for extraction, increasing existing resource estimates.

Seam	Longyear	Svea Nord	Svarteper	Askeladden
Lower limit (cm above seam base)	118	102	83	66
Upper limit (cm above seam base)	147	127	104	89
Sample Thickness (cm)	29	25	21	23
Nitrogen Pyrolysis yield (mg/g Coal)	190	71	172	195

Table 4.5 – Yields from nitrogen retortion of bulk samples of the Svea Nord, Longyear, Svarteper and Askeladden Seams

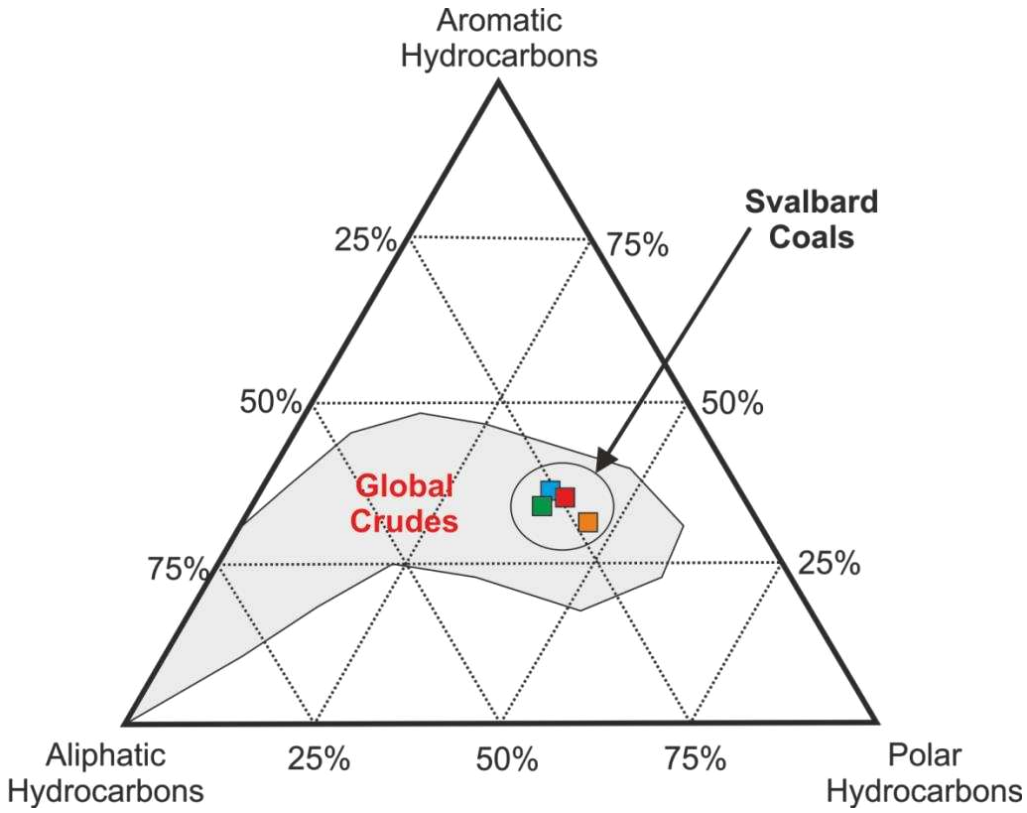

Fig. 4.6 – Composition of the oil yielded from nitrogen retortion compared to global crude oils (adapted from Lundegard and Knott, 2001) showing the retortion products composition within the range of natural crude oils

4.3.5 Resource Estimate for the Eastern Central Tertiary Basin

Orheim, (1982) estimated using Monte Carlo simulation that the coal within the CTB represented a maximum resource of 3,300Mt of which 600Mt was recoverable. Assuming a density of hydrocarbons at around 6.3bbl/ton and an average yield of 175mg/g coal, the maximum resource size could be as much as 3,638 Mbbl hydrocarbons in place with 661Mbbl hydrocarbons accessible by mining.

In-situ retortion methods would access the considerably larger deposits estimated by Orheim, (1982), which if used alongside coal gasification technology could yield significant quantities of liquid and gaseous hydrocarbons. However, the economics of such a scheme would depend upon a number of factors including distribution of oil prone material, recovery rates, oil quality, groundwater conditions and coal seam continuity which would require further study.

4.4 Maturity of the Svalbard Coals

The upper Todalen coals have been shown in the previous section to be sub-mature with PI values of around 0.1 (Maky and Ramadan, 2008). Previous vitrinite reflectance (R_0) studies from Adventdalen (Orheim et al. 2007, Manum and Throndsen, 1979, Throndsen, 1982, Paech and Koch, 2001) have indicated that the maturity of these

coals ranges from R_0 ~0.68% in the SW to as low as R_0 0.4% at the NE basin margin. This reflects the NE/SW trending synclinal structure of the basin.

A number of R_0 gradient estimates (Major and Nagy, 1972, Manum and Throndsen, 1979) have been produced for the Adventdalen region (0.17-032 % R_0/km) which has been used to infer a hyperthermal regime during burial (Paech and Koch, 2001) and extent of late Tertiary denudation (1.7km overburden loss; Manum and Throndsen, 1978).

However, Orheim et al. (2007) report a maturity gap between the Svea (R_0 0.78%) and Longyear seam (R_0 0.65%), seams which stratigraphically were only 40m apart. Orheim et al. (2007) proposed that the steep reflectance gradient was caused by insulation by the Svea seam had disrupted vertical heat transfer. Orheim et al. (2007) indicated that an alternative possibility was that a bitumen suppression effect could also be responsible, citing work by Diessel and Gammidge (1998). Apparent maturity gaps and maturity inversions appear relatively common within the Central Tertiary Basin, notably between Cretaceous and basal Tertiary material (Paech and Koch, 2001). This indicates that R_0 may not be as reliable an indicator of maturity in the CTB as previously thought.

4.4.1 Vitrinite Reflectance

Comparison of vitrinite reflectance of samples from the Svea Nord and Longyear seams (Table. 4.6) shows on a bulk basis the Svea Nord (SVA and SVB) and Longyear (LYR) samples reproduce the observed (Orheim et al. 2007) maturity gap closely (R_0 0.78/0.79% vs. 0.65% respectively).

However, examination at higher resolution shows the Lower Svea Nord and the Longyear to have very different trends up-seam. The R_0 of the Svea remains relatively constant (R_0 0.78%) whereas the Longyear varies significantly (R_0 0.78-0.52%) within the space of only 1.5m. The greatest change in reflectance occurs at around 80cm concurrently with the rise in oil potential described previously.

The different characters of the seams are further highlighted when examining the spread of reflectance data (Fig. 4.7). The distribution of vitrinite reflectance measurements from the Svea sample is relatively narrow around mean values (0.78±0.5%). The Longyear seam shows a much wider spread of data, particularly above 80cm with vitrinite reflectance measurements increasingly bi-modal (Fig.4.7). The Longyear seam also shows a gradual reduction in higher reflectance measurements up-seam.

4.4.2 Aromaticity of the Svea and Longyear Coals

Direct measurement of aromaticity (of which R_o is an indirect measurement) has been shown to be a useful tool in the derivation of

Seam	Seam Height (cm)	R_0	Pr/Ph	Pr/nc17	Ph/nC18	CPI(1)	Ts/Tm	c 29 βα/αβ	c30 βα/αβ	c31 S/(S+R)	c32 S/(S+R)	C33 S/(S+R)	C29/C30 αβ	C35/C34 αβ	C29 S/S+R	C29 B/B+A	TS/TH	MPI-1 [a]	Calculated R_0 [b]
			n-alkanes				Hopanes								Sterane			Aromatic	
Svea Nord	Bulk	0.78	7.1	0.9	0.1	1.05	0.95	0.05	0.07	0.64	0.62	0.63	0.75	0.31	0.54	0.46	0.23	0.60	0.76
Longyear	Bulk	0.65	13.40	4.50	0.20	1.10	0.93	0.05	0.10	0.64	0.63	0.61	0.75	0.41	0.56	0.49	0.19	0.63	0.78
Svea Nord	7	0.77	4.48	24.55	4.43	1.46	0.93	0.09	0.08	0.58	0.58	0.58	0.58	0.43	0.42	0.51	0.21	0.48	0.69
Svea Nord	82	0.78	4.82	2.80	0.43	1.54	0.93	0.08	0.12	0.60	0.60	0.62	0.60	0.16	0.48	0.5	0.19	0.65	0.79
Breinosa Svea	75	0.78	3.51	22.48	3.77	1.41	0.94	0.07	0.09	0.59	0.59	0.62	0.63	0.23	0.51	0.51	0.19	0.51	0.71
Breinosa Svea	50	0.78	6.29	17.33	2.01	1.50	0.95	0.10	0.11	0.60	0.60	0.61	0.59	0.14	0.54	0.5	2	0.51	0.70
Breinosa Svea	100	0.79	3.53	2.70	0.66	1.54	0.93	0.08	0.09	0.62	0.62	0.64	0.56	-	0.47	0.53	0.2	0.49	0.69
Breinosa Svea	125	0.76	26.54	75.45	1.87	1.42	0.92	0.08	0.10	0.59	0.59	0.62	0.47	0.19	0.45	0.55	0.2	0.47	0.68
Todalen	-	0.75	20.99	119.83	2.93	1.39	0.93	0.06	0.07	0.60	0.60	0.63	0.55	0.28	0.47	0.49	0.21	0.57	0.74
Svarteper	73	0.65	3.01	0.68	0.27	1.40	0.91	0.10	0.05	0.58	0.58	0.59	0.50	-	0.48	0.52	0.2	0.76	0.86
Svarteper	94	0.65	6.49	9.99	0.97	1.57	0.95	0.09	0.13	0.60	0.60	0.61	0.61	0.16	0.49	0.51	0.21	0.56	0.74
Askeladden	33	0.64	2.95	6.23	1.73	1.39	0.94	0.11	0.10	0.59	0.59	0.62	0.54	0.29	0.48	0.5	0.21	0.52	0.71
Longyear	143	0.501	3.46	7.75	0.18	1.40	0.92	0.08	0.06	0.58	0.58	0.60	0.51	0.49	0.43	0.51	0.2	0.51	0.71
Longyear	143	0.538	11.44	12.22	1.34	1.59	0.93	0.11	0.07	0.60	0.59	0.60	0.67	0.30	0.45	0.49	0.18	0.51	0.71
Longyear	136	0.561	10.13	20.67	1.56	1.53	0.94	0.10	0.11	0.60	0.57	0.60	0.60	0.31	0.43	0.50	0.2	0.49	0.69
Longyear	118	0.586	11.41	17.37	1.15	1.56	0.95	0.09	0.12	0.60	0.59	0.62	0.62	0.30	0.45	0.50	0.21	0.55	0.73
Longyear	83	0.628	13.42	15.42	0.81	1.62	0.93	0.08	0.09	0.61	0.58	0.61	0.60	0.03	0.41	0.52	0.22	0.49	0.69
Longyear	66	0.655	12.11	5.29	0.33	1.69	0.93	0.08	0.10	0.61	0.58	0.60	0.62	0.41	0.41	0.52	0.23	0.55	0.73
Longyear	29	0.74	12.31	6.20	0.35	1.72	0.93	0.10	0.10	0.60	0.58	0.59	0.62	0.31	0.40	0.51	0.18	0.54	0.73
Longyear	7	0.74	13.60	2.34	0.16	1.69	0.94	0.11	0.12	0.60	0.57	0.61	0.63	0.31	0.42	0.51	0.19	0.45	0.67

Table 4.6 – Vitrinite Reflectance (R_0), *n*-alkane, hopane, sterane and aromatic biomarker and maturity parameters within the Central Tertiary Basin coals. [a] *after* Cassani *et al.*, 1988, [b] *after* Radke and Welte, 1983

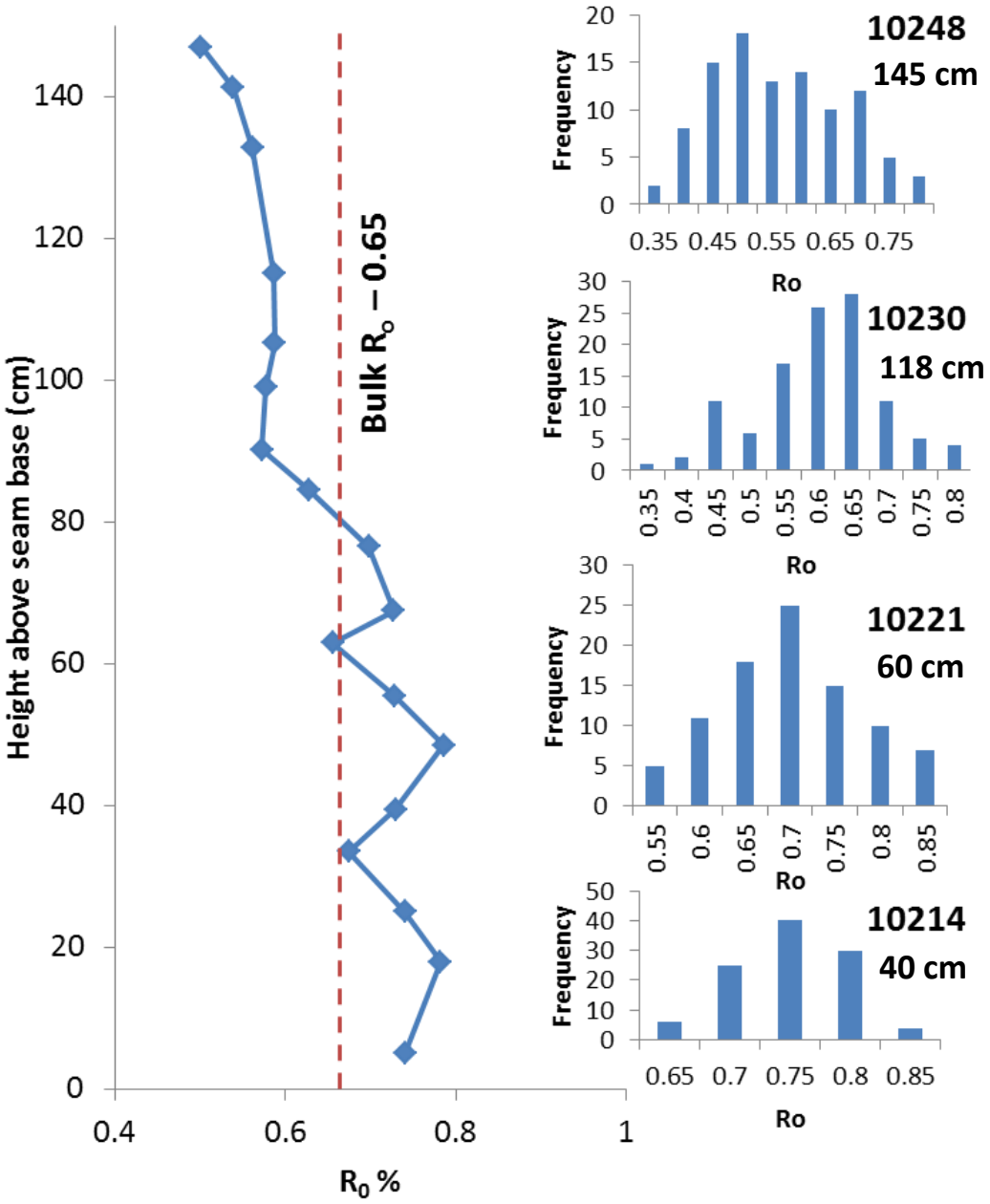

Fig. 4.7 - Variation in rank (R_0) within the Longyear seam in Mine 7, Adventdalen. Examination of the distribution of vitrinite reflectance values measured shows a shift to lower values, bi-modal distribution upseam.

maturity in some coals (Carr and Williamson, 1990; Stephens et al., 1985) due to the loss of aliphatic components with increasing maturity. Aromaticity in bulk samples of the Longyear and Svea seams.was compared using ^{13}C NMR (Fig.4.8).

The aromaticity (%) of the Svalbard coals differs greatly between the Longyear and Svea seams (50% vs. 70% respectively). Using the calibration of Carr and Williamson, (1990), equivalent R_0 values of 0.76 % (Svea) and 0.5% (Longyear). This is clearly not the case, as the Longyear seam bears no resemblance to a brown coal and has been shown to have entered the early oil window. Whilst, the Svea, which is not oil prone, exhibits an aromaticity consistent with its observed maturity. Consequently, the observed maturity gap between the Svea and Longyear seams must be caused by significant amounts of aliphatic (Type I/II) material within the Longyear seam.

To produce this suppression effect from normal bituminous Svea coal (75 parts aromatic: 25 parts aliphatic), additional aliphatic carbon within the oil prone Longyear coal would account for 33% of total carbon. This is approximately equivalent to 380-400mg/g TOC, which is very close to the HI values observed at the top of the seam. This observed additional macromolecular aliphatic material must therefore be the source of both the maturity gap and the Longyear seams oil potential.

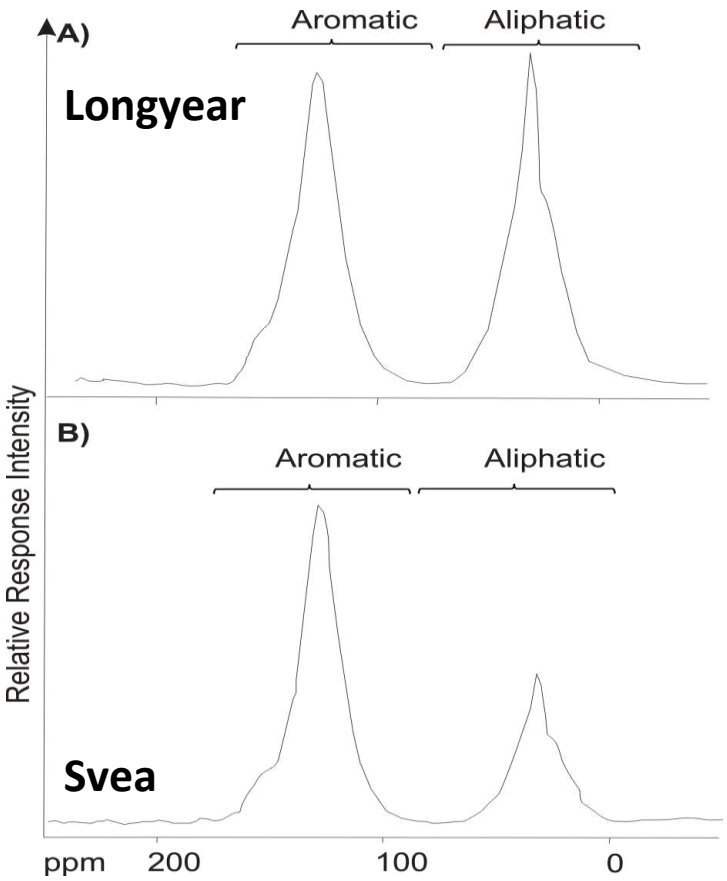

Fig. 4.8 Aromaticity of the Svalbard Coals (A) LYR and (B) SVB. Note the large difference between the seam indicating an apparent maturity equivalent to that of R_0 0.5% and 0.78% respectively (Carr and Williamson, 1990). This cannot be the case as the Longyear is not a lignite, therefore the Longyear is enriched with non-coaly aliphatics.

4.4.3 Organic Maturity Parameters

To examine the true maturity of the Svea Nord, Longyear, Svarteper and Askeladden seams, the Rock Eval T_{max} and organic geochemical biomarkers of Soxhlet extracted oils were used. T_{max}, like many maturity parameters is highly dependent upon source material (Peters 1986) but is considered of use for assessment of Type II material (420-460°C) and Type III (400-600°C; Tissot et al., 1987). Organic geochemical maturity parameters can be highly specific at low maturities but often reach equilibrium at around R_0 0.7%, making many of little use at higher maturities (Peters and Moldowan, 2005).

T_{max} ranges from 434–447°C for all the Svalbard coals indicating a maximum maturity in the early-mid oil window (Table. 4.3). Coals from the Svea Nord seam are slightly more mature than those in Adventdalen, consistent with the southward tilting of the Central Tertiary Basin. Values of T_{max} appear slightly high compared to PI values which indicate that the coals are sub-mature. This may be due to the extended oil window of coals compared to other conventional source rocks (Petersen, 2006)

Aliphatic maturity parameters for the Todalen coals are at or approaching equilibrium (Table. 4.6) indicating a maturity in excess of R_0 0.7%. Notably, both sterane and hopane maturity parameters shown no change up-seam in the Longyear (Fig.4.9) providing

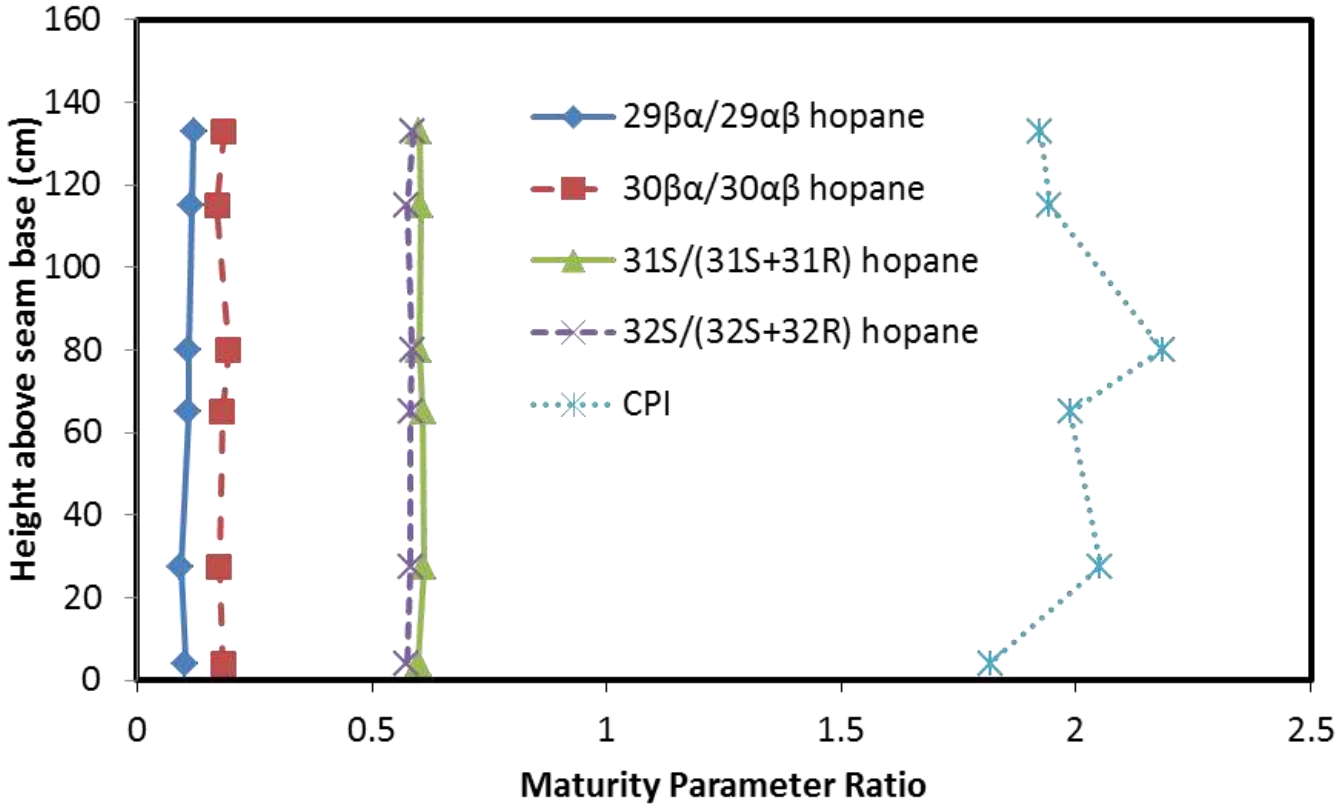

Fig. 9. Variation in hopane and *n*-alkane maturity parameters up-seam within the Longyear seam. Note little variation in maturity up-seam indicating no maturity gap.

further evidence of R_0 suppression at the top of the seam. It therefore indicates that R_0 values from the 'Svea' like lower Longyear seam are likely to represent the true maturity of the Longyear seam at around 0.76%,

Consideration of the aromatic Methylphenanthrene Index, MPI-1 (Radke et al., 1982; Radke et al., 1986 Radke, 1988) indicates there is a maturity gap between the two coals. However as the majority of the evidence presented above indicates otherwise and MPI-1 ratios can be affected by differences in source organic matter and migration (Peters et al., 2005) it is thought that the MPI-1 is a relatively poor indicator of the maturity of the Svalbard coals.

The geochemical evidence points to the two seams having comparable maturities and thermal histories. Significantly, the R_o maturity gap seen both within the Longyear seam and between the Svea and Longyear seams is not reproduced geochemically. It is thought that retardation of R_o by aliphatic enrichment of vitrinites is likely to play a dominant role in the steep reflectance gradient between the upper and lower Todalen seams. This places the Svalbard coals within the early to mid-oil window at peak burial, conforming to the production and migration of hydrocarbons described by this study and Orheim et al. (2007).

4.4.4 Implications for local and regional erosion models

Although previous local studies have noted significant R_0 variations between samples (Paech and Koch, 2001), the R_0 values used in these studies underestimate the maturity of the coals (0.65%, Paech and Koch, 2001; Manum and Throndsen, 1978 vs. ~0.78% this study). This is particularly true within the Adventdalen region where sampling is skewed towards the more easily accessible upper Todalen seams due to the Svea seams erratic thickness and distribution.

As a result of this the burial depth and loss of overburden must be greater than previously estimated (Manum and Throndsen, 1979, Paech and Koch, 2001). Also, the vitrinite reflectance gradient in the Adventdalen region between the Cretaceous and Tertiary is reduced to ~0.15%/km, similar to the estimates of Major and Nagy (1972) of 0.17%/km. This indicates that whilst the Central Tertiary Basin may still be classed as a hyperthermal basin (Paech and Koch, 2001) the reflectance gradient and inferred geothermal gradient was lower than presented by Manum and Throndsen (1979) of 0.33%/km.

Within a regional context, the Northern Barents including Svalbard (regarded as an uplifted NW edge of the Barents Shelf, Harland et al. 1997) was subjected to greater burial and subsequent uplift and erosion than previously thought (Paech and Koch, 2001, Manum and Throndsen, 1978) and consequently should be a greater source of

sediment load to the Southern Barents during the Tertiary. In addition, although hyperthermal conditions (Robert 1985) within the N. Barents Shelf during the late Cretaceous-Tertiary associated with N. Atlantic extensional tectonics is still inferred. The inferred influence of contemporaneous volcanism on geothermal gradient is thought to have been more limited than previously suggested (Paech and Koch, 2001).

4.5 Origins of the Oil Potential of the Longyear seam

Having demonstrated high oil yields from the coal it is now necessary to determine whether or not the coal is the source of the oil. Although this is expected, other sources are possible, for example the surrounding shale. This will also help determine the palaeo-environmental conditions required to form high latitude oil prone coals.

4.5.1 – Provenance of extracted hydrocarbons from the Longyear Seam

Alkane distributions (Fig. 4.10) within the Longyear seam are dominated by chain lengths in the range nC$_{20}$–nC$_{30}$ with peak concentrations around nC$_{23\text{-}24}$ consistent with a terrigenous/lacustrine source (Peters and Moldowan, 2005)

The high maturity of the Svalbard coals (R_o ~ 0.78) does not allow *n*-alkane distribution to be used as a clear indicator of the

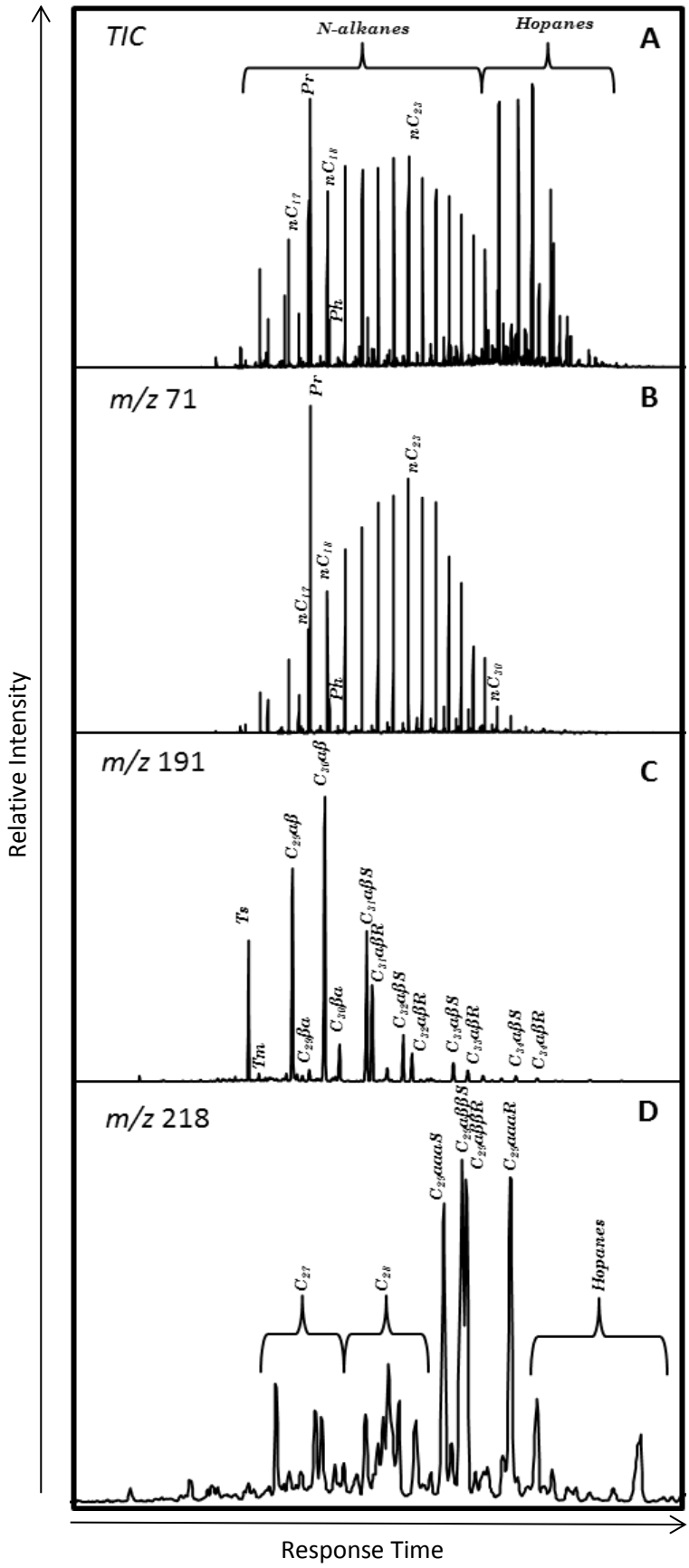

Fig. 4.10 Typical mass chromatogram from the Longyear coal at 117cm above seam base. (A) Total ion chromatogram. Note the high hopane concentrations. (B) *m/z* 71 chromatogram showing *n*-alkane distribution, peak concentrations at around nC_{23} (C) *m/z* 191 chromatogram showing hopane distribution (D) *m/z* 218 chromatogram showing sterane distribution

environment from which the bitumen is sourced. Maturity issues also prevent the use of established source proxies such as Paq (Ficken et al., 2000) and Phragmites preference index (Freese et al., 2008) and *n*-alkanes show little odd over even predominance, with carbon preference index values (CPI(1), Bray and Evans, 1961) close to maturity ~1.

The Pristane/Phytane (Pr/Ph) value of the Longyear seam are all >3. Pristane and phytane are considered a good indicator of redox conditions within sediments. Pristane formation is favoured by oxic conditions, phytane by reducing and therefore Pr/Ph ratios >3 are indicative of terigenous plant input.

The Pr/nC$_{17}$ ratio increases significantly up-seam, accompanied by an increase in the relative peak size of the hopanes, relative to the *n*-alkanes. Alexander et al., 1981 suggest that organic matter composition and post depositional biodegradation may increase the Pr/nC$_{17}$ ratio. Increasing biodegradation is considered more likely particularly due to the low preservation of lighter n-alkanes and lower peak intensities of the remaining alkanes when compared to other biomarker species

Gymnosperm biomarkers 4ß-19-norisopimarane, isopimarane/pimarane and ent-beyerane in oil from the Longyear seam indicate a terrestrial source. This is consistent with previous analysis by Ćmiel and Fabiańska (2004). The tricyclic diterpanes

isopimarane (or pimarane), 4ß(H)-19-norisopimarane and ent-beyerane are common constituents of gymnosperm resins with precursors found in decayed pine needle litter (Otto et al., 2005). 4ß(H)-19-norisopimarane has also been used as a higher plant indicator within source rocks from the Qaidam Basin, China (Hanson et al., 2001). No angiosperm biomarkers (oleanane, gammacerane) were detected.

The *m/z* 218 chromatogram (Fig. 4.10) shows the sterane composition of the free aliphatic maltene fraction of the Svalbard coals. These are dominated by C_{29} steranes with a complete absence of C_{30} steranes, which is indicative of a terrestrial source (Philp, 1994). Using the sterane discrimination diagram (Huang and Meinshein, 1979, Shanmugam, 1985), the sterane distribution of the Longyear seam is consistent with a higher plant terrigenous source (Fig.4.11).

The hopanes (Fig.4.10) are dominated by C_{29} and C_{30}, αß homologues with preservation of the C_{31-34} homohopanes. Hopanes comprise a significant component of bitumen in the Longyear coal and unusually can be seen in the TIC chromatogram (Fig. 4.10). High hopane contents are thought to be characteristic of terrestrially sourced bitumens (Peters and Moldowan, 2005).

The total absence of marine biomarkers (e.g. C_{27}/C_{30} steranes, Low Pr/Ph etc.) within the bitumen and residue phases rules out

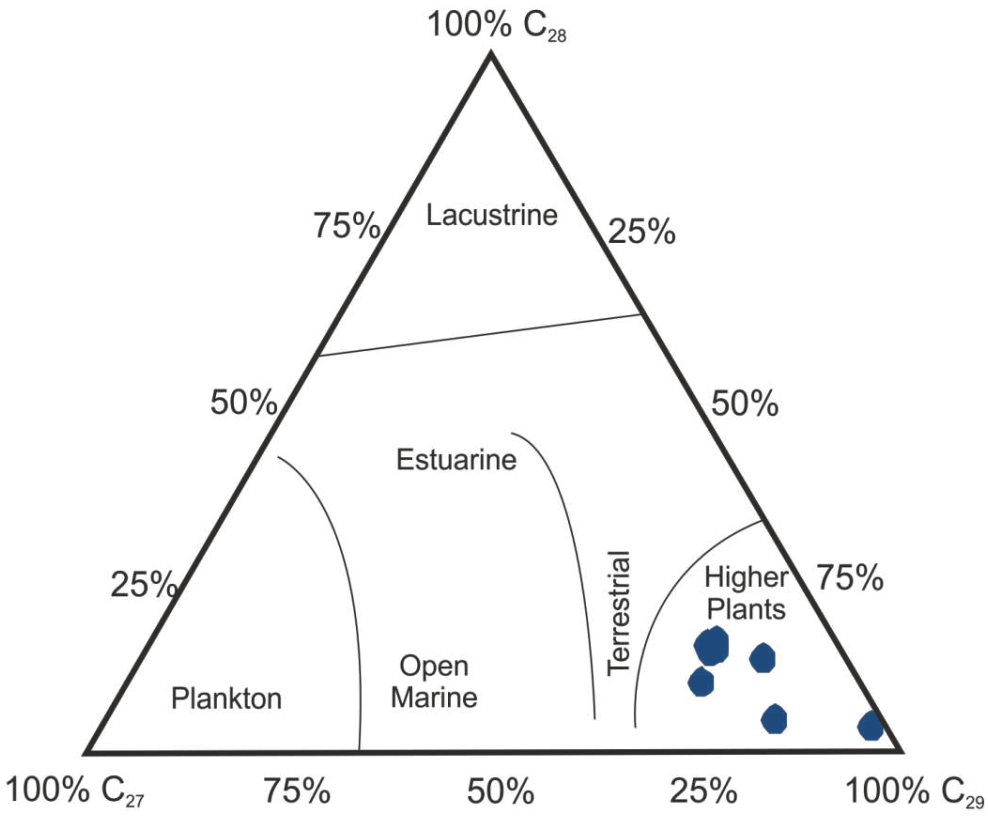

Fig. 4.11. Sterane discrimination diagram (*after* Huang and Meinshein, 1979) showing the dominance of terrigenous steranes within the Longyear coal.

migration from marine shales present deeper within the basin. It is therefore concluded that the bitumen contains significant terrestrial component, and is sourced entirely from the coal.

4.5.2 Peatland environment and Oil Potential

Coal Maceral analysis has been shown to reflect the hydrological conditions within peatland (Diessel, 1986). Maceral indices such as gelification index (GI) and Tissue Preservation Index (TPI) provide information regarding the wetness/dryness and humification/tree density respectively (Diessel, 1986, Casareo, 1996). Due to the virtual absence of macrinite GI is defined by (1) and TPI by (2) within the Svalbard coals;

$$(1) GI = \frac{Vitrinite}{Inertinite}$$

$$(2) TPI = \frac{Telovitrinite + fusinite + semifusinite}{Detrovitrinite + inertodetrinite}$$

In order to understand which peatland conditions were most favourable for subsequent oil potential, the maceral composition of the Svalbard coals was plotted on a GI vs. TPI diagram (Fig. 4.12, after Diessel, 1986, Casareo et al, 1996).

The Svea Nord and Breinosa Svea seams formed in peatlands with high TPI and low-intermediate GI values consistent with formation in a raised bog type environment. The oil prone Longyear, Svarteper and Askeladden seams by contrast show generally low TPI values

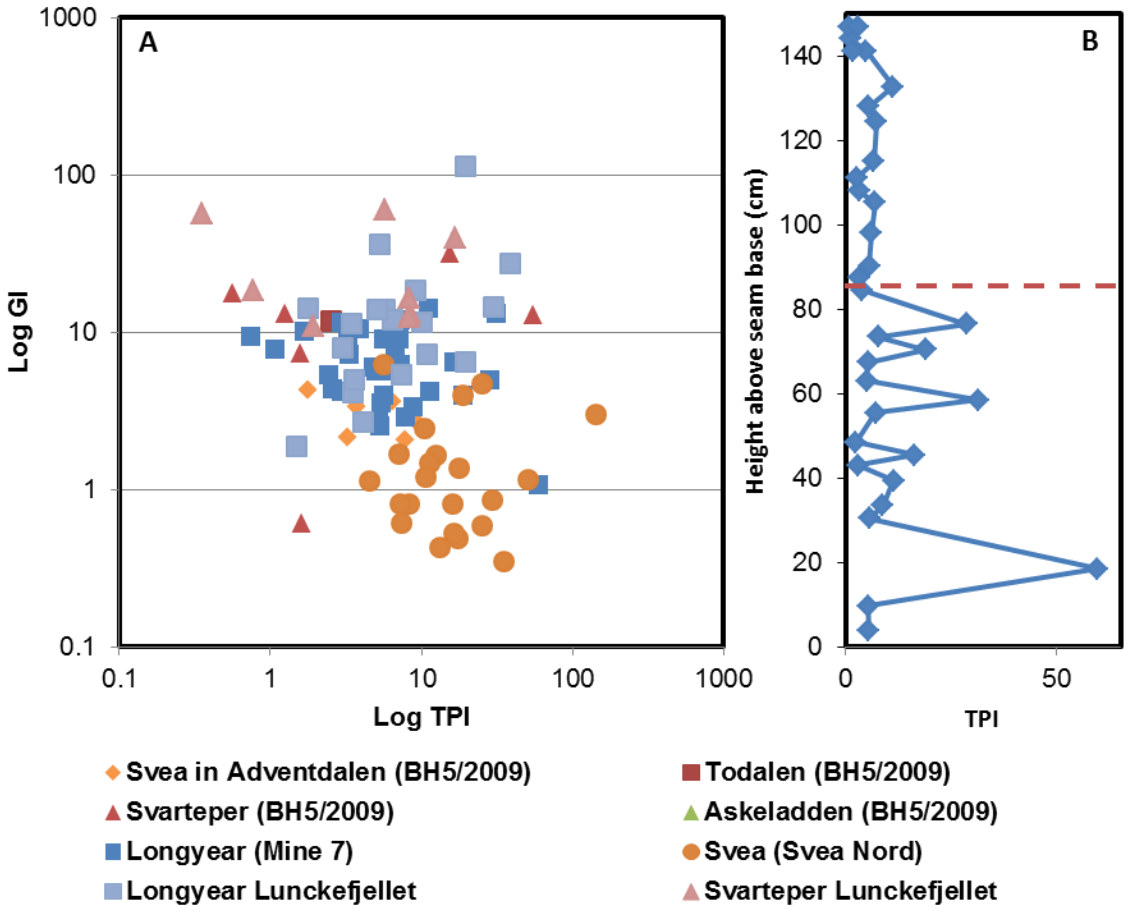

Fig. 4.12 (A). Tissue preservation index (TPI) vs. Gelification index (GI) (after Casareo et al., 1996) of the Svalbard Coals. Note that the coals with most oil potential are characterised by low TPI, high GI values.

and high GI values indicating that formation in a wet environment with high levels of humification/low tree density (Casareo et al. 1996, Diessel, 1986) are optimal for high latitude oil prone coal formation

Examination of the TPI profile (Fig. 4.12) of the Longyear seam shows that initially the hydrological supply to the Longyear seam was precipitation dominated and highly variable (high TPI and inertinite rich layers). At 80cm, the transition seen in oil yields is replicated in TPI values, dropping from ~28 to ~5. These values indicate a change to wetter, lower tree density conditions. This is consistent with replacement of the earlier 'Svea' like ombrotrophic (Precipitation supplied) raised bog with a rheotrophic (groundwater) fen. It is this fen environment which appears to provide the greatest oil potential which is likely associated with a thinner oxic zone.

The transition from raised bog to fen conditions is likely to be associated with rising sea levels. Higher base levels result in shallower groundwaters (Fan and Miguez-Macho, 2011; Gaiser et al., 2001) increasing the groundwater contribution to the peatland. Increasing regional groundwater input to the peatland end dependence upon local catchments and precipitation, leading to the more and hydrologically stable conditions which characterise fens.

Another important aspect of the environment is the supply of sulfur which is implicated in stabilising the aliphatic components within

the coal. Seawater is a significant source of sulfur to coastal regions with sea spray representing a major transport mechanism (Harkel, 1997). Rates of deposition of sea salt and sea salt sulfate decrease rapidly inland (Gustafsson 2000; Mahowald et al., 2006; Harkel, 1997) and consequently coal sulfur content should reflect the amount of marine input into the peatland.

The effect of increasing relative sea levels can be seen in the Longyear seam (Fig. 4.13). Sulfur contents remain relatively constant below 80cm (~0.5%; Fig. 4.13). Above 80cm, sulfur content increases rapidly along with the oil yield reaching a maximum of 2% S at the top of the seam (Fig. 4.13) consistent with previous work on the link between sulfur supply and perhydrous coal formation (Wilkins and George, 2002; Sandison et al., 2002)

4.5.3 Microbial Proccessing and Liberation of Oil Prone components

Marine influence prevents acidification of peatland, allowing optimum conditions for both aerobic and anaerobic decomposition, allowing separation of hydrogen rich components from insoluble ligno-cellulosic nucleus (Hao and Chen, 1992).

Hopanes originally thought to be confined to aerobic bacteria have also recently been found in anaerobic species *geobacter* (Härtner et al., 2005). This would indicate high hopane concentrations may be more reflective of overall bacterial activity rather than that of solely

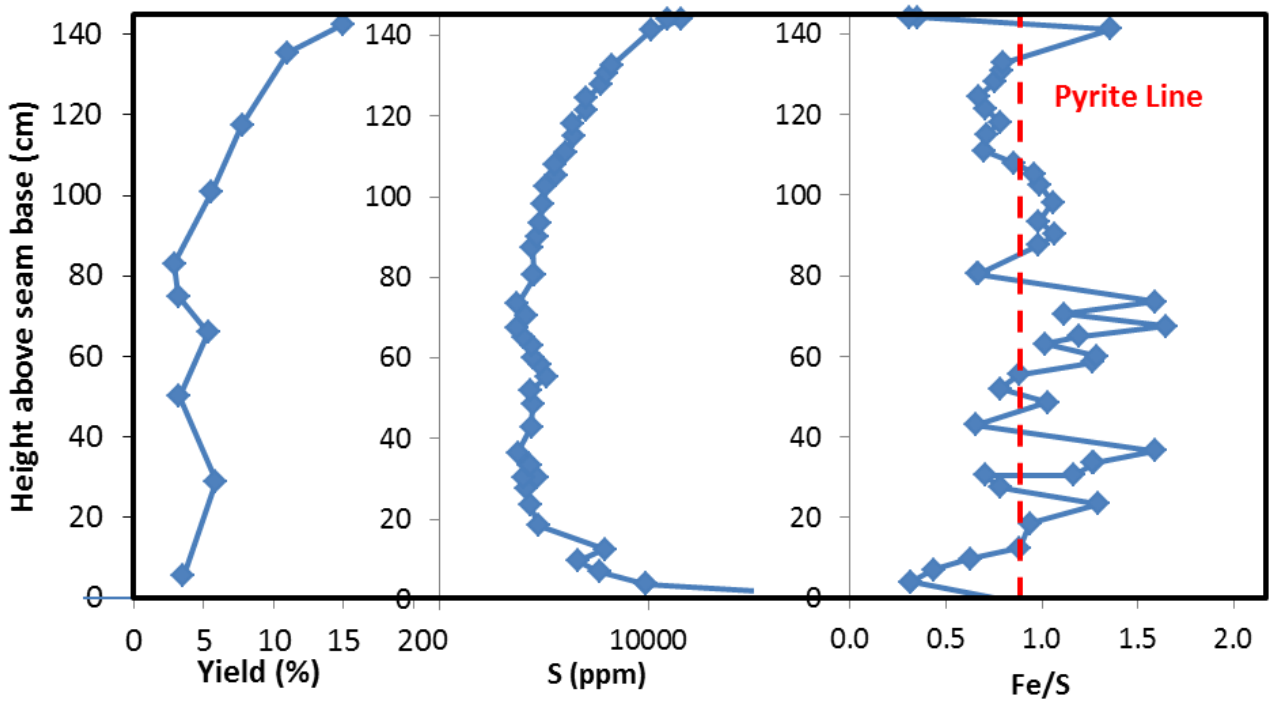

Fig. 4.13 Comparison of Soxhlet yield (%) with total coal sulfur and Fe/S ration within the Longyear seam. Note the rapid increase in sulfur concentration and shift from iron enriched to sulfur enriched conditions after 80cm above seam base.

aerobic species. High hopane concentrations also appear to be limited to marine influenced coals formed within coastal settings (Rathbone and Davis, 1993).

High hopane content also appears to be a common feature of high latitude perhydrous coals with the Taranaki coals, observed to contain approximately 60µg/g TOC in coals of similar rank to the Longyear seam (Vu et al., 2010). These have been interpreted as representing a considerable microbial biomass input to the coals (Vu et al., 2010).

In comparison the Longyear coal contains even higher total hopane concentrations of up to 100µg/g TOC (Table. 4.7) with amounts remaining relatively constant up-seam. These high hopane contents indicate that biodegradation during the formation of the Longyear seam was surprisingly high for the latitude. Hopanes also form a significant component of hydrocarbons generated from the coals (up to 15 wt%, Table. 4.7). The high content of bacterial lipids (classed as Type I kerogen), within the oils shows that not only did high biodegradation rates lead to liberation of hydrogen rich material, the bacteria themselves became a source of oil potential.

The conditions required to produce large bacterial communities within the Svalbard peatlands may have been due to climatological reasons. The Arctic has been identified as warmer and wetter than today, with winter temperatures rarely decreasing below freezing

Height above seam base (cm)	Total Hopane mg/g extract	Total Hopane µg/TOC
135.5	5.0	22.9
117.5	125.2	57.7
83	43.7	48.8
50	74.2	83.0
29	79.6	99.5
5.5	43.7	41.7

Table 4.7 – Concentrations of hopanes up-seam within the Longyear Seam at Mine 7 on an extract and TOC basis.

(Greenwood et al., 2010). Studies of primary productivity in analogous Palaeogene high latitude forests (Ellesmere Island) showed productivities similar to that of temperate old growth floodplain forests today (Williams et al., 2009).

Productivity within these peatlands would also be expected to be extremely seasonal. The transition between the short intense growing season and winter in Palaeocene Svalbard would be expected to be rapid, with deciduous Metasequoia Glyptostroboides, Taxodium and herbaceous plants such as sedges and reeds losing leaves or dying back quickly in order to maximise productivity.

Evidence from modern temperate soils (Avramides et al., 2009, Fierer et al. 2005) indicates that microbial communities however, are not unduly affected by the reduced organic input caused by lower temperatures and plant productivity experienced in winter. Rapid leaf fall would provide a nutrient rich litter during the dark polar

winter allowing microbial communities time to degrade surface layers efficiently. This would provide all the conditions required for the liberation of Type II hydrogen rich, functionalised molecules from bacterial decay of plant matter and Type I bacterial lipids including hopanes into the peat subsurface. This would produce the mixed kerogen type, characteristic of the upper Todalen coals.

4.5.4 Sulfur and Oil Potential

The availability of Fe (Fig.4.13) appears to be a major control upon the sulfur chemistry of the Longyear peatland. Sulfate reduction within organic coastal and marine sediments leads to precipitation of pyrite (FeS_2) with Fe/S values in excess of 0.9 required to convert all sulfur present to pyrite. Where Fe is in excess (Fe/S >0.9), as in the lower Longyear seam, sulfur is sequestered as pyrite and the remaining Fe deposited as Fe-carbonates. However, in the upper seam, additional supply of marine sulfur is shown to push the Fe/S ratio towards a system with excess sulfur (<0.9). This change in the availability of S coincides with the areas of greatest oil potential showing that whilst total sulfur content is important, the sulfur must be available i.e. the system must be Fe deficient relative to S.

High surface bacterial activity such as that seen in the Longyear seam causes the sub-surface of the peat to become anaerobic. Sulfate reducing bacteria produce H_2S in anaerobic conditions, when sulfur deposition exceeds iron supply, allowing the formation of organo-

sulfur molecules (Sinninghe Damsté and de Leeuw, 1990). This appears to be facilitated in the Longyear seam by deposition of marine sulfates.

The reaction of H_2S with organic matter within the peat occurs preferentially with functionalised molecules (Damsté and de Leeuw, 1990) liberated by microbial processing of hydrogen rich source material, preserving both carbon skeleton and functionality. These functionalised molecules include higher plant biomarkers (oleananes, trycyclic diterpanes, n-alkanes) and the bacteria themselves (hopanes). During later coalification this functionality is lost as a result of maturation, alongside the majority of the organoic sulfur.

Organo-sulfur molecule formation during early diagenesis, aided by the excess sulfur from marine deposition, would provide a method of binding and protecting hydrogen rich material produced by bacterial action within less reactive humic material (Hao and Chen, 1992) during subsequent diagenesis and coalification. This preservation effect would explain the excess hydrocarbon material observed within the Longyear seam (Fig. 4.2) and provides a plausible mechanism for the formation of perhydrous vitrinites, responsible for much of the Longyear coals oil potential.

4.6 Conclusions

The upper Svalbard coals (Longyear, Svarteper and Askeladden) are shown to have maximum oil yields in excess of 400mg/g coal with hydrous pyrolysis and Rock Eval yields comparable to many oil shales. The coals also show significant retortion potential with yields between 175-190 mg/g similar to values achieved on a sub-economic basis in the Kings Bay region during the 1920's.

The inferred maturity gap within the Svalbard coal is due to suppression of vitrinite reflectance by enrichment in hydrogen rich oil prone material. This has implications for local and regional basin models indicating reflectance gradients in the Adventdalen region consistent with lower estimates (0.15%/km) and greater burial and subsequent uplift within the N. Barents during the Tertiary.

Oil potential is thought to be due to the incorporation of hydrogen rich plant material and bacterial lipids into humic material, followed by preservation by organo-sulfur molecule formation. This process appears aided by the unusual conditions present at high latitude during the Palaeocene, namely the temperate climate, high seasonality, high productivity and pH regulation effect of a coastal position combined to form optimum conditions for perhydrous vitrinite formation.

Chapter 5

DEVELOPMENT OF THE SVEA SEAMS – PALAEOENVIRONMENT AND COAL QUALITY

5.1 Introduction

The Svea Seams, represents a significant current (Svea Nord) and future (Ispallen/ Svea Øst) economic coal resource on Spitsbergen. Therefore, to understand where the most economic deposits are it is important to understand the role of palaeo-geography and palaeo-environment in controlling coal quality within the Svea seams during formation.

Reported high ash, sulfur and phosphorus content variability in the Svea seam (Orheim et al. 2007) is poorly constrained with considerable quality variations both vertically and laterally within the seam. Another difficulty in the published data is the naming of the Svea as a single seam, rather than a number of separate lenses (Chapter 3). This may have contributed to the variation seen in the bulk properties of the Svea Seam. The lower oil potential and differing palaeogeographic distribution of the Svea seam should also provide a useful comparison and contrast with the oil prone, more laterally extensive, geologically later seams.

This Chapter will build upon the palaeogeographic reconstructions and conclusions presented in Chapter 3 using inorganic and organic petrographic techniques to study the interaction between the

peatlands and landscape/environment over time. In order to constrain the period of peatland formation and more generally constraints on possible carbon accumulation rates were considered. This will be used to develop models for predicting the location of potential coal quality issues

5.2 – The Svea Seams

The Svea seams have been the subject of relatively few published works (Orheim et al. 2007, Lüthje, 2008, Harland, 1997, Dallmann, 1999) with many limited to descriptions of coal thickness and extent. The bulk coal quality (Ash, S, P, Calorific value, fluidity) of the Svea seam has been characterised extensively by SNSK 2002-2013 and Orheim et al. 2007 (Table 5.1) for economic purposes, but the lack of high resolution data makes it difficult to put coal quality variations within the context of changing basinal/environmental controls.

The Svea Nord mine currently produces the majority of coal produced upon Spitsbergen (1.8Mt in 2010), however this mine is approaching the end of its life and faces increased problems with extraction and coal quality, particularly with ash content (SNSK 2010). The Svea Nord lens forms the southernmost of the 'valley type' deposits (Chapter 3) with the mine layout mirroring the shape of the deposit (figure 5.1).

At Svea Nord, coal reaches a maximum thickness of ~4.5m with greatest thickness and coal quality towards the centre of the lens

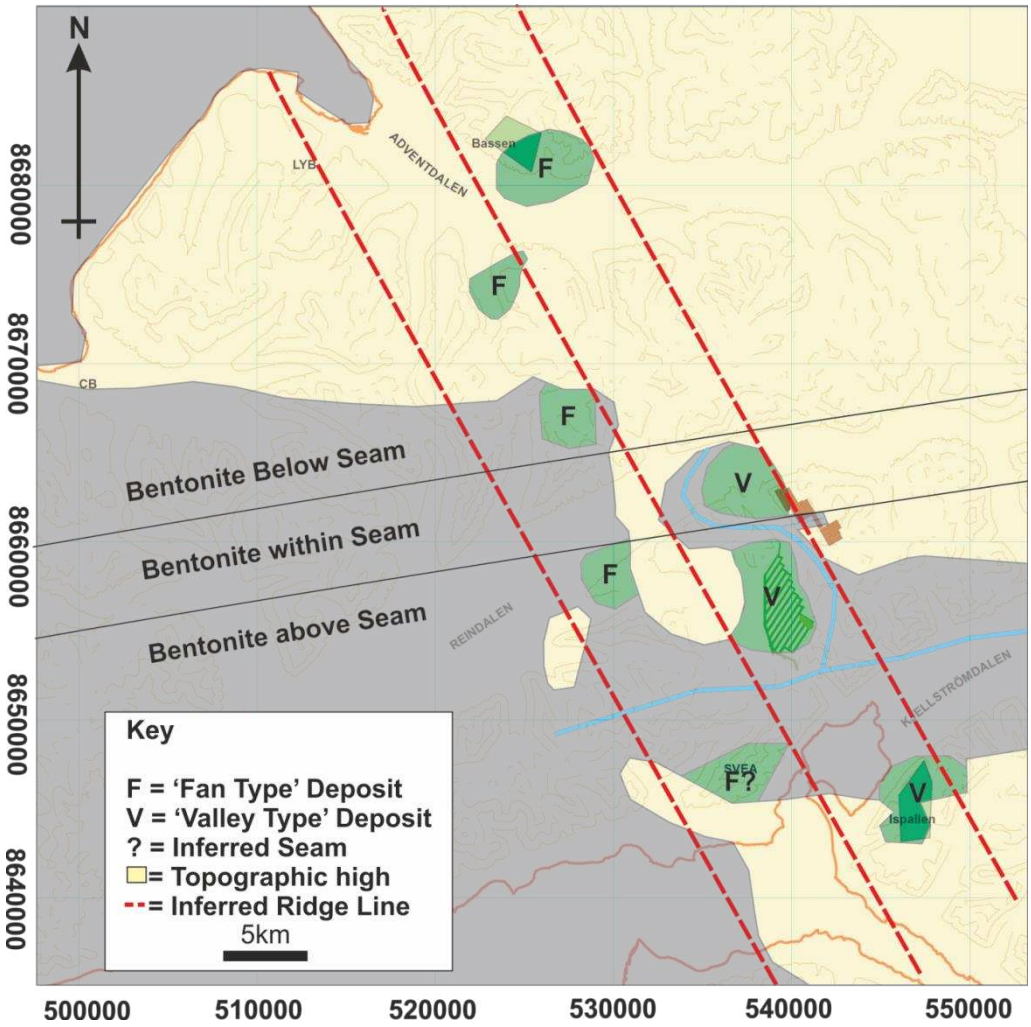

Fig. 5.1 – Map of the distribution of Svea Seams across the Central Tertiary Basin in Relation to the inferred 'structural highs' indicated in Chapter 3. Note that all the seams are adjacent to the ridge. Approximate location of seam is also given relative to the bentontite bed described in Chapter 3 showing that the seams were not formed concurrently. Sample locations are also given. Inferred seam from derived from historic mining in the area

(Figure 5.1). Towards the edge of the deposit the seam becomes thinner, increasingly vulnerable to splitting and coal quality diminishes. Future development and extraction of the Svea seam is focussed upon reworking of the former Svea Øst mine (Fan type?) and a possible new mine in the Ispallen region (Valley type) opposite the current Svea settlement (Figure 5.1)

The discontinuous nature (Figure 5.1) and lensoidal shape of the Svea seam is well documented (Orheim et al. 2007, Jochmann, 2004, this study). However, the Svea seams are also temporally discontinuous as shown by their stratigraphic position relative to a volcanic bentonite layer by the presence of a bentonite layer (assumed to represent a single volcanic event) above the Svea seam in the south, within the Svea seam in the Lunckefjellet region and below the Svea in the Adventdalen Region (Chapter 3). Consequently, the Svea seam will be referred to in this chapter by the nomenclature suggested in Chapter 3 in order to reflect the diversity of formation environments seen between the different Svea lenses.

5.3 – Persistence of the Svea Peatland

In order to understand how the supply of inorganic contaminants (dust, groundwaters, marine influence) changed over the lifetime of peatland accumulations, it is first helpful to estimate the length of time that the peatland existed.

5.3.1 – Estimation of deposition period from coal TOC

The simplest way to estimate the deposition period of a coal is to use the mean total organic carbon (TOC) of the seam and modern carbon carbon accumulation rates for peatlands at different latitudes (Large et al. 2003). By the Eocene, peatlands and forests at similar palaeo-latitude (Ellesmere Island) had productivities similar to that of old growth temperate forests in Europe today (Williams et al. 2009), with temperatures reported to have rarely fallen below 0°C (Greenwood et al., 2009). Consequently, long term carbon accumulation rates (LORCA) in Svalbard are likely to fall well within the range of Holocene peatlands in common with other Palaeogene peatlands (Large et al. 2003). Carbon accumulations rates from temperate peatlands (Large, 2007) are likely to be most appropriate for estimates of the period of deposition of the Svea coals.

LORCA rates from modern peatlands show a negative linear relationship with latitude with tropical peatlands exhibiting significantly elevated LORCA rates compared to boreal peatlands (Fig. xx; Large et al. 2011). Mean Tropical (Neuzil, 1997; Sorenson, 1993) and mean Boreal (Turenen et al. 2004) LORCA rates were therefore considered to provide maximum and minimum limits upon the period of peatland formation (Appendix I).

The length of peatland deposition estimate was calculated using the parameters detailed in Appendix I and equation;

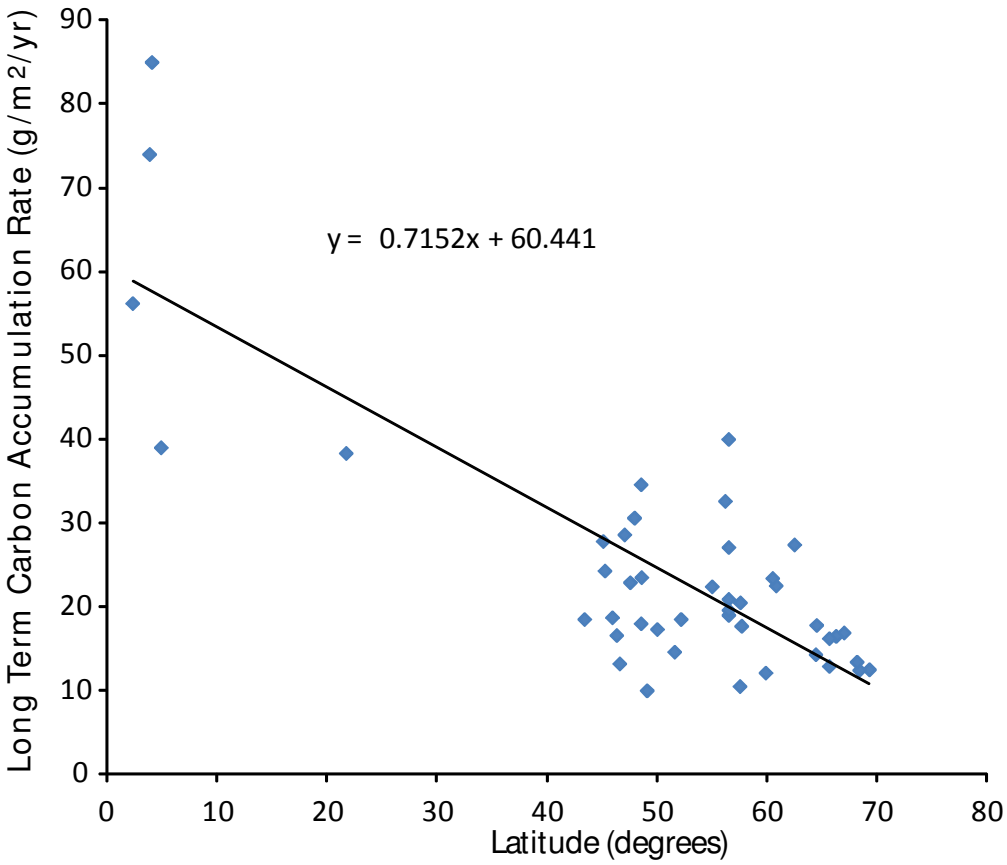

Fig. 5.2 Long Term Carbon accumulation rates (LORCA) g/m²/yr vs Latitude showing the linear decrease in LORCA rates from the equator to the poles (From Large et al., 2011)

$$Length\ of\ Peatland\ Deposition\ (Kyr) = \frac{\rho(\frac{kg}{m^3})h(m)TOC(\frac{\%}{100})}{LORCA(gm^{-3}a^{-1})}$$

Assuming temperate carbon (~27gCm^{-2}a^{-1} Turenen et al., 2004) accumulation rates and coal density between 1.2-1.3kg/m^3 (Orheim et al., 2007) the formation of the Svea Nord seam represents a period of between 177 and 192kyr. The maximum period of deposition of the Svea Nord seam is between 300-325Kyr in Boreal Conditions. By contrast, at tropical LORCA rates, the Svea Nord seam would have been deposited much faster at between 48-52kyr.

In some coals it is possible to identify Milankovitch cyclicity within coals enabling further constraint upon the length of deposition (Longyear seam, Chapter 6; Large et al., 2006) however the inorganic and organic petrographic parameters do not show any obvious cyclicity within the majority of the Svea seam. The Cu/Ti and Al/Ti ratios of the upper seam do exhibit some cyclicity at approximately 40cm/cycle which is similar to the 21kyr precessional cycles observed in the Longyear seam (Chpter 6), however these are not thought clear enough to warrant further statistical analysis. Consequently, the age of the Svea Nord seam should fall within the range of 170-200kyr as shown by carbon accumulation rates.

5.4 Coal Quality Issues in the Svea Seam

Identifying the coal quality issues affecting the value and future exploitation potential of the various Svea seams is more difficult

compared to the more laterally extensive upper Todalen seams due to the different and evolving hydrological/landscape conditions and time periods experienced within both the 'fan' and 'valley' type seams during deposition. Consequently, the coal quality data presented is representative of only the Svea peatlands, Svea Nord and Breinosa Svea from which they are sourced (Table. 5.1) which includes;

- Calorific Value
- Oil Potential/Coking Potential
- Ash, Sulfur and Phosphorus Content
- Seam Thickness and splitting (Chapter 3)

The Svea Nord and Breinosa Svea seams have a calorific content ranging from 6550 to 7901 kcal/kg which reflects the high volatile bituminous rank of this seam. This variation in calorific content is primarily controlled by ash/mineral content. The seams also have low oil potential (Chapter 4) and low free swelling index values at values considered too low for coking. Ash contents are generally <10% but range from 3-20% (Table.5.1)

The main elemental controls upon coal quality and resale value are by phosphorus and to a lesser extent sulfur. Phosphorus appears to be highly variable within the Svea seam (Orheim et al., 2007) and the controls upon the amounts and distribution of phosphorus rich

Location	Borehole	Description	Mean depth	Ash (%)	Sulfur (wt%)	Eff. B.v. kcal/kg	FSI
Svea Nord	BH3/2010	Hanging Wall	83.6	87.6	1.97	319	1.0
Svea Nord	BH3/2010	Coal	83.8	3.7	0.78	7829	8.0
Svea Nord	BH3/2010	Coal	84.0	2.9	0.67	7901	8.0
Svea Nord	BH3/2010	Coal	84.3	2.1	0.68	7887	7.5
Svea Nord	BH3/2010	Coal	84.5	4.3	0.75	7674	7.5
Svea Nord	BH3/2010	Coal	84.8	5.5	0.93	7584	8.0
Svea Nord	BH3/2010	Coal	84.9	57.4	2.29	3078	1.0
Svea Nord	BH3/2010	Coal Shale	85.1	81.6	5.15	757	1.0
Svea Nord	BH3/2010	Coal Shale	85.7	68.4	4.54	1845	1.0
Svea Nord	BH3/2010	Coal Shale	85.9	63.3	8.44	2209	1.0
Svea Nord	BH3/2010	Coal Shale	86.1	68.1	8.84	1765	1.0
Svea Nord	BH3/2010	Coal	86.3	17.5	3.46	6555	1.5
Svea Nord	BH3/2010	Coal Shale	86.4	81.6	1.99	822	1.0
Svea Nord	BH3/2010	Coal Shale	86.6	83.2	1.30	600	1.0
Svea Nord	BH3/2010	Coal Shale	86.8	72.0	1.92	1461	1.0
Svea Nord	BH3/2010	Coal	87.0	13.4	1.77	6816	1.5
Svea Nord	BH3/2010	Coal	87.2	6.6	1.40	7522	1.5
Svea Nord	BH3/2010	Coal	87.5	12.7	0.44	6511	1.5
Svea Nord	BH3/2010	Coal	87.7	12.2	0.57	6959	1.5
Svea Nord	BH3/2010	Coal	88.0	9.5	0.50	7084	6.0
Svea Nord	BH3/2010	Coal	88.2	8.4	0.62	7427	7.5
Breinosa Svea	BH5/2009	Coal	326.01	12.2	2.17	7184	8.5
Breinosa Svea	BH5/2010	Coal	326.26	10.5	2.20	7419	9.0
Breinosa Svea	BH5/2011	Coal	326.51	4.7	1.48	7993	8.5
Breinosa Svea	BH5/2012	Coal	326.76	17.3	3.97	6738	8.5
Breinosa Svea	BH5/2013	Coal Shale	326.94	79.3	9.03	784	1.0
Breinosa Svea	BH5/2014	Coal	327.13	8.2	1.83	7679	9.0

Table 5.1 – Typical Coal Quality Analyses from the Svea Nord seam and Breinosa Svea seam (SNSK data) ***FSI = Free Swelling Index***

coal is little understood. However, due to instrument problems (Chapter 2), ICP-AES phosphorus analysis was limited (detection limit >100ppm) leaving only the results from SEM-EDAX analysis to examine this. Sulfur contents range from 0.5-1% within the central region of Svea Nord rising to >2% at the edges of the deposit.

5.4.1 Major and Minor Elemental Composition of the 'Valley type' Svea Nord Coal

The average inorganic elemental composition of coals from the Svea Nord section (Table. 5.2; 5.3) were dominated by the lithophile elements (Al, Ti, Cu, Na, K) alongside Ca, Mg, Fe and S. However as discussed in Chapter 2, the dominance of Ca seen in the Lower Svea Seam may be due to application of a fire proofing $CaCO_3$ paste to the seam surface. This is thought to have contaminated a number of samples despite the washing procedure applied; consequently Ca data is considered unreliable. Phosphorous contents were generally above 100ppm (to a maximum of 5441ppm) in the lower Svea Nord Seam and were below detection in the upper seam.

In the lower Svea Nord (Table. 5.2) seam major elemental compositions are similar to those of Orheim et al. (2007). Minor elemental concentrations are also similar although both mean Sr and Ba values are closer to the maximum presented by Orheim et al. (2007).

	No of Samples	% of Samples Measured	Mean (ppm)	Minimum (ppm)	Maximum (ppm)	Median (ppm)	SD (ppm)
Al	89	98	5021	265	90817	2005	12937
Ca	80	88	15987	16	134785	3108	29392
Fe	90	99	5735	1111	33985	3522	6254
K	88	97	766	4.6	23077	23	3888
Mg	90	99	2061	106	25908	665	4379
Mn	90	99	20	1.0	230	5.4	34
Na	90	99	1360	171	5794	710	1441
P	77	85	600	B.D	5441	138	1154
S	90	99	3127	261	6393	3006	886
Ti	90	99	690	18	9052	80	1758
Ba	91	100	252	112	489	240	90
Co	91	100	3.5	0.8	17	2.4	3.3
Cr	91	100	16	0.6	185	3.1	34
Cu	89	98	5.9	B.D	101	3.0	12
Li	54	59	22	0.8	388	3.2	72
Ni	91	100	10	0.5	44	6.9	8.8
Pb	78	86	3.1	B.D	28	1.6	5.3
Rb	77	85	10	B.D	176	2.0	32
Sb	91	100	18	11	30	17	4.2
Sc	91	100	1.1	0.15	13	0.6	2.0
Sr	88	97	701	30	3864	258	956
U	22	24	71	2.8	170	52	59
V	91	100	20	0.2	357	1.4	63
Zn	91	100	8.1	1.3	43	4.8	9.2
Zr	91	100	20	0.9	211	4.6	41

Table 5.2 – Major and minor whole coal elemental composition of the Lower Svea Nord Seam at DT6/9

	Number of Samples	% of Samples Measured	Mean (ppm)	Minimum (ppm)	Maximum (ppm)	Median (ppm)	SD (ppm)
Al	52	98	1483	120	21762	865	3019
Ca	49	92	15286	21	90780	4980	24614
Fe	53	100	7106	1263	59817	3646	9740
K	39	74	298	0.7	10998	14	1759
Mg	53	100	1703	128	9204	865	2128
Mn	53	100	27	0.6	260	8.0	55
Na	53	100	1022	287	6410	832	904
P	35	66	227	3.4	1435	33	413
S	52	98	7931	2746	61088	6529	7857
Ti	53	100	149	12	4319	60	589
Ba	53	100	152	34	367	135	74
Co	53	100	0.8	BD	6.5	0.6	1.1
Cu	49	92	2.8	BD	13	1.7	3.0
Li	37	70	2.7	BD	65	0.6	11
Ni	51	96	4.4	BD	22	2.4	4.5
Pb	29	55	1.5	BD	11	1.0	2.4
Rb	44	83	5.5	BD	90	2.0	16
Sb	53	100	17	11	31	16	3.8
Sc	53	100	0.6	BD	7.2	0.3	1.0
Sr	53	100	639	26	5506	219	1067
U	12	23	69	3.6	325	31	94
V	53	100	11	BD	209	1.0	39
Zn	53	100	5.4	0.9	23	3.4	4.8
Zr	53	100	6.8	0.8	107	2.4	18.1

Table 5.3 – Major and minor whole coal elemental composition of the Upper Svea Nord Seam at DT6/9

In the upper seam (Table 5.3) the concentration of the lithophile elements (Al, Ti, K, Na) and S are closer to the minimum values presented by Orheim et al. (2007). However, Fe concentrations are closer to the maximum values presented.

Comparison of both seams with the trace element data from Orheim et al. (2007) also shows similar low trace element concentrations (Table 5.2; 5.3). Both Ba and Sr dominate minor elemental composition in both this study and Orheim et al. (2007).

A Correlation Matrix was used (Fig.5.3; 5.4) to identify relationships between different elements in the lower and upper seams. Regression showed that all the relationships discussed subsequently were significant to at least >90% confidence (*t*-Stat >2, P values <0.1; see attached disc). This shows that many of the elements analysed can be grouped with the lithophile elements (Al, K, Na, Ti) including Co, Li, Pb, Rb, Sc, V and Zr. In the upper seam, the lithophile group of elements is limited to Al, K, Na, Ti however this may be due to lower minor elemental concentrations in this seam. This lithophile group is often thought to represent dust controlled deposition into the peatland (Lawrence and Neff, 2009). Another group identified in both the lower and upper seams is generally associated with groundwater input to the peatland (Todd, 1980). In the lower seam it comprises Fe, Mg, Mn. Calcium is also likely to

	Al	Ca	Fe	K	Mg	Mn	Na	P	S	Ti	Ba	Co	Cu	Li	Ni	Pb	Rb	Sb	Sc	Sr	U	V	Zn
Ca	-0.14																						
Fe	0.27	0.36																					
K	**0.75**	-0.09	0.33																				
Mg	0.04	**0.47**	**0.72**	0.02																			
Mn	0.19	**0.44**	**0.96**	0.22	**0.73**																		
Na	0.31	-0.14	-0.01	0.11	-0.14	-0.12																	
P	0.12	-0.09	0.01	-0.06	-0.06	-0.05	0.70																
S	-0.42	-0.21	-0.43	-0.56	-0.23	-0.37	0.18	0.39															
Ti	**0.63**	-0.18	0.25	**0.71**	-0.02	0.15	0.24	-0.03	-0.52														
Ba	**0.51**	0.14	0.35	0.42	0.09	0.28	0.53	0.58	-0.33	**0.57**													
Co	**0.62**	-0.19	0.16	**0.66**	-0.09	0.03	0.47	0.18	-0.42	**0.90**	0.57												
Cu	0.37	-0.16	0.14	0.44	-0.03	0.07	0.08	0.00	-0.34	0.39	0.29	0.34											
Li	**0.62**	-0.11	0.37	**0.99**	0.02	0.27	0.16	-0.08	-0.64	**0.73**	0.44	**0.67**	0.39										
Ni	0.44	-0.18	0.24	**0.58**	-0.07	0.13	0.17	-0.01	-0.38	0.46	0.34	0.49	0.34	0.73									
Pb	**0.67**	-0.17	0.51	**0.96**	0.20	0.43	0.28	0.01	-0.58	**0.77**	**0.53**	**0.76**	0.46	**0.95**	**0.63**								
Rb	**0.92**	-0.15	0.61	**0.95**	0.57	0.62	0.21	-0.07	-0.63	**0.74**	**0.52**	**0.62**	0.43	**0.84**	**0.53**	**0.82**							
Sb	-0.14	0.68	0.09	-0.07	0.21	0.12	0.05	0.11	-0.05	-0.13	0.16	-0.08	-0.22	0.06	-0.08	-0.02	-0.16						
Sc	**0.94**	-0.16	0.20	0.55	0.01	0.10	0.52	0.23	-0.29	**0.61**	**0.51**	**0.65**	0.31	0.40	0.38	**0.61**	**0.79**	-0.13					
Sr	0.00	**0.50**	0.06	-0.10	0.14	0.07	0.34	0.56	0.29	-0.13	0.39	-0.03	-0.12	-0.10	-0.03	-0.07	-0.10	0.60	0.04				
U	0.14	0.41	0.79	0.40	0.32	0.69	-0.06	0.32	-0.37	0.05	0.26	0.07	-0.08	0.29	0.43	0.41	0.59	0.23	0.04	0.11			
V	**0.75**	-0.15	0.34	**0.98**	0.02	0.23	0.24	-0.04	-0.58	**0.85**	**0.52**	**0.76**	0.47	**0.96**	**0.58**	**0.95**	**0.91**	-0.14	**0.69**	-0.12	0.23		
Zn	0.48	0.05	0.44	**0.63**	0.15	0.37	0.01	-0.11	-0.44	**0.70**	0.40	**0.55**	0.35	**0.71**	0.39	**0.68**	**0.67**	0.00	0.37	-0.05	0.35	**0.69**	
Zr	**0.68**	-0.17	0.30	**0.88**	-0.02	0.17	0.43	0.21	-0.45	**0.81**	**0.59**	**0.85**	0.43	**0.88**	**0.54**	**0.94**	**0.77**	-0.06	**0.67**	0.02	0.23	**0.90**	**0.62**

Fig. 5.3 – Correlation Matrix comparing the major and minor elemental composition of the Lower Svea Nord Seam at DT6/9

Red = lithophile associated elements Blue = Groundwater associated elements

	Al	Ca	Fe	K	Mg	Mn	Na	P	S	Ti	Ba	Co	Cu	Li	Ni	Pb	Rb	Sb	Sc	Sr	U	V	Zn
Ca	-0.07																						
Fe	-0.04	0.61																					
K	**0.96**	-0.10	0.04																				
Mg	-0.05	**0.79**	**0.64**	-0.02																			
Mn	-0.10	**0.68**	**0.96**	-0.01	**0.72**																		
Na	**0.94**	-0.19	-0.16	**0.85**	-0.15	-0.22																	
P	0.18	0.28	-0.20	-0.03	-0.03	-0.18	0.18																
S	-0.22	0.25	**0.73**	-0.26	0.11	**0.57**	-0.09	-0.25															
Ti	**0.95**	-0.12	-0.01	**0.99**	-0.04	-0.04	**0.85**	-0.03	-0.10														
Ba	0.15	0.15	-0.16	0.04	0.00	-0.12	0.13	0.35	-0.21	0.06													
Co	0.12	0.29	-0.10	-0.05	0.02	-0.09	0.11	0.47	-0.09	-0.05	**0.55**												
Cu	0.17	0.23	-0.10	0.11	0.03	-0.06	0.10	0.62	-0.26	0.09	**0.70**	**0.69**											
Li	0.42	0.25	-0.06	0.79	0.19	-0.07	0.12	0.23	-0.08	-0.09	0.42	**0.95**	0.57										
Ni	-0.04	0.04	-0.07	-0.06	-0.04	-0.04	-0.06	0.59	-0.13	-0.07	-0.06	0.30	0.23	0.57									
Pb	0.07	0.68	-0.10	-0.08	0.10	-0.09	0.02	0.78	-0.20	-0.07	**0.56**	**0.96**	**0.72**	**0.97**	**0.64**								
Rb	0.11	0.37	-0.10	-0.04	0.01	-0.09	0.07	0.88	-0.09	-0.04	**0.56**	**0.95**	**0.71**	**0.99**	0.33	**0.95**							
Sb	-0.01	-0.07	0.02	-0.04	0.01	0.04	0.00	0.19	0.00	-0.06	0.48	0.03	0.30	-0.03	-0.09	-0.03	-0.04						
Sc	0.08	0.33	-0.15	-0.05	-0.05	-0.13	0.11	0.46	-0.07	-0.04	**0.52**	**0.76**	**0.56**	0.47	0.24	**0.77**	**0.85**	0.03					
Sr	0.04	0.13	-0.11	-0.07	0.03	-0.12	0.04	0.40	-0.11	-0.06	0.29	-0.03	0.08	-0.02	-0.13	-0.08	-0.06	0.36	0.11				
U	-0.50	-0.28	-0.04	-0.48	-0.09	0.05	-0.50	-0.48	-0.13	-0.28	0.43	-0.31	0.02	-0.29	-0.35	-0.33	-0.38	0.84	-0.29	0.81			
V	0.10	0.35	-0.10	-0.04	0.04	-0.09	0.07	0.43	-0.08	-0.04	**0.50**	**0.95**	**0.62**	**0.97**	0.28	**0.97**	**0.97**	-0.06	**0.80**	0.01	-0.31		
Zn	0.08	0.22	-0.04	-0.02	0.12	-0.01	0.00	0.17	-0.11	0.04	**0.59**	0.46	0.44	**0.57**	0.08	**0.58**	0.48	0.18	0.43	0.11	0.23	**0.51**	
Zr	0.12	0.26	-0.10	-0.02	0.01	-0.10	0.10	0.39	-0.07	-0.02	0.48	**0.97**	**0.65**	**0.98**	0.28	**0.98**	**0.95**	-0.08	**0.71**	-0.10	-0.34	**0.97**	**0.43**

Fig. 5.4 – Correlation Matrix comparing the major and minor elemental composition of the Upper Svea Nord Seam at DT6/9

Red = Lithophiles, Blue = Groundwater associated, Green = Marine sulfur associated, Orange = trace metals (clastic supply?)

be included within this group however the addition of extra $CaCO_3$ by contamination has affected this relationship. In the upper seam where contamination is lower this group comprises Fe, Mg, Mn and Ca.

Sulfur is relatively independent of the element groups identified previously although it shows increasing affinity with Fe in the upper seam, probably due to pyrite formation. This implies a different environmental control upon sulfur deposition from the other groups identified, which due to its coastal position may be attributed to marine influence

This section shows that the ash and inorganic elemental composition of the Svea Nord Seam at this location can be attributed to three major sources. These comprise a major source of lithophile and transition metals (namely dust), a Ca/Mg/Fe groundwater source and a source of sulfur

5.4.2 – Composition of Local Clastic sediments within the Svea Nord Peatland

The composition of the sediments adjacent to the peatland is important for understanding how the provenance of clastic material changed over the life time of the seam. To study this, the sediment parting within the Svea Nord seam was sampled and analysed. The composition of the sediment parting (Table 5.4) will then be used in future sections to indicate where local sediment was a dominant

	No of Samples	% Samples Measured	Mean (ppm)	Minimum (ppm)	Maximum (ppm)	Median (ppm)	SD (ppm)
Al	23	100	62487	20110	90029	62425	17864
Ca	23	100	1399	395	2998	1055	782
Fe	23	100	49477	7448	82963	51534	21941
K	23	100	17754	11386	21587	18699	3115
Mg	23	100	4276	2302	5466	4166	718
Mn	23	100	87	20	124	94	24
Na	23	100	10094	6286	14346	10634	1987
P	23	100	221	174	265	222	24
S	23	100	34912	1168	73675	37425	23839
Ti	23	100	4872	3413	5871	5088	777
Fe/S	23	100	2.7	1.1	14.1	1.4	3.3
Ca/Mg	23	100	0.3	0.1	0.7	0.2	0.2
Al/Ti	23	100	13.2	3.4	18.1	13.9	4.0
Fe/Ti	23	100	10.8	1.9	23.4	10.6	6.1
Ca/Ti	23	100	0.3	0.1	0.8	0.2	0.2
Cu/Ti	23	100	0.004	-	0.007	0.004	0.002

Table 5.4 – Major and minor elemental composition and elemental ratios from the Svea Nord Split at DT6/9

control upon coal quality and in which conditions where they favourable.

The Svea Nord split is dominated by Al, Fe and Na probably representing the Al-Silicates and clay minerals. The local sediment is Ca depleted relative to the coals. SEM-EDAX analysis showed that sulfur is primarily found in the form of pyrite (FeS_2) with the Fe/S ratio showing enrichment in Fe compared to S (Appendix III).

The Ca/Mg ratio is low indicating a possible marine or coastal influence upon the parting. Al/Ti, Fe/Ti ratios are at approximately mean continental crust values (Rudnick and Gao, 2003) with Ca depleted compared to MCC.

The Cu/Ti ratio of the local sediment is depleted in Cu compared to atmospheric dust values (~0.01; Lawrence and Neff, 2009) which should allow easy differentiation between local and distal dust sources.

5.4.3 Major and Minor Elemental Composition of 'Fan Type' Breinosa Svea

Unlike the Svea Nord seam, the Breinosa Svea contains significant amounts of ash (~18%, Table. 5.4) with a dominance of Al, Fe and S (Table.5.4). As this is an inferred fan deposit, formed adjacent to a gulley system and formed during the last stages of Svea seam formation, this difference is not entirely unexpected. The minor

	No of samples	% Samples measured	Mean (ppm)	Minimum (ppm)	Maximum (ppm)	Median (ppm)	SD (ppm)
Al	8	100	17236	4658	54766	13607	15946
Ca	8	100	2693	554	3324	2859	896
Fe	8	100	22005	4797	85779	13079	26476
K	8	100	3819	398	19285	1535	6350
Mg	8	100	1667	1053	4174	1375	1027
Mn	8	100	50	18	142	35	39
Na	8	100	3636	2030	7802	3077	2011
S	8	100	29527	15200	84503	20242	23529
Ti	8	100	1022	180	4197	655	1299
Ba	8	100	249	161	431	184	108
Co	8	100	4.8	0.6	15	3.0	4.9
Cr	8	100	23	2.0	83	17	25
Cu	8	100	10	2.1	30	6.6	8.8
Li	6	75	10	1.1	24	8.4	7.7
Ni	8	100	14	0.4	49	11	16
Pb	8	100	6.8	0.3	24	4.7	7.4
Rb	8	100	29	3.3	142	12	46
Sb	8	100	20	13.9	32	17	7.2
Sc	8	100	3.0	0.3	5.7	2.4	1.8
Sr	8	100	513	132	1526	179	622
U	5	62.5	151	29	545	32	224
V	6	75	66	1.0	203	39	72
Zn	8	100	27	1.1	93	12	33
Zr	8	100	73	3.2	117	74	39

Table 5.5 – Major and minor elemental composition of the Breinosa Svea at BH9/2009

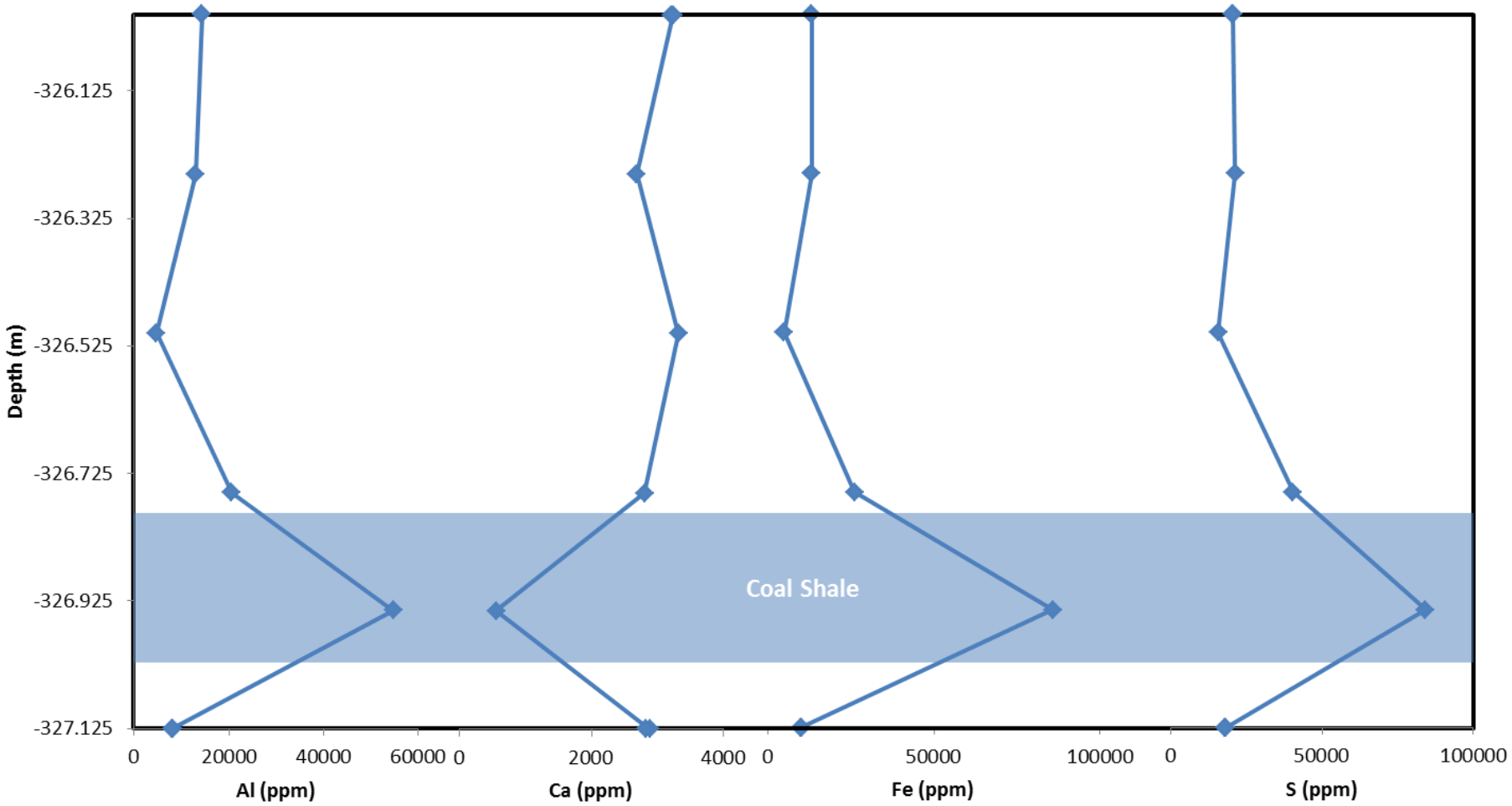

Fig 5.5 –Distribution of Al, Ca, Fe and S within the Breinosa Svea at BH5/2009. Note the similar distributions of each element

elements are dominated by Ba and Sr as in the Svea Nord Seam (Table 5.4).

All major and minor elements show similar profiles up-seam (Fig.5.5) with a high ash base, replaced at the top by lower ash conditions as the peatland grew and became increasingly isolated from clastic influence. The homogeneity of the major elemental profiles suggests a single control on coal quality within this seam, namely local clastic sedimentation.

During initiation of the peatland, the peat would form at the base of the gulley, overlying a former debris fan due to its favourable hydrological supply. At this point the peatland would have vulnerable to clastic sedimentation as it was not thick enough to divert surface flow around it during rain events. As the peatland grew and stabilised, the thickness of the peat became sufficient to prevent this, leading to the lower ash contents seen in the upper part of the Svea seam. This probably represents a relative increase in the role of dust deposition within the lithophile elements within the coal.

5.5 – Controls upon Coal Quality within the 'Valley Type' Svea Nord Seam

Unlike the Breinosa Svea (whose ash contents are primarily controlled by clastic sedimentation), the complexity of the distribution of ash and inorganic elements within the 'Valley Type'

Svea Nord Seam is thought sufficient to warrant further investigation. In the Svea Nord Seam, a number of elements have been shown in previous sections to be controlled by similar processes, allowing them to be grouped. This section will discuss each of the element groups and suggest the most likely palaeo-environmental control in each case.

5.5.1 Hydrological Controls upon Coal Quality

Unlike the Longyear (Chapter 6), Svarteper and Askeladden Seams (Chapter 7), the Svea seams were dependent upon small local catchments for their water supply (Chapter 3) and consequently upon local climate. The inherent vulnerability of hydrological supply to the peatland should therefore exert a significant control upon the supply and distribution of inorganic elements to the peatland. In order to understand the evolution of hydrological and redox conditions within the Svea peatland coal maceral analysis is used (Chapter 4; Diessel and Gammidge, 1998) alongside commonly used inorganic geochemical parameters.

5.5.1.1 – Coal Macerals and the hydrological development of the Svea Nord Seam

The lower Svea Nord Seam fluctuates between vitrinite dominated (49.8±19.2%) and inertinite dominated (41.8±17.1%) with relatively low liptinite contents (3.7±3.2%; Table 5.5). Vitrinite in the lower

seam is dominated by telovitrinites (34.1±15.7%), unlike the upper Svea seam and later seams within the Todalen Member.

The upper seam is vitrinite dominated (76.9±14.1%), which unlike the lower seam is composed primarily of detrovitrinites (52.9±14%). Inertinite is lower within the upper seam but remains a significant component of the coal (22.9±13.7%) with liptinite forming a minor constituent of the coal (3.3±1.6%; Table 5.6).

The high variation seen in coal maceral composition in the upper and lower Svea seams fits well with previously published Svea data (Orheim et al., 2007) with vitrinite values ranging between 50% and 70%.

5.5.1.2 – Hydrological Development of the Lower Svea Nord Seam

Vitrinite and inertinite show significant fluctuation in the lower seam reflecting the hydrological instability within the peatland (Diessel and Gammidge, 1998) due to local hydrological controls. The first 20cm of the Lower Svea Nord Seam show low vitrinite, inertinite conditions with high liptinite and mineral matter (Fig. 5.6; Fig. 5.7). This probably reflects the transition of the peatland from a waterlogged soil/clastic wetland to raised bog conditions.

After the initiation phase (50cm), vitrinite increases slowly up-seam, accompanied by a drop in liptinite and inertinite (Fig.5.6). Liptinite is dominated by sporinite and liptinites and is generally associated

	No of samples	% Measured Samples	Mean (%)	Minimum (%)	Maximum (%)	Median (%)	SD (%)
Vitrinite	*25*	*100*	*49.8*	*11.2*	*84.6*	*48.0*	*19.2*
Telovitrinite	*25*	*100*	*34.1*	*9.6*	*63.6*	*30.8*	*15.7*
Telinite	*25*	*100*	*4.2*	*0.0*	*18.0*	*2.8*	*5.1*
Collotelinite	*25*	*100*	*29.9*	*0.4*	*63.6*	*29.2*	*17.9*
Detrovitrinite	*25*	*100*	*14.0*	*1.2*	*54.8*	*9.6*	*16.0*
Collodetrinite	*4*	*16*	*10.1*	*4.4*	*20.0*	*8.0*	*6.9*
Inertinite	*25*	*100*	*41.8*	*2.8*	*68.4*	*44.4*	*17.1*
Fusinite	*25*	*100*	*16.1*	*2.0*	*51.2*	*13.3*	*10.2*
Semifusinite	*25*	*100*	*23.5*	*0.8*	*56.8*	*25.8*	*12.4*
Funginite	*5*	*20*	*2.0*	*1.2*	*4.4*	*1.2*	*1.4*
Inertodetrinite	*22*	*88*	*2.0*	*0.0*	*9.2*	*1.5*	*2.0*
Liptinite	*25*	*100*	*3.7*	*0.4*	*13.6*	*2.0*	*3.2*
Sporinite	*25*	*100*	*2.0*	*0.0*	*13.6*	*1.2*	*2.9*
Liptodetrinite	*5*	*20*	*1.4*	*0.0*	*2.0*	*1.6*	*0.8*
Cutinite	*24*	*96*	*1.0*	*0.0*	*4.8*	*0.4*	*1.2*
Minerals	*23*	*92*	*7.5*	*0.8*	*72.4*	*3.6*	*14.5*

Table 5.5 – Coal Maceral composition of the Lower Svea Nord Seam at DT6/9

	No of Samples	% Measured Samples	Mean (%)	Minimum (%)	Maximum (%)	Median (%)	SD (%)
Vitrinite	11	100	76.9	46.6	94.2	82.0	14.1
Telovitrinite	11	100	16.4	8.8	25.0	15.0	5.5
Telinite	11	100	10.3	4.0	20.0	10.0	4.5
Collotelinite	11	100	6.1	0.8	20.0	4.8	5.5
Detrovitrinite	11	100	52.9	34.0	72.8	52.8	14.0
Collodetrinite	11	100	7.5	2.0	22.8	5.6	6.0
Inertinite	11	100	22.9	10.0	54.8	21.6	13.7
Fusinite	11	100	10.3	4.0	27.2	6.8	7.0
Semifusinite	11	100	11.2	4.0	27.2	8.8	7.0
Funginite	11	100	1.5	0.4	2.8	1.6	0.9
Liptinite	10	91	3.3	0.0	5.2	3.6	1.6
Sporinite	10	91	0.2	0.0	0.4	0.0	0.2
Liptodetrinite	10	91	1.9	0.0	4.0	2.0	1.2
Cutinite	10	91	1.2	0.0	2.4	0.8	0.7
Minerals	10	91	5.4	0.0	39.2	1.6	11.4

Table 5.6 – Coal Maceral composition of the Upper Svea Nord Seam at DT6/9

with increased mineral matter. Inertinite in the Lower Svea seam is elevated compared to later seams, (50-70% Svea vs. <20% Longyear) indicating generally drier conditions. This reflects the instability of a local hydrological supply, with supply dependent upon local precipitation.

The greater frequency of fusinite rich layers within the Svea Seam, compared with the Longyear seam (Chapter 6) implies that the Lower Svea Nord seam was more vulnerable to fire damage, due to the less hydrologically stable conditions. However, peaks in fusinite appear to be relatively cyclic (~40-50cm) implying that the fire frequency was controlled by an external factor, such as by the frequency of ignition events, not by the dryness of the peat which appears to have remained relatively dry throughout the formation of the Lower Svea Nord Seam. Clearer evidence for such a climatological control on fire frequency is seen more clearly and discussed in more detail within the Lower Longyear seam (Chapter 6).

The TPI (Diessel, 1992; Diessel and Gammidge, 1998, Casareo et al., 1996) is thought to reflect the degree of preservation of source materials with higher values indicating higher tree density and thicker oxidising layer preserving more organic structures (Diessel and Gammidge, 1998). The GI shows the ratio of macerals formed in wetter conditions (namely vitrinites) and macerals favoured by

conditions that favour extensive combustion affected by oxidation/desiccation (inertinites).

Analysis of the GI and TPI profiles within the Lower Svea Nord Seam (Fig. 5.7) show that after an initial wetter colonisation phase, the peatland was relatively dry (GI <1) and with high tissue preservation/plant density (TPI >1). The peatland appears to have become both wetter and more degraded/reducing towards the top of the seam peaking at ~190cm above seam base. This general trend is punctuated by a series of wetter (higher GI) and drier (lower GI) events.

This was then followed by around 30cm of drying leading up to split formation with a peak in fusinite immediately preceding splitting. This suggests that peat will start to collapse as water budget decreases as well as developing a relatively aerated surface layer that is prone to fire. This leaves the peatland vulnerable to clastic sedimentation either from the flooding of the valley floor or washed on from the valley side. This sedimentation then terminated peat accumulation in all but the centre of the peatland.

5.5.1.3 – Hydrological Development of the Upper Svea Nord Seam

The upper Svea Nord Seam exhibits generally higher vitrinite (~80%) contents with more similarity to the lower Longyear seam than to the Lower Svea Nord Seam (Fig. 5.8). Re-establishment of

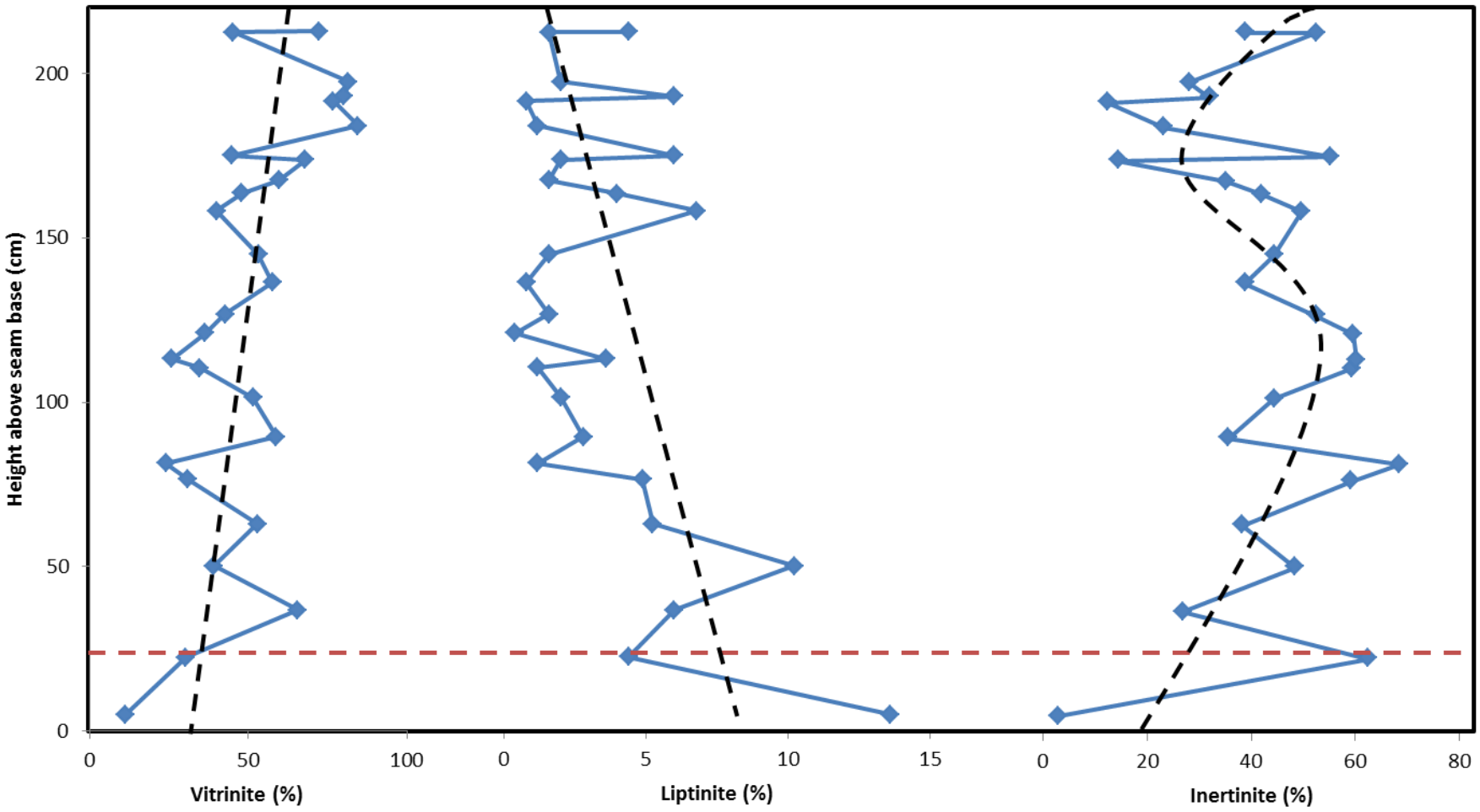

Fig. 5.6 – Vitrinite, Liptinite and Inertinite profiles up seam within the lower Svea Nord Seam. Note that vitrinite increases upseam, liptinite decreases and inertinite exhibits a weakly cyclic distribution. Repeats plotted

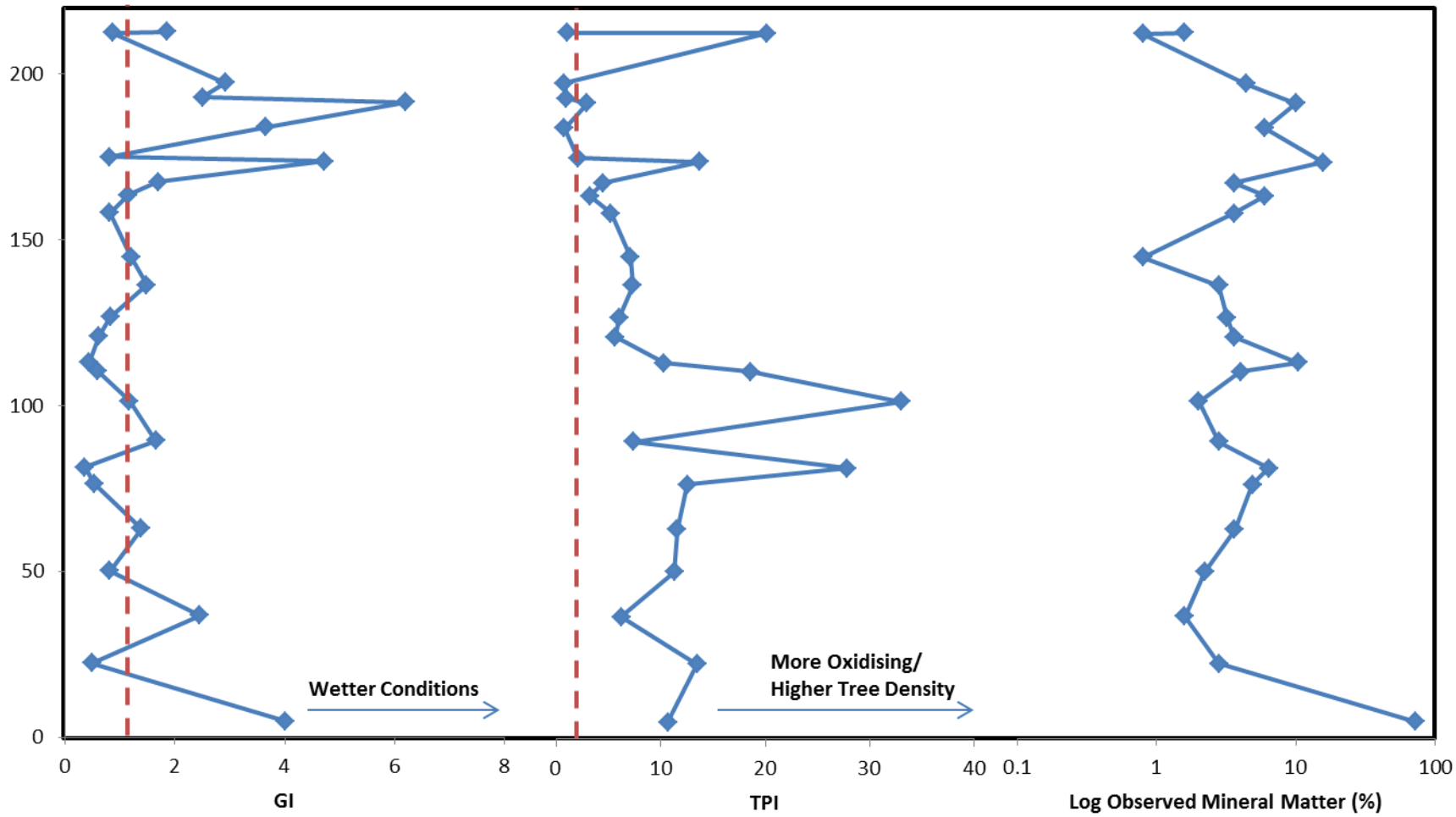

Fig. 5.7 – TPI, GI (*after Casareo et al., 2006)* and observed mineral matter profile within the Lower Svea Nord Seam. Note the drying events within the lower TPI profile and the increasingly wet conditions as indicated by higher GI values at the top of the seam

the seam at this location after splitting was characterised by wetter (high GI) and more degraded peats (TPI ~1) which initially contained significant mineral matter (~60%; Fig 5.9).

The upper peatland was generally wetter than the lower peatland (GI ~6 vs <1 previously) indicating increasing hydrological stability and increased groundwater component. This may be due to a relative rise in sea level raising water tables, the underlying split acting as conduit for groundwaters, increased precipitation or a combination of each.

Evidence of only one significant period of drier peat conditions is recorded at 328cm above seam base (GI < 1, TPI > 1. As in the lower seam this was followed by an increase in mineral matter indicating collapse of the peat surface allowing sediment to be washed onto the peat surface. In more marginal areas of the Svea Seam a second splitting event occurs (Chapter 3) with the observed increase in mineral matter from the central peatlands thought to be an expression of this.

After splitting the peatland returned to relatively stable hydrological conditions with dominance of vitrinite macerals, Low TPI values and GI > 1. This is consistent with a change to a more hydrologically stable regime, less dependent on local catchment and variations in precipitation. It is at this time that observation of perhydrous vitrinites occur (Appendix I), which has been shown

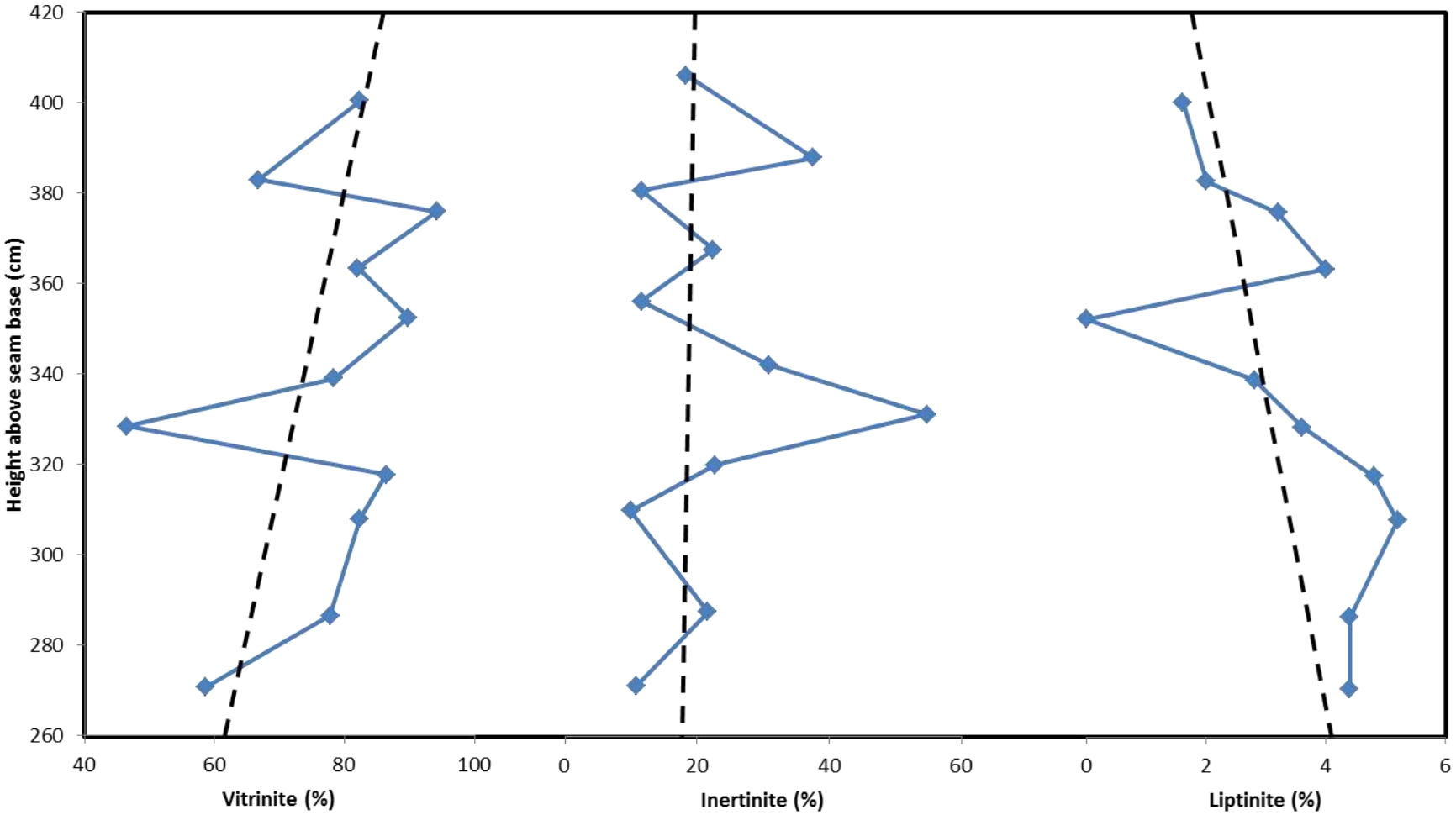

Fig. 5.8 – Vitrinite, inertinite and liptinite profile up-seam within the upper Svea Nord Seam showing increasing vitrinite, stable inertinite and decreasing liptinite up-seam.

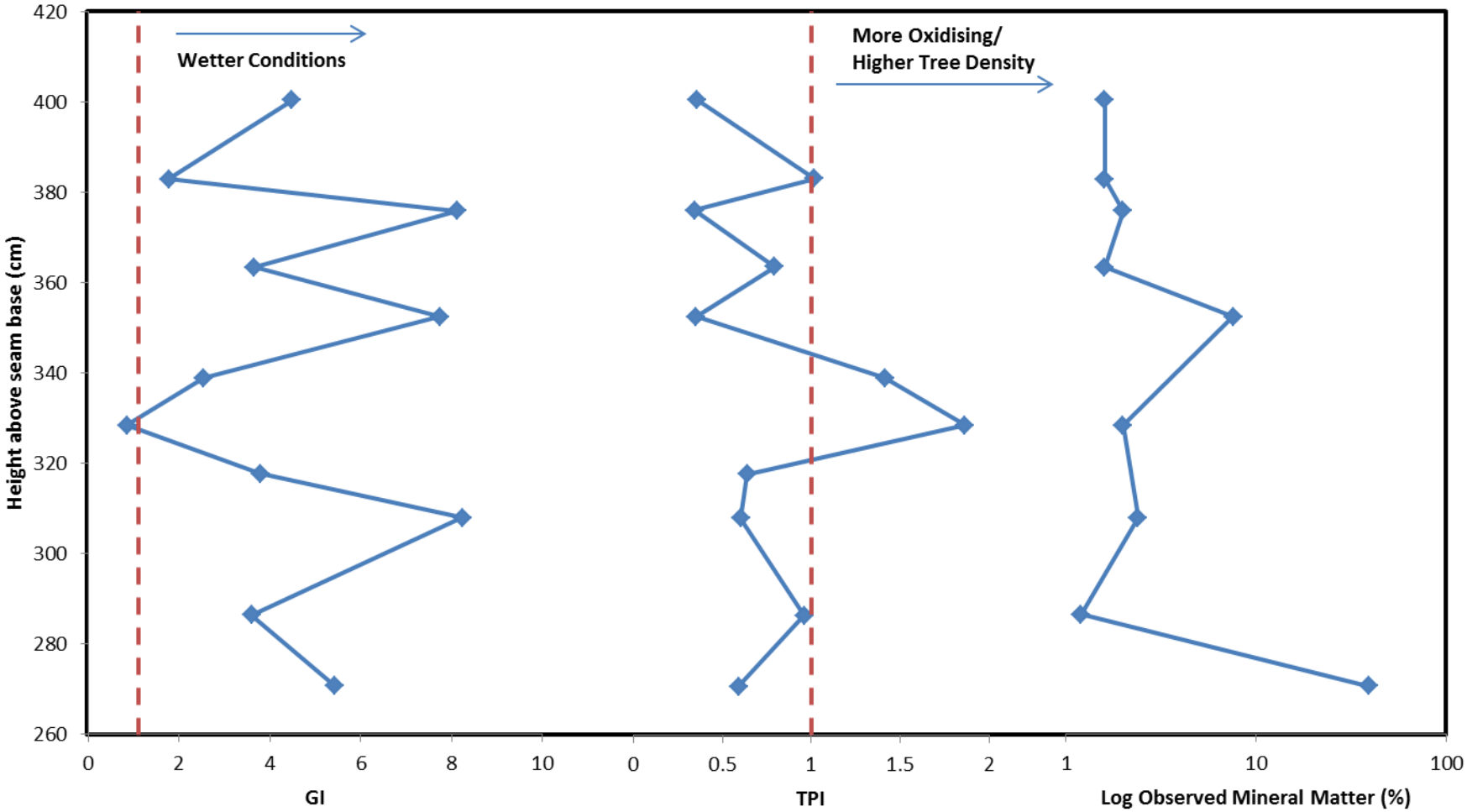

Fig. 5.9 – TPI, GI (*after Casareo et al., 2006)* and observed mineral matter profile within the Upper Svea Nord Seam. Note the wetter conditions and fewer drying events within the upper seam compared to the lower seam

previously within the Longyear seam to be an indicator of oil potential (Chapter 4). This would therefore indicate that up-seam the environment of the Upper Svea peatland was becoming increasingly similar to that within the Longyear seam namely more fen-like.

The termination of the seam at this location appears to have been characterised by a slight drying of the peatland followed by a period of soil formation before eventual marine transgression. This is evidenced by numerous root cortex tissues and sclerotinite within the top 30cm of coal (Appendix I). This indicates a transition to mineral soils with plant colonisation. This indicates the Svea Nord Seam was followed by increased clastic floodplain deposition and following a drop in the water table, exposing the peat surface to flooding.

5.5.1.4 – Effect of peatland hydrology upon the inorganic composition of the Svea Nord seam

The hydrological regime within the Lower Svea Nord seam appears to have had at first glance very little effect upon the lithophile elements with lithophile element profiles remaining relatively stable and with little of the variation expected within a raised peatland. However, two large 'saw tooth' features occur within the Al/Ti, K/Ti, Fe/Ti and other immobile element profiles (Fig. 5.10; 5.11) at 110cm and 145cm above seam base. These coincide with periods of

increased inertinite contents within the coals indicating drier more oxidising conditions (Fig.5.12). These areas of Ti enrichment coincide with a peak in fusinite indicating combustion during this period.

The effect of drought has been shown to result in acidification of peat due to the oxidation of stored reduced sulfur (Dillon et al., 1997; Scott et al., 1998). The decrease in pH leads to an increase in dissolved metals (Tipping et al., 2002) and loss from the peatland The amount of metals leached is dependent upon the severity of the drought; however after sustained drought metals leached from the peatland cannot be replaced by current and future metal deposition. Other reasons for these features include formation of a soil with downward transport and leaching or oxidation of reduced Fe discharge to the surface by groundwater after combustion/collapse of the peatland.

Al appears to have been highly mobile throughout the formation of the Lower Svea Nord Seams deposition and is therefore distributed evenly throughout the lower seam (Fig.5.10). The variability of the water table and acidity within the Svea Nord Seam at this time allowed Al to be remobilised by diffusion or groundwater flow, enhanced by the oxidising conditions within the peat (Takeno, 2005).

Consequently, although groundwater is not the source of the lithophile elements in the lower Svea Nord seam, it appears that

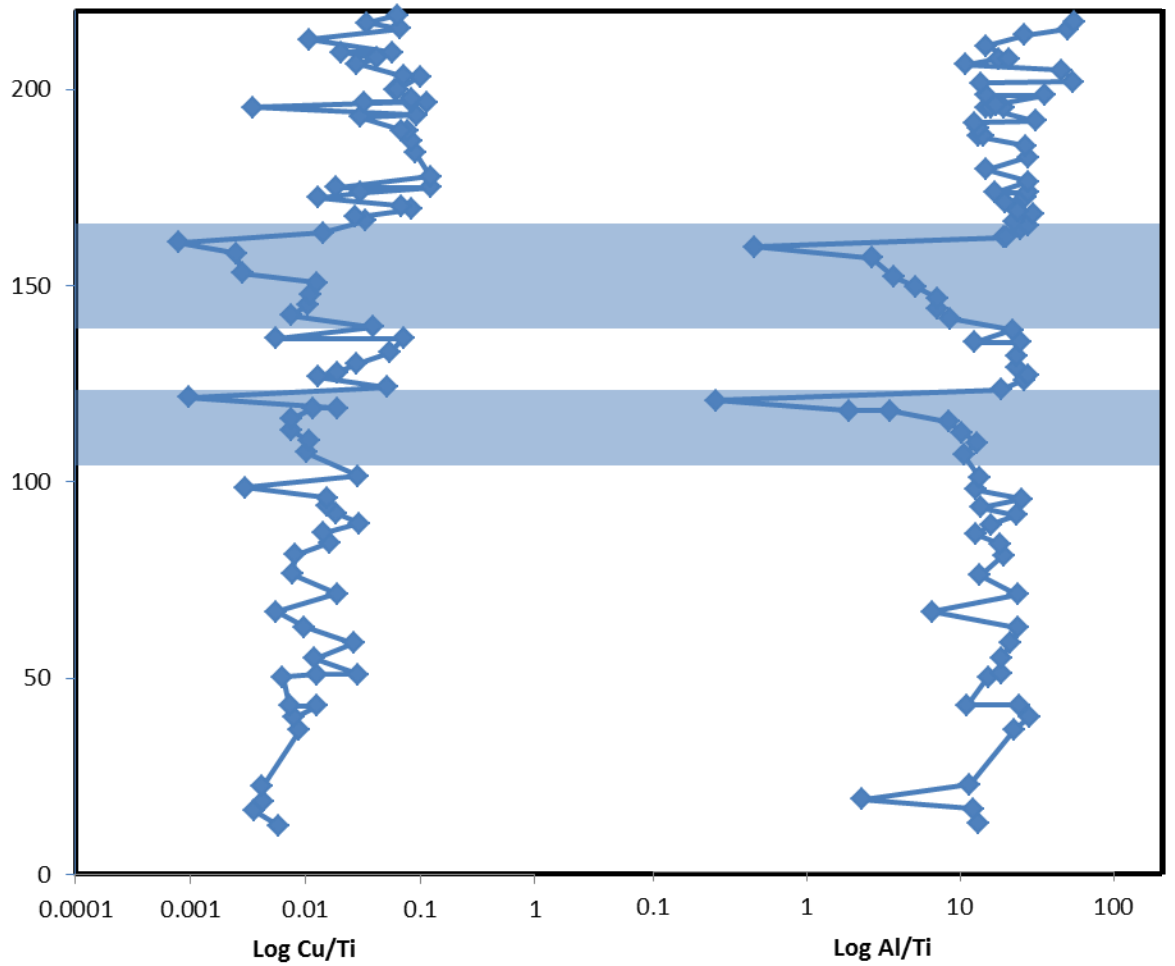

Fig. 5.10 – Log Cu/Ti, Log Al/Ti profile from the Lower Svea Nord Seam, Note the 'saw tooth' profile at 110cm and 160cm indicating acidification and leaching of the peatland. Errors ±5% of displayed values

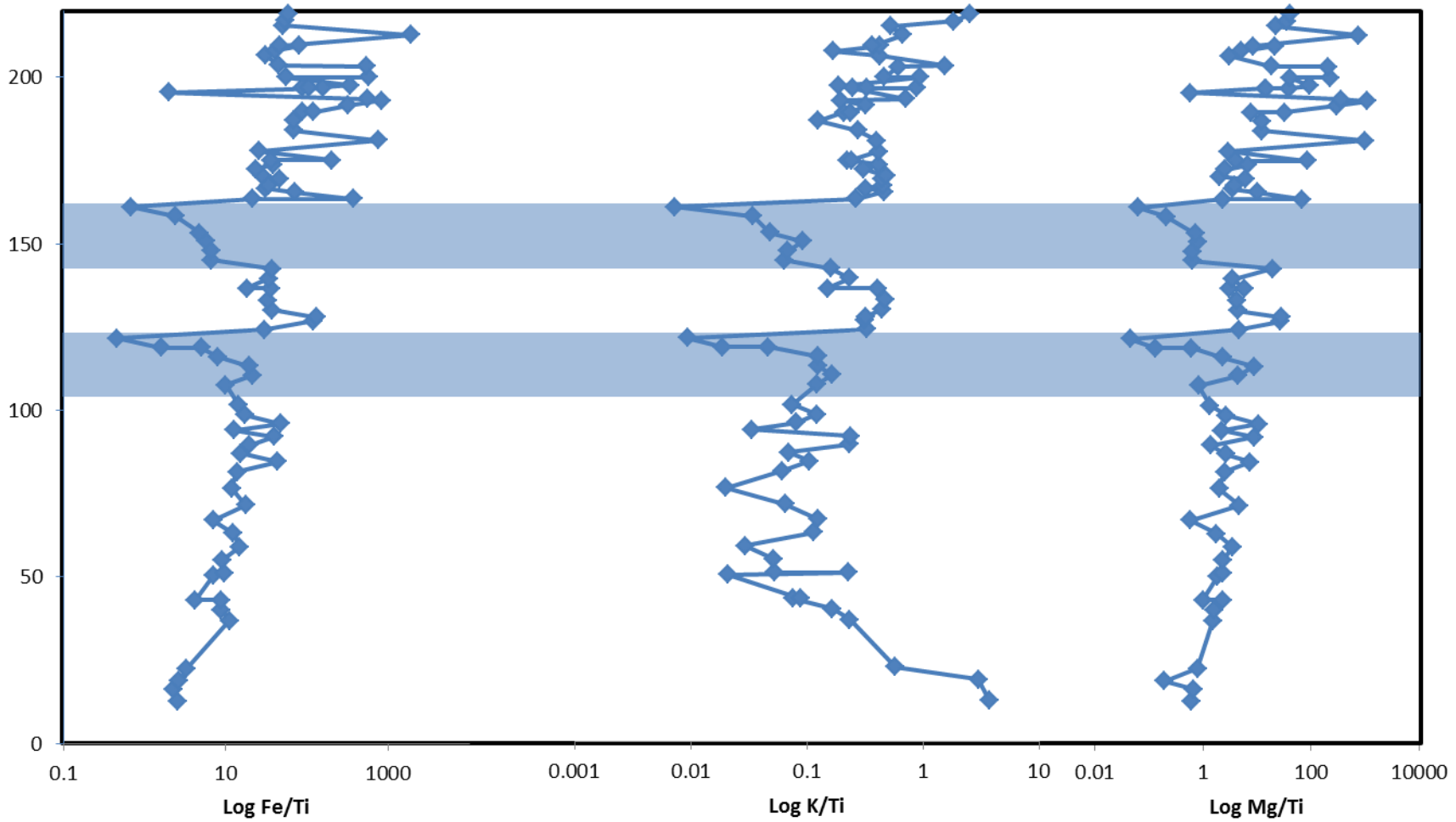

Fig. 5.11 – Log Fe/Ti, Log K/Ti, Log Mg/Ti profile from the Lower Svea Nord Seam, Note the 'saw tooth' profile at 110cm and 160cm indicating acidification and leaching of the peatland. Errors ±5% of displayed values

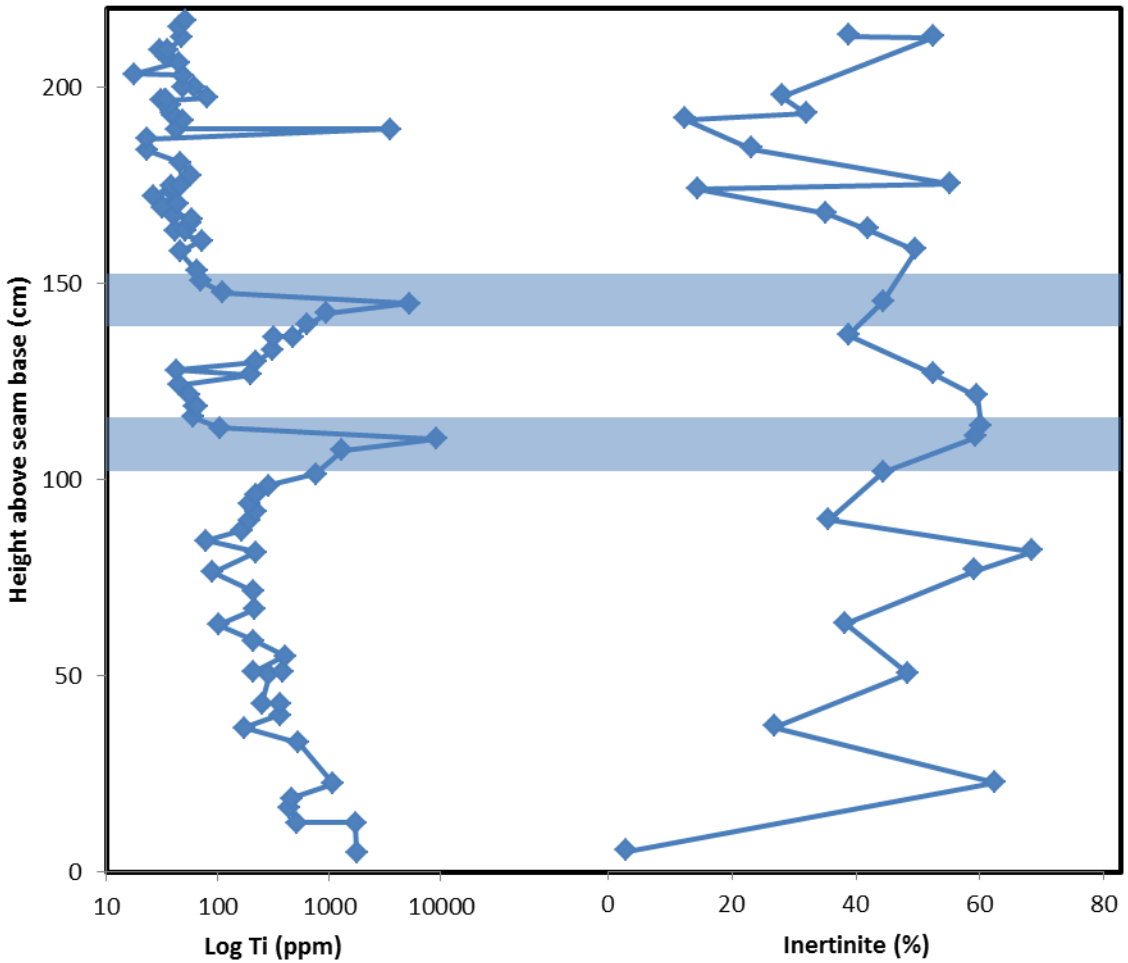

Fig. 5.12 – Log Ti and inertinite profile from the Lower Svea Nord Seam. Note peak Ti occurs slightly after peak inertinite Ti Errors ±5% of displayed values

peatland hydrology influences their distribution, particularly during prolonged drought (high inertinite intervals).

5.5.1.5 - Phosphorus and peatland fires

A study by Smith et al., (2001) showed that during peat fires within the everglades total carbon, total nitrogen and total organic phosphorus decreased. This is partially explained by the volatilisation of carbon and nitrogen; however phosphorus appears to be fixed within the peat as inorganic phosphate minerals. Smith et al., (2001) also report an increase in calcium fixation which is associated with the formation of Ca-Mg phosphates such as apatite and crandallites. Although inorganic phosphorus is more bioavailable to certain plants and this study covers only recent peats, it is conceivable that fire may provide a mechanism for the enrichment of phosphorus in coals.

It is intriguing that the Svea Nord Seam (Orheim et al., 2007) is both phosphorus & fusinite (charcoal) rich with mineral compositions dominated by crandallites and apatite (appendix I), supporting the hypothesis that wild fires were a significant control upon P concentrations in the Svea Nord seam.

The distribution of P within the section sampled shows the highest concentrations in the first 2m of the lower seam (Fig. 5.13) with few P problems in the upper seam reflecting the more hydrologically stable, groundwater dominated conditions in the upper seam.

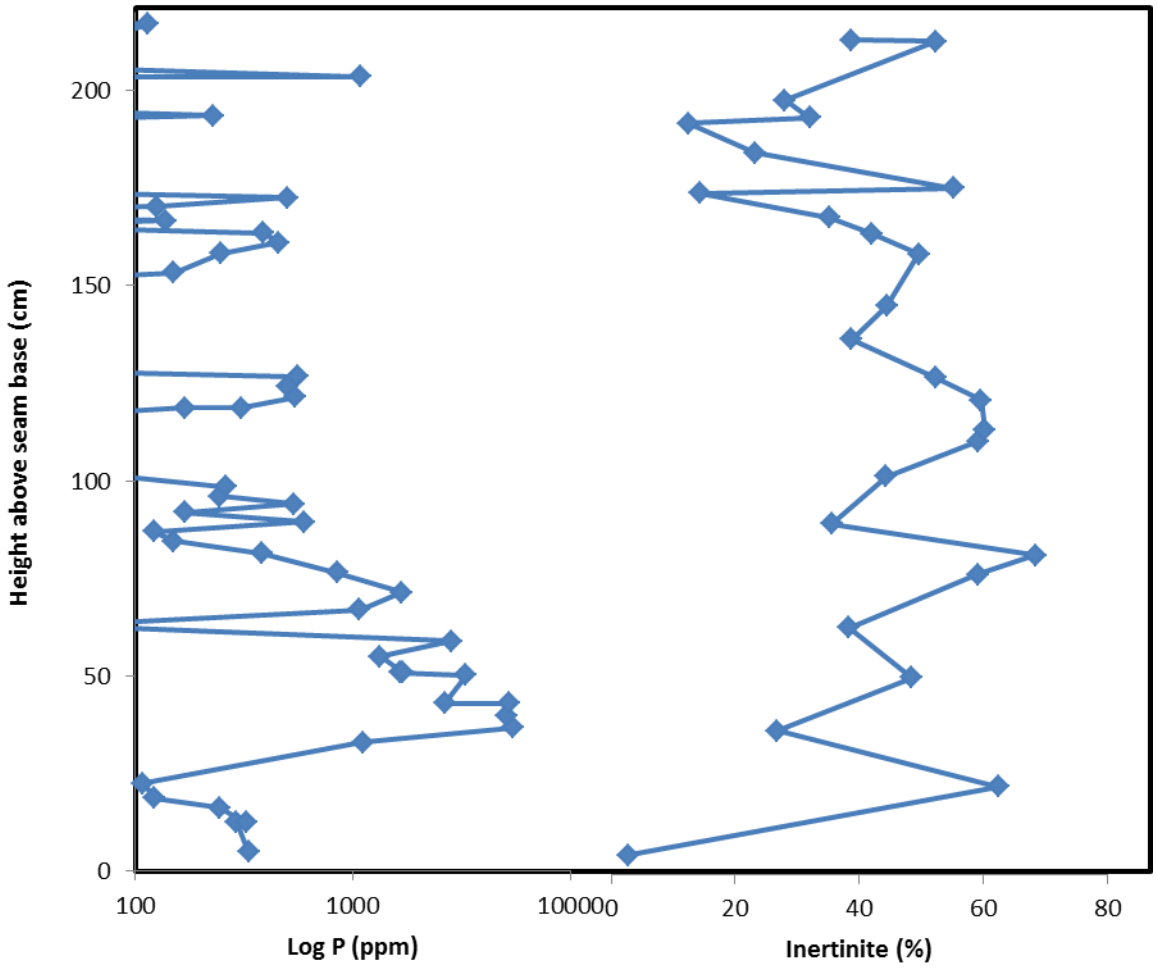

Fig. 5.13 – Log P and inertinite profile from the Lower Seam, Note P is concentrated within the more inertinite rich bottom of the seam

P Errors ±5% of displayed values

Another control on phosphorus could be associated with stabilisation of P by acidification, increasing the concentration of Al in solution linked to drier peatlands

Although the data is limited by the equipment constraints (high detection limits etc.) it does imply a possible causal link between dry peatland/fire and phosphate within the lower Svea Nord Seam, which in turn is controlled by the hydrological stability of the peatland during the period of deposition.

5.5.2 Dust deposition and the Lithophile elements

The lithophile elements, have been subject to local remobilisation within the Lower Svea Nord Seam, however the close correlation between the lithophile elements (Fig. 5.3) indicates that they must have had similar sources, the two most obvious of which are clastic sedimentation and aeolian wind-blown dust.

The provenance of the lithophile elements to the Svea Nord coal is important as it controls the elemental composition of the peatland, influencing both gross ash content and the concentration of problem elements. To consider the orgins of the lithophile elements the concentrations were normalised to Ti.

Examination of the Al/Ti and Na/Ti profile for the Lower Svea Nord Seam (Fig. 5.10) show values close to that of MCC indicating a MCC source (Rudnick and Gao, 2003). However this does not allow

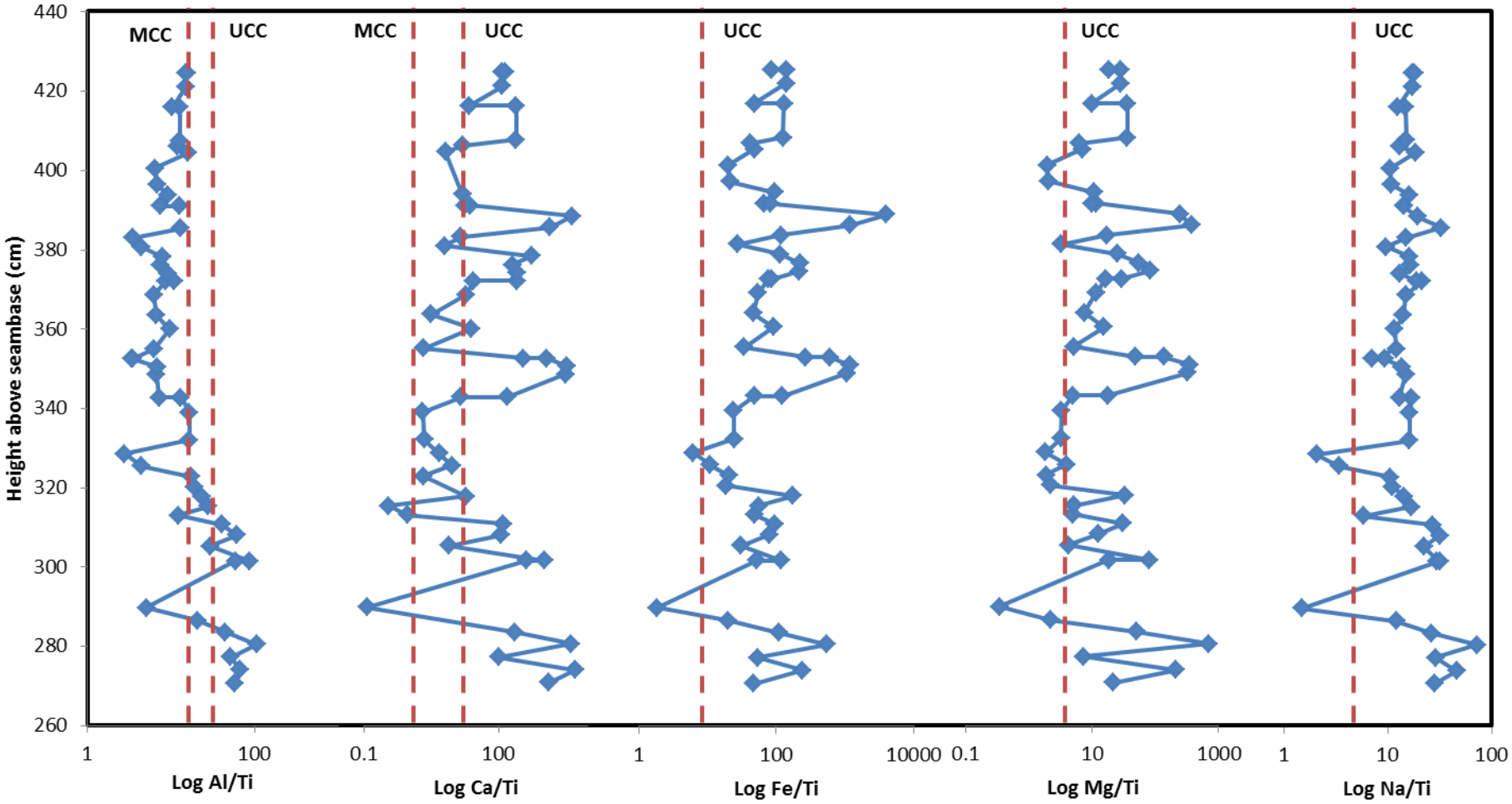

Fig. 5.14 – Major element profiles normalised to Ti in the Upper Svea Nord Seam. Note the lithophiles show values close to mean continental crust (*Rudnick and Gao,2003)* whereas Fe and Ca are relatively enriched. Errors ±5% of displayed values MCC = Mean Continental Crust UCC = Upper Continental Crust

the discrimination between local clastic supply and more distal dust supply.

In the upper seam, the Al/Ti and Na/Ti ratios show more variability upseam (Fig.5.14) with peaks values coinciding with peak inertinite indicating dry conditions. Al is enriched closest to the split but decreases to MCC values at the top of the seam. Na/Ti and K/Ti remain at around MCC values with Fe enriched compared to MCC due to groundwater deposition. However, there is still difficulty differentiating between local clastic and Aeolian source for the lithophile elements.

Dust deposition rates in the Svalbard region today (Mahowald et al., 2006) are low ($0.20 gm^{-2} yr^{-1}$). During the Palaeocene, the continental configuration had some similarities to that of today and therefore Palaeocene Svalbard may have had similar dust deposition rates. Consequently, if the concentrations of the lithophile elements and ash are low (<10%) within the Svea Seam a dust provenance is likely and where it is higher a clastic source is more likely. As the both the upper and lower seams are relatively low ash (excepting during initiation and termination of the seam), a dust provenance for the lithophile elements is considered likely.

Cu is enriched within dust and the record of atmospheric deposition of Cu is well preserved within peatland environments (Nieminen et al., 2002). Therefore, the examination of the Cu/Ti record (Fig. 5.15;

5.16) should provide an indication of the provenance of the lithophile elements within the Longyear seam during different climatic conditions. Local sediment making up the split has already been shown previously to have a Cu/Ti composition of 0.004 (Section 5.42) whereas the Cu/Ti composition of mean global dust is 0.01 (Niemenen et al., 2002). This difference therefore allows the provenance of the lithophile elements to be determined.

Examination of the Cu/Ti ratio from the lower Svea Nord Seam shows Cu/Ti values broadly similar to those seen within mean continental dust (0.01; Fig.5.15; Lawrence and Neff, 2009). Values similar to the local sediment source are broadly associated with prolonged drought and combustion events where the collapse of the peat surface allowed clastic deposition or locally derived dust supply to dominate.

In the upper seam the Cu/Ti ratio is again generally similar to that of mean continental dust (Fig.5.16). As in the lower seam, values corresponding with local dust/clastic sources are found during drier periods and during wetter periods are closer to MCD values. This may be due to intensification of the hydrological cycle during warmer wetter periods (Chapter 6)

These wet-dry cycles appear to exhibit a degree of cyclicity of around 40cm/cycle. This cyclicity is similar to that observed in the Longyear seam, which has been inferred to be precession controlled (Chapter

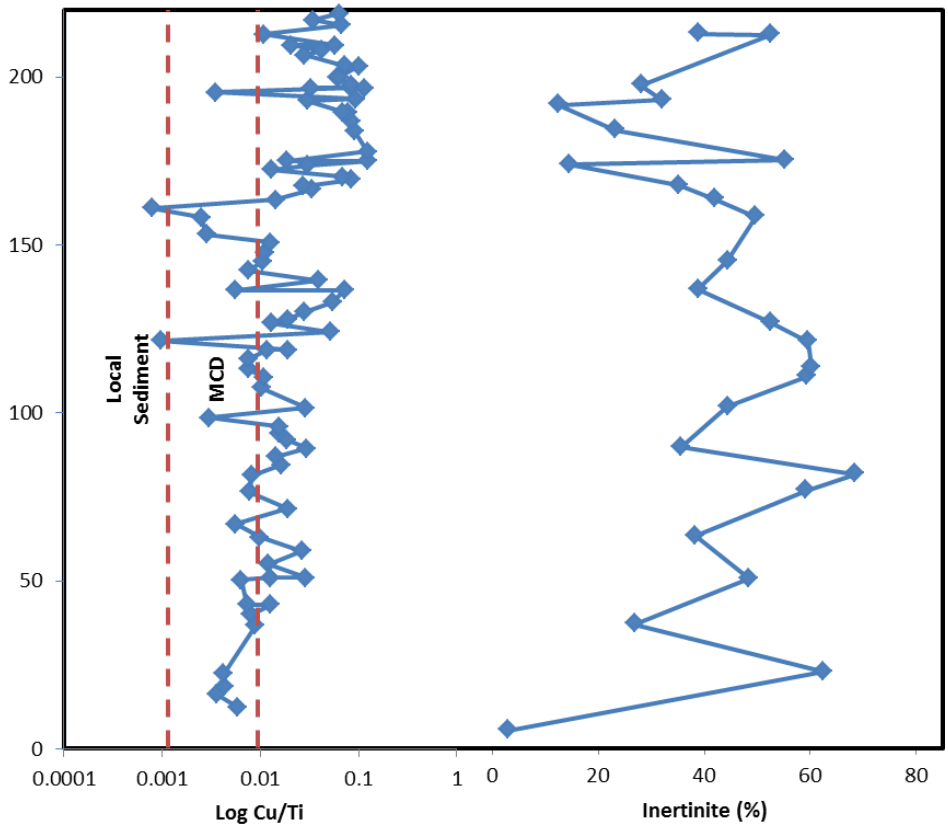

Fig. 5.15 – Log Cu/Ti and inertinite profile from the Lower Svea Nord seam showing values consistent with mean continental dust (MCD; Lawrence and Neff, 2009) except during peak inertinite where local clastic sediment is deposited

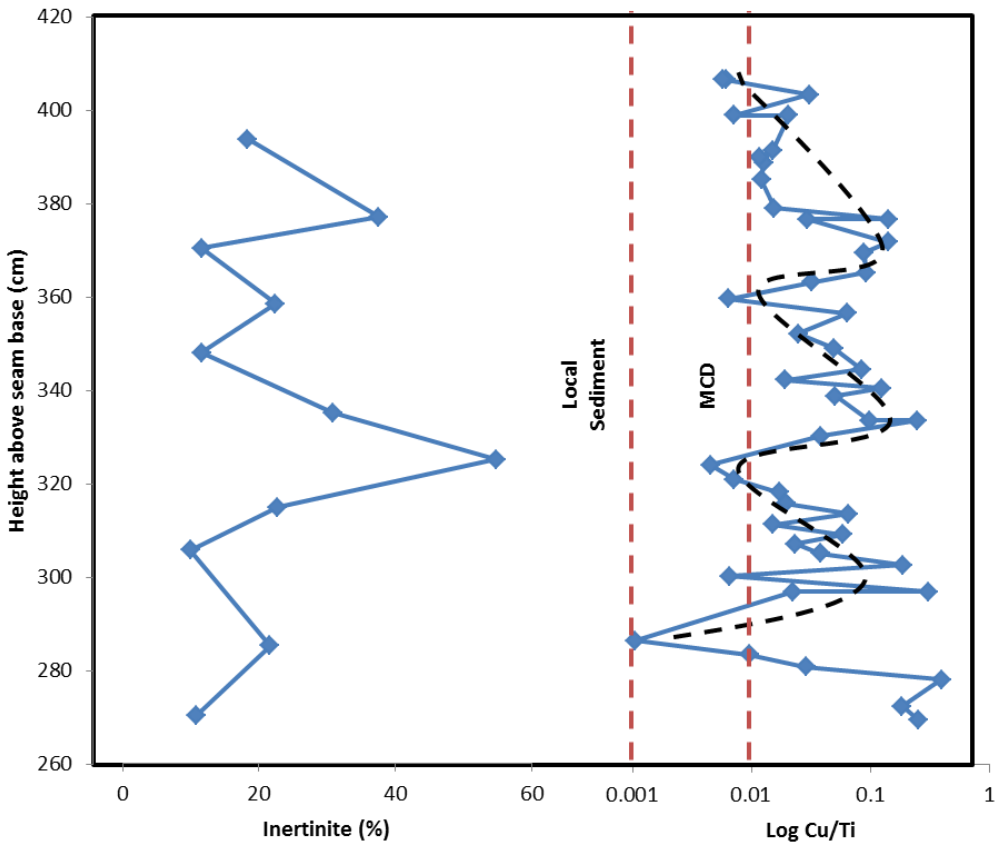

Fig. 5.16 – Log Cu/Ti and inertinite profile from the Upper Svea Nord seam showing values consistent with mean continental dust (MCD; Lawrence and Neff, 2009) this alternated between more Cu rich and more typical MCD values on cyclic basis (40cm cycles)

6). If this is correct it would indicate that the upper Svea Nord seam at this location took ~80kyr to form and lithophile element concentration controlled by precessional cycles similar to the Longyear seam.

It is therefore considered that the predominant control upon the supply of lithophile elements (away from the sources of clastic sediment such as the upper slopes and valley bottom) within the upper and lower Svea Nord Seam is precessional controlled dust cycles with dust from local sources dominating during drier periods and more distal dust sources during wetter periods. In the lower seam these cycles are less well expressed due to the overwriting effect of the acidic conditions within the peat within the more mobile lithophile elements (Al, Na, K) leading to a number of leaching events and averaging of the lithophile element profile up-seam (particularly Al).

5.5.3 Marine supply of Sulfur to the peatland

Sulfur concentrations within the lower Svea Nord Seams remain constant throughout the seam (~0.35%). This would indicate a stable supply of S to the peatland (Fig.5.17) likely derived from a combination of atmospheric and groundwater sources. The exception to this trend is seen at the seam base where values are significantly lower. As this occurs at the transition between clastic

wetland and peatland conditions, this may be caused by residual flow within the peatland flushing S from the system.

In the upper seam, sulfur concentrations increase gradually from 0.5% at the resuming of the seam to 1.2% at the termination of the seam (Fig.5.18). This shows the supply of sulfur increased during this period indicating the increasing influence of a new source of sulfur during the latter stages of peat formation. As the Svea Nord Seam was covered with marine sediments relatively quickly (5m) after termination, marine influence is a likely source of this extra sulfur.

Using the model of Large et al. (2011) for sea salt sulphate deposition at high latitude vs. distance inland (Chapter 6) the difference between the base and termination of the seam is equivalent to the coastline advancing from in excess of 8km away from the seam to within 1.5km of the coastline. The shape of the curve also matches that modelled closely indicating that sea sulphate deposition were responsible for the extra sulfur seen within the upper seam.

Upon termination clastic input likely became too great for peat formation to continue, replacing the peatland with coastal floodplain. This termination occurred further away from the coastline than within the Longyear seam which terminated only when within 250m-500m from the coastline.

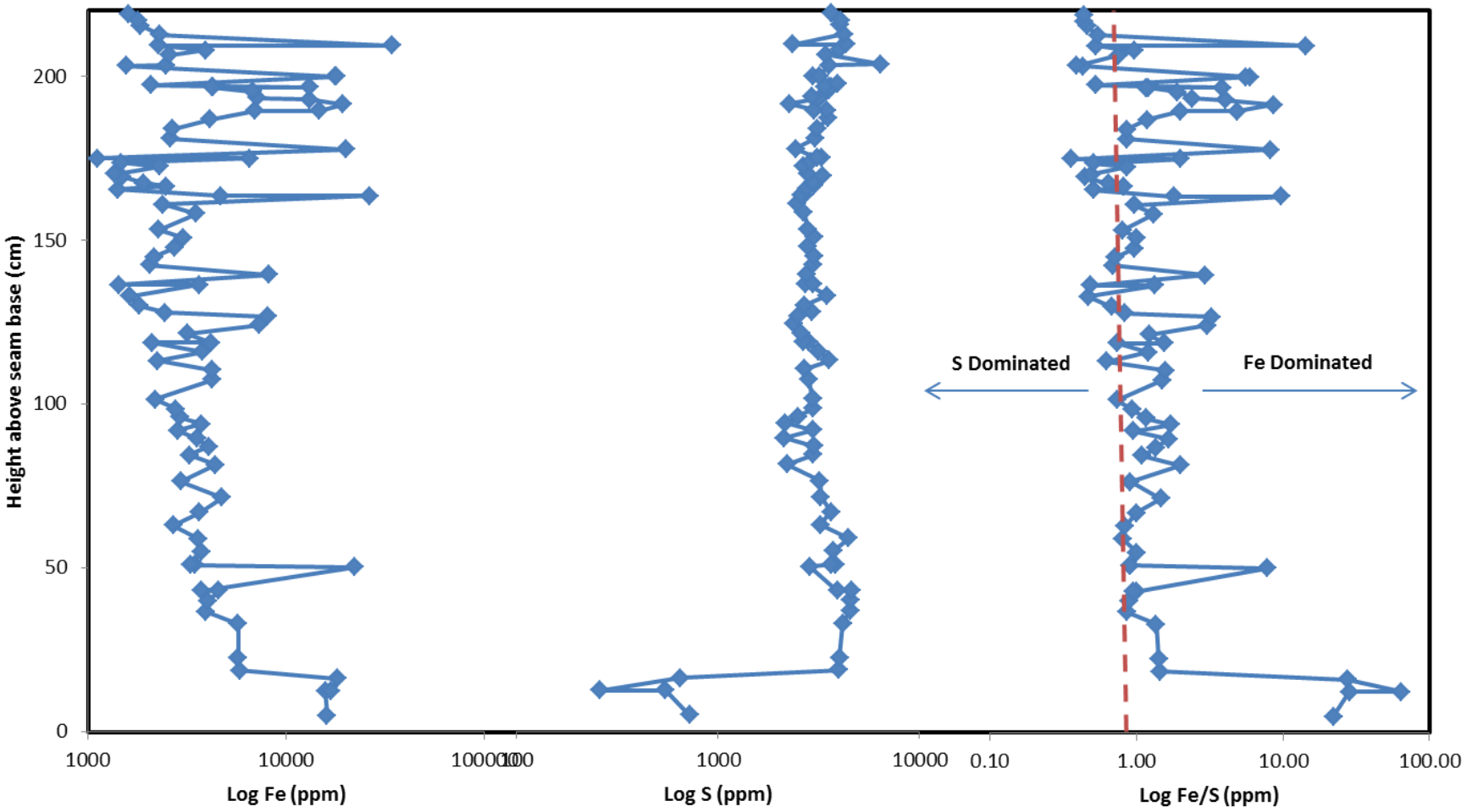

Fig. 5.17 – Log Fe, Log S and Log Fe/S ratio in the Lower Svea Nord Seam showing constant S concentrations up-seam, variable Fe and a Fe enriched peatland system with little free sulfur, indicating low oil potential (Chapter 4) Max deviation ±5% from displayed values

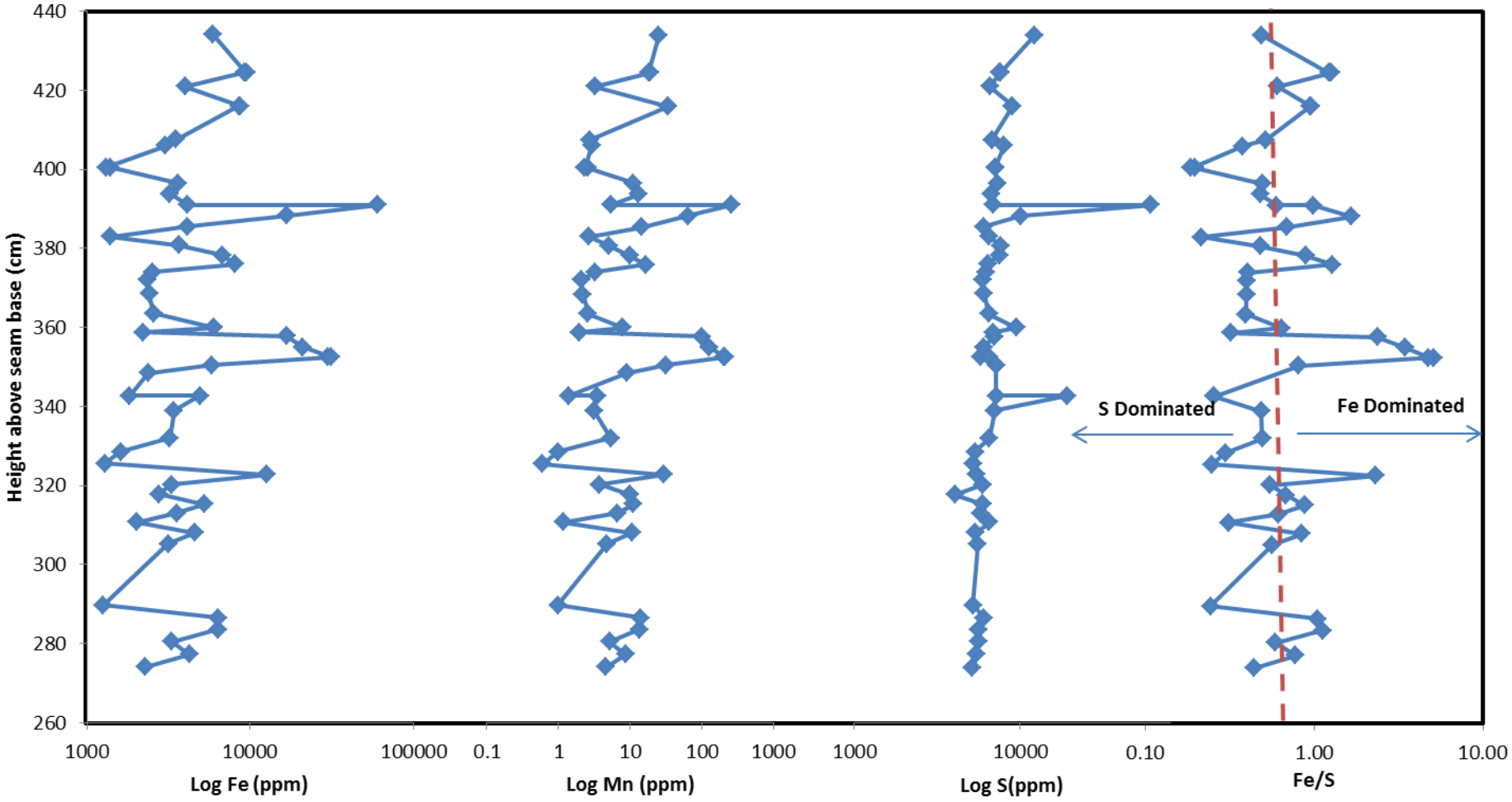

Fig. 5.18 – Log Fe, Log S and Log Fe/S ratio in the Lower Svea Nord Seam showing gradually increasing S concentrations up-seam, variable Fe and a S enriched peatland system with free sulfur, indicating higher oil potential (Chapter 4). Max deviation ±5% from displayed values

This may be due to differences in the topographic framework that existed between the Svea Nord Seam and the Longyear seam. The Longyear in a broad coastal plain would have groundwater relatively evenly across the plain whereas the topographic depressions in which the Svea was situated would act as conduits for hydrological flow making it more vulnerable to rising water tables.

The Fe/S ratio within the Svea Nord seam is primarily controlled by Fe as the S concentration does not increase significantly (Fig.5.17; 5.18). The Lower Svea seam is consistently enriched in Fe (Fig.5.17) leading to high Fe/S ratios (>0.9) indicating that there is little free sulfur within the system to produce oil prone coal (Chapter 4). The upper Svea seam however is enriched in S (Fe/S < 0.9; Fig.5.18) compared to Fe suggesting that the uppermost 1.5m of the seam may be oil prone. The only areas where the Fe/S ratio is above 0.9 are within drier periods (high inertinite), which is similar to that seen within the Longyear seam (Chapter 4; Chapter 6).

The main source of sulfur evolved over the duration of the Svea Nord Seam with increasing marine influence (due to an advancing shoreline/transgression) in the upper seam. This evolution led to a gradual shift of the Fe/S ratio from low to high oil potential conditions.

5.6 Palaeo-environmental Development of the Svea Seams

Integrating the palaeogeographic (Chapter 3), organic petrographic, organic and inorganic petrographic data presented previously, a detailed depositional history of the Svea seams can be presented.

The initiation of the Svea seams began within the southernmost valleys and depressions formed during the uplift and erosion of the Cretaceous peneplain. These were marked by a number of braided stream beds which produced the Grønfjorden beds. Over time the valley bottoms became waterlogged, formed clastic marshes (Fig.5.19). These became increasingly dominated by organic matter initiating the peatland proper.

The hydrological supply to the lower Svea Nord peatland was limited by a local catchment and a dependence upon precipitation. This resulted in a vulnerability to oxidation and combustion.

During combustion events the surface of the peatland collapsed to the water table allowing sediments to wash on to the peatland forming thin ash layers. (Fig.5.19) Otherwise, clastic supply to the lower Svea Nord peatland was primarily through dust deposition with dust sourced locally during dry periods and from further afield during wetter periods due to the intensification of the hydrological cycle.

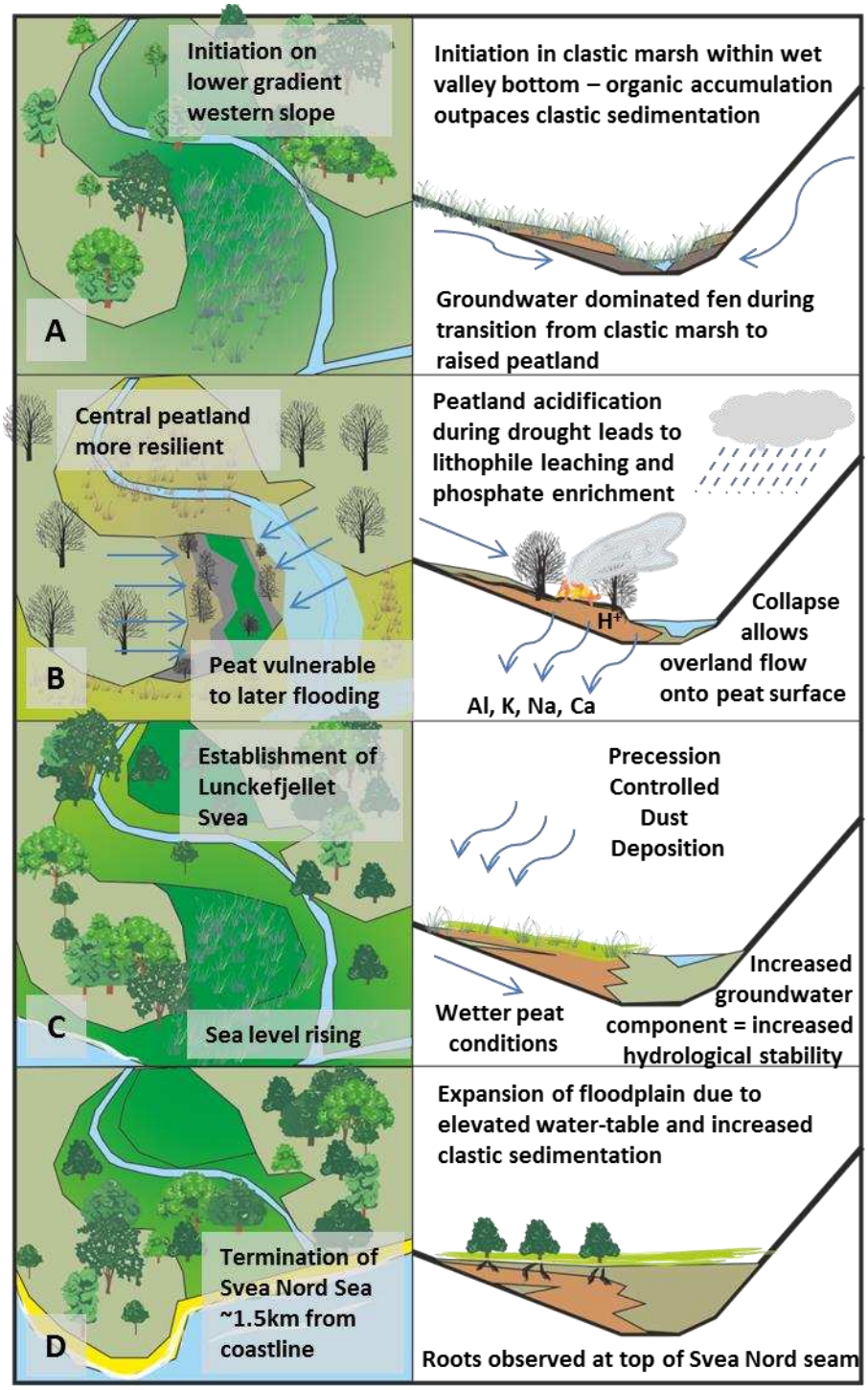

Fig. 5.19 Palaeo-environmental development of the Svea Nord Peatland from initiation to termination (A) Initiation of the peatland (B) Conditions within the Lower seam and split development (C) The upper Svea Nord Seam (D) Termination of the Svea Nord Seam. This shows increasing marine influence over the Svea Nord Seam, associated with rising relative sea levels.

On two occasions (Fig.5:19) severe drought caused acidification of the peatland and leaching of more mobile metals from the peatland surface, with conditions remaining acidic enough during the entire lower peatland to effectively homogenise the distribution of Al within the peat.

The peatland dried out again towards the top of the lower seam, culminating with a fire that burnt the peat surface to the water table. This led the peatland to become vulnerable to inundation and sediment to be washed from the slopes above onto the peatland, initiating splitting (Fig.5.19). This splitting event terminated peatland accumulation across the valley except for the very centre of the raised bog.

Peatland formation resumed with a much more stable hydrological supply due to a combination of raised water tables (Fig.5.19) due to sea level rises and increased groundwater input to the peatland (possibly due to supply through the split).

The upper peatland was less acidic, wetter and more reducing than previously allowing the preservation of fluctuations in the amounts of dust supplied to the peatland. These fluctuations showed some cyclicity at ~40cm/cycle which is similar to those attributed to 21kyr precessional cycles within the Longyear Seam (Chapter 6). The same trends in dust provenance as the lower seam were seen with

local sediment sources dominating during dry periods and from more distal locations in wetter periods.

This continued until the termination of the seam where rising sea levels caused water tables to rise faster than peat could accumulate, increasing clastic supply to the Svea Nord area and causing vegetated flood plain material to accumulate. This was then buried underneath marine sediments relatively quickly after the cessation of peat formation.

Peat formation then shifted northward with deposition of the Lunckefjellet Svea occurring concurrently with the deposition of volcanic ash. This formed the bentonite layer seen within the geological record today. As sea levels increased Svea peatland formation shifted to the base of gulleys within the peneplain such as the Breinosa Svea. Similar depositional environments can be seen in the Adventdalen region today (Fig.5.19)

These 'fan type' peatlands (Fig. 5.19) were smaller in size than the earlier peatlands and were vulnerable to clastic material from the top of the gulley washing onto the peatland. This lead to a clastic control upon most of the elements, leading to high ash contents compared to the earlier Svea Seams. Due to the more stable hydrological supply these peatlands were wetter but were of poorer quality and were more short-lived than the Svea Nord peatland.

The seams were then buried by subsequent sedimentation, buried and rapidly uplifted to the positions seen today where it was exploited in mines around the Svea Area (Fig.5.1).

5.7 Conclusions

The Svea seams represent the infill of the Grønfjorden valleys and the colonisation of fans at the base of gulleys across the central tertiary base. Deposition began and was greatest in the southernmost valleys (Svea Nord, Lunckefjellet Svea, Ispallen Svea) and shifted to predominantly 'fan type' deposits during the late Svea period. The main controls upon the coal quality of Svea Nord 'valley type deposits were (Fig.5.20);

- Groundwater/Hydrological Conditions – most important in the lower seam, instability leads to acidification of peatland and remobilise lithophile elements, primary source of Fe, Ca, Mg, Mn
- Aeolian dust supply – Controls absolute lithophile element concentrations, overwritten by peatland hydrology in lower seam. Controlled by precessional cycles in upper seam
- Marine sulphate deposition – Increasing supply in upper seam due to increasing proximity of seam
- Clastic supply – washed onto seam surface after combustion event and during the initiation and termination of the seam.

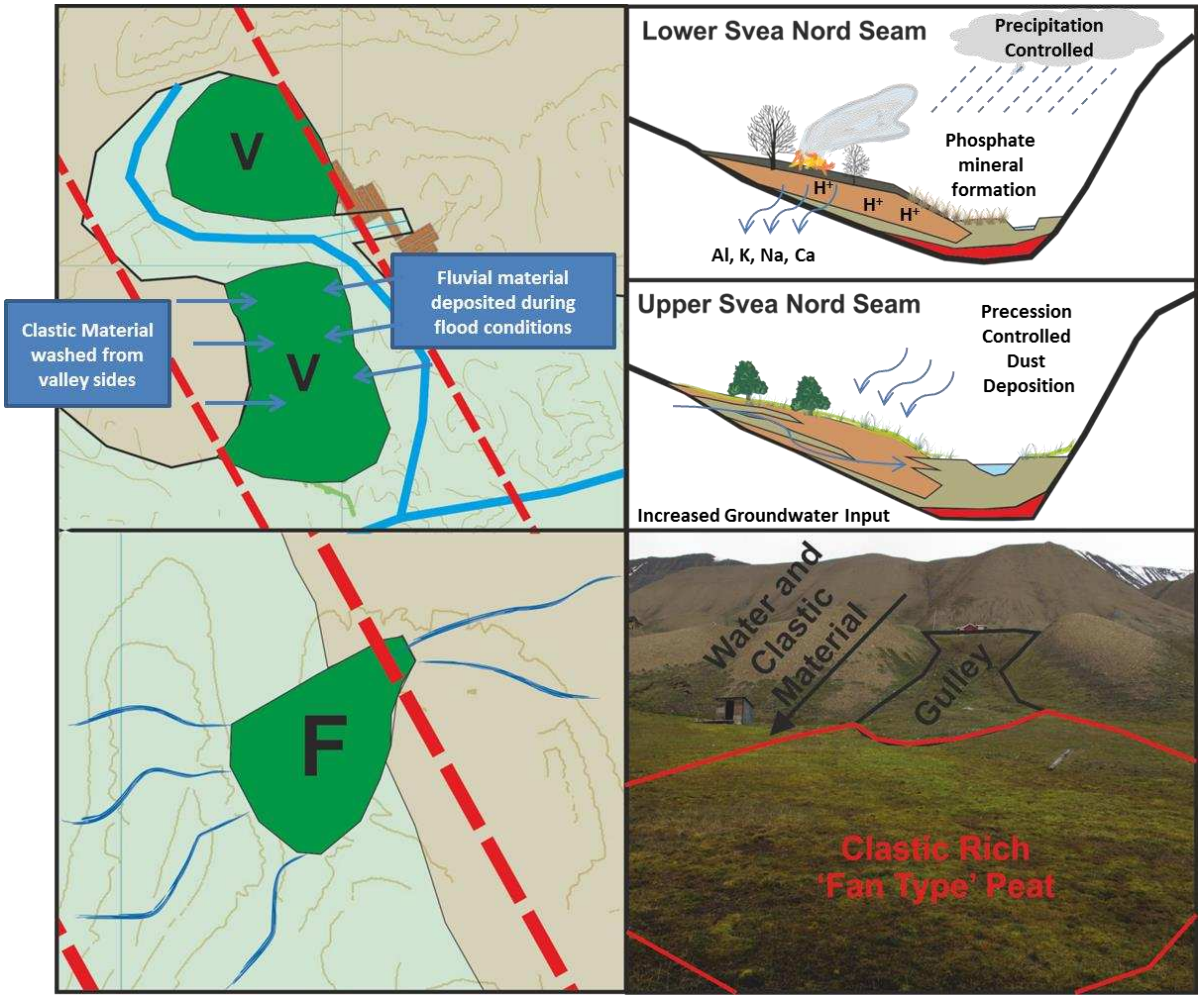

Fig.5.20 – Summary diagram of the major controls upon coal quality within the Svea Nord Sea, (A) and Breinosa Svea (B). Note that the 'fan type' peat deposits can still be seen in Adventdalen today and would be expected to produce very ash rich coals (*source M. Jochmann)*

The main control upon the 'fan type' Breinosa Svea is the hydrological stability provided from the adjacent topography and underlying fan. However, as a result clastic supply significantly exceeds inorganic material from other sources (Fig.5.20). This explains the reduced seam thickness and poorer coal quality which characterise the 'fan type' seams.

Chapter 6

THE PALAEOENVIRONMENTAL EVOLUTION OF THE LONGYEAR SEAM AND ITS EFFECT UPON COAL QUALITY

6.1 Introduction

The Longyear has been exploited within the Adventdalen region since the earliest period of mining on Svalbard. The Longyear seam was initially mined close to the settlement of Longyearbyen before moving eastward as supplies of good quality coal were exhausted. Coal is currently extracted at Mine 7 (Gruve 7, Adventdalen) with a mine under construction at Lunckefjellet (close to Svea Nord) and a future mine site at Bassen (opposite mine 7).

The Longyear seam has also been shown to be oil prone (Chapter 4, Orheim et al. 2007, Marshall et al. 2013) and therefore has the potential for either in-situ or ex-situ retortion of significant quantities of hydrocarbons. In addition, although coal quality of this seam are the subject of a number of publications (Ćmiel and Fabiańska, 2004; Orheim et al. 2007; Lewińska-Preis et al., 2009) and potential controls discussed, these have not been placed within the context of the hydrological landscape discussed in Chapter 3. Landscape hydrology controls the balance of groundwater, clastic, atmospheric influences on quality allowing coal quality to be predicted at different locations in the peatland.

This Chapter will build upon the palaeogeographic reconstructions and geological histories presented in Chapter 3 in order to understand and predict coal quality across the basin. This will be achieved by using inorganic and organic geochemical techniques. This will be supplemented with organic petrographic techniques which will be used to examine the hydrological development of the Longyear Seam. As in the Svea, the period of peatland formation will be constrained by estimating depositional period using TOC and modern LORCA rates and consideration of possible orbital signals within lithophile element profiles. This will then be used to consider changes in dust deposition and climate during the period of the deposition of the Longyear seam

6.2 The Longyear Seam

The Longyear seam has been the subject of most of the published works (Orheim et al. 2007; Ćmiel and Fabiańska, 2003; Lüthje, 2008; Harland, 1997; Dallmann, 1999, Lewinska-Preis et al., 2009) however many are limited to descriptions of coal thickness and extent. The bulk coal quality (Ash, S, P, Calorific value, fluidity) of the Svea seam has been characterised extensively by Store Norske Spitsbergen Kulkompanie AS (SNSK; period-2002-2013), Orheim et al. 2007 (Table 6.1) for economic purposes, but the lack of high resolution data makes it difficult to put coal quality variations within the context of changing basinal/environmental controls.

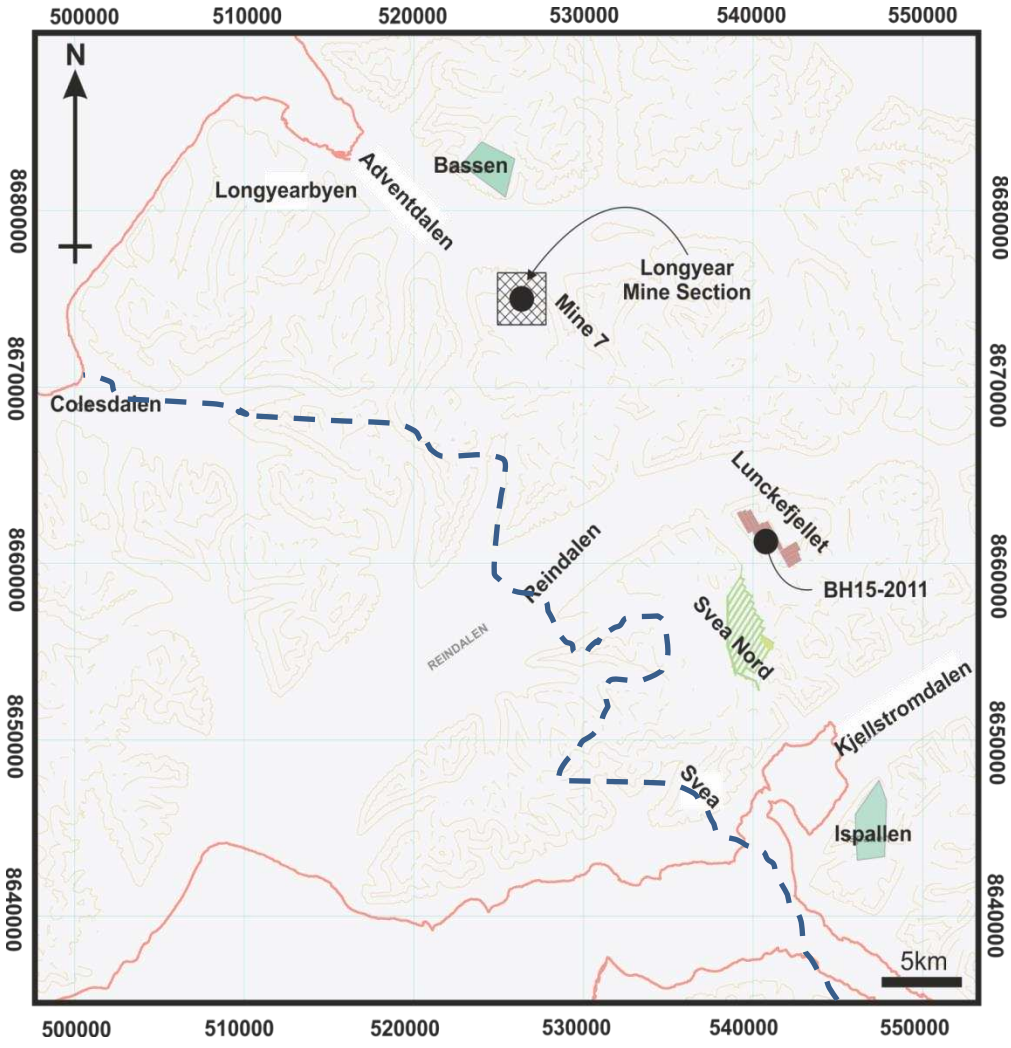

Fig. 6.1 – Sample locality map of the NE Central Tertiary Basin with locations of currently operational and prospective mines.

Blue dashed line – Maximum extent of the Longyear seam (Chapter 3)

Mine 7 in Adventdalen is currently the only mine exploiting the Longyear seam (63 Kt in 2010), however this mine is approaching the end of its life and faces increased problems with extraction and coal quality, particularly with ash and sulfur content (SNSK 2010). Previous mining at mines 1-6 in Adventdalen has ceased due to exhaustion of economic coal stocks (Coal quality and seam thickness issues). A new mine in Lunckefjellet is currently under construction close to the Svea Nord Mine which exploits the Longyear seam representing a coal resource of approximately 11.1Mt (SNSK 2010). Future development of the seam is likely to shift to the north of Adventdalen and the Bassen/Operafjellet region (Fig.6.1).

At Mine 7 (Fig.6.1), coal reaches a maximum thickness of ~2m with lowest sulfur coal within the centre of the deposit away from the inferred channels indicated in Chapter 3. Splitting of the seam also appears to originate from these depressions. High thickness, high sulfur coal (>2wt%) occur adjacent to the mine entrance, and to the east of the deposit, which would require processing to bring sulfur content to an acceptable level.

At Lunckefjellet, coal thickness reaches a maximum of around 2.5m with highest sulfur contents and ash originating from the inferred palaeo-coastline (Chapter 3). In Bassen, maximum thickness is also around 2.5m with generally lower sulfur content (Fig. 6.1). The

future (post-Bassen) exploitation of the Longyear seam is dependent upon the balance of oil potential (Chapter 2) and coal quality and how much sulfur can be removed by retortion to extend economic reserves of the seam. However, further work on a more palaeo-geographically diverse set of samples would be required to ascertain this.

6.3 Period of Deposition of the Longyear seam.

In order to understand how the supply of inorganic contaminants (dust, groundwaters, marine influence) changed over the lifetime of the Longyear peatland, it is first important to estimate the length of time that the peatland existed.

6.3.1 Carbon Accumulation rates

The simplest way to estimate the deposition period of a coal is to use the mean total organic carbon (TOC) of the seam and modern carbon carbon accumulation rates for peatlands at different latitudes (Large et al. 2003). By the Eocene, peatlands and forests at similar latitude (Ellesmere Island) had productivities similar to that of old growth temperate forests in Europe today (Williams et al. 2009), with temperatures reported to have rarely fallen below 0°C (Greenwood et al., 2009).

Consequently, long term carbon accumulation rates (LORCA) in Svalbard are likely to fall well within the range of Holocene

temperate peatlands in common with other Palaeogene peatlands (Large et al. 2003).

LORCA rates from modern peatlands show a negative linear relationship with latitude with tropical peatlands exhibiting significantly elevated LORCA rates compared to boreal peatlands (Large et al. 2011). Mean Tropical (Neuzil, 1997; Sorenson, 1993) and mean Boreal (Turenen et al. 2004). As the balance of productivity and decay is unlikely to lie outside the current climatic range LORCA rates were considered suitable for determining maximum and minimum limits for the period of peatland formation (Appendix II).

The length of peatland deposition estimate was calculated using the following parameters (Appendix II) and equation;

$$Length\ of\ Peatland\ Deposition\ (Kyr) = \frac{\rho(\frac{kg}{m^3})h(m)TOC(\frac{\%}{100})}{LORCA(gm^{-3}a^{-1})}$$

Assuming temperate carbon accumulation rates ($27gCm^{-2}a^{-1}$) and coal density of $1.3kg/m^3$ (Orheim et al., 2007) the formation of the Longyear seam at this site represents a period of 59kyr. The maximum period of deposition of the Longyear seam is 99kyr in Boreal Conditions ($16gCm^{-2}a^{-1}$). By contrast, at tropical LORCA rates ($\sim100gCm^{-2}a^{-1}$) the Longyear seam would have been deposited much faster at 16kyr.

6.3.2 Orbital Cycling

Constrained by the predicted length of deposition of the Longyear seam derived from TOC and LORCA rates, the period of deposition of the Longyear seam can be determined in more detail. This is achieved through locating and examining evidence of orbital cyclicity within the coal (Large et al. 2003; 2004; 2007 Briggs et al. 2005; 2007; Briggs, 2007). The methodology and rationale (Chapter 2) behind this technique have been discussed previously and are therefore only a summary is presented in this Chapter

Using the temperate estimates for the length of deposition of the Longyear seam, it would be expected that the only orbital cycles likely to be present in the Longyear seam are 21kyr precession cycles. This is due to the fact that the Longyear peatland did not exist for the length of time required for multiple obliquity (41kyr) and eccentricity (95-136kyr) cycles to be recorded within the core.

Consequently, it would be expected that in temperate conditions precession cycles would be expected to have a frequency of 1.9 cycles m^{-1}. At boreal carbon accumulation rates it would be expected that precession cycles would have a frequency of 3.18 cycles m^{-1}.

The lithophile elements (Al, Ti, Cu) are good targets for finding orbital cycles within coals as dust (a major contributor of lithophile elements to peatland) is highly susceptible to changes in climate (Mahowald et al.,2004). This is particularly true within low ash

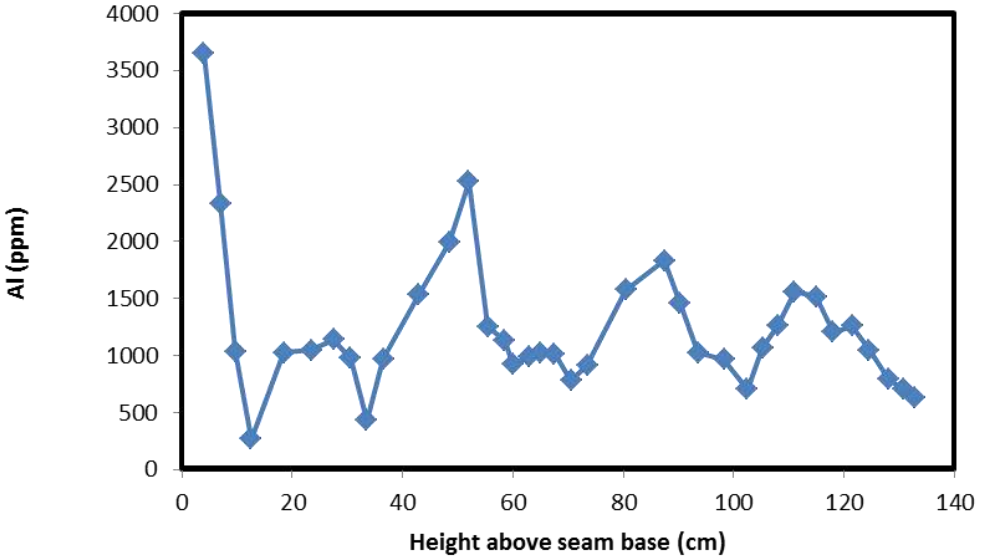

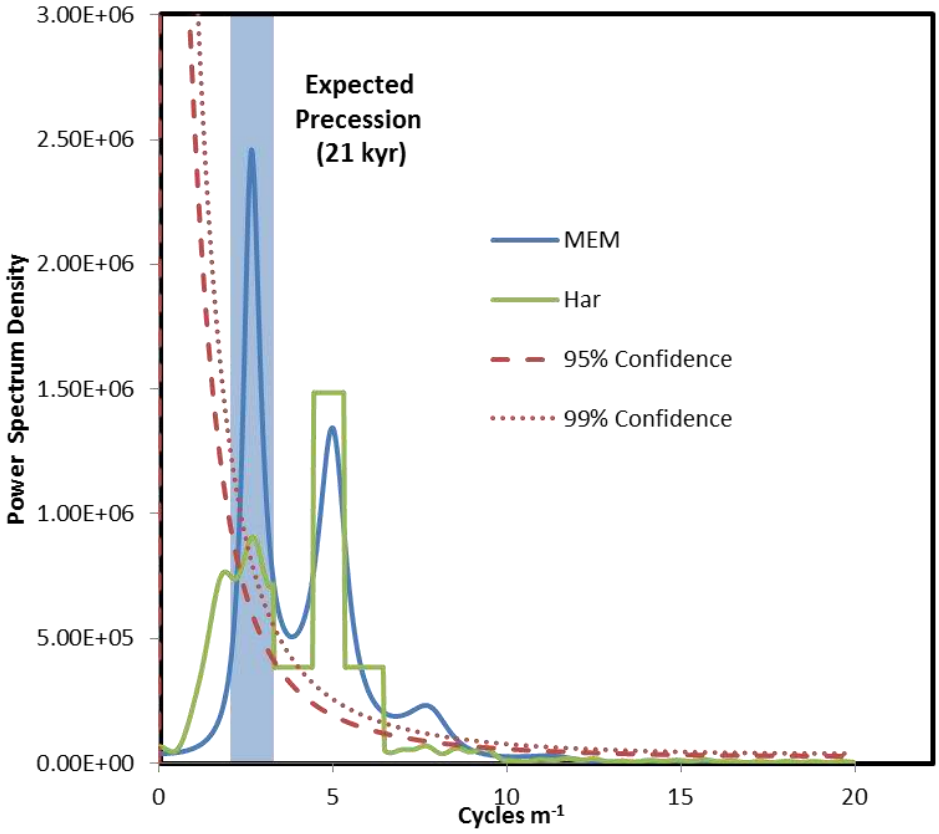

Fig. 6.2 – (Top) - Al profile of the Longyear seam at Mine 7 as a time series shows a series of apparent cycles. (Bottom) Power spectrum of the Al concentration of the Longyear seam. Expected precession component calculated from number of 21kyr cycles expected/m at Tropical and Boreal LORCA rates. Shows that the cycles are consistent with a precessional control on Al and indicating estimates from LORCA rates are generally accurate (Har = Harmonic

coals as dust deposition forms the primary supply of inorganic material to the peatland; therefore global orbital cycles are more likely to be preserved compared to peatland with significant clastic input.

Only one significant periodic component was identified from the Al record from the Longyear seam (Fig.6.2). This component has a spatial frequency of 2.66m^{-1} for Al. This fits well within the expected orbital frequencies from precession. This spatial frequency is also similar to those observed within the Upper Svea Seam (~40cm/cycle).

The spatial frequencies of each component are slightly lower than expected possibly indicating that carbon accumulation rates in the Longyear were between temperate and boreal LORCA rates. This may be a consequence of the high seasonality of net primary productivity due to high latitude, lower preservation of peat than expected or the effect of averaging TOC and coal density throughout the seam in the carbon accumulation model. In addition due to the low number of cycles observed (as a consequence of low seam thickness) any estimates of depositional period are relatively uncertain

Nevertheless, it is considered that the significant spectral peak at spatial frequency (2.6m^{-1}) may equate to the 21kyr precession cycle. This is due to its position within the predicted range for precession

from LORCA rates and its replication within three elemental records from within the Mine 7 section. Assuming the 2.6 cycle m^{-1} component represents the 21kyr precession cycle, depth can be converted into time. This constrains the internal timeframe of the 1.5m seam at mine 7 to approximately 83.8kyr.

Using this new constraint on peatland formation to estimate carbon accumulation rates at this time produces a mean LORCA value of 19.5$gCm^{-2}yr^{-1}$, representing productivity between that of a modern boreal (16$gCm^{-2}a^{-1}$; Turenen, 2004) and temperate peatland (27$gCm^{-2}a^{-1}$; Large et al., 2003). This reflects Svalbard's position on the boundary between warm temperate and cold temperate conditions (Scotese, 2001). In addition the supply and perhaps source of dust to the peatland appears to have a precessional control during this period with implications for understanding patterns of climate and atmospheric dust deposition within the basin.

6.4 Controls upon Coal Quality within the Longyear Seam

The primary coal quality issues affecting the value and future exploitation of the Longyear seam (Table 6.1) are;

- Calorific Value
- Oil Potential/Coking Potential
- Ash Content

Location	Borehole	Description	Mean Depth (m)	Ash (%)	Sulfur (%)	Eff. B.v. kcal/kg	FSI
Breinosa	BH5/2009	Coal	313.1	8.0	3.76	7635	8.5
Breinosa	BH5/2009	Middle Stone	313.3	75.7	4.53	1212	1.0
Breinosa	BH5/2009	Middle Stone	313.6	85.9	3.86	396	1.0
Breinosa	BH5/2009	Middle Stone	313.9	88.0	3.95	274	1.0
Breinosa	BH5/2009	Middle Stone	314.1	82.3	6.47	646	1.0
Breinosa	BH5/2009	Coal	314.4	13.6	3.72	7249	8.5
Breinosa	BH5/2009	Coal	314.6	13.1	5.14	7261	8.0
Breinosa	BH5/2009	Coal	314.8	10.4	5.11	7353	9.0
Breinosa	BH5/2009	Coal	315.1	83.5	5.85	534	1.0
Breinosa	BH5/2009	Coal	315.4	82.1	3.83	660	1.0
Breinosa	BH5/2009	Coal	315.6	8.2	4.43	7448	8.5
Lunckefjellet	BH15/2011	Coal	375.2	8.8	5.60	7456	8.5
Lunckefjellet	BH15/2011	Coal	375.4	2.3	1.34	7952	7.5
Lunckefjellet	BH15/2011	Coal	375.7	3.9	1.29	7802	7.5
Lunckefjellet	BH15/2011	Coal	375.9	8.2	1.46	7383	7.5
Lunckefjellet	BH15/2011	Coal	376.2	7.2	2.24	7455	8.0
Lunckefjellet	BH15/2011	Middle Stone	375.9	77.8	5.96	1082	1.0
Lunckefjellet	BH15/2011	Coal	376.6	23.6	9.51	6008	6.0
Lunckefjellet	BH15/2011	Ash rich Coal	376.8	41.9	9.23	4255	2.0

Table 6.1 – Coal Quality (Ash, Sulfur, Calorific Value and Free Swelling Index (FSI) from Longyear Seam Coals at Breinosa (Mine 7) and Lunckefjellet areas (Source SNSK)

- Sulfur Content
- Seam Thickness and splitting (Chapter 4)

The calorific content of the coals reflects its high volatile bituminous rank with values ranging from 6394 kcal/kg to 7859kcal/kg in BH5/2009 and BH15/2009. The Longyear seam has a free index of between 4 and 9 in the two boreholes above. The Free Swelling Index indicates coals suitability to coking with high values representing coking potential. Consequently, the Longyear seam can be classified as having a medium to high coking potential. Ash contents range from 4.1% to 16.2% with sulfur contents ranging from 0.5-5% in BH5/2009 and BH15/2012.

The oil potential of the Longyear seam has been shown to be significant with oil yields dependent upon hydrological conditions and marine influence (Orheim et al., 2007; Chapter 4). The relative importance of these controls upon the inorganic elemental composition of the coals will be examined in greater detail later within this Chapter

6.5 Controls on Major and Minor Elemental Composition of the Longyear Seam

A number of commonly major and minor elements were analysed by ICP-AES analysis (Chapter 2) to characterise the inorganic composition of the Longyear coals at Lunckefjellet and Mine 7. The average major and minor elemental composition of coals from the

Element	No of Samples	% of Samples Measured	Mean (ppm)	Minimum (ppm)	Maximum (ppm)	Median (ppm)	SD (ppm)
Al	44	100	1759	265	7528	1101	1697
Ca	44	100	10977	1825	65357	6612	13158
Fe	44	100	5276	2935	14170	5108	1852
K	44	100	89	11	426	69	74
Mg	44	100	2577	554	6651	2446	1306
Mn	44	100	11	B.D	76	8	14
Na	44	100	1488	637	3100	1352	542
S	44	100	6062	3679	13758	4898	2417
Ti	44	100	357	31	2784	122	636
Ba	43	98	202	85	576	170	97
Co	39	89	1.2	B.D	5.6	0.9	1.2
Cr	43	98	10.6	0.8	123.8	9.7	19.5
Cu	41	93	4.5	B.D	40.4	2.3	8.3
Li	44	100	1.3	B.D.	11.9	0.7	1.9
Ni	36	82	8.5	B.D	112.8	5.8	18.5
Pb	28	64	3.1	2.1	4.8	2.8	0.8
Rb	14	32	2.2	1.3	3.8	1.9	0.7
Sb	43	98	31.6	24.5	39.1	31.3	2.5
Sc	43	98	1.3	B.D	20.2	0.5	3.2
Sr	43	98	285	89	1654	193	327
V	43	98	20.3	B.D	704.0	1.7	106.9
Zn	36	82	1.3	B.D	4.2	1.2	0.8
Zr	43	98	16.1	B.D	258.6	6.6	39.2

Table 6.2 – Major and minor elemental composition of the Longyear Seam at Mine 7. B.D = Below detection

Element	No of Samples	% Measured Samples	Mean (ppm)	Minimum (ppm)	Maximum (ppm)	Median (ppm)	SD (ppm)
Al	16	100	3333	230	16097	1398	4606
Ca	16	100	11596	170	101624	2924	25130
Fe	16	100	8367	2470	34135	6346	7433
K	16	100	460	24	3032	56	996
Mg	16	100	2072	378	16953	1024	4010
Mn	16	100	83	7	415	38	112
Na	16	100	1541	1166	2152	1374	323
P	16	100	169	14	826	64	217
S	16	100	12693	3619	32530	7930	9617
Ti	16	100	255	38	986	166	295

Table 6.3 – Major Elemental composition of the Longyear Seam at Lunckefjellet

mine 7 section (Table 6.2) is dominated by Ca, Fe and S species with relatively lower lithophile element (Al, Ti, Cu, Na, K) concentrations. Phosphorus contents within the Longyear at this location were below detection limits.

Al contents were generally lower than reported by Orheim et al. (2007) with similar Fe and S concentrations. Mean Ca concentrations appear to be significantly higher than reported previously. This difference may be a feature of the different sampling scales used as Orheim et al. 2007 analysed bulk samples rather than high resolution samples. Comparison with trace element data from Orheim et al. (2007) shows similar low trace element concentrations with Ba and Sr concentrations greatest.

Examination of the major elemental composition of the Longyear coals from Lunckefjellet BH15/2011 (Table. 6.3) shows that they are again dominated by Ca, Fe and S. At this location Al concentrations are significantly higher than at mine 7 with mean concentrations (3333 ppm) similar to those reported by Orheim et al. (2007).

6.5.1 Determining Controls upon the Major and Minor Elemental Composition of the Longyear Seam.

In order to examine possible controls upon the inorganic composition of the Longyear seam it is first necessary to establish which elements have similar distributions up-seam, which would imply a similar control. This was achieved through the use of correlation

matrices and checked using regression. Regression showed that all the relationships discussed subsequently were significant to at least >90% confidence (*t*-Stat >2, P values <0.1; see attached disc).

Using a Correlation Matrix (Fig.6.3) the major and minor elemental composition of the Longyear seam at mine 7 are compared. Many of the elements analysed can be grouped with the lithophile elements (Al, Ti, Cu). This group comprises Al, K, Na, Ti, Ba, Co, Cr, Cu, Li, Sc, Sr, V, Zr. This group is often associated with dust or clastic deposition (Lawrence and Neff, 2009; Rudnick and Gao, 2003).

Another group comprises Ca, Mg and Mn concentrations probably linked to groundwater (or marine influence for Mg; Weis et al., 2002). Also the distribution of Fe shows some similarities to Ca group elements. Sulfur concentrations are relatively independent of the other element groups identified previously, reflecting a different control, such as atmospheric marine deposition or volcanogenic supply (Todd, 1980).

Correlation of the major elements within the Longyear coal at Lunckefjellet produces similar groupings to those at Mine 7 (Fig. 6.4). The elements can be grouped into the lithophile group comprising Al, K and Ti and a second groundwater based grouping comprising Ca, Fe, Mg, Mn and S. Na concentrations appear independent of the other major elemental concentrations at this location.

	Al	Ca	Fe	K	Mg	Mn	Na	S	Ti	Ba	Co	Cr	Cu	Li	Ni	Pb	Rb	Sb	Sc	Sr	V	Zn
Ca	-0.20																					
Fe	0.04	0.38																				
K	**0.89**	-0.23	-0.03																			
Mg	-0.38	**0.63**	0.39	-0.46																		
Mn	0.18	**0.70**	**0.69**	0.12	0.25																	
Na	**0.86**	-0.32	0.00	0.71	-0.39	0.12																
S	**0.79**	-0.25	0.10	**0.75**	-0.48	0.05	0.56															
Ti	**0.89**	-0.13	0.31	**0.79**	-0.23	0.30	**0.84**	0.66														
Ba	**0.74**	-0.23	0.00	**0.68**	-0.32	-0.02	**0.68**	0.76	**0.68**													
Co	**0.79**	-0.09	-0.11	**0.65**	-0.18	0.01	**0.66**	0.66	**0.68**	**0.85**												
Cr	**0.65**	0.01	-0.05	0.48	-0.08	0.11	**0.57**	0.51	0.49	**0.66**	**0.81**											
Cu	**0.82**	-0.10	-0.09	**0.68**	-0.18	0.03	**0.70**	0.68	**0.68**	**0.86**	**0.96**	**0.89**										
Li	**0.73**	-0.07	-0.19	**0.58**	-0.24	0.04	**0.59**	0.61	0.49	**0.63**	**0.81**	**0.95**	**0.88**									
Ni	**0.54**	-0.02	-0.06	0.33	-0.05	0.06	**0.55**	0.42	0.38	**0.55**	**0.70**	**0.98**	**0.80**	**0.92**								
Pb	0.21	-0.07	-0.27	0.17	-0.20	-0.13	0.12	0.02	0.06	0.07	0.25	0.32	0.28	0.41	0.38							
Rb	0.34	-0.18	0.09	0.24	-0.14	0.11	-0.24	0.49	-0.28	-0.50	-0.04	0.01	-0.02	0.57	0.07	-0.28						
Sb	0.08	0.33	0.09	0.04	0.32	0.16	0.02	0.11	0.08	0.20	0.32	0.41	0.40	0.34	0.41	0.14	-0.34					
Sc	**0.74**	-0.09	-0.05	**0.81**	-0.22	0.02	0.48	0.67	**0.64**	**0.75**	**0.80**	**0.52**	**0.79**	**0.56**	0.34	0.23	0.49	0.18				
Sr	**0.75**	0.01	0.01	**0.64**	-0.08	0.09	**0.54**	0.72	**0.64**	**0.88**	**0.89**	**0.68**	**0.89**	**0.69**	0.56	0.21	-0.24	0.32	**0.82**			
V	0.56	-0.04	0.05	**0.73**	-0.14	0.05	0.32	0.53	**0.53**	**0.64**	**0.63**	0.37	**0.63**	0.36	0.18	0.19	0.08	0.17	**0.95**	**0.69**		
Zn	0.34	0.34	0.25	0.37	0.34	0.21	0.03	0.40	0.31	0.41	**0.56**	0.37	**0.51**	0.36	0.22	0.17	0.35	0.41	**0.65**	**0.69**	**0.64**	
Zr	**0.64**	-0.06	-0.04	**0.77**	-0.18	0.02	0.40	0.55	**0.56**	**0.66**	**0.69**	0.43	**0.68**	0.45	0.24	0.21	-0.05	0.15	**0.97**	**0.72**	**0.97**	**0.64**

Fig. 6.3 – Correlation matrix of major and minor elemental composition of the Longyear Seam at Mine 7. Red = Lithophile associated, Blue = Ca associated

	Al	*Ca*	*Fe*	*K*	*Mg*	*Mn*	*Na*	*P*	*S*
Ca	-0.14								
Fe	-0.03	**0.97**							
K	**0.96**	-0.10	0.03						
Mg	-0.22	**0.96**	**0.95**	-0.15					
Mn	-0.30	**0.90**	**0.89**	-0.26	0.84				
Na	0.28	-0.18	-0.08	0.18	-0.28	-0.07			
P	0.45	-0.16	-0.13	0.32	-0.19	-0.36	0.39		
S	**0.54**	**0.69**	**0.72**	0.52	0.54	0.53	0.11	0.10	
Ti	**0.96**	-0.17	-0.06	**0.98**	-0.24	-0.32	0.24	0.31	0.50

Fig. 6.4 – Correlation matrix of major elemental composition of the Longyear Seam at Lunckefjellet

Red = Lithophile Blue = Marine Supply

The incorporation of Fe and S into the Ca associated group marks a difference between Lunckefjellet and Mine 7. This may be due to the more vulnerable coastal location of Lunckefjellet (Chapter 3) compared to mine 7, allowing more Fe to be retained within the peatland due to interaction with marine supplied S at the site. Na concentrations remain much the same as at mine 7 (Table 6.2), therefore the low correlation with the lithophile group is surprising. This will be investigated further in later sections.

This section shows that the ash and inorganic elemental composition of the Longyear seam can be attributed to two major sources. These comprise a major source of lithophile and transition metals and a Ca/Mg source. Supply of Fe and S to the peatland appears to be controlled to a certain extent by these main groups but is significantly affected by other environmental factors. The behaviour of the inorganic elements at the two sites examined remains generally similar with minor differences. These can be explained by the balance of groundwater, atmospheric, marine aerosol and clastic deposition.

6.5.2 – Groundwater controls upon the Longyear Seam

Increased oil yields have been shown to be associated with the transition of the Longyear seam from a more ombrotrophic (precipitation fed) peatland to a more rheotrophic (groundwater fed) system (Chapter 4). As previously shown in Chapter 4 the

hydrological conditions and redox conditions of a peatland can be represented using coal maceral analysis.

6.5.2.1 Coal Macerals and the hydrological development of the Longyear Seam

The Longyear seam at Mine 7 shows that the coal is dominated by macerals from the vitrinite group, comprising 75%±7.5%, with lesser amounts of inertinite (14.4%±8.2%) and liptinite group macerals (7.3%±3.8%; Table 6.4.). This is similar to other published maceral compositions which report mean vitrinite contents of between 70 & 90% (Ćmiel and Fabiańska, 2003; Orheim et al., 2007).

Vitrinite remains relatively constant about the mean, however analysis of the sub-maceral group detrovitrinite (representing fine degraded organic matter indicating wetter conditions; Diessel and Gammidge, 1998) exhibits a shift of around 10% at 80cm above seam base (Fig.6.5). As shown in Chapter 4 this coincides with an increase in oil yields and represents a transition to wetter conditions.

Liptinite contents are greatest during higher detrovitrinite conditions and are dominated by sporinites and liptinites probably indicating aolian supply and deposition from surrounding areas, enrichment due to biodegradation or vegetational transition to more hydrogen rich vegetation. Inertinite formation (indicative of more oxidative conditions) is focussed below the transition during periods

of low detrovitrinite formation. This indicates a more hydrologically vulnerable beginning to peatland deposition at mine 7. The Tissue Preservation Index (TPI; Diessel, 1992; Diessel and Gammidge, 1998, Casareo et al., 1996) is thought to reflect the degree of preservation of source materials with higher values indicating higher tree density and oxidation and lower values associated with greater microbial decomposition (Diessel and Gammidge, 1998). The Gelification Index (GI) shows the ratio of macerals formed in wetter conditions (namely vitrinites) and macerals affected by oxidation/desiccation (inertinites).

Analysis of the TPI and GI profile (Fig.6.6) shows the same transition at 80cm between drier and wetter conditions. The transition from drier to wetter conditions is preceded by a peak in fusinite contents during both such events in the Longyear seam. Fusinite (fossilised charcoal; Scott, 2000; Scott, 2002) is thought to represent a combustion event. This may reflect the burning of the peat surface to the water table leading to the loss of any topography the peatland had. This would firstly make the peatland at this location relatively wetter and more dependent upon groundwater and also vulnerable to inundation from fluvial or marine sources. This shift in water balance also could lead to the drying of the peat in areas of relatively strong peat and collapse in areas of weak peat collapse, leading to inertinite expressions being different within different parts of the peatland. In more vulnerable areas, such as

	Mean (%)	Minimum (%)	Maximum (%)	Median (%)	Mode (%)	SD (%)
Vitrinite	75.0	50.4	86.0	76.2	81.2	7.5
Telovitrinite	54.1	19.2	79.6	55.6	62.0	13.8
Collotelinite	54.1	19.2	79.6	55.6	62.0	13.8
Detrovitrinite	20.9	1.2	49.2	19.4	20.4	11.2
Inertinite	14.4	6.0	46.8	12.5	9.2	8.2
Fusinite	3.7	0.0	15.6	2.0	4.0	4.4
Semifusinite	6.2	0.4	44.0	4.2	3.6	7.5
Funginite	2.4	0.0	4.8	2.4	1.2	1.2
Inertodetrinite	2.1	0.0	5.2	1.8	0.8	1.5
Liptinite	7.3	2.4	16.4	6.4	4.4	3.8
Sporinite	4.3	0.0	13.6	3.6	3.6	3.4
Liptodetrinite	0.1	0.0	0.8	0.0	0.0	0.2
Cutinite	2.5	0.4	7.0	2.0	2.0	1.6
Resinite	0.5	0.0	2.8	0.0	0.0	0.8
Minerals	3.8	0.4	10.0	3.2	3.2	2.5

Table 6.4 – Maceral compositon of the Longyear seam at Mine 7 showing a dominance of vitrinite macerals

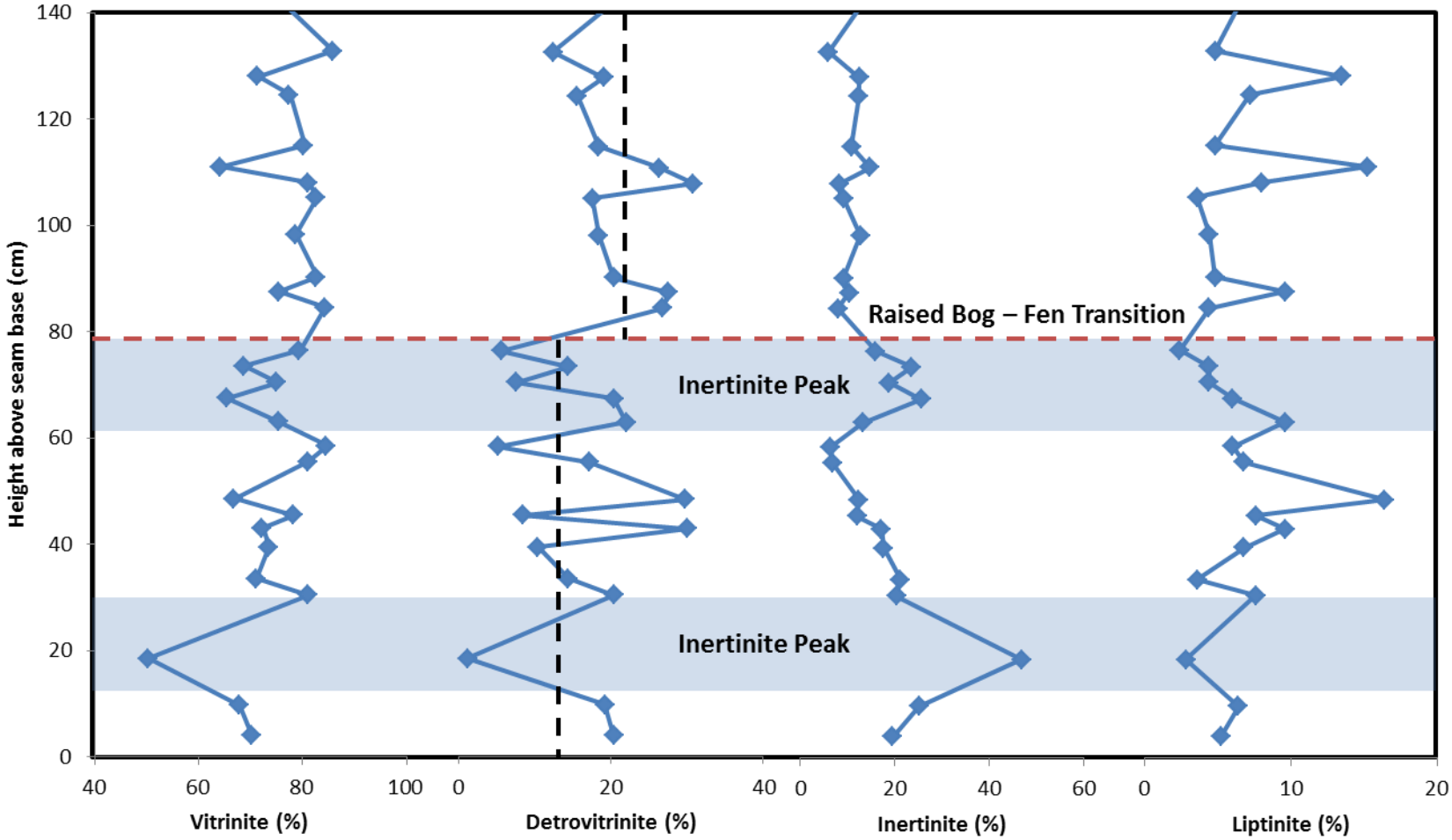

Fig. 6.5 – Vitrinite, Detrovitrinite, Inertinite and Liptinite profile upseam within the Longyear Seam at Mine 7. Note the transition at 80cm between raised bog-fen conditions causing elevated detrovitrinite and lower more stable inertinite.

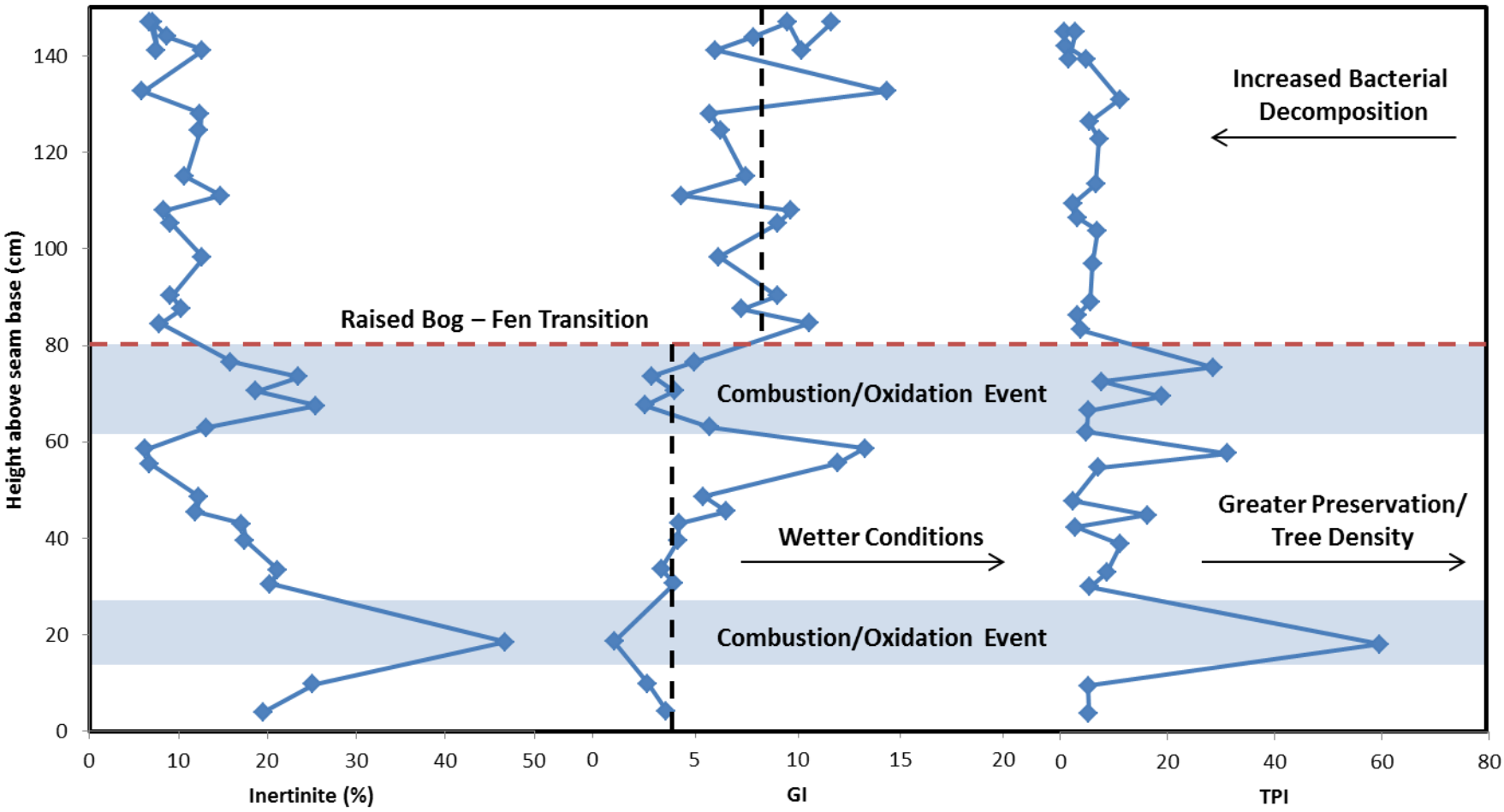

Fig. 6.6 – Inertinite, GI and TPI profile from the Longyear seam at Mine 7 showing the transition to wet conditions and increasingly degraded organic matter (reducing conditions) Max deviation 5%, Inertinite peak primarily fusinite

the persistent lows identified in Chapter 3 this event could have represented by clastic sedimentation (splitting).

At Mine 7 the peatland was able to return to raised bog conditions after the first combustion event but was unable to recover after the second. This is probably happened within the context changes in the overall hydrological budget at this site due to a combination of sea-level rise and groundwater discharge leading to a more groundwater influenced peatland to form. This shallowing of the water table in coastal peatlands in response to rising base levels has been observed within more recent peatlands (Waller et al. 1999; Gaiser et al. 2001).

After 80cm the peatland system shifted to a wetter, more reducing fen conditions. This was probably accompanied by a change in vegetation from more woody to more herbaceous material. However, further palynological work would be required to confirm this. The transition also heralded a shift in hydrological supply to groundwater dominance and increased stability due to rising sea level. The consequence of this would be a more homogenous and hydrologically stable peatland. Accordingly, the upper seam is observed to be much less vulnerable to oxidation and combustion events than the lower Longyear seam.

The Longyear seam at mine 7 can be seen to have two characters with around 80cm (~45,000 years) of greater rainfall influence and

more local supply. This is shown by greater peat thickness adjacent to topographic highs and highly variable TPI and GI values in the lower part of the seam.

At ~45000 years after initiation the peatland received a much more stable hydrological supply, consistent with a more regional groundwater input leading to consistently wetter conditions and more fen like conditions (as evidenced by increased GI and detrovitrinite contents). This period fits well with the German Wadden Sea model proposed by Lüthje, 2008.

The Lunckefjellet section is dominated by vitrinite (81.2±7.5%; Table. 6.5) with lesser amounts of inertinite (10.5±8%) and liptinite (5.5±3%). Vitrinite again does not vary significantly up-seam (Fig.6.7) with the rapid decrease at -259.5m depth attributed to higher ash content. Detrovitrinite contents gradually increase upseam with a minor shift at approximately around -259.7m depth. Inertinite contents remain relatively constant upseam with a peak at -259.5m depth associated with higher ash contents. Liptinite is most variable at the bottom 40cm of the seam before remaining relatively constant after -259.9m depth.

The TPI and GI profile (Fig. 6.8) of the Longyear seam at Lunckefjellet show a clearer picture of peatland hydrology with a transition from relatively high and variable TPI values to consistently low TPI values occurring between 259.9-259.7m depth.

	Mean (%)	Minimum (%)	Maximum (%)	Median (%)	Mode (%)	SD (%)
Vitrinite	81.2	59.6	90	82.8	74.8	7.5
Telovitrinite	59.1	17.2	83.6	60.2	48.8	16.3
Telinite	0.5	0	2.2	0.4	0	0.6
Collotelinite	58.5	17.2	83.2	58	48.4	16.3
Detrovitrinite	22.1	4.4	46	21.8	30	12.1
Inertinite	10.5	0.8	31.6	7.6	6	8.4
Fusinite	3.7	0	20.4	1.2	0.4	5.6
Semifusinite	4.6	0.8	12.8	4.4	4.4	3.0
Funginite	2.2	0	5.6	2	2	1.7
Liptinite	5.5	1.6	15.2	4.4	4.4	3.0
Sporinite	2.4	0.8	5.2	2.4	2.8	1.2
Cutinite	1.9	0	4.4	1.6	2.4	1.1
Resinite	1.2	0	8	0.8	0.8	1.7
Minerals	4.6	0.4	20.8	2.4	2	5.8

Table 6.5 – Maceral composition of the Longyear seam at Lunckefjellet showing the dominance of vitrinite group macerals in these coals

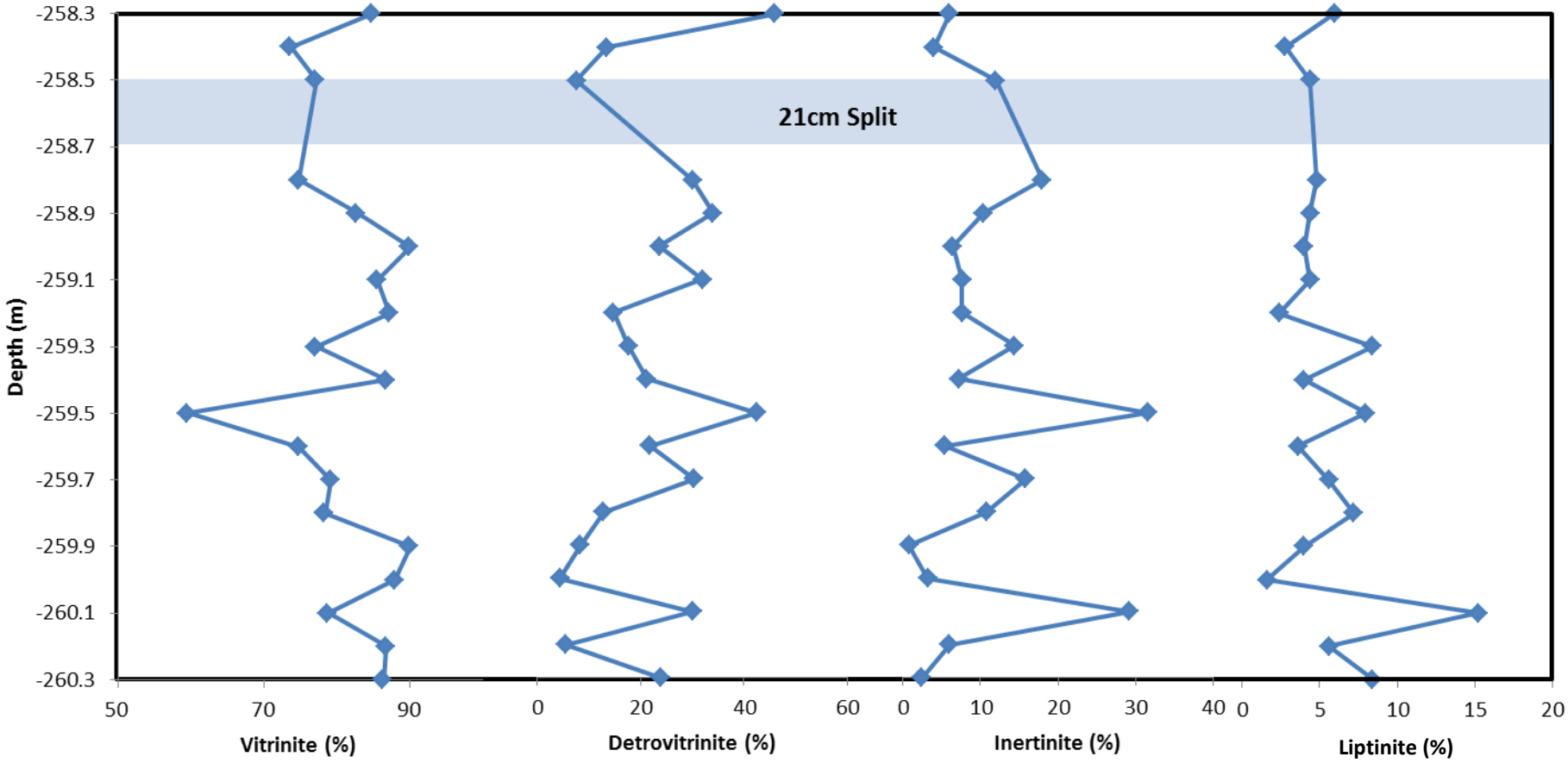

Fig. 6.7 – Vitrinite, Detrovitrinite, Inertinite and Liptinite profile upseam in the Longyear at Mine 7 showing a shift to wetter conditions ~ 259.7m depth

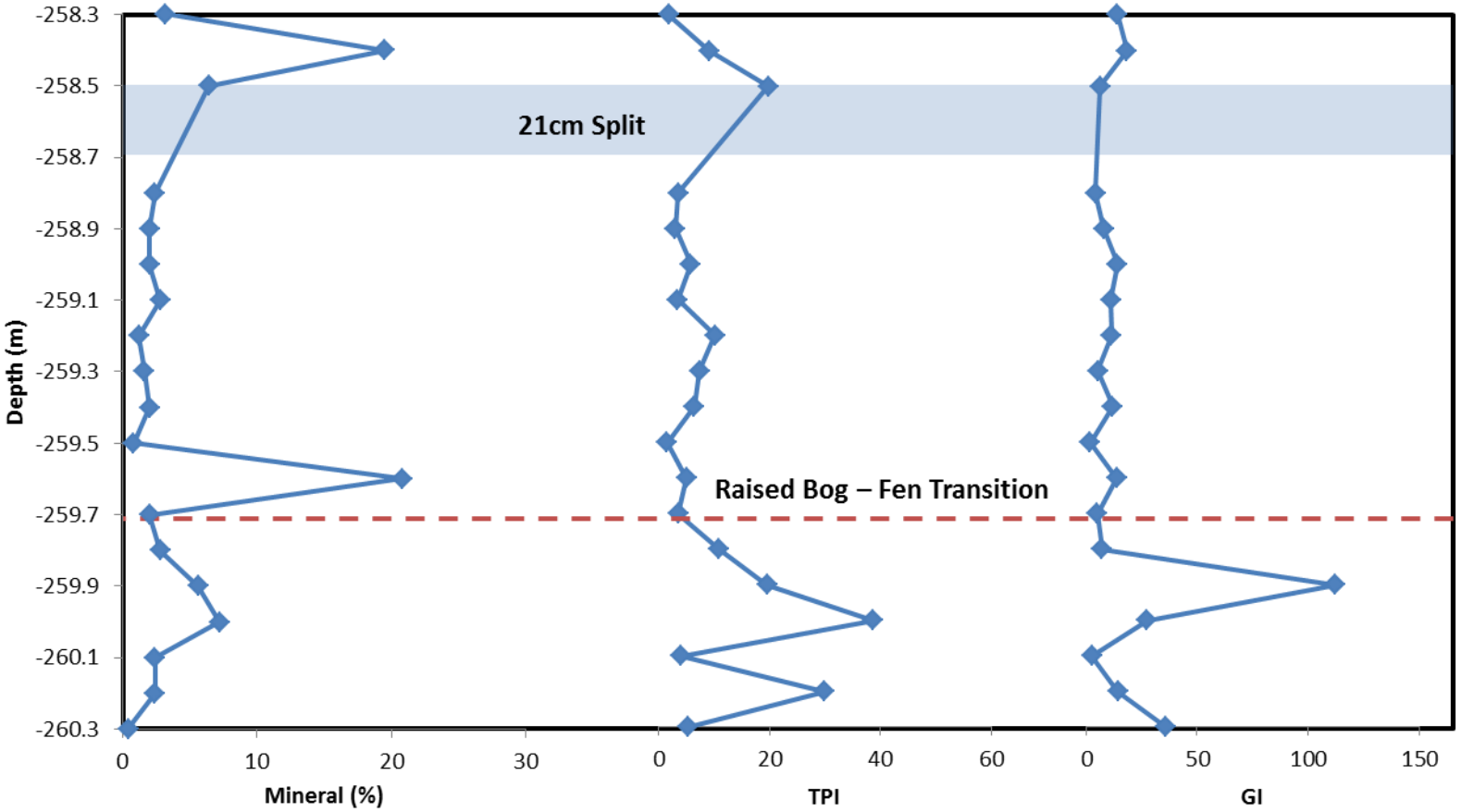

Fig. 6.8 – % Observed Mineral Matter, GI and TPI profile for the Longyear seam at Lunckefjellet showing a transition at ~259.7 followed by an increase in observed mineral matter

This transition appears to be similar to that seen at Mine 7, however it occurs earlier (~60cm) within the section. It is also followed by an increase in observed mineral content consistent with increased clastic input to the peatland at this location. The palaeogeographic reconstruction of at Lunckefjellet shows this location to be close to an inferred tidal channel (Chapter 3). Consequently, this area of peatland is likely to have been more vulnerable to clastic influence during the transition from raised peatland to fen. This is confirmed by the increase in mineral content at the transition. This transition would also be expected mark a boundary between lower and higher oil yields (as explained in Chapter 4), however further analysis would be required to confirm this.

The relatively early position of the transition at Lunckefjellet is not entirely unexpected. The Lunckefjellet area is adjacent to an apparent depression or embayment that was subject to little or no coal deposition during the emplacement of the Longyear seam (Chapter 3). This means that the Lunckefjellet region became rapidly more marine influenced once sea level rose with transition occurring at around 40-60cm (21-33kyr) after seam initiation. This indicates that Mine 7 was formed at slightly higher elevation and further inland, allowing local controls on hydrological supply to persist for an extended period before regional groundwater supply was established compared to Lunckefjellet.

The transition therefore does not represent a single event but should reflect the time of transition from predominantly terrigenous controls to regional groundwater influence. The raised bog-fen transition would be expected to be earliest within lower lying more coastal areas (W Lunckefjellet), and later in slightly higher more protected topographically influenced areas (Mine 7) and later still in more inland regions such as Bassen.

6.5.2.2 Groundwater influence and the Ca-group elements

The change in hydrological regime had varying effects upon the inorganic distribution and concentrations of the major elements within the Longyear seam (Fig. 6.9; 6.17). The lithophile elements (Al, Ti, Cu, Na, K) appear unaffected by the change indicating an external control upon their concentration.

Examination of the mineral composition of the Longyear seam (SEM EDX; Appendix I) shows that the mineral composition of the Longyear seam at mine 7 is dominated by Ca/Fe carbonates and pyrite (FeS_2). The Ca/Fe carbonates comprise Calcite ($CaCO_3$), Ankerite ($Ca(Fe.Mg.Mn)(CO_3)_2$) and Siderite ($FeCO_3$). The presence of these minerals explains the close relationship between Ca, Mg, Mn and Fe) within these coals.

The minerals primarily infill small voids within inertinite macerals, possibly indicating that deposition occurred during deposition /diagenesis. There is little evidence of post diagenetic carbonate

mineral deposition in veins. This is similar to the observations of Orheim et al. (2007).

The distribution of Ca, Mg, and Fe at Mine 7 however shows a marked change at 80cm above seam base (Fig.6.9). The highest concentrations of these elements appear to occur alongside fusinite peaks, immediately prior to the onset of wetter conditions. This could be due to groundwater discharge of Fe onto the peatland surface/near surface followed by reduction to Fe-carbonates

The total inorganic carbon concentration within the coals also increased at this time. After the transition the profiles become more stable indicating that during fen conditions the supply and conditions within the peatland remained relatively constant.

Ca group elements (Ca, Fe, and Mg) represent one of the most common constituents within groundwater (Todd, 1980). In the Longyear seam the Ca group elements are enriched during periods of high inertinite, this is in part due to the increased groundwater input expected following peatland collapse and the extra porosity provided within inertinite macerals. In the upper seam, groundwater supply is more constant leading to the distribution of Ca-group elements within the coal to remain constant.

Examination of the Ca/Mg compared to marine and continental sources (Berner and Berner, 1997; Wedepohl, 1995) can indicate

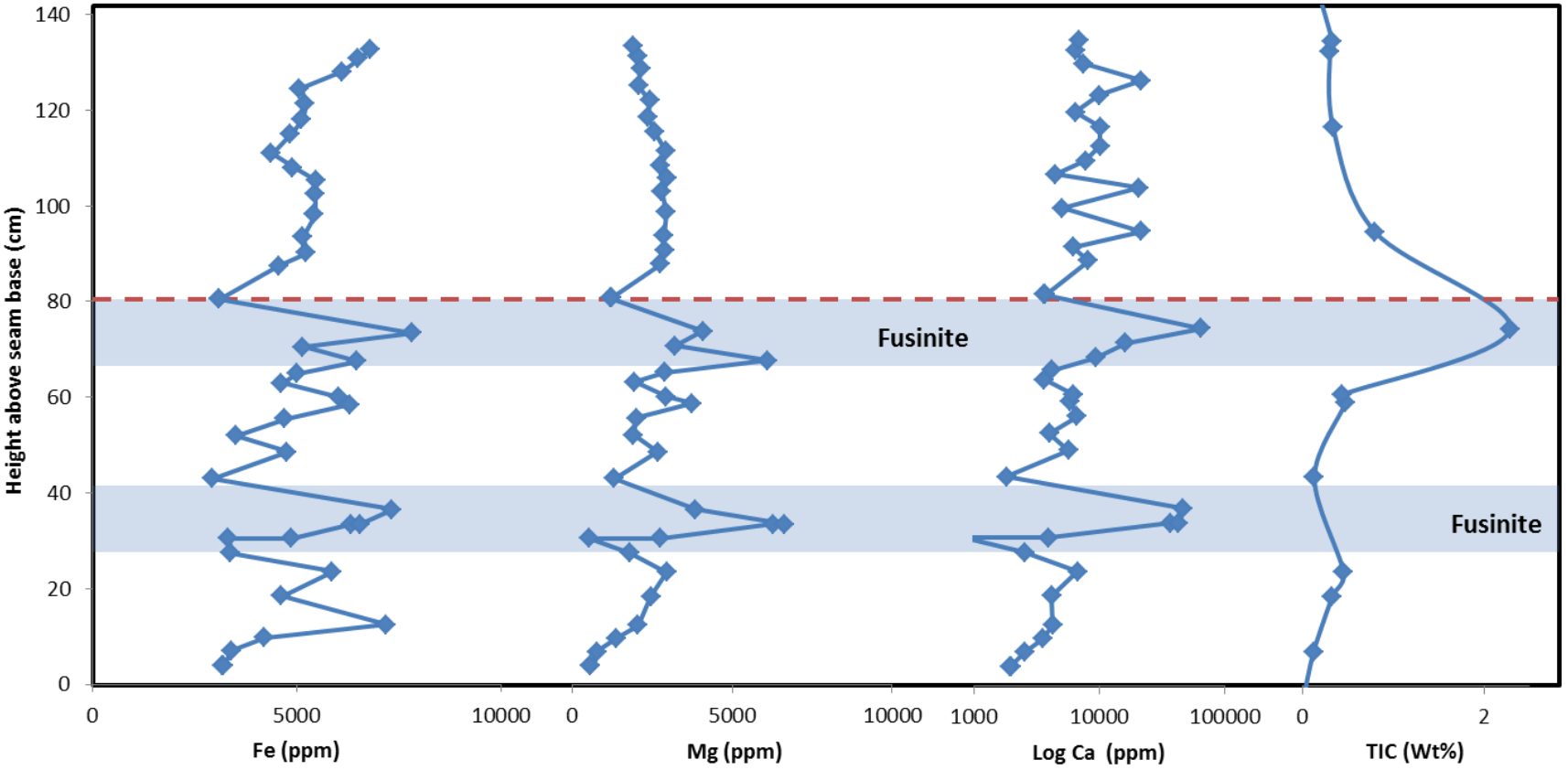

Fig. 6.9 – Fe, Mg, Ca and TIC profile upseam in the Longyear at Mine 7 showing concentration in fusinite rich areas, indicates deposition within higher porosity areas, post deposition. Max Deviation from point shown ±5%

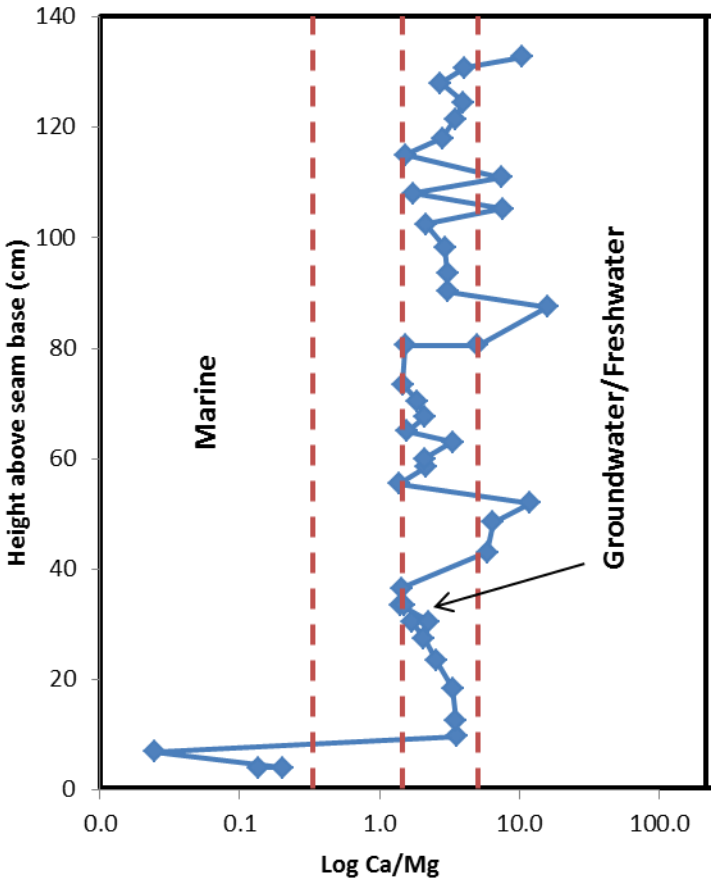

Fig. 6.10 – Ca/Mg ratio within the Longyear seam at Mine 7 showing compositions broadly in the range of coastal and continental rainfall (Weiss et al., 2002 and references therein) Max Deviation from point shown ±5%

hydrological character. Mg is enriched within marine and Ca within terrestrial systems (Weiss et al., 2002)

The Ca/Mg ratio at both Mine 7 (Fig. 6.10) and Lunckefjellet generally fluctuates between continental and marine coastal rainfall values, with values at mine 7 closer to that of coastal rainfall. This only changes in areas of secondary carbonate formation within inertinite causing the Ca/Mg to increase due to the precipitation of significant amounts of Ca within inertinite pore space.

Fe concentrations show significant enrichment compared to MCC (Fig. 6.16), this excess is probably associated with remobilisation of Fe, during groundwater-rock interactions with the underlying Carolinefjellet marine shale (as with Ca) and deposition under reducing conditions (Butler and Rickard, 2000).

The groundwater control upon the Ca-group elements can be defined by the amount of groundwater supplied to the peatland and groundwater character. In the two locations studied, the lower seam is generally characterised by fluctuating groundwater influence controlled by combustion events and subsequent peatland collapse. In addition the extra porosity provided within high inertinite horizons led to increased Ca group preservation. In the upper seam, the dominance of the groundwater control leads to a relatively constant supply of Ca group elements to the peatland. The

provenance of groundwater appears to be a mixture of coastal and inland rainfall interacting with underlying marine shales.

6.5.3 – Climatic Controls on Atmospheric Dust Supply

Lithophile (Al, Cu, K, Na) elements within peatlands are primarily derived from atmospheric dust deposition (Lawrence and Neff, 2009) and clastic sedimentation (Rudnick and Gao, 2003). The Longyear coal generally contains relatively low ash content (Table 6.1) favouring a dust source for the lithophile elements. In addition, Large et al., (2011) present a method for predicting the amount of specific elements expected from dust sources within coals. This has proven useful for predicting dust supplied Ti concentrations within a number of Cenozoic coals (Large et al., 2011).

Briefly, to predict the amount of lithophile elements derived from dust within the coal, requires latitudinal gradients in organic accumulation, mass loss from coalification and dust deposition and composition to be defined. Modern latitudinal gradients from peatlands at various latitudes were compiled and plotted to define the relationship between organic matter accumulation and latitude (Fig.6.11).

Mass loss due to coalification was modelled with the assumption that CO_2 and CH_4 were lost initially followed by H_2O. Although this is not strictly correct it reproduces coalification trends published from the USGS coal database (Bragg et al., 1998; Fig.6.11).

Atmospheric dust deposition was estimated from the modern dust deposition map of Mahowald et al., (2006; Fig.6.12) and Mean Continental Dust data from Lawrence and Neff (2009). The use of the modern dust deposition map is thought suitable in the Cenozoic due to similar paleogeography at the time (Scotese, 2001). To test the model Large et al., (2011) predicted Ti within several Cenozoic coals (Fig.6.13) and compared the results to actual concentrations. The modelled and actual values were very similar demonstrating the strength of the technique.

When applied to the Longyear and Lunckefjellet coals, assuming a dust deposition rate of 1 $gm^{-2}a$ and TOC of 78%, and carbon accumulation rate of ~20 $gCm^{-2}a^{-1}$ (as calculated previously), the mean concentration of lithophile elements within the coals reproduce or fall below those predicted by the model making a dust source highly plausible (Table 6.6). K is persistently low within the Longyear coal seam indicating remobilisation or K depleted source region. It is therefore thought that dust supply represents the dominant control upon lithophile concentrations within the Longyear seam.

Dust supply during the formation of the Longyear seam appears to be controlled by Milankovitch precessional cycles (Section 6.32). Global dust deposition rates are highly dependent upon global and regional climate with the warmer wetter conditions of the

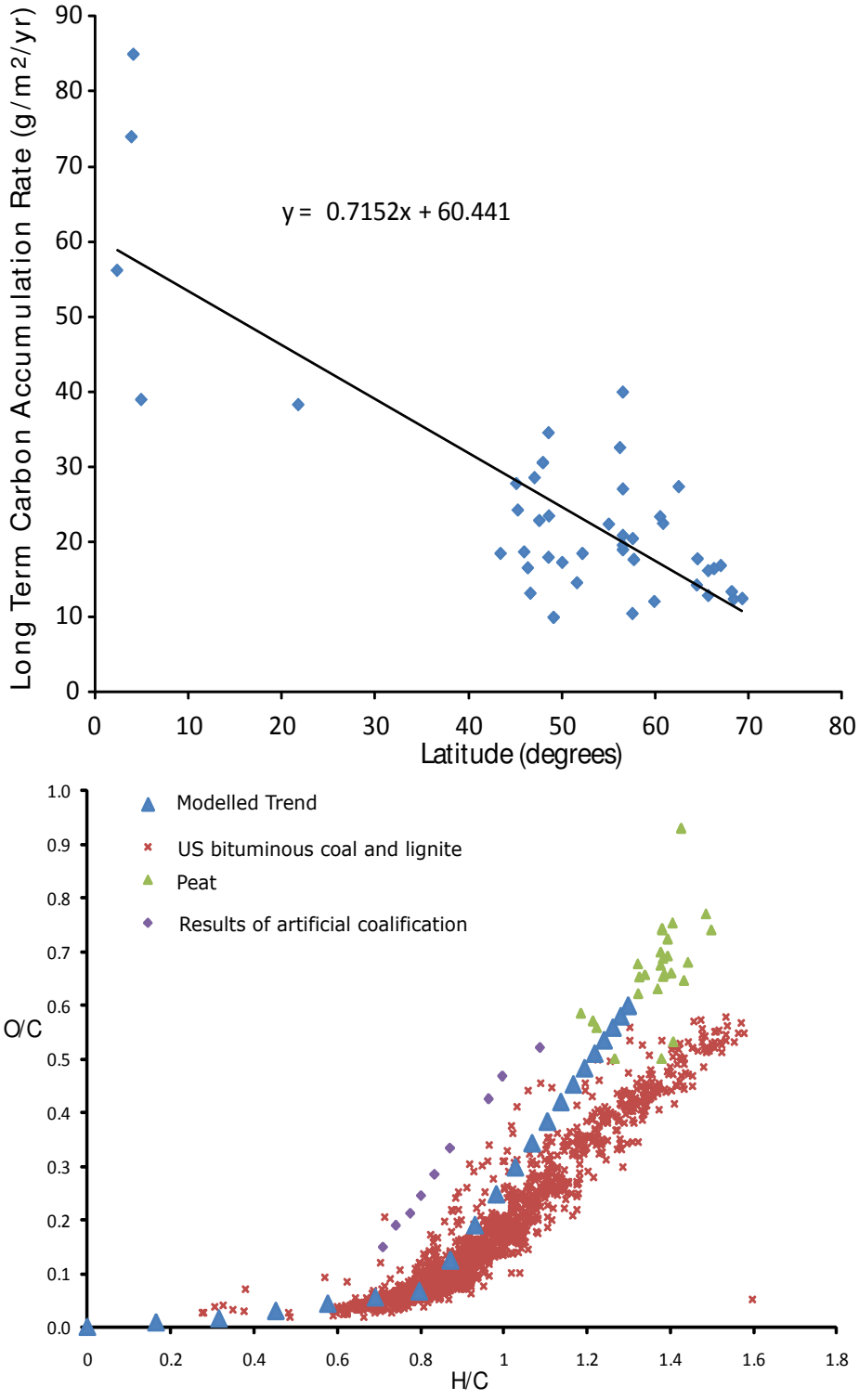

Fig. 6.11 – (Top) Modern trend in Long Term Carbon Accumulation rates with Latitude (Large et al., 2011) showing decreasing LORCA towards the poles

(Bottom) The trend used to predict mass loss during coalification plotted on a van Krevelen diagram and compared to the USGS Coals (Bragg et al., 1998) and the results of artificial coalification (Mursito et al., 2010).

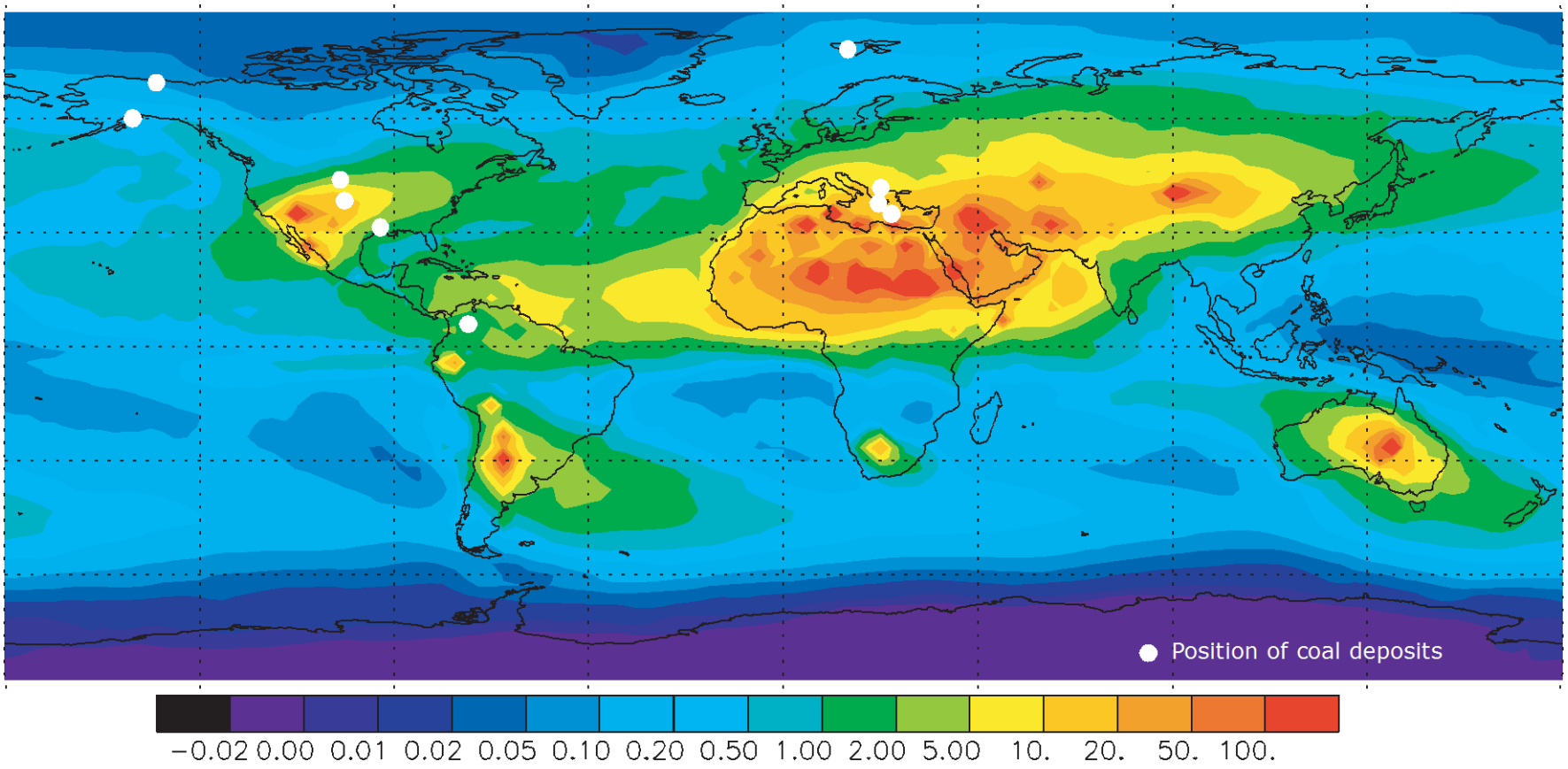

Fig. 6.12 – Predicted recent mineral dust deposition rates (Mahowald et al., 2006)

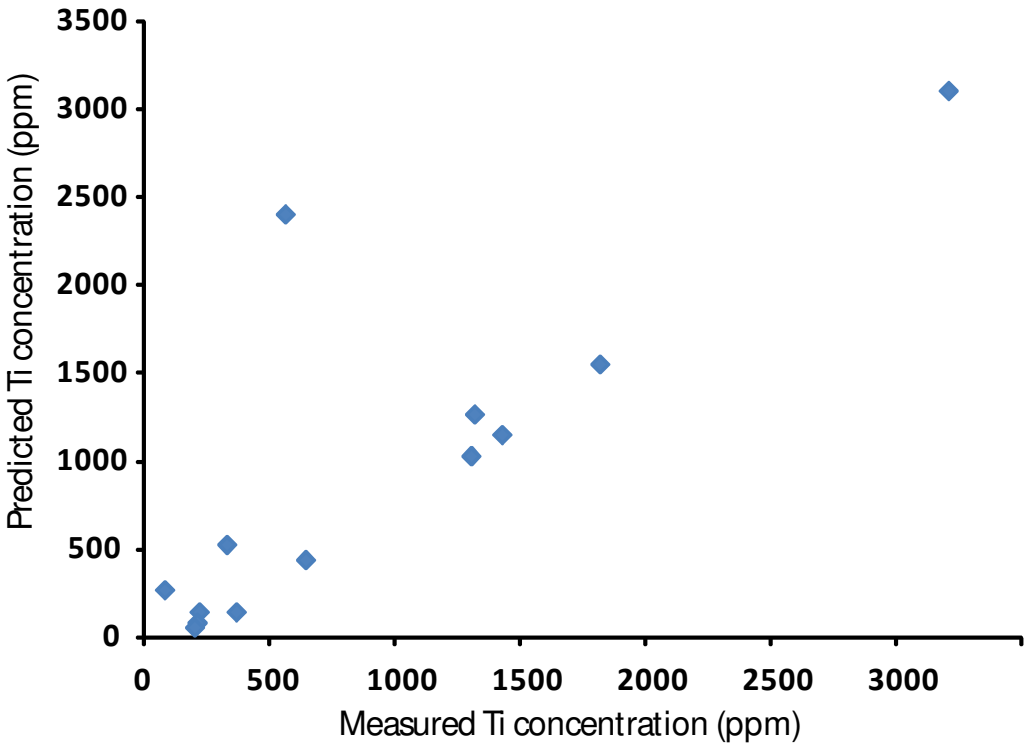

Fig. 6.13 – Measured vs. predicted Ti concentrations within Cenozoic coals (Large et al., 2011). Close agreement indicates that the techniques should be valid.

	Dust (Predicted) ppm	Mine 7 ppm	Lunckefjellet ppm
Al	4858	1759	3333
K	1596	98	460
Na	832	1488	1541
Ti	347	357	255
Pb	5.6	3.1	-
Cu	3.1	4.5	-

Table 6.6 – Predicted dust contribution for peatland (assumed dust deposition 1g/m²/yr) and the actual composition of the Longyear seam, note the close correlation of Ti, Cu and Pb (the most immobile lithophile element with that predicted). K is low due to its mobility within peats

interglacial periods producing up to 3-4 times less dust globally than in the drier colder interglacial periods (Mahowald et al. 1999; 2002).

The Al, Ti, K and Na profile (Fig. 6.14) shows that the lithophile element record fluctuates between higher and lower concentrations four times within the 1.5m Longyear seam. There also appears to be a lag between peak Al, Ti, K concentrations and Na concentrations with highest values approximately 10cm after that of the other lithophile elements.

6.5.3.1 - Peatland fires and the Arctic Palaeocene Climate

Dust deposition rates (and consequently higher lithophile element coal concentrations) would be expected to be higher in more arid, cooler periods and vice versa. This has been explained by increased surface gustiness (Engelstaedter and Washington, 2007), decreased vegetative density, reduced hydrological intensity and reduced pCO_2 (Mahowald et al., 1999) during cooler periods (the best studied of which is the last glacial maximum). Some studies even suggest that once high dust conditions have been initiated, dust generating conditions are further enhanced by seeding Fe limited parts of the ocean (Archer et al. 2000; Bopp et al., 2003), further drawing down CO_2 and also through increased albedo at the tropics (Claquin et al. 2003).

Drier periods would also be expected to be characterised by higher fusinite contents (Scott et al., 2000; Scott et al., 2002) reflecting high

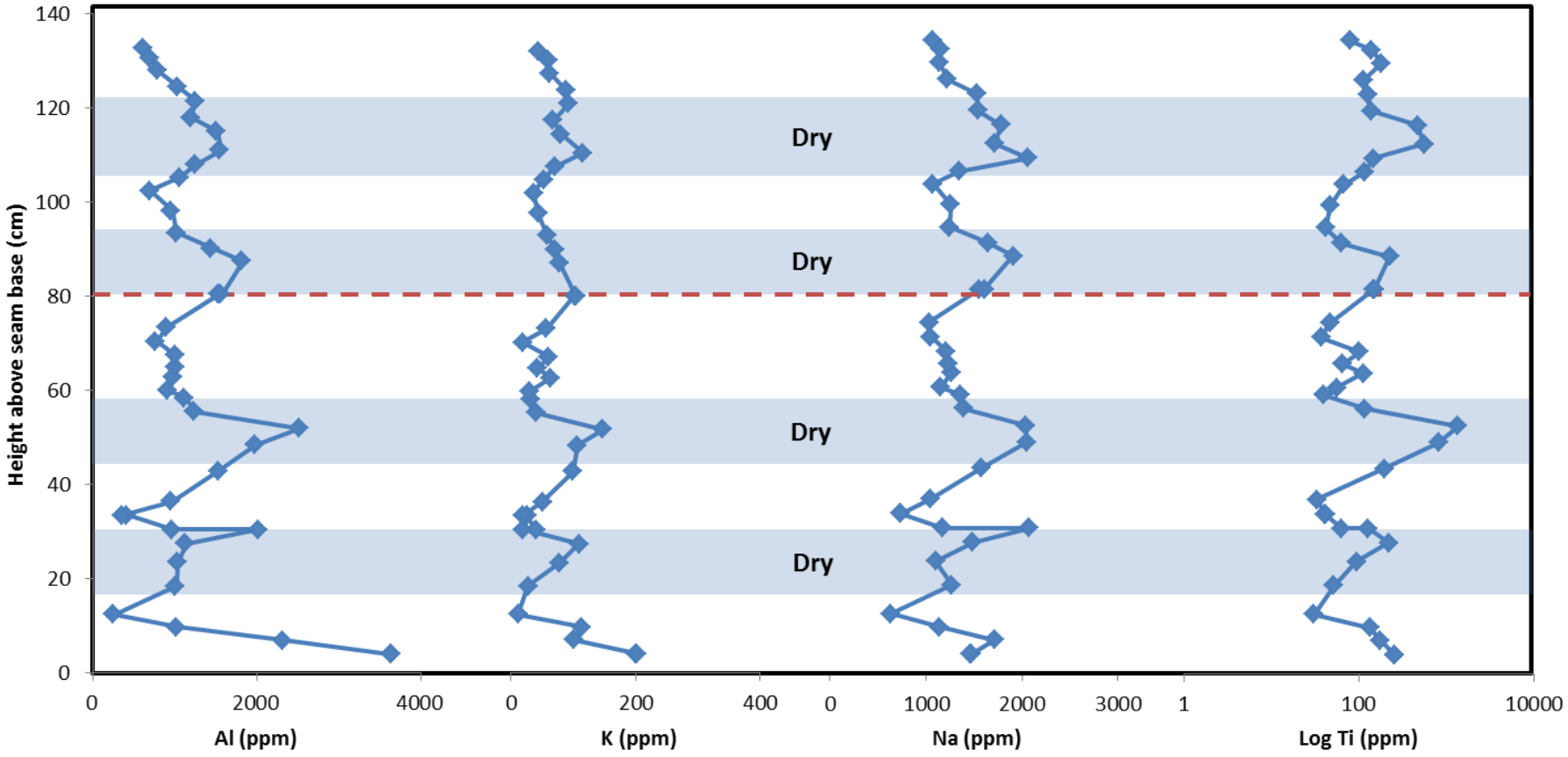

Fig. 6.14 – Lithophile elements (Al, K, Na, Ti) profiles upseam in the Longyear at Mine 7. High values indicate dustier periods/ drier periods. Max Deviation from point shown ±5%

oxidation and combustion within the peatland. However, in the Longyear seam the periods of highest dust input to the peatland are associated with the lowest fusinite contents (Fig.6.15). This is unexpected as peatland fires appear to be more common within wetter periods.

A number of reasons for this are proposed; that the local conditions during the Palaeocene were drier than the global trend which controlled the dust flux, or that the intensification of the hydrological system associated with a warmer wetter climate led to increasing lightning strike frequency. This is most pronounced in the hydrologically less stable lower part of the seam.

The effect of modern global warming upon forest fire frequency in boreal regions has been the subject of a number of publications (Stocks et al., 1998; 2001; Carcaillet et al., 2001; McCoy and Burn, 2005). Natural forest fire initiation is closely related to lightning strike frequency (McCoy and Burn, 2005; Anderson et al., 2006). Currently, in boreal regions, the Northern Arctic Air Mass is relatively stable and not generally associated with lightning (Carcaillet et al., 2001). Consequently, forest fire initiation is dependent upon the penetration of unstable marine air masses that create the necessary conditions for lightning and ignition (Carcaillet et al., 2001).

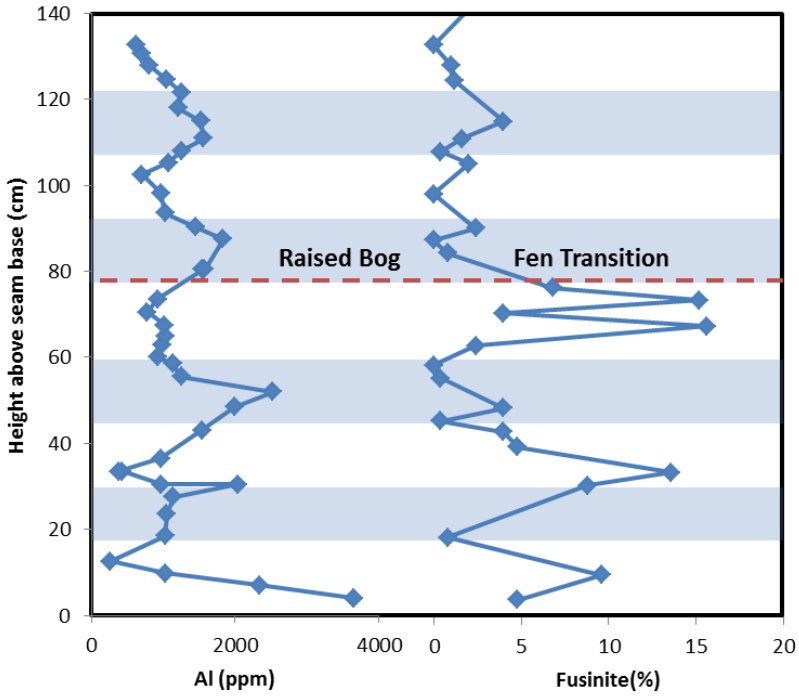

Fig. 6.15 – Al and fusinite profile showing fires during locally wetter periods, this indicates that although peatland hydrology made large fires possible the causes of the fires may be external for example ignition by lightning. When hydrology was more stable the peatland was harder to burn and so the fire cycles seen were not as prominent. Max Deviation from point shown +5%

If such a stable northern air mass were to exist in the Early Palaeocene, its expansion during cooler periods would lead to dry peatland conditions without significant peatland fires due to lack of ignition (Fig. 6.16). However as global conditions became warmer, more unstable air masses could penetrate further northwards due to the intensification of the hydrological system.

At the PETM, proxies of sea surface temperature indicate temperatures ranging from 18-23°C in the Arctic Ocean (Sluijs et al. 2006) indicating that the atmospheric gradient during the Palaeocene was low. However, evidence of ice rafted deposits and of glendonites within sediments from the Van Mijenfjorden group (Spielhagen and Tripati, 2009) and more widely within Palaeogene Arctic (Moran et al., 2006; Tripati et al. 2008; St John, 2008) indicates, that at least periodically, conditions at the shallow seafloor were between 0-4°C (Spielhagen and Tripati, 2009).

This contrast shows that rather than being constant the climate of the Arctic in the Palaeocene fluctuated significantly from colder to warmer conditions. Consequently, the climate response to global warming (and fire frequency) during the Palaeocene may be very similar to those seen from modern global warming, namely increased northward penetration of more intense rainfall events and higher lightning initiated peatland fires.

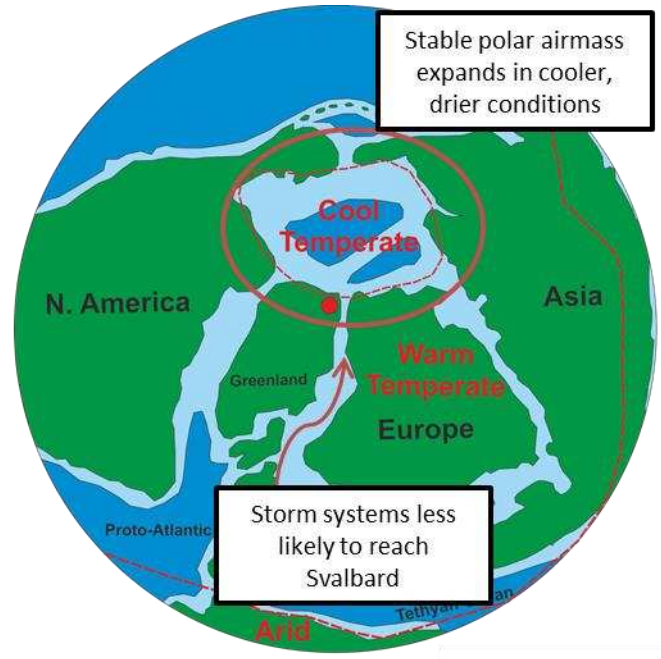

Fig. 6.16 – Palaeogeographic/climatological model of the Arctic region in the Palaeocene (After Scotese, 2002) showing conditions during globally cooler periods and during periods more intense hydrological cycling.

6.5.3.2 – Provenance of dust supply to the Longyear seam

The provenance of the dust supply to the Longyear coal is important as it controls the particle size and elemental composition of the dust deposited upon the peatland, influencing both gross ash content and the concentration of problem elements.

To compensate for expected variations in coal density and dust deposition rate throughout the Longyear seam the lithophile elements were normalised to Ti in the sections from Mine 7 (Fig.6.17) and Lunckefjellet (Fig.6.18). Al, K Na show values varying between MCC and UCC values (Rudnick and Gao, 2003) which is consistent with supply only from a dust source. K is depleted in both locations relative to Ti in MCC, which is due either to the lithology of the source region or loss due to mineral dissolution in the peat.

The Na/K ratio has been associated with the supply of clastic material to peatland within intermontane basins in the Rockies (Weimer and Land, 1975) with lower values indicating higher clastic input and vice versa. At both locations (Lunckefjellet; fig 6.18 and Mine 7 Fig. 6.19) the Na/K ratio remains relatively constant around 10. At mine 7, the ratio is lowest at the base of the seam inferring initiation within a more clastic marsh or lacustrine environment. At Lunckefjellet, the seam becomes increasingly clastic upwards as

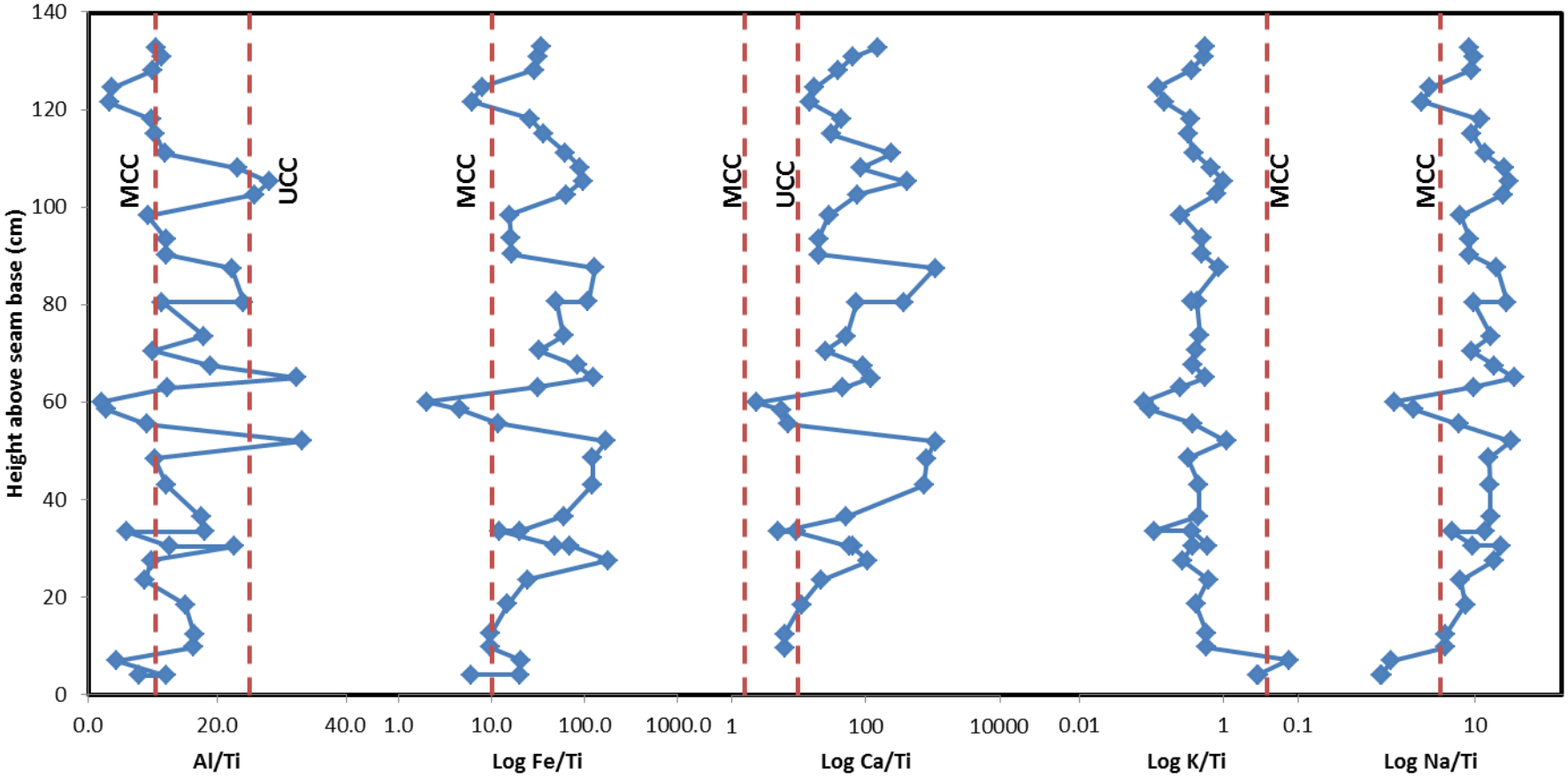

Fig. 6.17 – Al/Ti, Fe/Ti, Ca/Ti, K/Ti, Na/Ti ratio profiles upseam in the Longyear at Mine 7 showing that Al is consistent with Mean Continental Crust Values (MCC) but that Fe and Ca are enriched probably due to groundwater supply. UCC = Upper Continental Crust Max Deviation from point shown ±5%

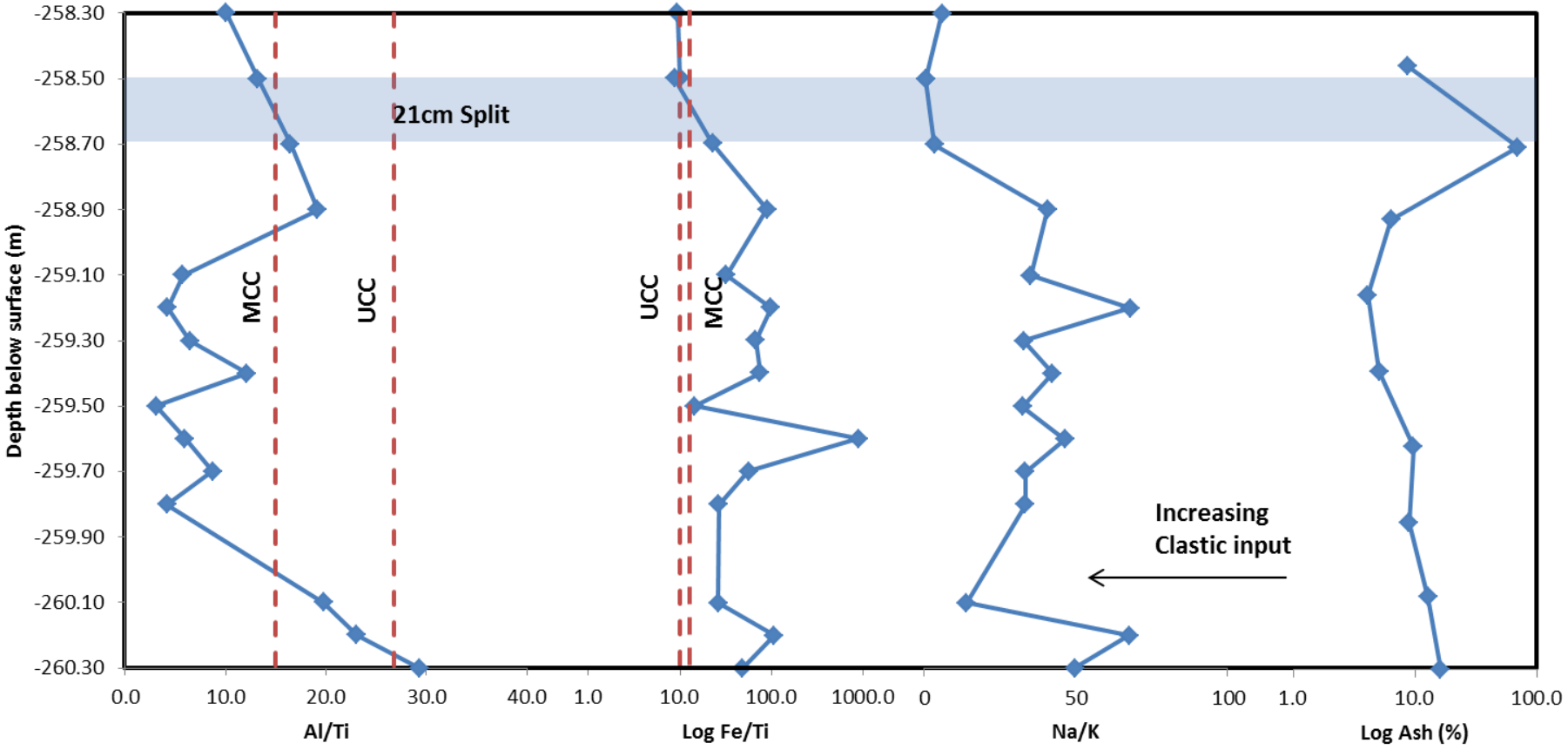

Fig. 6.18 – Al/Ti, Fe/Ti, Na/K and Ash content of the Longyear Seam at Lunckefjellet MCC= Mean Continental crust UCC = Upper Continental Crust

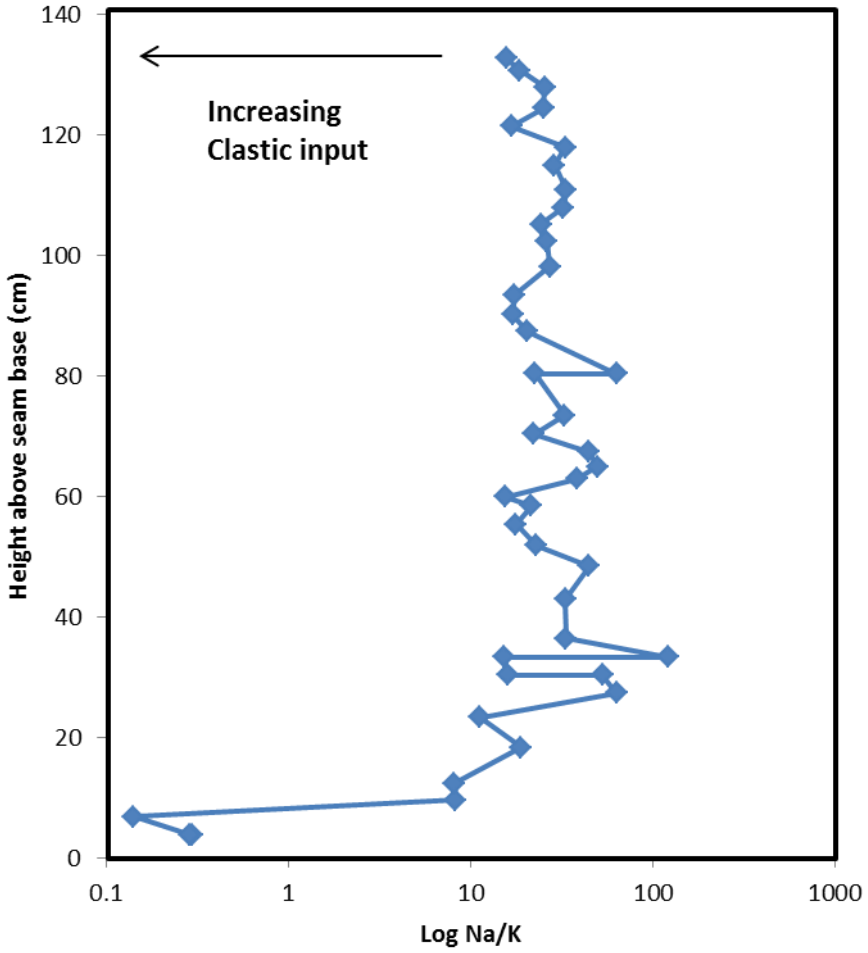

Fig. 6.19 – Na/K profile of the Longyear Seam at Mine 7 showing increased clastic input at the base of the seam

shown by increasing ash, approaching the split as would be expected.

Fe and Ca, as previously reported (Section 6.5.2.2) are enriched by groundwater interaction with underlying Cretaceous marine shales and therefore dust plays only a minor role in the distribution and concentration of these elements within the Longyear coal.

Cu is enriched within dust and the record of atmospheric deposition of Cu is well preserved within peatland environments (Nieminen et al., 2002).

Examination of the Cu/Ti record (Fig. 6.20) should provide an indication of the provenance of the lithophile elements within the Longyear seam as Cu is generally enriched in dust (Lawrence and Neff, 2009). The Cu/Ti ratio of local sediment is defined by the composition of the sediment forming splits within the Svea seam and that immediately above and below the Longyear Seam. Mean Continental dust Concentrations (MCD) were taken from Lawrence and Neff (2009).

The Cu/Ti ratio in the Longyear coal shows the same offset of that observed in Na profile (10cm). The lowest Cu/Ti ratios (corresponding to local sediments) occur during the driest periods (high Al,Ti,K). This is then followed by significant enrichment in Cu during the beginning of wetter conditions before declining towards the next dry period. This could correspond with a more distal Cu

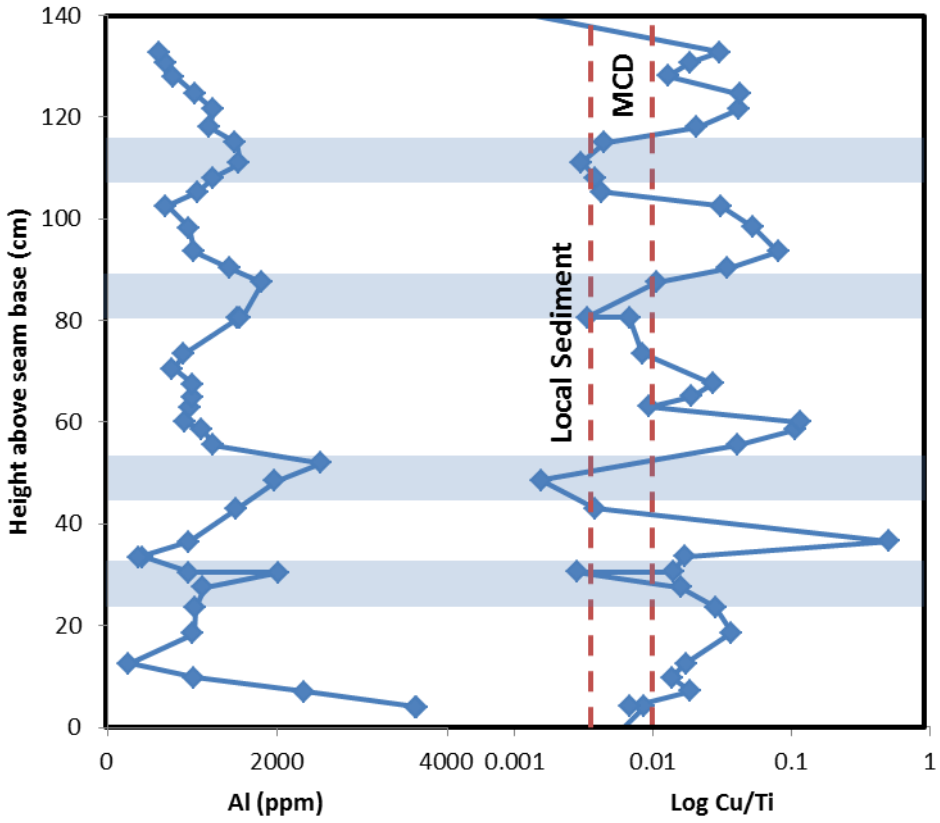

Fig. 6.20 Al and Cu/Ti profile of the Longyear at Mine 7 showing that in drier periods, dust was locally derived and in wetter periods less dust was delivered but from a more copper enriched distal source. MCD = Mean Continental Dust (Lawrence and Neff, 2009) Max Deviation from point shown ±5%

rich dust source during wetter periods or possibly due to very fine grained distal dust preferentially partitioned into plant-matter and coarser local dust less available for plant uptake.

Using the model of a stable polar air mass during dry, cooler periods the northward transport of distal dust would be prevented leading to a predominantly local supply. During initiation of locally wetter periods northward transport would be enhanced with transport of Cu enriched or finer global dust northward before the increased vegetation density etc reduced dust production (Fig.6.16).

The high values of Cu/Ti (Fig. 6.20; above MCD values; Lawrence and Neff, 2009) may be explained either by the presence of a distal Cu rich source region or through the incorporation of Cu into vegetation, leading to relative enrichment compared to Ti. Certain plant species (eg. Fernandes and Enriques, 1991) are significantly enriched with regard to Cu. Whereas Ti would be vulnerable to physical transportation within the peatland during wetted conditions, incorporation of Cu into plants would effectively sequester Cu in place leading to the enrichment seen.

This section shows that dust supply of lithophile elements remained dominant throughout the deposition of the Longyear seam. Dust appears to be controlled by precessional cycles with dry, colder periods characterised by local dust supply and wetter periods more distal supply. During the more hydrologically unstable lower seam

formation, fires frequency increased during globally warmer conditions, reflecting the intensification of the hydrological cycle and greater lightning strike frequency.

6.5.4 - Marine Controls on Coal Sulfur

Marine influence is both direct and indirect within the Longyear seam with the indirect effect of rising sea level upon the carbonate minerals and coal character discussed in Section 6.5.2.2). Large et al. (2011) accounting solely for sulfur deposition from sea spray (a major source of marine sulfur to the coast; Mahowald et al., 2006) shows the expected sulfur concentration at low (0°), medium (45°) and high (70°) latitude at various distances from an inferred coastline (Fig.6.21) although prevailing wind may have a role.

Sea salt sulphate deposition rates in the study were derived from an empirical formula for sea salt sulfur deposition, $y= 1.0941x^{-0.5527}$ (Hossain and Easa, 2011) where x is distance in km and y is expected sulfur deposition rate ($mg/m^2/d$). To account for additional sulfur supply a low pre-industrial atmospheric S deposition rate was added (Stevenson et al., 2003), assuming 75% of sulfur in peat is retained (Moore et al., 2005). The resulting sea salt sulphate deposition rates were then inputted into the model outlined in the previous section (Large et al., 2011)

At low latitudes, the zone of coal predicted to be affected by sea salt sulphate deposition would be much thinner than at higher latitude

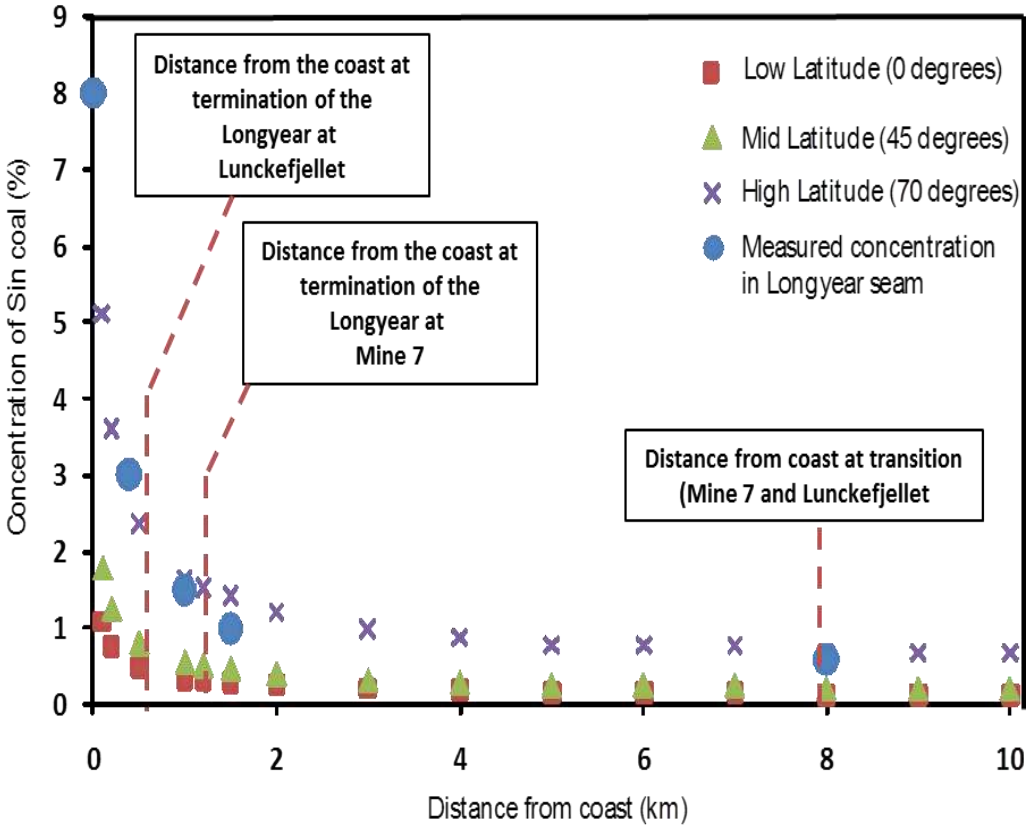

Fig. 6.21 – Modelled effect of sea salt sulphate deposition at low, medium and high latitude and a measured transect inland from an inferred tidal channel shows close correlation. Using this model the Longyear terminated at 1km from the coast in mine 7 and 0.5km in Lunckefjellet

(0.2km vs. 4km) due to the much greater carbon accumulation rates. Predicted values were then compared to a re-drawn transect from the Longyear seam at Lunckefjellet (Aspøy, 2011). Distance from the coast was measured as distance from a mudstone–coal transition interpreted as a tidal channel. Measured sulfur from the Lunckefjellet transect shows very similar values to those predicted from high latitude (Fig.6.21).

As shown in Chapter 4, sulfur remains relatively constant at 0.5% to the raised bog-fen transition at Lunckefjellet and Mine 7 (Fig.6.22). Using the model provided above this would represent a distance from the coastline of in excess of 4km during this period. Sulfur deposition during this period therefore represents the background contribution of groundwater and coastal aerial deposition. However in a large bog much of the shallow groundwater will be sourced within the peat and have composition that reflects the transport of atmospheric deposition through the near surface.

Post-transition coal sulfur rises rapidly, at both sites with the same parabolic curve as predicted by Large et al. (2011). This indicates that in response to a steady rise in sea level, the zone of high sea salt sulphate deposition moved inland. At Lunckefjellet (BH15/2011) the coastline reached within 0.5km (4% S) of the site before the termination of the seam with a split, probably representing coastal inundation. At Mine 7 further from the coast

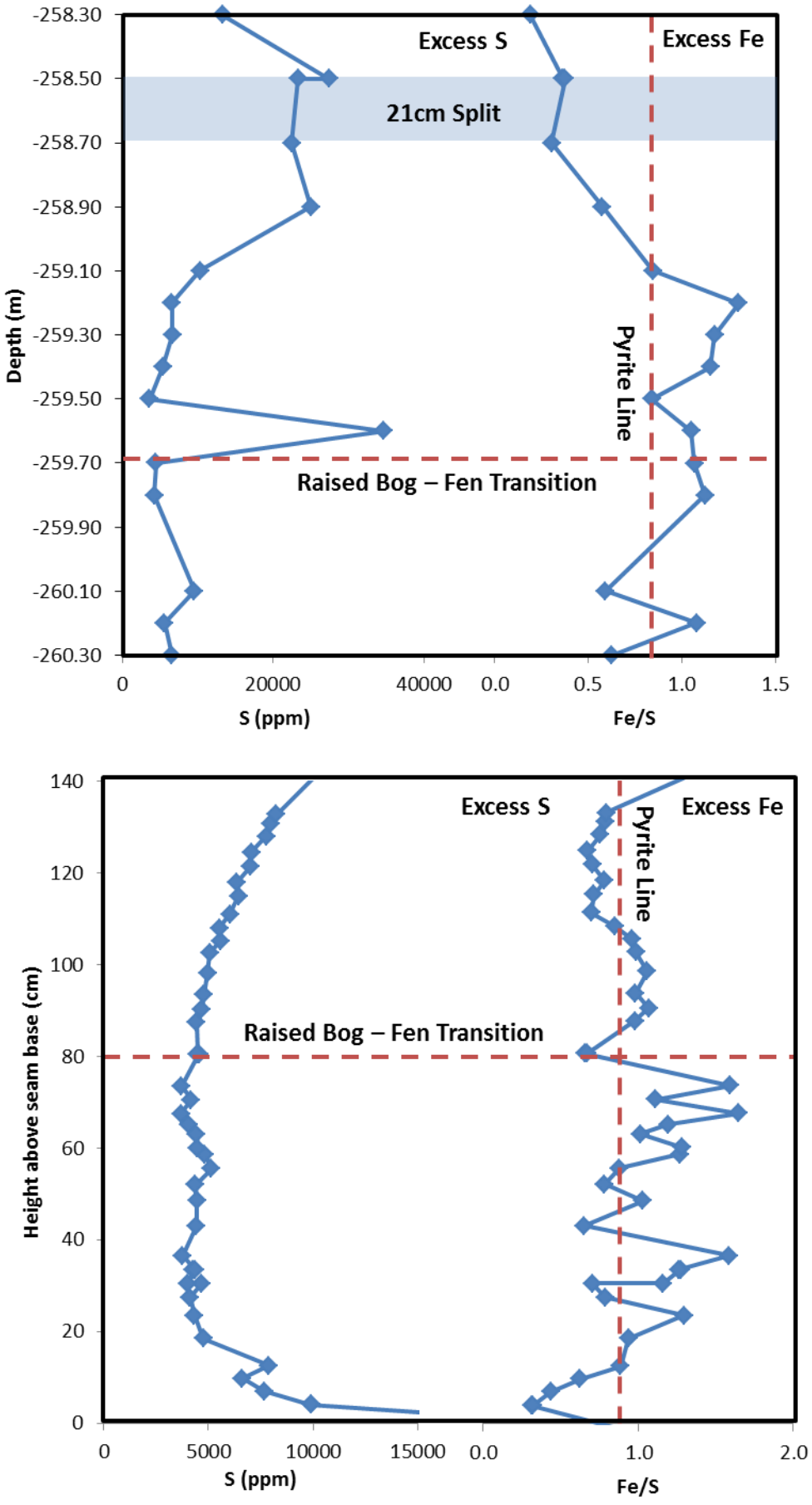

Fig. 6.22 - (Top) S and Fe/S profile for the Longyear at Lunckefjellet (Bottom) S and Fe/S profile for the Longyear at Mine 7. Pyrite line from atomic ratio of Fe/S in pyrite Max Deviation from point shown ±5% Base of seam at bottom of graph

and less vulnerable the coastline reached 1.5km (1% S) of the site before termination of the seam. This may have been due to rising groundwaters associated with sea-level rise outpacing peat accumulation. This difference in suggested termination between the two sites is attributed to the variation between coastal plain gradient due to palaeogeographic position (Chapter 3).

The Fe/S ratio is thought to have a significant control upon the oil potential of the Longyear coal (Chapter 4). This is largely driven by S supply as Fe supply does not vary significantly during the formation of the highest yield coals (Fig. 6.9). This in turn as shown previously is affected by the proximity to the coastline.

The Fe/S profile of the Longyear at Mine 7 and Lunckefjellet (Fig.6.22) show that close to the raised bog-fen transition the Fe/S ratio switches from Fe enriched to Fe depleted. This is due to an increase in marine S supply. Economically, a balance is required, with sufficient sulfur and alkalinity to produce oil prone coals but not so coastal that the S and ash content of the coals renders them unsellable. With the limited samples analysed this would be predicted to be within 2 km and 4 km from the inferred palaeo-coast, however further work and a more numerous and palaeo-geographically diverse dataset would be required to confirm this.

6.5.5 – Clastic Depositional Controls at Lunckefjellet

In areas of peatland more vulnerable to clastic sedimentation dust deposition is superseded as the dominant control upon the inorganic composition of the Longyear seam. These areas lie adjacent to the coastline, tidal inlets, fluvial channels and depressions within the peatland which makes them prone to inundation during storm events, high flow events or to rising sea levels.

In the Lunckefjellet region, soon after initiation, the Longyear seam became rapidly more coastal due to its proximity to a natural depression, previously representing coastal lake/lagoonal conditions (Chapter 3). The area most vulnerable to inundation were focussed upon a depression (Tidal Channel) situated centrally within the Lunckefjellet deposit and to the inferred estuary/tidal inlet south of Lunckefjellet (Chapter 3).

BH15/2011 is positioned towards the inland edge of the central tidal inlet (Chapter 3) and contains a single split to the top of the seam of 20cm. Unlike the section at mine 7, examination of the lithophile elements (Al, Ti, Na, K) shows little cyclicity (Fig. 6.22). This may be due to the lower sampling density in this area or indicate that the lithophile element profile at Lunckefjellet reflects a greater clastic component than seen elsewhere in the peatland, as a result of closer proximity to the tidal channels.

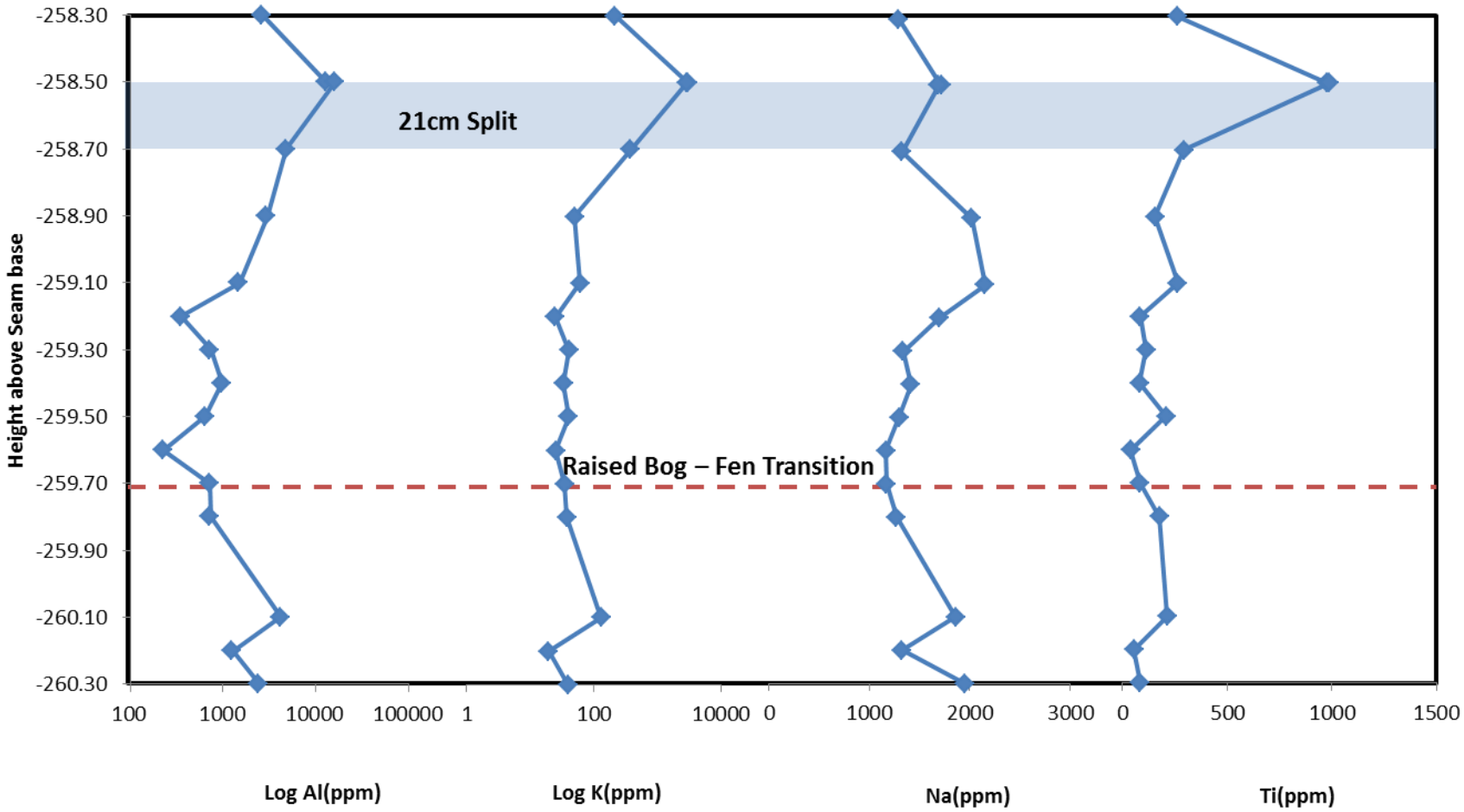

Fig. 6.23 – Al, K, Na, Ti profile showing increasing clastic deposition towards the top of the Longyear seam at Lunckefjellet. Max Deviation from point shown ±5%

6.6 – Plant communities forming the Longyear Seam

Examination of plant fossils from the wider Palaeogene sediments of the Central Tertiary Basin (Denk et al., 1999; Fig. 6.24) and from a single observed plant fossil (*Acer Arcticus?*; Denk et al., 1999) within BH14/2011 (Fig.6.24) shows that a mixture of temperate gymnosperm and angiosperm species.

The fossil record is dominated by members of the *Taxodiaceae, Pinus, Cupressaceae, Glyptostrobus* and *Metasequoia* gymnosperm species with lesser amounts of *Nyssidium, Quercus, Carex, Poacites* and Populus angiosperm species (Fig.6.24). In addition a wide variety of other temperate species such as Hawthorne, Ivy, Bog Rosemary, Iris, Thistle and Fern can be found. This indicates that the flora which formed the Longyear peatland comprised a mixture of gymnosperm, angiosperm and herbaceous angiosperm species (Fig.6.24)

6.6.1 – Organic Biomarkers

The tricyclic diterpanes have been suggested as highly specific biomarker molecules (Noble, 1986; Peters and Moldowan, 2005). Previous studies of these molecules (Ćmiel and Fabiańska, 2003) indicated that the Longyear coal from Bjeorndalen contained primarily pimarane, 4β(H)-19-norisopimarane and lesser amounts of ent-beyerane. This was thought indicative of significant *pinaceae* input to the peatland. When the m/z 123 from the Mine 7 section

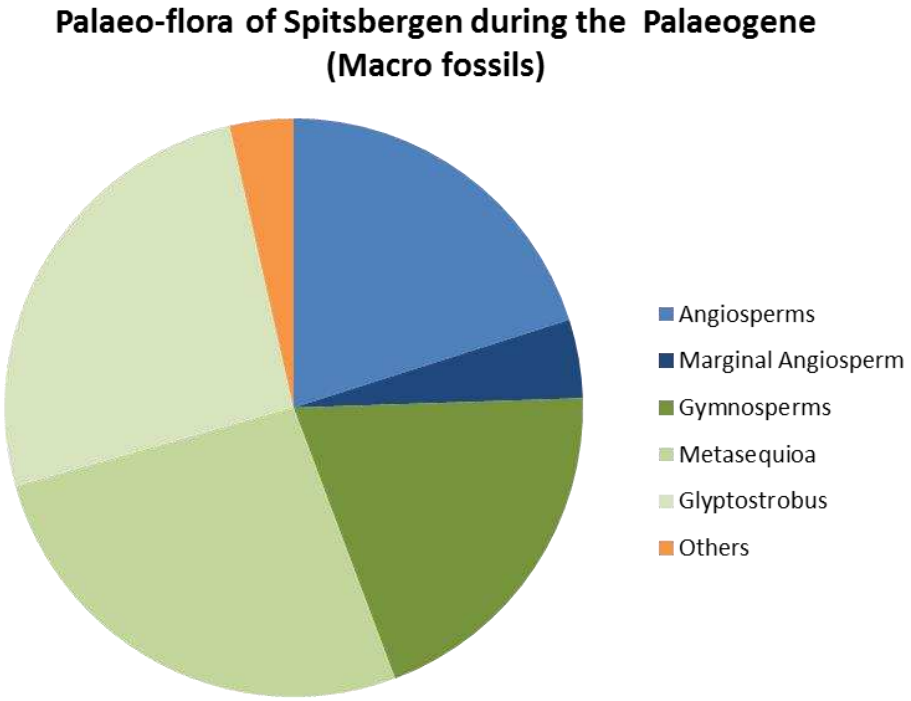

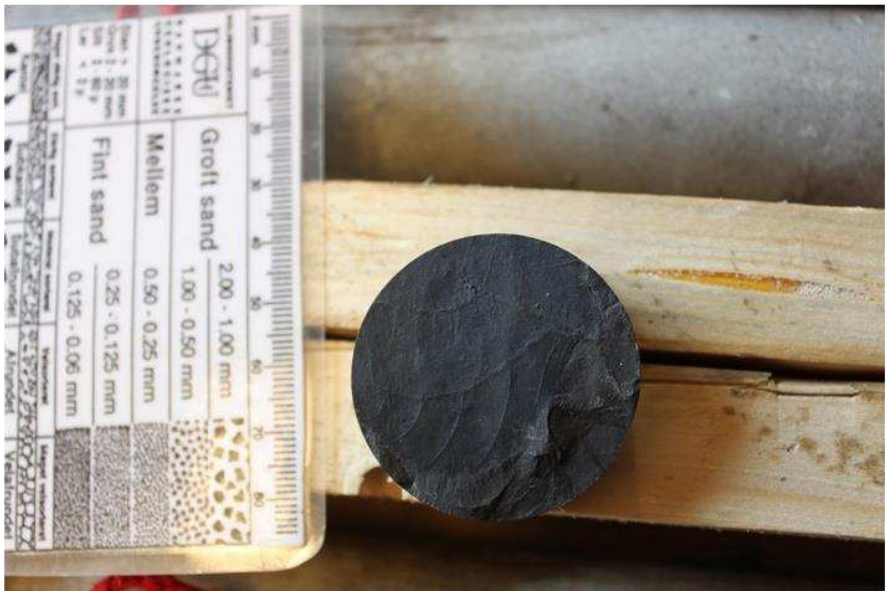

Fig. 6.24 - (Top) Macrofossils from the Palaeogene of Svalbard (Source Denk et al., 1999)

Bottom- Possible *Acer Arctica* fossil from a split in the Longyear seam in BH14/2011

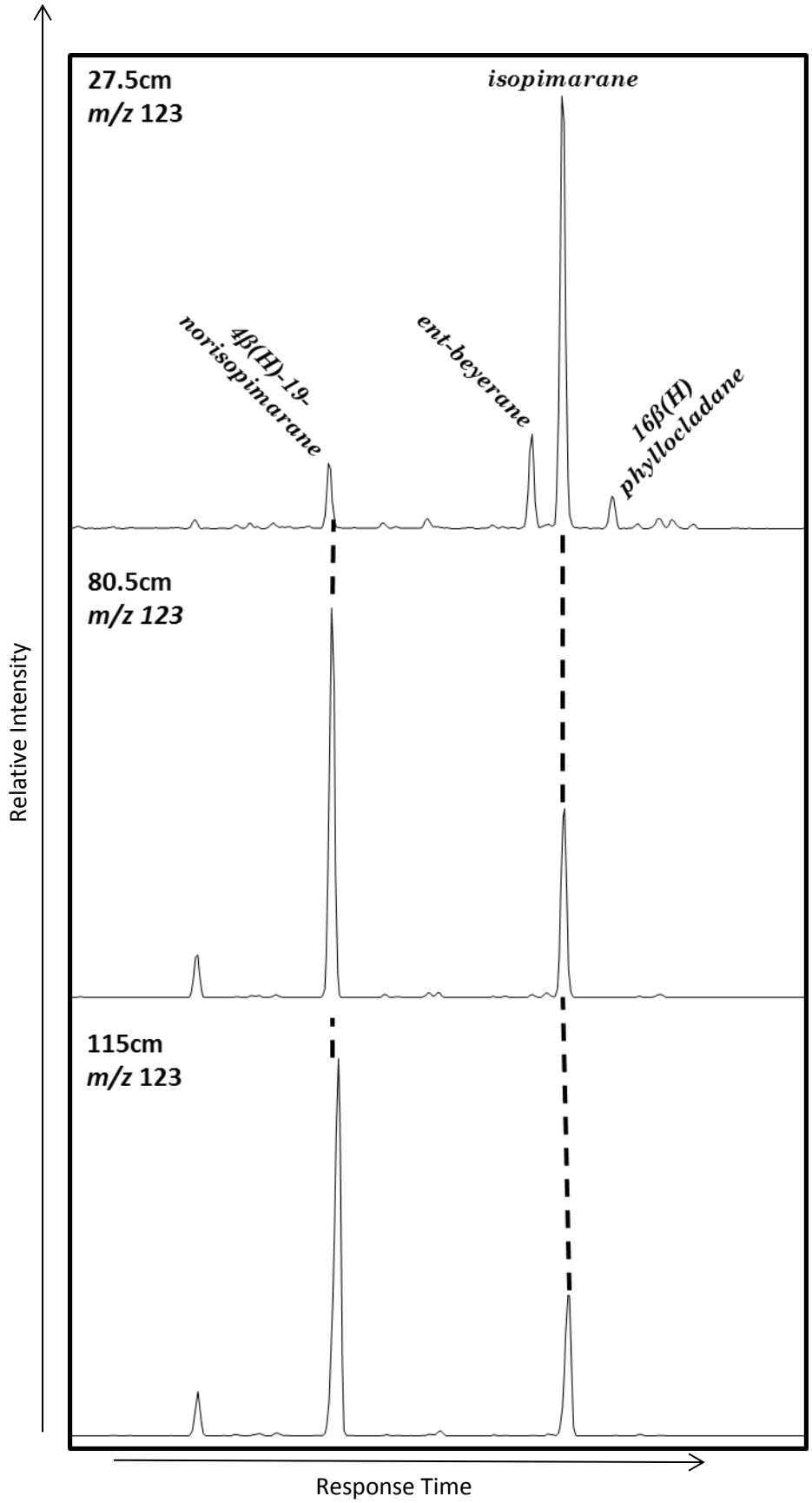

Fig. 6.25 – m/z 123 mass chromatograms showing the tricylic diterpanes showing a dominance of isopimarane and 4β-(H)-19-norisopimaranes in the Longyear seam at Mine 7

was examined (Fig.6.25) the same distribution was seen with pimarane and norisopimarane dominating with lesser amounts of ent-beyerane supporting an important pine and gymnosperm component to the peatland at this location. The presence of ent-beyerane and lack of ent-kaurane within the Longyear seam may indicate a limnic rather than paralic setting (Schulze and Michaelis, 1990).

The absence of angiosperm biomarkers within the Longyear coals is strange as the fossil evidence indicates that they formed a significant component of the flora of the Central Tertiary Basin. However, angiosperms are significantly less resilient to biodegradation than gymnosperms (Faix et al., 2009). High hopane contents are observed (indicative of aerobic bacterial community) within the Longyear seam (Section 6.7; Chapter 4). The high levels of bacterial activity and susceptibility of angiosperms to biodegradation may have preferentially enriched both the fossil and biomarker record in gymnosperms.

6.7 Bacterial Communities within the Longyear seam

High hopane concentrations, aerobic bacterial biomarkers (Peters and Moldowan, 2005) observed within the Longyear seam has been shown to be a significant control upon oil potential of the seam (Chapter 4). However, further examination of the hopanes and associated 2-methyl hopanes and 3–methyl hopanes may also yield

further information regarding the size and type of bacterial communities and subsurface redox conditions. In addition it may provide an indication of how the relative size of the greenhouse gas flux evolved throughout the seam.

Hopanes are thought to be derived from aerobic bacterial membrane lipids such as bacteria-hopaneterol. The function of these molecules is primarily associated with cell membrane permeability and adaption to extreme conditions (Ourisson and Rohmer, 1982; Ourisson et al., 1987). The hopanoid precursor molecules have been recorded in anaerobic species *Geobacter* (Hartner et al., 2005) but are more generally associated with oxic bacteria. Hopanes are relatively resistant to maturation and biodegradation with bio-hopanoid forms being converted to geo-hopanoid forms during burial (βα to αβ; Peters and Moldowan, 2005). In addition hopanoids have been shown to be rapidly incorporated within kerogen (between 0-350 years; Farrimond et al., 2003) indicating the hopane composition is likely to be fixed during early burial and diagenesis.

The 2α and 3ß methyl-hopanes have been shown to be a feature of many source rocks (Farrimond et al., 2004; Talbot et al., 2008). They have very different origins with 2α methyl-hopanes originating almost solely from cyanobacterial sources (Summons et al., 1999)

Cyano-bacteria are found across a wide range of surface environments, responsible for around 50% of productivity within

modern oceans (Talbot et al., 2008). Nitrogen fixing cyanobacteria species such as *Trichodesmium* & *Crocosphaera* have also been shown to contribute significantly to the global nitrogen budget (Montoya et al., 2004).

3-Methylhopanes precursors are less common in sediment than they are in geological samples (Farrimond et al., 2004) but when detected are often closely associated with Type I methanotrophs (Neunlist and Rohmer, 1985; Cvejic et al., 2000) although they have been also detected in acetic bacteria (Simonin et al., 1994). The ubiquity of 3 methyl-hopanes in the geological record (compared to their relative rarity with modern sediments) indicates that there are undiscovered biological precursor molecules or mechanisms from known molecules that require further investigation.

Type I methanotrophs are found predominantly in low methane, surface conditions (Hanson and Hanson, 1996) similar to those expected within fluvial and peatland conditions. Consequently, examination of the 3-methyl hopanes may provide indications regarding how the methtrophic efficiency of the peatland changed over the lifetime of the Longyear peatland.

Hopanes within the Longyear seam are dominated by the C_{29}-C_{30} αβ hopane (geohopanoid) form with lesser amounts of the C_{31}-C_{35} homo-hopanoids reflecting the maturity of the coal (Fig. 6.26; Chapter 4). Quantification of the hopanes (Chapter 2) with 5β-

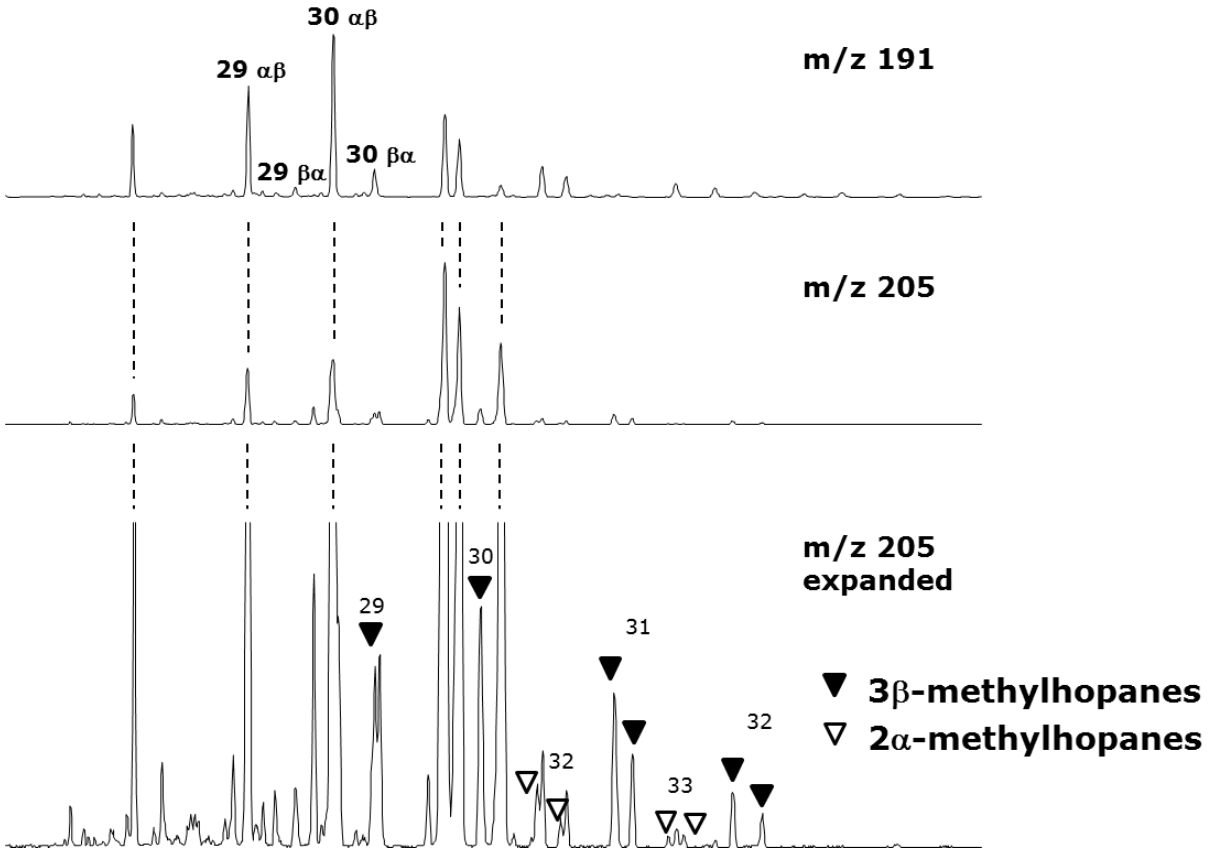

Fig. 6.26 - m/z 191 and m/z 205 mass chromatograms identifying the main hopanes, 2-methyl hopanes and 3-methyl hopanes (identified from Farrimond et al., 2004)

	Hopane or methylhopane Concentration (µg/g oil or extract)		
	Total Hopanes	**2-Methyl Hopanes**	**3-Methyl Hopanes**
Longyear Coal	**5000-125000**	**10-60**	**50-300**
		Oils	
Lacustrine			
Offshore West Africa	920-2600	27-160	31-210
China	760	20	17
Marine or Mixed			
Offshore West Africa	200-2700	15-100	12-72
Offshore Norway	76-1100	2-35	1-14
Germany	300-1600	11-60	10-38
Iran	200-1000	17-170	9-31
Others	240-760	5-37	6-24
		Source Rocks	
Lacustrine			
Offshore West Africa	1300-2900	18-57	70-300
Green River (USA)	1400	18	200
Marine			
Offshore West Africa	270-2000	8-220	8-64
Offshore Norway	300-940	9-22	8-13
Kimmeridge Clay (UK)	110	3	1.8
Marl Slate (UK)	550	26	10
Toarcian (UK)	870-1100	15-20	16-22
Toarcian (Italy)	550-1000	13-130	5-9
Livello Selli (Italy)	70	2.2	1.9
Serpiano (Switzerland)	1100-2400	260-970	16-35
Bahloul Fm. (Tunisia	1700-2200	130	32-38

Table 6.7 – Comparison of the hopane and methyl-hopane content of the Longyear coal with other coals and source rocks (from Farrimond et al., 2004)

cholane allows the comparison of the Longyear coal with other source rocks (Table. 6.7). This shows that the conditions in the Longyear seam were more suited to the formation and preservation of hopanoids than within other marine, lacustrine and coal source rocks (including the Svea).

Examination of bio-hopanoids in modern sediments has been used to make sometimes highly specific inferences regarding the relative size and compositions of various bacterial communities (Talbot and Farrimond, 2007). Consequently, this suggests that this should be applicable to older sediments.

There are a number of complications and assumptions that need to be made in order to interpret how the size and compositions of bacterial communities in geological samples;

1. The same specificity possible at lower maturity is generally not possible and therefore is restricted to very general groups of bacteria eg. Cyanobacteria, Type 1 methanotrophs
2. Quantification of total hopane content (using 5β-cholane) is assumed to represent a significant amount of the aerobic microbial biomass and therefore is regarded as a proxy for the aerobic bacterial community.

3. Any interpretation of the size and composition of the 2 and 3 methyl-hopanes limited to the species in which they have already been linked (eg. Farrimond et al., 2004; Talbot et al., 2007; Talbot and Farrimond, 2007)
4. Post depostional biodegradation is low, and verified by examination of the organic composition and specific biodegradation parameters (as defined in Peters and Moldowan, 2005).
5. Must be examined within the context of the hydrological and palaeo-environmental history at the point analysed.
6. Hopane concentration dependent upon both source input and preservation, evidence for differential preservation up-seam must be taken into account.

The Longyear seam is considered to have minor biodegradation, excellent hopane preservation (as demonstrated in Chapter 2), a well-defined palaeo-hydrological history. Therefore, taking into account the above caveats, it was considered that the Longyear hopane record was suitable for basic examination of the bacterial communities present within the Longyear seam over its 85kyr formation.

6.7.1 Size and Composition of Bacterial Communities

The distribution of hopanes and methyl hopanes changes significantly upseam (Table 6.8; Fig. 6.27; 6.28). Both the methyl

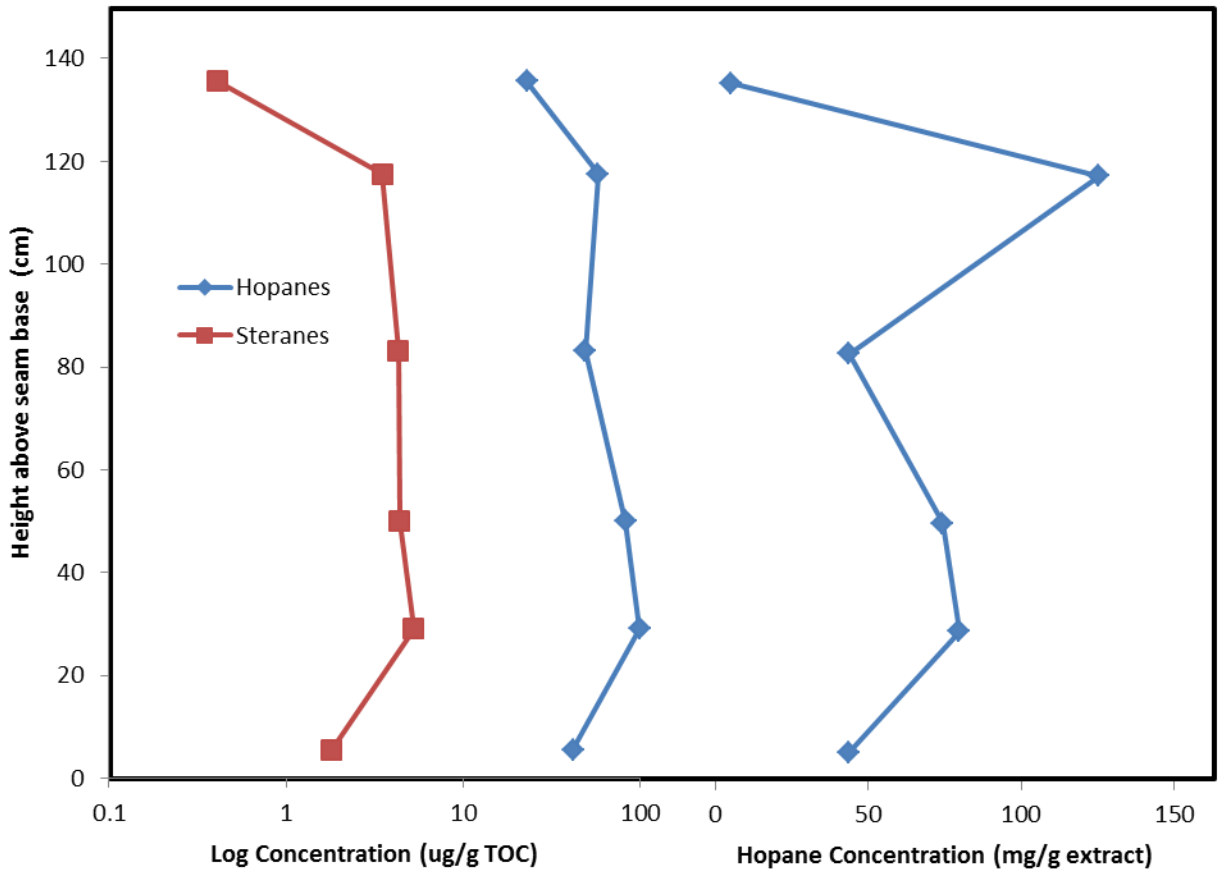

Fig. 6.27 – Log hopane/sterane concentration (µg/g TOC) and hopane concentration (mg/g extract) showing the distribution and percentage hopanes upseam in the Longyear at Mine 7

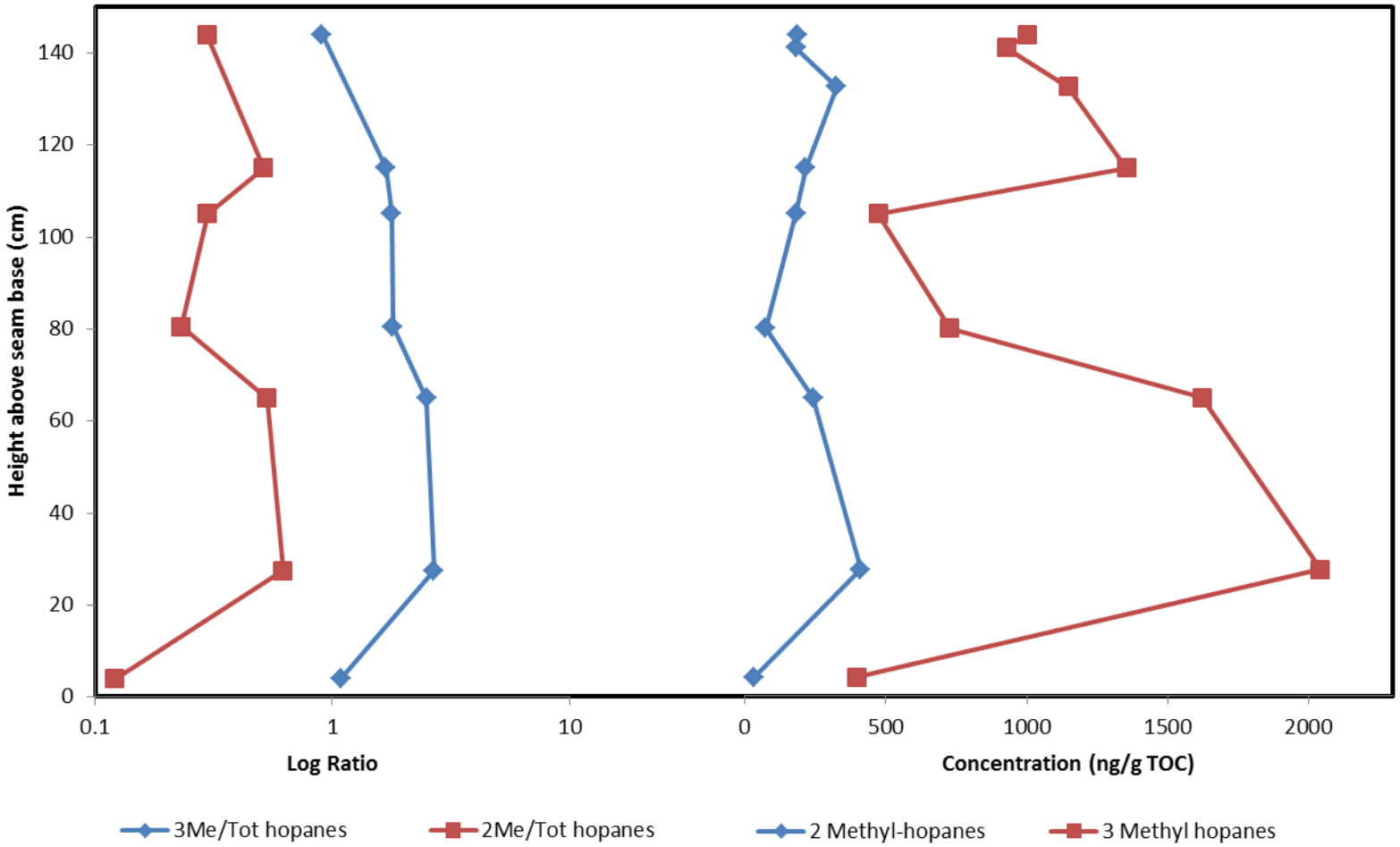

Fig. 6.28 – Ratio of 3-Methyl hopanes to total hopanes and 2-methyl-hopanes to total hopanes and concentration of 2-methyl hopanes and 3-methyl hopanes upseam within the Longyears seam at mine 7.

-hopanes and hopanes concentrations are greatest below 80cm before decreasing slightly during fen conditions. Considering the hopane free phase hopane concentration/g extract basis shows an increase in the in the upper seam. However, this is a result of the loss of n-alkanes due to biodegradation (Chapter 4).

The higher total hopane and methyl-hopane concentrations (Fig.6.27; 6.28) seen in the lower Longyear seam show close association with raised bog conditions. As hopanes and methyl-hopanes are primarily associated with aerobic bacterial species, it would be expected that these bacteria would thrive in more oxic conditions. Raised bog conditions in the Longyear seam can be characterised by lower groundwater condition and more oxic redox conditions promoting aerobic bacterial growth. During later fen conditions, where the water table is higher, the thickness of the aerobic zone is reduced, restricting the size of the bacterial community it could support

The relationship between total hopanes and the methyl-hopanes (Table 6.8, Fig. 6.27; 6.28) also shows the importance of the oxic zone to the relative success of the Type I methanotrophs and cyanobacteria. Both cyanobacteria (2-Methyl) and methanotrophs (3-Methyl hopanes) form a greater proportion of the bacterial community in raised bog conditions.

Methanotroph and Cyanobacteria communities appear to recover towards the top of the seam. However, whereas 3-methyl hopanes remain the same or decreases as a proportion of total hopanes, 2-methyl hopanes increase. This is likely to be due to increasing amounts of open water (associated with rising sea levels) increasing photosynthetic communities, including cyanobacteria.

This implies that the major control upon hopane producing bacteria within the Longyear peatland was the height of the water table, indirectly controlled by sea level.

6.7.2 Implications for carbon cycling during the Palaeocene.

The peatland methane flux, a potent greenhouse gas (Berner and Berner, 1997) is of particularly interest within the context of the Palaeocene Arctic particularly leading up to the Palaeocene-Eocene Thermal Maximum (PETM). Previous studies indicate that the rapid warming seen at the PETM was caused by the sudden destabilisation of methane hydrates at basin margins, due to global warming (Sloan et al., 1992; Dickens, 2003; Pancost et al., 2007).

Pancost et al., 2007 using compound specific isotope analysis on hopanes also suggests that methane fluxes within mid-latitude peatlands were also elevated during this period. However, little has been done to consider the conditions prior to the PETM, which has been shown to have varied between warmer and cooler conditions

Height above seam base (cm)	Total hopanes (µg/g TOC)	Total hopanes (mg/g extract)	2Me (ng/g TOC)	3Me (ng/g TOC)	3Me/2Me	2Me/Tot hop	3Me/Tot hop
4	42.0	5.0	33.8	398.7	8.9	0.1	1.1
27.5	96.0	125.2	410.8	2042.1	4.3	0.6	2.7
65	99.0	128.0	240.9	1621.4	4.7	0.5	2.5
80.5	83.0	43.7	73.0	726.0	7.8	0.2	1.8
105	49.0	74.2	181.0	473.1	6.0	0.3	1.8
115	58.0	79.6	214.9	1353.2	3.3	0.5	1.7
144	60.0	43.7	184.6	1001.0	3.0	0.3	0.9

Table 6.8 – Hopane concentration and hopane ratios at increasing height above seam base (cm)

(Sluijs et al., 2006 Tripati et al., 2008; Spielhagen and Tripati, 2009).

High latitude peatlands were common in the Palaeocene with deposits found upon within Svalbard and the wider Arctic (Scotese, 2002) with methane released from these peatlands possibly providing a 'smoking gun' for later marine methane hydrate destabilisation at the PETM. This is particularly plausible as the high latitude methane flux forms the basis for the formation of polar stratospheric clouds, which have been shown to significantly increase winter temperatures in the Arctic (Sloan et al., 1992; Sloan and Pollard, 1998). Therefore the large bacterial and methanotroph communities seen in the Longyear seam may have had a significant effect upon regional and global climate, particularly if replicated in other high latitude peatlands of the period.

The rapid decrease in 3 methyl hopane concentrations (and therefore Type I methanotrophs) at the raised bog-fen transition suggests a significant decrease in the ability of the peatland to trap and process biologically produced methane. As methanogens are anaerobic bacteria (Dworkin et al., 2006) they do not form a significant component of the hopanes. However, the methanotrophs can be considered as an indirect proxy for the methane flux from the peatland.

The Longyear seam shows an 80% drop in the 3-methyl concentrations across the raised bog-fen transition before recovering

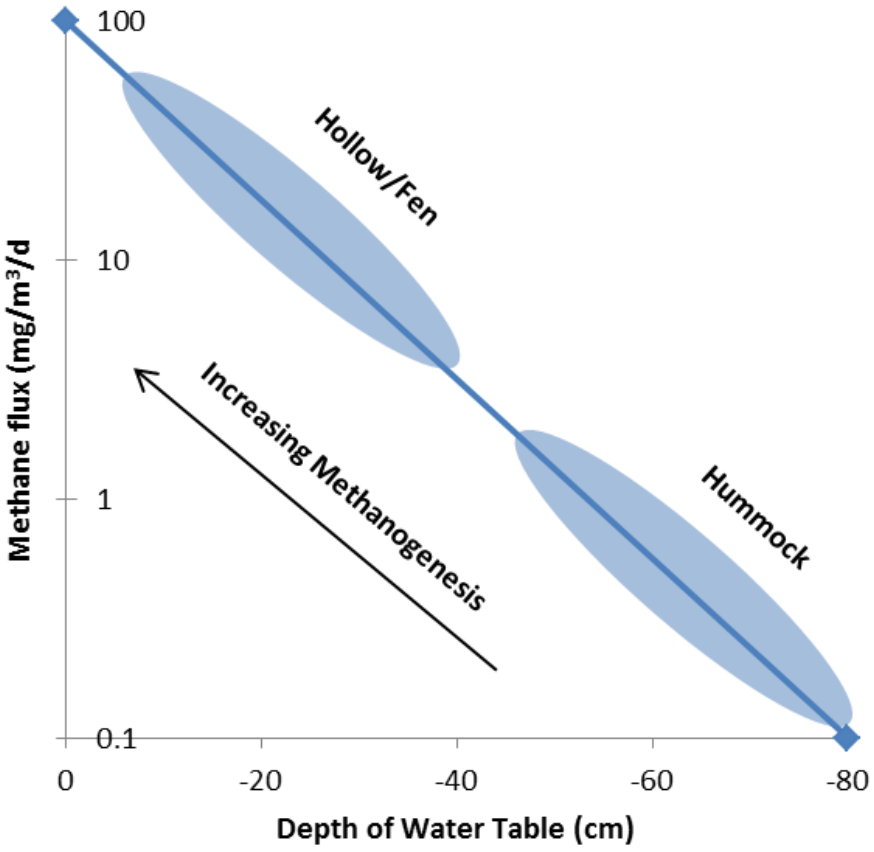

Fig. 6.29 – Relationship between water table depth and methane flux (after Bubier et al., 2003) showing greatest methane flux at the shallowest water table depth.

to ~60% of former values (Fig.6.28). This is consistent with observations by Bubier et al., (1993) where the methane flux showed a negative linear relationship between depth of water table and atmospheric methane flux (Fig.6.29).

In raised peatlands with similar LORCA rates as the Longyear the average methane flux is around $8gCm^{-2}yr^{-1}$ (Laine et al., 2007).

Assuming the amount of methane captured by methantrophy decreased by 80% the flux would increase to around $14.4gCm^{-2}yr^{-1}$. This is consistent with the atmospheric methane flux of methane reported from fens ($15gCm^{-2}yr^{-1}$; Suyker et al., 1996).

Using the more conservative 38% decrease within Fig. 6.28 seen in methantrophy the CH_4 flux is estimated to be around 11.2g $Cm^{-2}yr^{-1}$, between fen and raised bog values. Assuming the size of the Longyear peatland was approximately $600km^2$, this would indicate an increase in methane flux of 1920 tCH_4yr^{-1} or an extra 76.8MT over the ~40Kyr period of fen compared to raised bog conditions.

These estimates although very simplified (e.g. assuming a 1:1 relationship between methyl-hopane concentration and methantrophic community size and methane flux) fit within modern constraints and models (Bubier et al., 1993; Suyker et al. 1996; Laine et al., 2007). This serves to demonstrate that minor fen development in the Palaeocene would have a significant effect upon

atmospheric methane concentrations particularly if repeated across all peatlands at high latitude.

The consequences of this would be expected to be higher annual regional temperatures due to polar stratospheric cloud formation; however this appears to be short-lived, as evidenced by the presence of glendonites in the Basilika Member indicate subsequently cooler conditions.

This work shows that the Longyear coals are good candidates for studying the effect of bacterial communities and subsequent high latitude methane release upon mid-Palaeocene climate. However, further work is needed to confirm and expand on this including examination of the isotopic and composition of the hopanes (Pancost et al., 2007) and calibration of total hopanoid concentrations and bacterial activity within modern samples.

6.8 Palaeo-environmental Development of the Longyear Seam

Integrating the palaeogeographic (Chapter 3), organic petrographic, organic and inorganic petrographic data presented previously, a detailed depositional history of the Longyear seam can be presented. Immediately prior to the formation of the Longyear seam, the coastal plain consisted of a number of coastal lakes with sediment coarsening to the SW, representing upper and lower coastal marsh

and shoreface sediments. The plain was also dissected by a number of channels (Fig. 6.30; Chapter 3)

The Longyear seam began at the basin margins (Bassen, Lunckefjellet) in response to a drop in relative sea levels. The peatland expanded over recently abandoned coastal plain and salt marsh rapidly, reaching its maximum extent early within the peatlands history. To the west of the Lunckefjellet region, a depression overlying the Svea Nord valley remained saturated forming a lacustrine/lagoonal deposit limiting peat formation to its fringes. During this period the hydrological supply to inland parts of the peatland were primarily supplied by local groundwater and precipitation which made it vulnerable to oxidation and combustion.

Global precession controlled wet-dry cycles controlled the majority of the sediment to the peatland with local supply dominant in dry periods followed by distal dust when the hydrological system intensified during warmer, wetter periods. This intensification also caused stormier weather leading to lightning controlled fires. Background levels of sulfur were supplied from a combination of coastal rainfall and sea spray. In areas close to channels/depressions, (BH15/2011), the peat was subject to more clastic sedimentation associated with flooding events/storm events.

During this period vegetation density was thought to be higher comprising more trees amongst which occurred *Acer Arcticum*

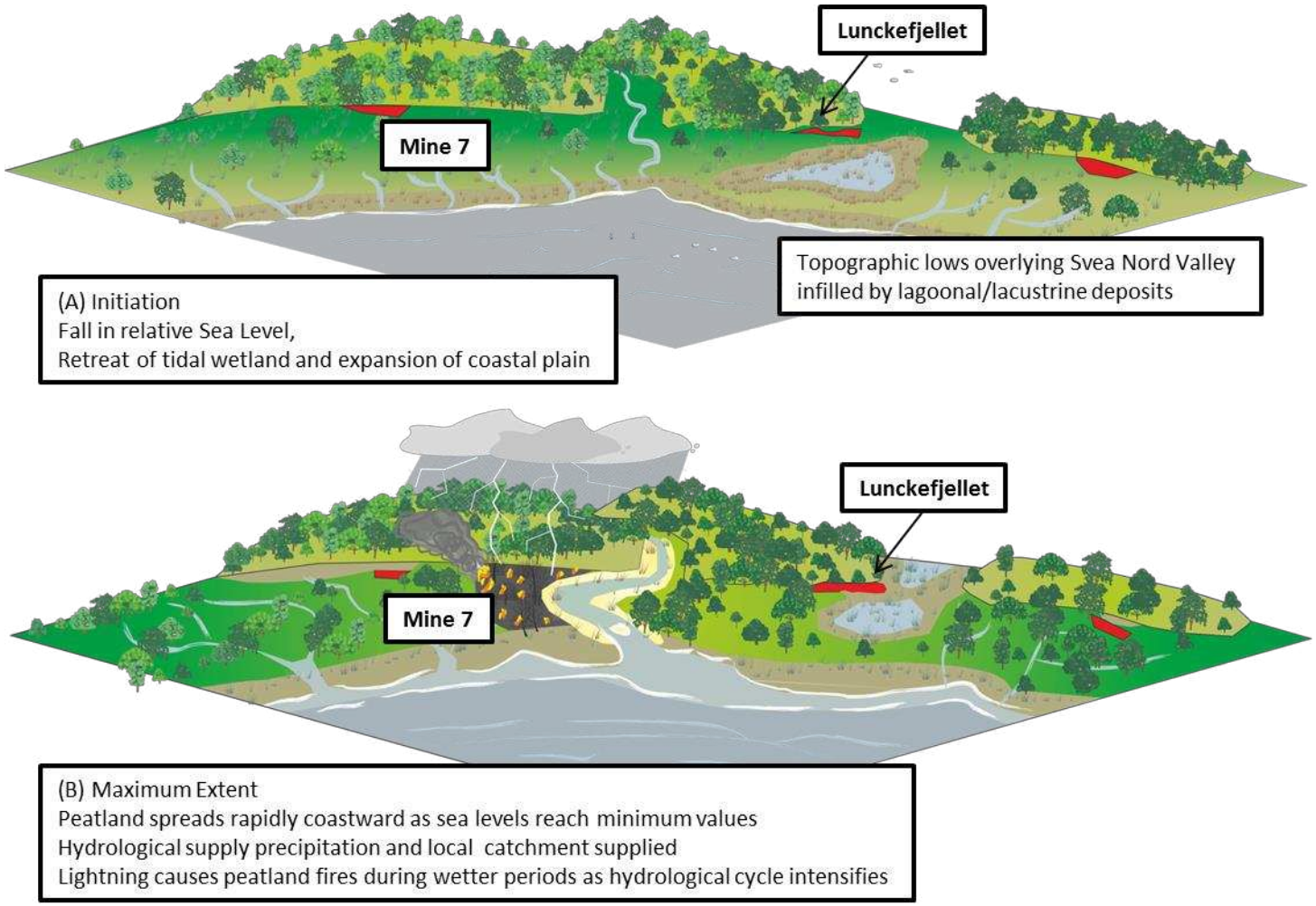

Fig. 6.30 – Palaeo-environmental reconstruction of the initiation of the Longyear seam and conditions within the Lower Longyear seam

(Fig.6.24) which was found within the core and members of the *Pinaceae* (pimarane and isopimarane). Other species reported from the Aspelintoppen Formation such as birch, metasequoia and gingko (Uhl et al., 2007) are also likely to be present as conditions were similar. The climate and high seasonality of Arctic at this time also led to unusually high biodegradation of organic material throughout the deposition of the Longyear peatland.

After approximately 20kyr, relative sea level began to rise with the low gradient coastal floodplain inundated steadily. Peat accumulation continued unaffected by this sea level rise in the northern interior basin due to a wider coastal plan.

However, adjacent to the Svea Nord valley depression, coastal waters penetrated inland until meeting the steeper slopes of the Lunckefjellet high. At this location raised sea-levels led to the a higher water table within the adjacent peatland leading to a transition to fen conditions. This was probably accompanied by a change in vegetation, leading to lower vegetation density (As evidenced by TPI) and replacement of trees with smaller more herbaceous plants, (however this would require further palynological study to confirm).

The raised bog-fen transition occurred later within the mine 7 region as would be expected further from the advancing coastline. At mine 7, the primary supply of lithophile group elements remained from

(A) Raised Bog – Fen Transition
Rising Sea levels expand into the Svea Nord Depression rapidly moving the coastline inwards towards Lunckefjellet.
The closer coastal proximity causes groundwaters to rise within the Lunckefjellet region causing a transition to fen conditions
In the North the process of raised bog – fen transition occurs more slowly, due to the thicker coastal plain with more coastal areas affected first and more landward regions later.

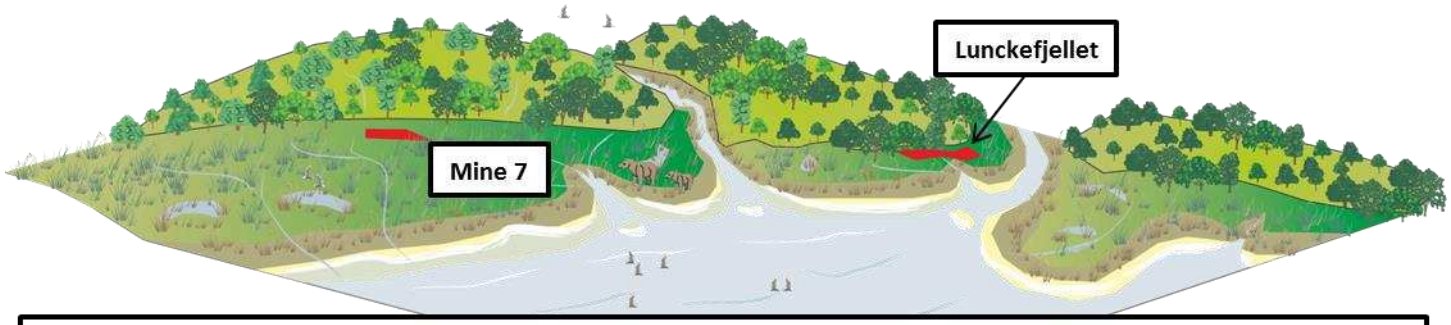

(B) Stabilisation of the fen
Hydrological Supply becomes more groundwater dominated, with thickest peatlands situated at the break in slope between Topographic highs and the coastal plain. Former depressions act as conduits for sediment and sulfur to the peatland interior

Fig. 6.31 – Palaeo-environmental reconstruction of the conditions at the raised bog-fen transition and during the upper Longyear seam

dust, however at BH15/2011 Lunckefjellet, this was supplemented by clastic sedimentation, due to its proximity to local depressions, providing a conduit for subsequent inlets/channel. This clastic supply overwrote the precessional cycles observed within the Longyear at mine 7 (Fig. 6.31)

Rising sea levels led to an increase in S supply at both locations and raised and stable water table maintaining a constant supply of Ca and Fe to the peatland. The elevated water table and fen conditions led to redox conditions within the peatland to reduce the thickness of the oxic layer. Thinning of the oxic zone led to greater preservation of aliphatic oil prone components and a reduction in oxic bacterial activity. As a result the atmospheric methane flux is thought to have increased during the upper Longyear seam with implications for the global carbon budget at that time. Continued rising sea levels led to increasing clastic and sulfur supply to both mine 7 and Lunckefjellet, resulting in splitting at Lunckefjellet, probably due to flooding due to a combination of marine incursion and raised water tables. Within the context of the hydrological landscape model this represents a very wet surface over which clastic material can easily be transported. This reflects the total water budget within the peat which in this case is dominated by groundwater discharge (Fig. 6.31)

Termination of the Longyear seam was dependent upon the locations vulnerability to flooding, with more coastal areas or those

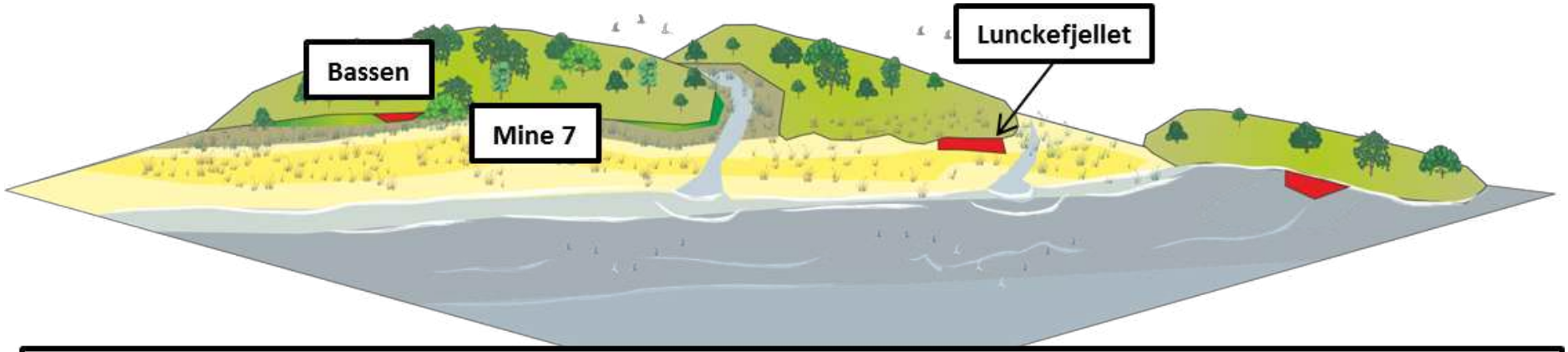

Fig. 6.32 – Palaeogeographic reconstruction of the conditions present immediately after the termination of the Longyear seam.

close to depressions affected sooner than those in the interior. Most areas were covered rapidly by fine-medium sand shore-face facies material (Fig.6.32). During this period at mine 7 titanoid pantodonts of species *Thulitheripus Svalbardii* (Lüthje et al., 2010) walking on the surface of the peat, left footprint impressions which were filled with sand indicating this was land, albeit very wet land, at this time.

At Bassen, the seam is covered by silt, tidal flat facies material, occurring several metres above the seam before replacement with shoreface sands. This suggests that the height of the floodplain was sufficient to allow peat accumulation to continue after the rest of the peatland had been lost, and forcing a more gradual transition to marine conditions.

Once buried the Longyear seam was buried relatively rapidly, with the hydrogen rich plant and microbial material protected within organo-sulfur compounds. At peak burial, early-mid oil window, hydrocarbons were generated and trapped within vitrinites and pore spaces within the coals. The coal was then rapidly uplifted to their present position, before being subjected to significant glacial erosion.

6.8 Conclusions

The Longyear seam represents a coastal peatland with coal quality controlled by the relative position of the coastline and small-scale topography controlled by underlying landscape features. In the

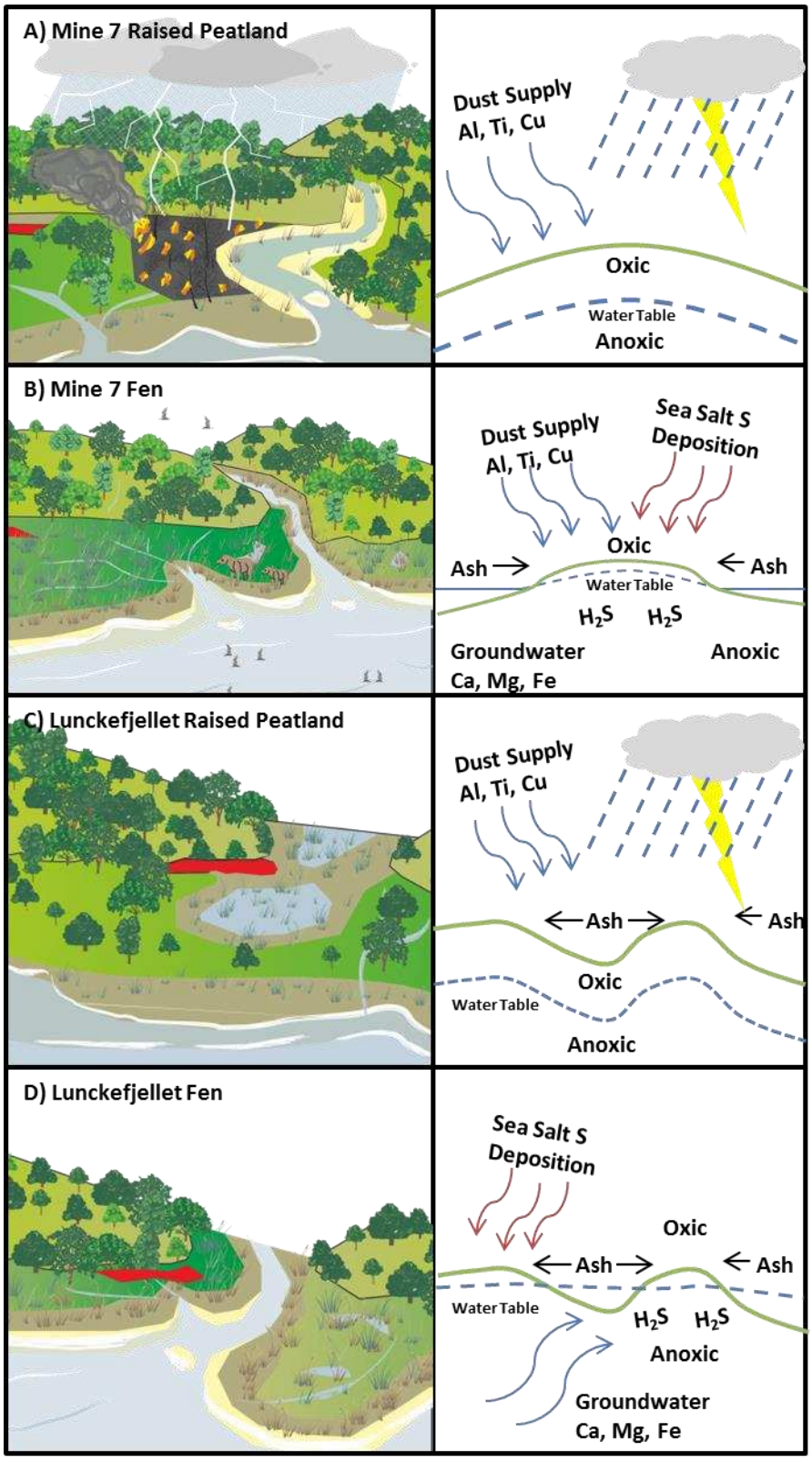

Fig. 6.33- Summary diagram of the major controls on coal quality within the Longyear seam at Mine 7 and Lunckefjellet before and after the raised-bog – fen transition

Mine 7 region the major controls upon coal quality are shown to be (Fig.6.33);

- Precession controlled dust supply of lithophile and heavy metal elements with local sources dominating during dry periods and distal sources during wetter periods associated with strengthening of the hydrological system
- Groundwater supply of Ca, Mg, Fe and Mn to the peatland supplied from underlying shales and later infilling of cleats during early burial/diagenesis within fusinite rich layers
- Supply of S from sea salt sulfur deposition with amount determined by relative distance from inferred coastline.
- Oil potential controlled by degree of hydrological stability and size of bacterial community with later fen conditions more suitable than ombrotrophic peatland

The controls upon coal quality at Lunckefjellet are broadly the same as at Mine 7 (Fig.6.33) however adjacent channels and steeper slope gradient, causes the coastal sulfur gradient to be compressed and clastic sediment supply to be greater than seen at Mine 7

Chapter 7

DEVELOPMENT OF THE SVARTEPER AND ASKELADDEN – PALAEOENVIRONMENT, COAL QUALITY AND FUTURE POTENTIAL

7.1 Introduction

The Svarteper and Askeladden seams which have been hitherto regarded as of too poor quality for large scale exploitation (Major & Nagy, 1972), nevertheless represent a significant coal resource. The coal seams were formed during the last phase of Palaeocene coastal plain sedimentation in the Central Tertiary Basin with peat deposition retreating N-NE to the basin margins (Chapter 3).

Significant increases in the sulfur and ash content in the Svarteper and Askeladden seams (Orheim et al. 2007) indicate a change in the dominant controls upon coal quality during the late Todalen period. The dependence of coal oil potential upon sulfur and marine influence (Chapter 4) indicates that high oil yields may be achieved through Nitrogen Pyrolysis. This suggests that rather than being uneconomic these coals may have significant future economic potential and so require further study.

The objective of this chapter is to briefly examine how the Svarteper and Askeladden peatlands adapted to increasing marine influence and marginal setting, and its effect upon subsequent coal character.

This will be achieved by examining both the organic petrography and inorganic chemistry of the coals.

7.2 – The Svarteper and Askeladden Seams

The Svarteper and Askeladden seams have been the subject of relatively few published works (Nøttvedt, 1985; Harland, 1997; Dallmann et al. 1999; Orheim et al. 2007; Lüthje, 2008) with many limited to descriptions of coal thickness and extent. The bulk coal quality (Ash, S, P, Calorific value, fluidity) of the Svarteper seam has been characterised extensively by SNSK 2002-2013 and Orheim *et al.* (2007) however it was considered of secondary interest compared with the more valuable Longyear and Svea seams.

As shown in Chapter 3 the Svarteper seam is laterally extensive, reaching a thickness in excess of 2m with approximately the same distribution of that seen in the Longyear seam. The Askeladden seam, which is in some places indistinguishable from the Svarteper seam, while in others it is separated by as much as 10m of sediments (Nøttvedt, 1985). The focus of peatland formation shifted northward in the Askeladden seam, accompanied by an increased variability of thickness (0.3m to almost 3m).

Nøttvedt (1985) favours a deltaic origin for the post Longyear Todalen member with the Svarteper and Askeladden seams representing delta plain sedimentation. Nottvedt (1985) also noted that the flood plain was dissected by a number of fluvial/tidal

channels, and due to its more marginal setting was frequently flooded. This vulnerability to marine influence is used to explain the coal quality issues within this seam.

7.3 – Coal Quality within the Svarteper and Askeladden Seams

The primary coal quality parameters affecting the value of the Svarteper and Askeladden seams in BH5/2009 & BH15/2011 (Table 7.1) are:

- Calorific value
- Oil potential/coking potential
- Ash content
- Sulfur content

As high volatile bituminous coals the calorific value of the Svarteper and Askeladden seams ranges from 6200-7100 kcal/kg with values reflecting the varying ash content. The coals also have been shown to have significant oil potential (Chapter 4), with high fluidity values indicating potential as a coking coal. However, the economic potential of these coals is limited by ash, and particularly sulfur content. Unlike, the Svea seam, the phosphorus content is not considered a problem in these coals, and is often below detection limits in these coals (<100ppm).

Location	Borehole	Sample no	Seam	Depth (m)	Ash (%)	Sulfur (%)	Eff.b.v.kcal/kg	FSI
Breinosa	BH5/2009	10313	Askeladden	-295.725	7.5	4.3	7706.0	8.5
Breinosa	BH52009	10314	Askeladden	-295.95	31.6	6.3	5444.0	4.5
Breinosa	BH52009	10316	Askeladden	-296.39	18.1	5.6	6795.0	6.0
Breinosa	BH52009	10315	Askeladden	-296.445	13.7	6.1	7163.0	9.0
Breinosa	BH52009	10307	Svarteper	-300.215	17.5	6.3	6872.0	7.5
Breinosa	BH52009	10308	Svarteper	-300.425	16.3	5.7	6992.0	6.0
Breinosa	BH52009	10309	Svarteper	-300.63	24.0	6.2	6263.0	3.0
Breinosa	BH52009	10310	Svarteper	-300.855	75.0	5.5	1285.0	1.0
Breinosa	BH52009	10311	Svarteper	-301.095	57.2	9.1	2928.0	1.0
Breinosa	BH52009	10312	Svarteper	-301.285	13.9	8.3	7089.0	9.0
Lunckefjellet	BH15/2011	10317	Svarteper	-246	23.1	8.1	6058.0	4.5
Lunckefjellet	BH15/2011	10319	Svarteper	-246.2	25.7	5.9	5845.0	4.5
Lunckefjellet	BH15/2011	10321	Svarteper	-246.4	21.1	7.9	6318.0	4.5
Lunckefjellet	BH15/2011	10323	Svarteper	246.6	21.4	8.4	6271.0	4.5

Table 7.1 – SNSK Core Data from BH5/2009 (Breinosa Region) and BH15/2011 (Lunckefjellet Region) for the Svarteper and Askeladden Seams

Location	Breinosa	Breinosa	Breinosa	Breinosa	Breinosa	Breinosa	Breinosa	Breinosa	Breinosa	Breinosa
Borehole	BH5/2009	BH5/2010	BH5/2011	BH5/2012	BH5/2013	BH5/2014	BH5/2015	BH5/2016	BH5/2017	BH5/2018
Sample no	10313	10314	10316	10315	10307	10308	10309	10310	10311	10312
Seam	Askeladden	Askeladden	Askeladden	Askeladden	Svarteper	Svarteper	Svarteper	Svarteper	Svarteper	Svarteper
Depth (m)	-295.725	-295.95	-296.39	-296.445	-300.215	-300.425	-300.63	-300.855	-301.095	-301.285
Al_20_3	3.1	0.8	5.4	1.2	2.1	2.5	4.8	9.9	8.8	0.7
CaO	0.82	0.42	0.92	1.84	0.64	0.71	0.47	2.21	0.36	0.55
FeO	4.6	3.3	6.6	5.3	5.5	4.1	5.2	6.3	11.5	8.2
K_2O	0.309	0.070	0.735	0.099	0.213	0.250	0.582	1.936	1.244	0.050
MgO	0.30	0.09	0.38	0.29	0.25	0.33	0.38	0.58	0.51	0.22
MnO_2	0.006	0.003	0.011	0.005	0.005	0.005	0.006	0.016	0.012	0.005
Na2O	0.53	0.20	0.52	0.43	0.39	0.49	0.52	0.94	0.77	0.25
SO_3	12.6	9.7	15.1	14.4	14.7	13.0	14.8	12.2	23.4	18.9
TiO_2	0.17	0.06	0.30	0.07	0.16	0.13	0.25	0.78	0.54	0.04
Ba	272	488	619	326	387	509	728	721	362	312
Co	2	7	4	2	4	4	5	12	8	2
Cr	22	35	26	17	22	27	29	86	60	19
Cu	4	11	10	2	11	13	19	27	34	1
Li	5	46	29	7	22	21	13	132	71	3
Ni	9	20	17	9	15	19	21	37	25	8
Pb	4	11	8	4	6	6	8	18	14	5
Rb	6	39	17	7	13	17	38	54	71	4
Sb	34	33	33	33	31	31	16	29	31	32
Sc	3	4	3	1	4	4	6	8	7	2
Sr	490	985	1026	512	658	587	431	678	323	529
U	-	41	8	-	21	-	217	59	120	44
V	115	58	33	10	38	49	67	184	117	43
Zn	10	48	31	11	23	35	39	72	64	16
Zr	42	67	79	12	25	31	39	118	83	32

Table 7.2 – Major and Minor elemental composition of the Svarteper and Askeladden Seams from BH5/2009 (Breinosa)

(Al_2O_3 – TiO_2 = Oxide wt%, Ba-Zr ppm)

Sample ID	10317	10318	10319	10320	10322	10323	10324	10325
Location	Lunckefjellet	Lunckefjellet	Lunckefjellet	Lunckefjellet	Lunckefjellet	Lunckefjellet	Lunckefjellet	Lunckefjellet
Seam	Svarteper	Svarteper	Svarteper	Svarteper	Svarteper	Svarteper	Svarteper	Svarteper
Depth	-246.00	-246.10	-246.20	-246.30	-246.40	-246.50	-246.60	-246.70
Al_2O_3	8.35	5.84	4.04	2.81	0.38	0.83	0.98	0.50
CaO	0.08	0.31	0.73	0.69	1.43	1.36	1.31	6.05
FeO	5.60	7.46	2.70	6.00	4.45	7.02	4.95	10.79
K_2O	1.47	0.71	0.47	0.29	0.01	0.07	0.06	0.03
MgO	0.60	0.34	0.34	0.27	0.26	0.24	0.26	0.31
MnO	0.02	0.02	0.01	0.01	0.01	0.01	0.01	0.21
Na_2O	0.02	0.02	0.01	0.01	0.01	0.01	0.01	0.21
PO_3	0.04	0.05	0.05	0.06	-	-	-	-
SO_3	11.87	17.23	9.15	15.36	12.58	16.95	13.96	23.50
TiO_2	0.56	0.30	0.22	0.14	0.06	0.08	0.07	0.03

Table 7.3 - Major elemental composition (oxide wt%) of the Svarteper Seam at BH15/2011 (Lunckefjellet)

A detailed examination of the inorganic composition of the coals (Table 7.2(a), 7.2(b)) shows that the coals are dominated by Fe/S species and lithophile elements (Al, Ti, Na, K) at both locations. When correlated against each other (Table 7.4) for both locations, a number of elemental relationships within the coals. These include;

- Fe and S species
- The lithophile elements (Al, Ti, Mg, Mn, Na, K and to a lesser extent Fe)
- Ca minerals
- Metals (Ba, Pb, Ni, Cu, Zn, Co, Li, Sc, Rb)

The relationship between Fe and S can be attributed to the presence of Fe sulphide minerals primarily pyrite (FeS_2). The lithophile elements are thought to represent predominantly clastic material, with the metals group representing a combination of heavy mineral deposition and possibly enrichment within organic materials. The Ca minerals are likely to have formed from a groundwater source.

Unlike, the Longyear and Svea seams, the non-correlation between Cu and the lithophile elements indicates that dust was not a significant input of mineral matter into the Svarteper and Askeladden seams.

	Al	*Ca*	*Fe*	*K*	*Mg*	*Mn*	*Na*	*S*	*Ti*	*Ba*	*Co*	*Cr*	*Cu*	*Li*	*Ni*	*Pb*	*Rb*	*Sb*	*Sc*	*Sr*	*U*	*V*	*Zn*
Ca	0.27																						
Fe	0.73	-0.04																					
K	0.97	0.43	0.61																				
Mg	0.93	0.45	0.68	0.89																			
Mn	0.95	0.48	0.66	0.96	0.92																		
Na	0.94	0.47	0.63	0.93	0.97	0.92																	
S	0.51	-0.26	0.93	0.34	0.51	0.40	0.43																
Ti	0.97	0.40	0.63	1.00	0.89	0.95	0.94	0.36															
Ba	-0.10	-0.41	-0.28	-0.13	-0.19	-0.18	-0.26	-0.16	-0.16														
Co	0.17	-0.05	-0.30	0.23	0.08	0.05	0.05	-0.35	0.20	0.62													
Cr	0.33	0.09	-0.16	0.36	0.29	0.21	0.26	-0.22	0.33	0.47	0.95												
Cu	0.40	0.28	-0.24	0.51	0.35	0.36	0.38	-0.38	0.49	0.47	0.85	0.83											
Li	0.22	0.04	-0.19	0.25	0.18	0.12	0.12	-0.24	0.22	0.49	0.95	0.98	0.76										
Ni	0.16	-0.06	-0.31	0.20	0.11	0.06	0.06	-0.32	0.17	0.72	0.98	0.93	0.86	0.93									
Pb	0.33	0.04	-0.15	0.39	0.21	0.23	0.19	-0.26	0.36	0.54	0.97	0.96	0.85	0.95	0.94								
Rb	0.36	0.27	-0.25	0.49	0.24	0.31	0.29	-0.42	0.46	0.44	0.88	0.84	0.95	0.78	0.84	0.91							
Sb	0.00	0.27	0.10	-0.02	0.09	0.10	0.02	-0.01	-0.03	-0.61	-0.23	-0.10	-0.36	0.00	-0.31	-0.15	-0.31						
Sc	0.33	0.04	-0.23	0.40	0.25	0.22	0.28	-0.30	0.38	0.56	0.92	0.91	0.94	0.84	0.92	0.89	0.90	-0.43					
Sr	-0.36	-0.41	-0.19	-0.41	-0.49	-0.31	-0.61	-0.17	-0.44	0.34	0.09	-0.04	-0.23	0.13	0.09	0.11	-0.14	0.35	-0.20				
U	0.12	0.15	-0.19	0.21	0.08	0.06	0.22	-0.18	0.21	0.36	0.19	0.12	0.48	-0.06	0.24	0.14	0.48	-0.89	0.48	-0.68			
V	0.31	-0.05	-0.16	0.30	0.26	0.14	0.29	-0.20	0.29	0.29	0.76	0.86	0.65	0.79	0.72	0.74	0.64	-0.11	0.82	-0.22	0.23		
Zn	0.29	0.05	-0.25	0.37	0.18	0.20	0.17	-0.36	0.34	0.59	0.97	0.91	0.91	0.90	0.95	0.97	0.94	-0.23	0.90	0.07	0.27	0.67	
Zr	0.37	-0.01	-0.09	0.38	0.25	0.30	0.20	-0.22	0.34	0.53	0.85	0.88	0.70	0.89	0.83	0.91	0.74	0.03	0.77	0.30	-0.10	0.75	0.84

Table 7.4 – Correlation Matrix between major and minor elements within the Svarteper and Askeladden Seams, BH5/2009

The maceral composition (Table 7.5 & 7.6) of the Svarteper and Askeladden seams is similar to that of the upper Longyear Seam with high vitrinite content ( ) and low inertinite content ( ) and those reported by Orheim et al. (2007). Liptinite values are elevated compared to those reported, but this may be due to the higher magnification used in this study. In addition, liptinite concentrations appear to be related to ash content with liptinite dominated by sporinite.

7.4 – Palaeo-environmental Development of the Svarteper Seam

The Svarteper seam formed upon reduced coastal plain compared to the Longyear with deposition focussed in the NE CTB (Chapter 3). From the reconstructions it is thought, the Lunckefjellet borehole (BH15/2011) was situated further inland than that at Breinosa (BH5/2009) and therefore should be subject to less marine influence. The Breinosa core also appears to be situated on a peninsula of peatland bordering an estuary/tidal channel to the east and an embayment to the west (Chapter 3, Fig. 3.20;3.21).

Both cores contain approximately the same thickness of coal (70-80cm), however in the Breinosa region the Svarteper seam is split by 30cm of clastic sedimentation. This demonstrates the relative vulnerability of the seam at this location to inundation by storm events, rises in sea level and flooding events.

Location	Breinosa	Breinosa	Breinosa	Breinosa	Breinosa	Breinosa	Lunckefjellet	Lunckefjellet	Lunckefjellet	Lunckefjellet	Lunckefjellet	Lunckefjellet	Lunckefjellet	Lunckefjellet
Borehole	BH5/2009	BH5/2009	BH5/2009	BH5/2009	BH5/2009	BH5/2009	BH15/2011	BH15/2011	BH15/2011	BH15/2011	BH15/2011	BH15/2011	BH15/2011	BH15/2011
Sample no	10307	10308	10309	10310	10311	10312	10317	10318	10319	10320	10322	10323	10324	10325
Seam	Svarteper	Svarteper	Svarteper	Svarteper	Svarteper	Svarteper	Svarteper	Svarteper	Svarteper	Svarteper	Svarteper	Svarteper	Svarteper	Svarteper
Depth (m)	-300.215	-300.425	-300.63	-300.855	-301.095	-301.285	-246	-246.1	-246.2	-246.3	-246.4	-246.5	-246.6	-246.7
Collotelinite	71.7	67.6	29.2	-	5.6	26.8	50.8	35.6	56.8	54.4	19.6	10	31.2	61.2
Detrovitrinite	2.7	8.8	30	3.2	22.8	46.4	12.4	12.4	6.8	11.6	54.4	58	34	13.6
Fusinite	2.3	0.4	0.4	5.2	1.6	2.4	1.2	-	-	-	1.6	0.4	0.8	-
Semifusinite	3.4	2	0.4	-	-	2.4	2.4	0.4	0.8	0.8	1.2	-	2.4	1.6
Funginite	-	-	-	-	-	0.8	1.2	0.4	0.8	1.6	1.2	0.8	2.8	3.2
Inertodetrinite	-	-	7.2	-	-	0	-	-	-	1.6	-	-	-	1.2
Sporinite	5.4	5.6	4	11.2	-	0.4	3.6	6.8	6.4	3.2	2.8	6.4	4	2.8
Liptodetrinite	-	-	7.2	-	-	-	0.4	0.8	0.4	-	-	-	0.4	0
Cutinite	5.2	6.8	8.4	7.6	8.8	5.2	5.6	-	-	3.6	8.4	10.8	6.8	2
Minerals	9.2	8.8	13.2	65.2	50	15.6	23.2	43.6	28	23.2	10.8	13.6	17.6	14.4
Total Vitrinite	74.4	76.4	59.2	3.2	28.4	73.2	63.2	48.0	63.6	66.0	74.0	68.0	65.2	74.8
Total Telovitrinite	71.7	67.6	29.2	0.0	5.6	26.8	50.8	35.6	56.8	54.4	19.6	10.0	31.2	61.2
Total Detrovitrinite	2.7	8.8	30.0	3.2	22.8	46.4	12.4	12.4	6.8	11.6	54.4	58.0	34.0	13.6
Total Inertinite	5.7	2.4	8.0	5.2	1.6	5.6	4.8	0.8	1.6	4.0	4.0	1.2	6.0	6.0
Total Liptinite	10.6	12.4	19.6	26.0	20.0	5.6	9.6	7.6	6.8	6.8	11.2	17.2	11.2	4.8
Total Mineral	9.2	8.8	13.2	65.2	50.0	15.6	23.2	43.6	28.0	23.2	10.8	13.6	17.6	14.4
V/I	13.1	31.8	7.4	0.6	17.8	13.1	13.2	60.0	39.8	16.5	18.5	56.7	10.9	12.5
TPI	55.2	15.6	1.6	1.6	0.6	1.3	8.5	5.8	16.8	8.3	0.8	0.4	1.9	8.4
GI	13.1	31.8	7.4	0.6	17.8	13.1	13.2	60.0	39.8	16.5	18.5	56.7	10.9	12.5

Table 7.5 – Maceral Composition of the Svarteper seams at BH5/2009 (Breinosa) andBH15/2011 (Lunckefjellet), Point Count (500 counts, 50x lens) ***TPI = Tissue Preservation Index, GI = Gelification Index, V/I = Vitrinite/Inertinite (see Chapter 2 for calculations)***

Location	Breinosa	Breinosa	Breinosa	Breinosa
Borehole	BH5/2009	BH5/2010	BH5/2011	BH5/2012
Sample no	10313	10314	10316	10315
Seam	Askeladden	Askeladden	Askeladden	Askeladden
Depth (m)	-295.725	-295.95	-296.39	-296.445
Collotelinite	20.2	23.4	19.6	12.8
Detrovitrinite	38.2	40.2	35.2	44.4
Fusinite	3.8	2.4	3.2	2
Semifusinite	2.2	3.2	2	1.2
Funginite	1.2	0.8	0.8	0.8
Inertodetrinite	-	-	0.4	0.8
Sporinite	2	2	3.2	4.2
Liptodetrinite	2	1.2	3	2.2
Cutinite	2	1.5	2.3	2.7
Minerals	28.4	25.3	30.3	28.9
Total Vitrinite	58.4	63.6	54.8	57.2
Total Telovitrinite	20.2	23.4	19.6	12.8
Total Detrovitrinite	38.2	40.2	35.2	44.4
Total Inertinite	7.2	6.4	6	4
Total Liptinite	6	4.7	8.5	9.1
Total Mineral	28.4	25.3	30.3	28.9
V/I	8.1	9.9	9.1	14.3
TPI	0.69	0.72	0.70	0.36
GI	8.1	9.9	9.1	14.3

Table 7.6 – Maceral Composition of the Askeladden seam at BH5/2009 (Breinosa), Point Count (500 counts, 50x lens) *TPI = Tissue Preservation Index, GI = Gelification Index, V/I = Vitrinite/Inertinite (see Chapter 2 for calculations)*

Comparison of the vertical maceral profile of the two locations (Fig. 7.1) shows that both begin with increased inertinite concentrations (5%) dropping rapidly to around (1%) after 20cm. This fall in inertinite is accompanied by an increase in liptinite (mainly sporinites) and a rise in ash content.

At 30cm the Breinosa seam splits, leading to a decrease in organic maceral content and a decrease in woody material (vitrinites). Conversely in the Lunckefjellet region ash content of the seam remains constant (Fig. 7.2) and the maceral composition of the peatland became dominated by detrovitrinite (~60%) and sporinite (~15%).

After splitting at Breinosa, the inertinite contents at both localities increase (~6-8%) before rapidly decreasing again to ~1% at around 20cm below the top of the seam. This is then followed by an increase in inertinite content (~5%) and the termination of the seam.

Observed Mineral Matter (Fig. 7.2) gradually increases up seam at Lunckefjellet whereas as ash content peaks during split formation before falling back to pre-split levels at Breinosa.

7.42 – Hydrological Controls upon the Svarteper Seam

Examination of TPI and GI (Chapter 2 for methods; Diessel and Gammidge, 1998) allows examination of wetness of peatland and degree of preservation of organic matter/tree density (Fig.7.2). TPI

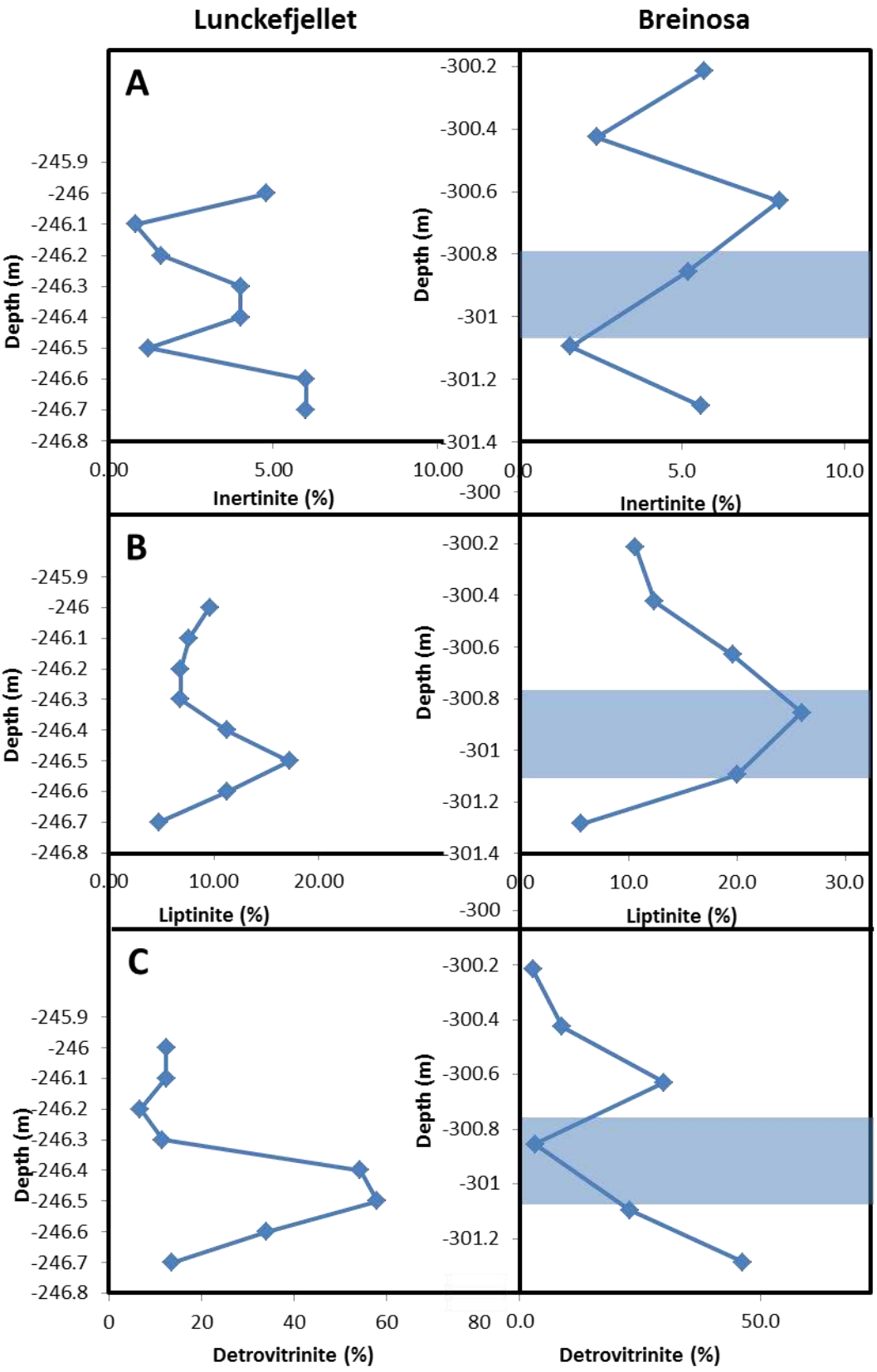

Figure 7.1 – Vertical maceral profile for the Lunckefjellet and Breinosa Svarteper (A) Inertinite (%) (B) Liptinite (%) (C) Detrovitrinite (%) *Blue Box - split*

shows that tissue preservation/tree density was low at both locations; however tree density/preservation increased towards the end of the Svarteper seam at Breinosa. This is associated with drier conditions (higher more variable maceral content), and may represent the replacement/colonisation of the peatland by forest in response to higher clastic supply.

The generally high GI values for the Svarteper seams indicate a significant groundwater input to the peatland, with conditions similar to modern day coastal fens. In this respect peatland conditions are thought to be similar to those seen within more coastal parts of the Longyear seam.

In the Lunckefjellet region, GI indicates that the peatland became wetter at around the same period as splitting in the Breinosa region. This indicates that there was a basin wide flooding event at around 30cm above seam base, probably associated with increased water tables. The Lunckefjellet core being in a less vulnerable position than that at Breinosa was not completely flooded at this time, but the effect of higher sea levels are reflected by raised groundwater levels, leading to more reducing conditions in the peatland.

When sea level fell, groundwater supply also reduced leading to drier peat conditions (greater oxidation), as shown by an increase in inertinite post-split in both areas. This was followed by a period of

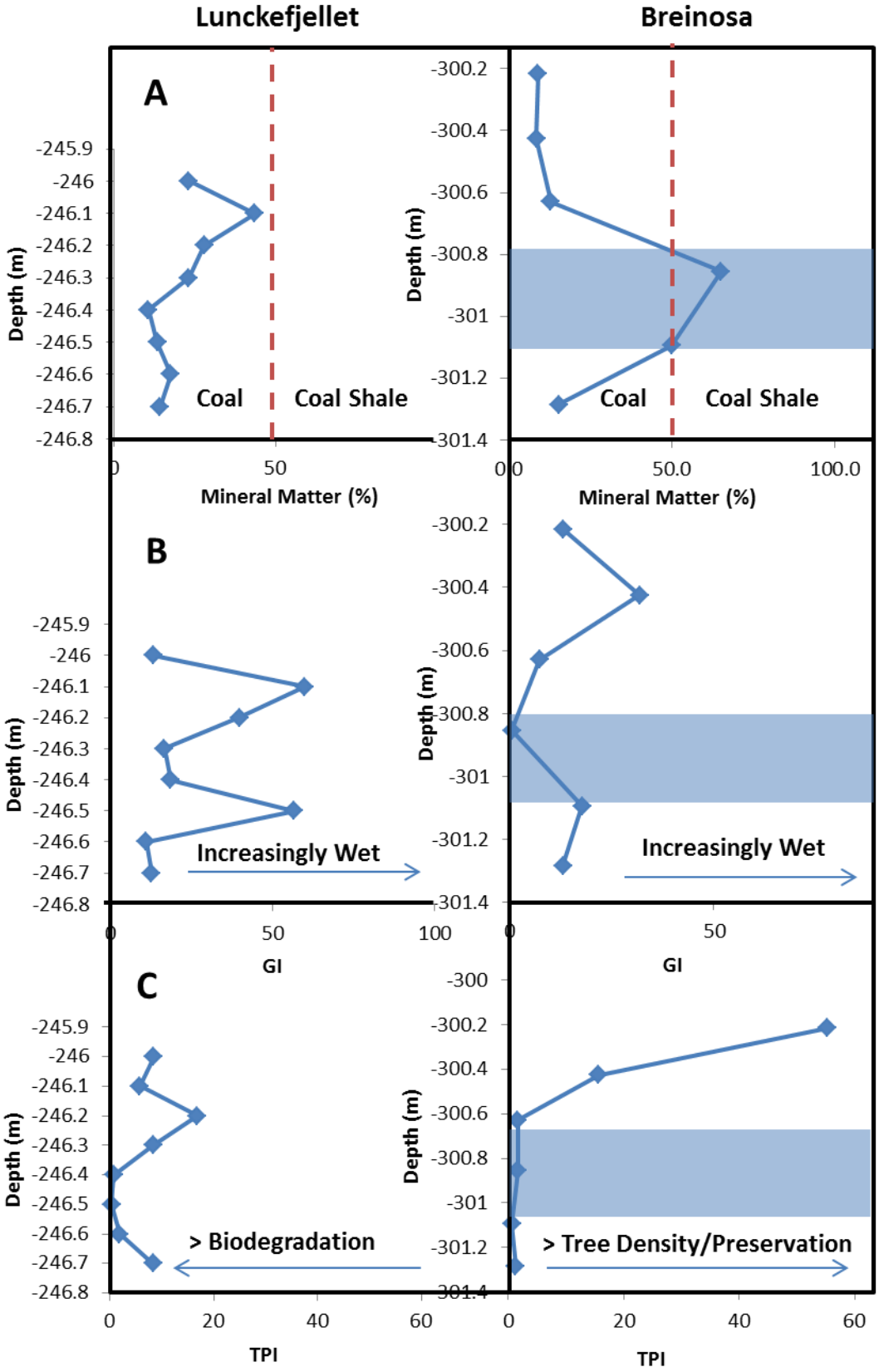

Figure 7.2 – Vertical maceral profile for the Lunckefjellet and Breinosa cores (A) Mineral Matter (%) (B) GI (Gelification Index; see chapter 2) (C) TPI (Tissue Preservation Index; see chapter 2)
Blue Box - split

higher groundwater supply conditions before replacement by clastic marsh/floodplain material.

The apparent periodicity of the dry/wet cycles (~2.5 cycles/m) may indicate that relative sea level was controlled by precessional (~20kyr) orbital cycles as seen in the Longyear seam. It is in these wetter periods that the greatest oil potential is seen (Chapter 4). Consequently, further study of the observed cyclicity may prove useful in the prediction of oil potential within these seams.

The maceral evidence from the Svarteper seam supports the conclusions by Nøttvedt, (1985) that the peatland was vulnerable to flooding due to the thin nature of the coastal plain and high marine influence. It also does not preclude the possibility that by this period the coastal plain had a more deltaic character (Nøttvedt, 1985), with indications of a number of possible channel deposits within the palaeogeographic reconstructions (Chapter 3).

7.4.3 Controls upon inorganic species within the Svarteper Seam.

Ombrotrophic peatlands receive the majority of their inorganic species from dust whereas rheotrophic peatlands are significantly influenced by ground and surface waters (Shotyk, 1996). To examine the provenance and major controls upon the elemental groups previously identified (Section 7.3) a number of geochemical

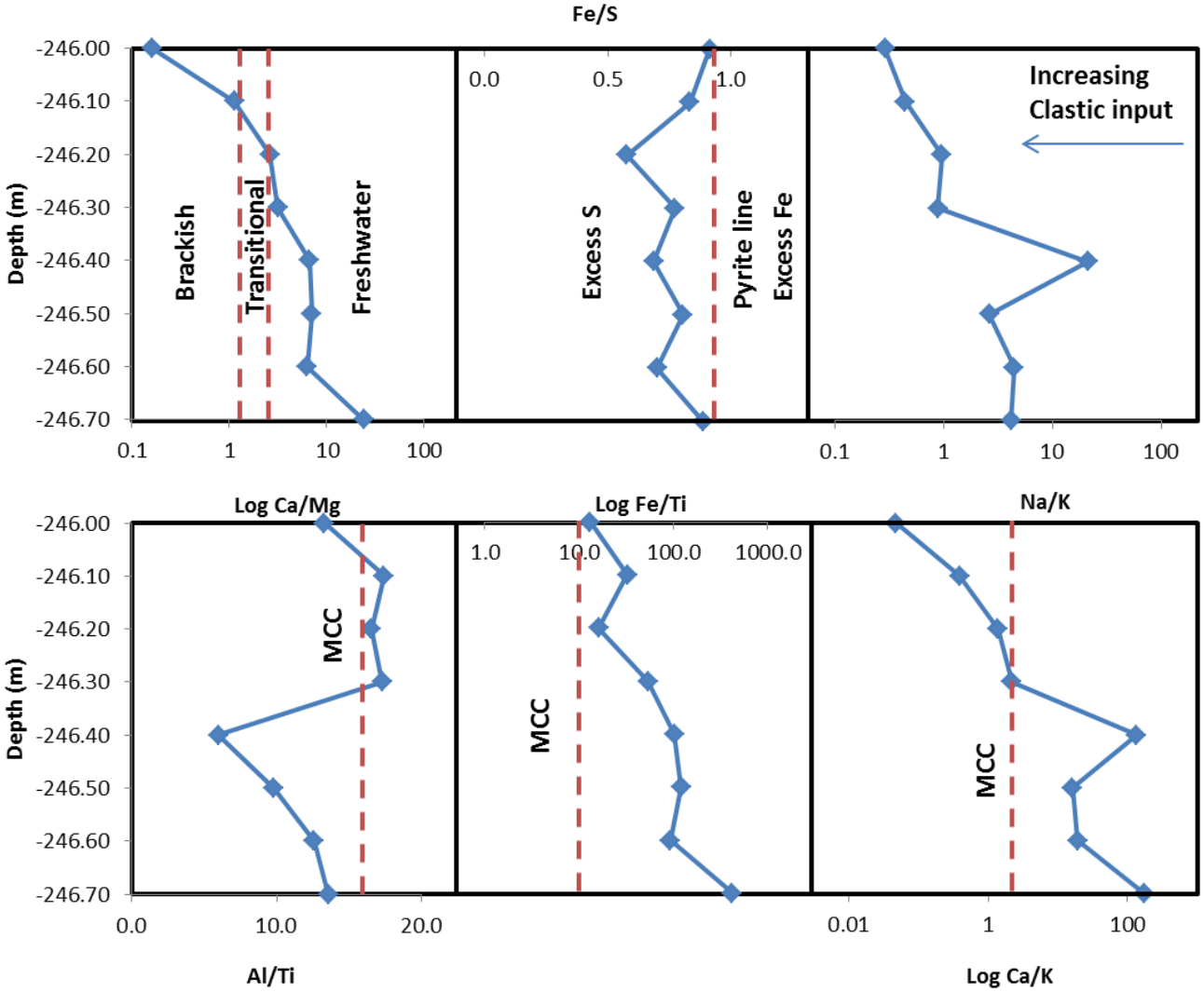

Fig. 7.3 – Geochemical Parameters from BH15-2011 (Lunckefjellet) ***Top Row (left-right) – Ca/Mg (Water Compositions Berner and Berner, 1997) , Fe/S , Na/K Bottom Row – Al/Ti, Fe/Ti, Ca/K (MCC values Rudnick and Gao, 2003)***

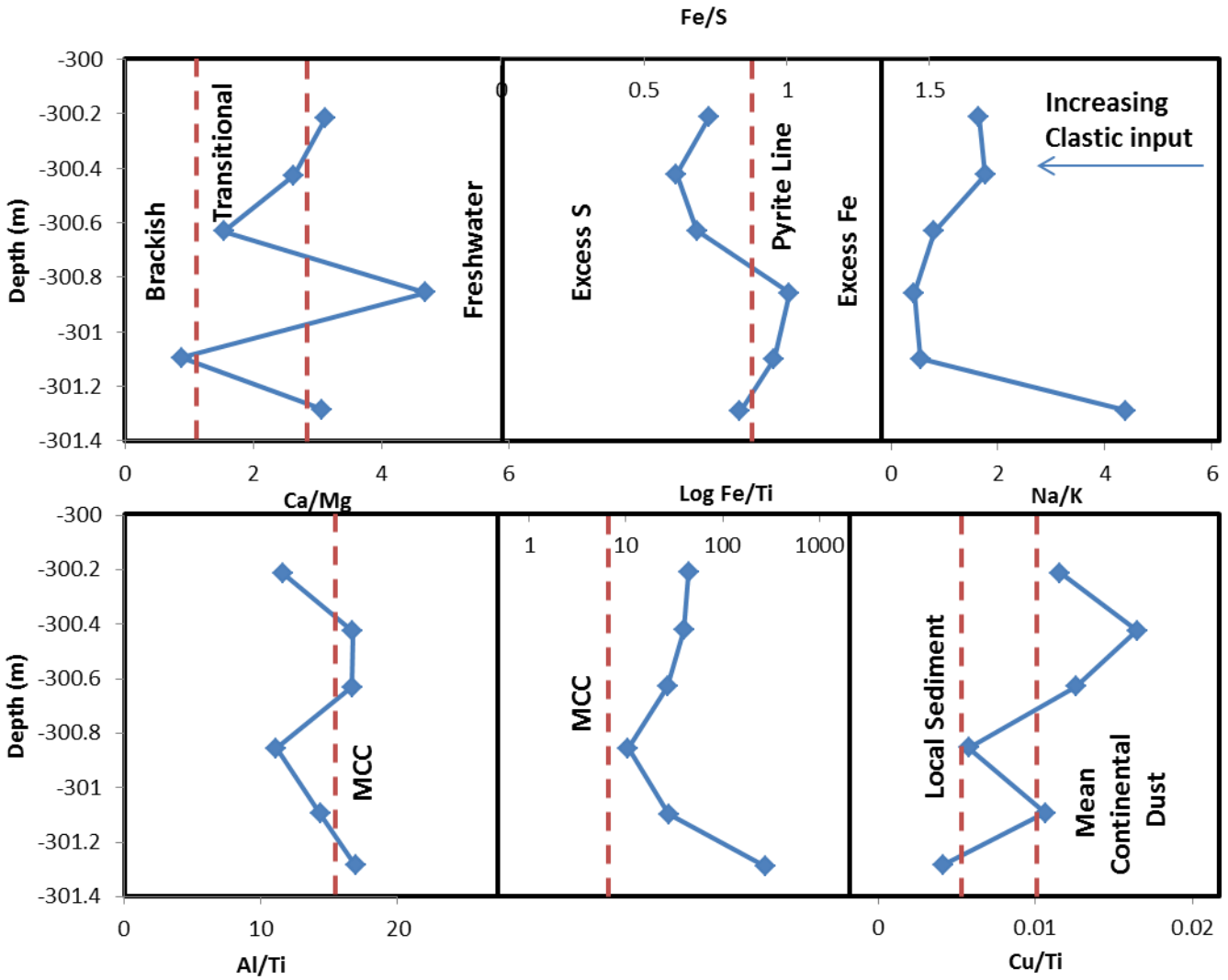

Fig. 7.4 – Geochemical Parameters from BH5-2009 (Breinosa) Svarteper Seam *Top Row (left-right) – Ca/Mg (Water Compositions Berner and Berner, 1997) , Fe/S , Na/K Bottom Row – Al/Ti, Fe/Ti, Cu/Ti (MCC values Rudnick and Gao, 2003)*

parameters (Fig.7.3 & 7.4) were normalised to Ti and compared to mean continental crust (MCC; Rudnick & Gao, 2003).

At both the Breinosa and Lunckefjellet the coals are significantly enriched in iron compared to MCC values (~9). At the split (Breinosa) values approach MCC values indicating that the clastic sediment supplied to the peatland was of average composition. A likely source for the excess iron could be remobilisation of Fe from the underlying Carolinefjellet shales by groundwater. This has also been observed in the Svea (Chapter 5) and Longyear (Chapter 6) seams.

In the Lunckefjellet region the Fe/Ti ratio slowly decreases to mean values representing that the groundwater control upon Fe is gradually reduced and replaced by a dominantly clastic sediment control. In the Breinosa region, post splitting the groundwater control remains a significant control upon iron up until the termination of the seam. This is probably due to a wider coastal plain at this location and large catchment to the NE.

The Al/Ti ratio remains around MCC values in both seams indicating that Al and the other lithophile elements (Al, Ti, Na, K) are primarily controlled by clastic sediment with average composition. This is unlike the Svea and Longyear seams whose lithophile element profiles are primarily controlled by dust variations. This is supported by the fact that copper and lithophile

elements do not correlate in the Svarteper seam, whereas in the Longyear seam and Svea seam they are closely related to dust input.

During splitting at Breinosa, Al concentrations drop in both seams relative to Ti. This coincides with increased inertinite concentrations and an inferred drop in the water table. Acidification of peat pore waters would remobilise Al leaching and transporting from the peatland. This may represent a brief period of palaeosol formation within the peatland.

The Na/K ratio (Fig.7.3 & 7.4) has also been inferred as a proxy for clastic sediment supply in coals (Weimer and Land, 1975). In the Svarteper coals Na/K reduces from seam base to seam termination indicating increasing clastic supply to the peatland. This fits with reports by Nøttvedt (1985) of the seams vulnerability to inundation and wash over.

The Ca/Mg ratio (Fig.7.3 & 7.4) should reflect the provenance of peat pore waters with Ca enriched in continental/groundwater conditions and Mg in seawater (Berner and Berner, 1997). The decreasing influence of groundwater on peatland is again seen in the Lunckefjellet region with values becoming increasingly marine.

Groundwater supply to the more northerly Breinosa region appears to have remained relatively constant during the formation of the Svarteper seam, as shown by the relatively constant Ca, Fe and Mn . The split in this region was initiated by flooding by marine waters.

Once sea-levels dropped this was followed by a pulse of freshwater as groundwater occupied the previously flooded coastal plain.

Marine influence upon the coastal plain increased from the Longyear coals to the Svarteper coals. The Svarteper peatland also became increasingly marine up-seam as shown by increasing sulfur, reflecting a gradual increase in sea level. Sulfur supply from seawater and thin coastal plain ensured that unlike the Longyear seam, the entire Svarteper seam was enriched in sulfur compared to iron. This 'free' sulfur was then available to produce organo-sulfur molecules and bind hydrogen rich material (Chapter 4) and increasing the seams oil potential.

7.5 The Askeladden seam

A short period after the termination of the Svarteper Seam, the Askeladden seam built from the northernmost part of the basin (likely Bassen region) towards the SW. The coastal plain at this period was significantly narrower than previously with no deposition of Askeladden seam within the BH15-2011 core (Lunckefjellet).

The inorganic elemental composition (Table 7.2, Fig. 7.5) of the Askeladden seam at Breinosa (BH5/2009) is very similar to that of upper Svarteper seam (fig 7.5) with various parameters (Al/Ti, Fe/Ti, Na/K, Cu/Ti) indicating significant local clastic supply, and significant marine influence (Fe/S, Ca/Mg). This is supported by the

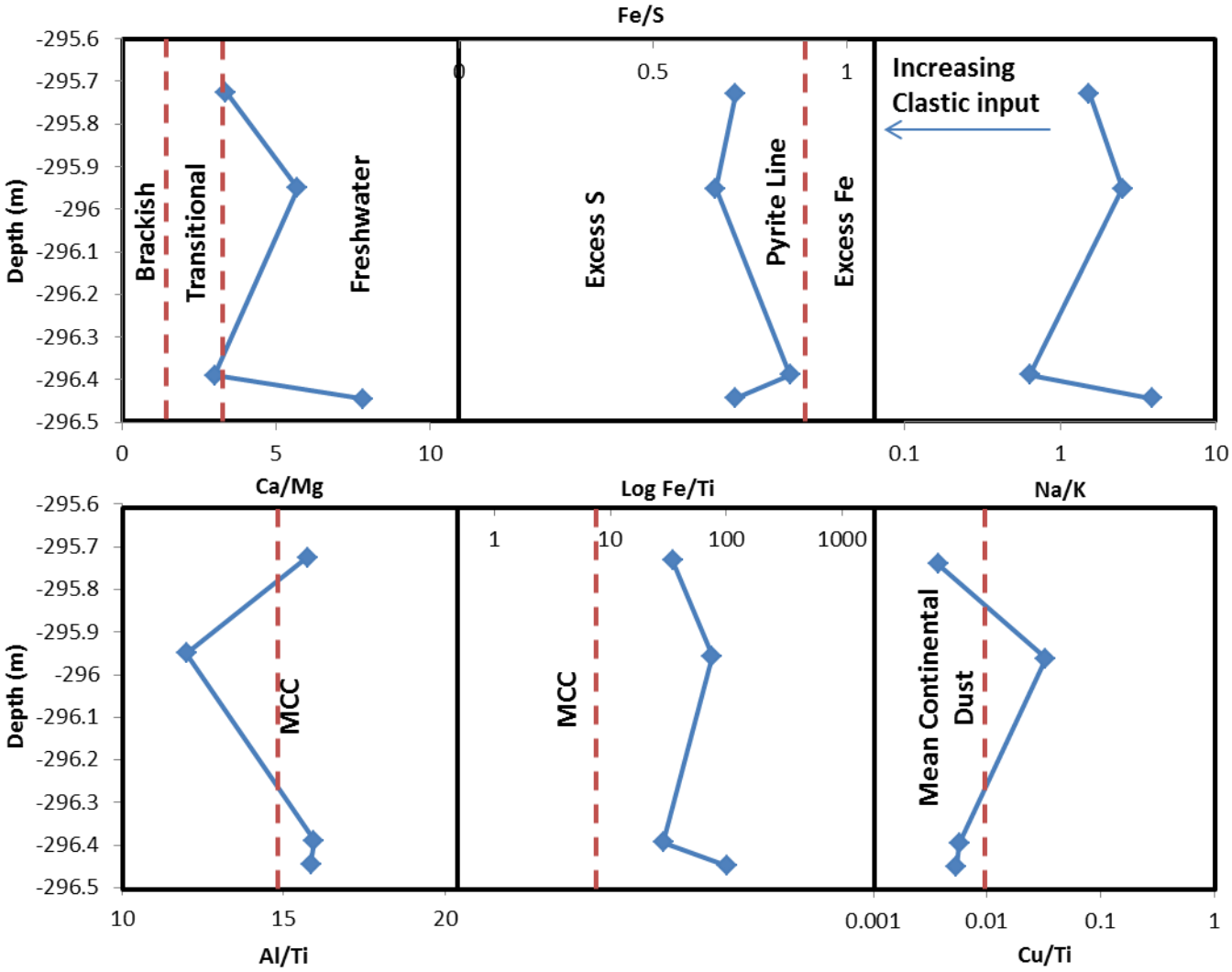

Fig. 7.5 – Geochemical Parameters from BH5-2009 (Breinosa) Askeladden Seam *Top Row (left-right) – Ca/Mg (Water Compositions Berner and Berner, 1997) , Fe/S , Na/K Bottom Row – Al/Ti, Fe/Ti, Cu/Ti (MCC values Rudnick and Gao, 2003)*

high ash and sulfur contents reported by SNSK for this core (Table.7.1).

Low GI and TPI values (Table 7.6) from the Askeladden seam supports formation in a clastic marsh environment. This is accompanied by observations of significant framboidal pyrite and dispersed mineral matter throughout the coal indicating flow of clastic material through the peatland during this period.

Consequently, the Askeladden represents the most marginal of peatland environments within the Todalen member which was vulnerable to flooding, leading to the coal quality issues identified (Section 7.3) and its sporadic occurrence and thickness.

7. Conclusions

The Svarteper and Askeladden seams represent a transition from a rheotrophic fen to clastic marsh/flat conditions. The seams were vulnerable to inundation with higher slope gradients to the N and NE preventing retreat, forcing peat formation to be limited to the thin coastal plain. The proximity to steeper slopes also meant that sediment was washed over the peatland in high rainfall events. Due to the thin coastal plain marine influence would be expected to be high across the peatland with the lowest sulfur coals restricted to the Bassen region, due to its position away from the coastline. The

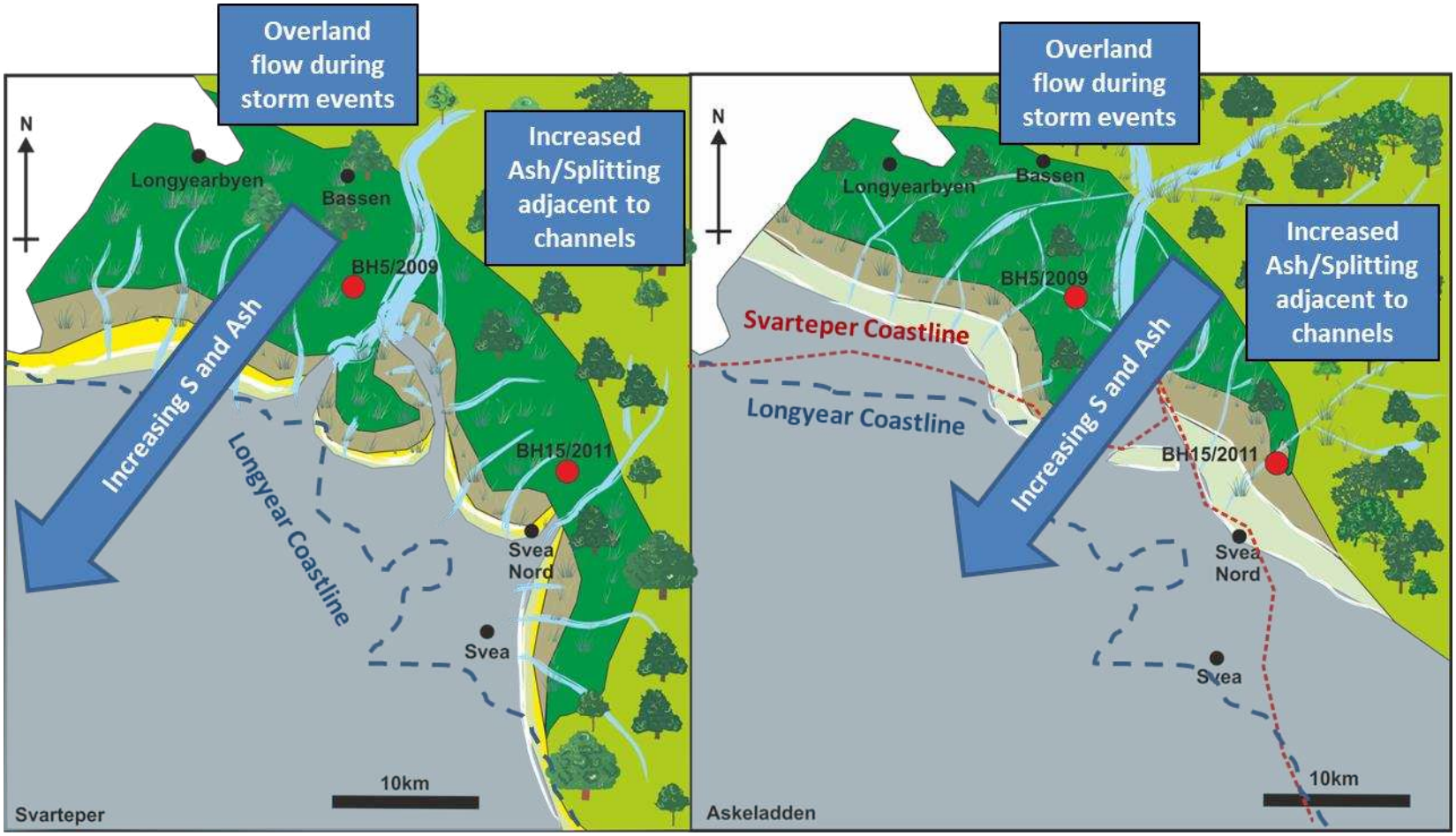

Fig. 7.6 – Summary diagram showing the main sources of Ash and sulfur from the Svarteper and Askeladden Seams alongside a demonstration of increasing marine influence from the deposition of the Longyear seam to the Svarteper/Askeladden area. The primary controls are S from seawater, Ash from marine and fluval flooding events and Fe/Ca from groundwater. Highest quality and thickest coal would be expected in the Bassen area for both seams due to its relatively sheltered position at the NE edge of the coastal plain. N.B the rapid northeasterly retreat of peatland from the Longyear to Svarteper Askeladden period represent the final infilling of the underlying palaeotopography

extent and sulfur enrichment of the Svarteper peatland would make it a particular target for in-situ/ex-situ extraction of oil.

The summary diagram (Fig. 7.6) shows that the best coal quality and thickest seams would be expected in the Bassen region, due to its relatively inland location, and favourable conditions for coal initiation (evidenced by the presence of an Endalen coal seam).

Sulfur supply would be expected to increase in a SW direction toward the palaeo-coast. The same is likely to be the case for ash content, as more coastal peats would be expected to be most vulnerable to sea-level rise and storm events. Peats deeper within the peatland but adjacent to channels would also be likely to have higher ash contents with the channels acting as conduits for clastic material and seawater during flooding events. Unlike the Longyear, dust supply is thought to have very little effect upon the inorganic elemental composition of the Svarteper and Askeladden seams as the supply of clastic sediment was too great.

The Svarteper and Askeladden seams may therefore be classified as a coastal clastic marsh system whose restricted floodplain and marine influence produced the high ash, high sulfur character which limits the coals economic value today.

Chapter 8

CONCLUSIONS AND FUTURE WORK

This study has integrated both palaeogeographic and geochemical data from the Todalen coals to provide insight into the impact of landscape, climate and sea-level upon paralic high latitude peatlands and subsequent coal quality and thickness. The discovery of significant oil potential may also prove to be of significant future value, both as an oil resource and as a model for oil prone coal exploration within the wider Arctic.

The objective of this chapter is to create a unified palaeo-environmental model of coal formation over the lifetime of the Todalen Member, discuss how the controls upon coal quality evolved over time.

8.1 Palaeo-environmental development of the Todalen Mbr.

The Todalen member is comprised of a number of transgressive-regressive cycles which gradually in-filled the underlying Carolinefjellet peneplain. This evolving landscape had a significant effect upon the distribution and character of the coals formed. The development of coal forming environments within the Todalen Member can be seen in Fig. 8.1-8.4

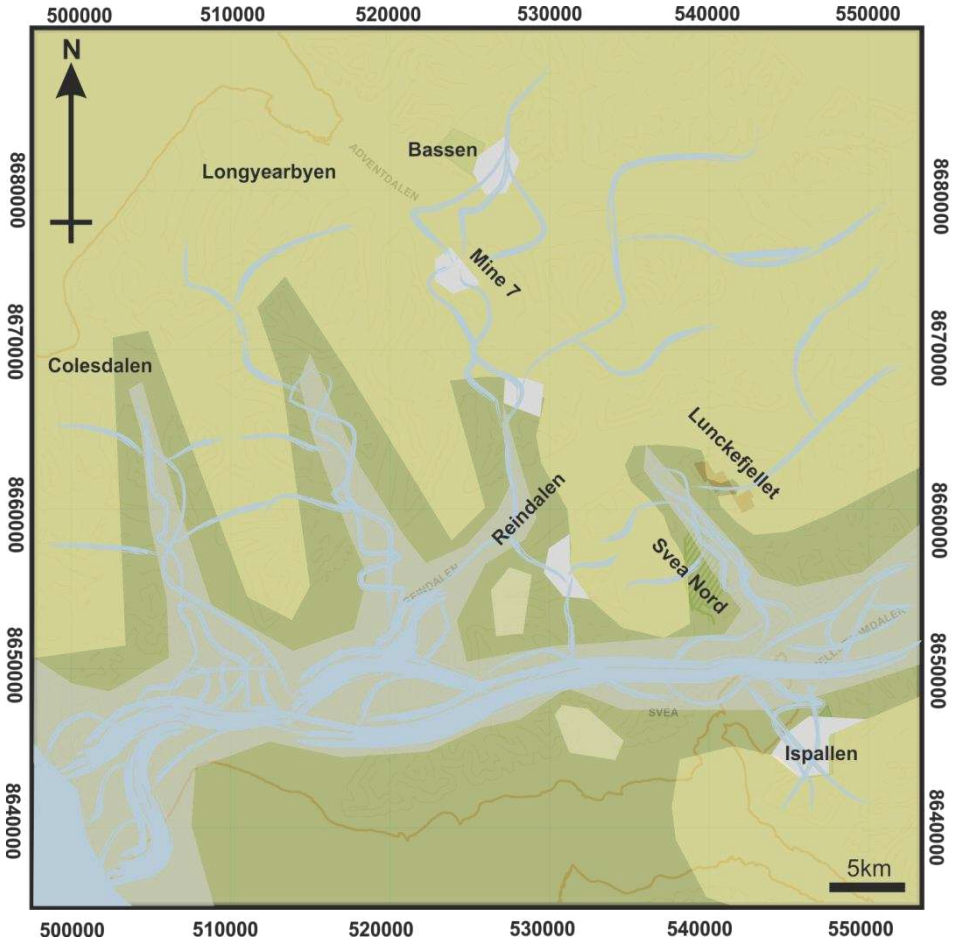

Fig. 8.1 – (Left) Reconstruction of the Gronfjorden valleys presuming the valley system identified extends to the previously identified swells and troughs.

Compression and movement between Greenland and Svalbard during the Late Cretaceous, led to uplift and a hiatus lasting at least 40Myr (Harland, 1997). This study shows that the peneplain created was structurally controlled with valleys forming in structural depressions, probably representing draping over underlying structures within the basement. These valleys were initially the focus of braided river formation, forming the Grønfjorden Bed. This was followed by a brief period of silt deposition, before the development of the Svea Seams (Fig.8.1)

Svea Seam formation occurred in two forms, the fan type and valley type. Deposition occurred initially in the south and moved northward over time, as evidenced by a bentonite layer. The Svea Nord seam formed over a period of ~160,000kyr and represents the largest lens of those formed during the Svea period (Fig. 8.2)

In the Lower Svea Nord Seam the peat was vulnerable to desiccation and fire due to its reliance upon local precipitation and hydrology. This probably led to the high coal phosphate contents observed at this location. Lithophile elements were primarily supplied from dust as evidenced by the generally low ash contents within the seam (<10%) but have been extensively leached from the peat during acidification events associated with drying. A charcoal horizon at the top of the lower seam immediately prior to splitting indicates that the peatland probably burnt to the water table in most areas allowing clastic sedimentation (Fig. 8.2)

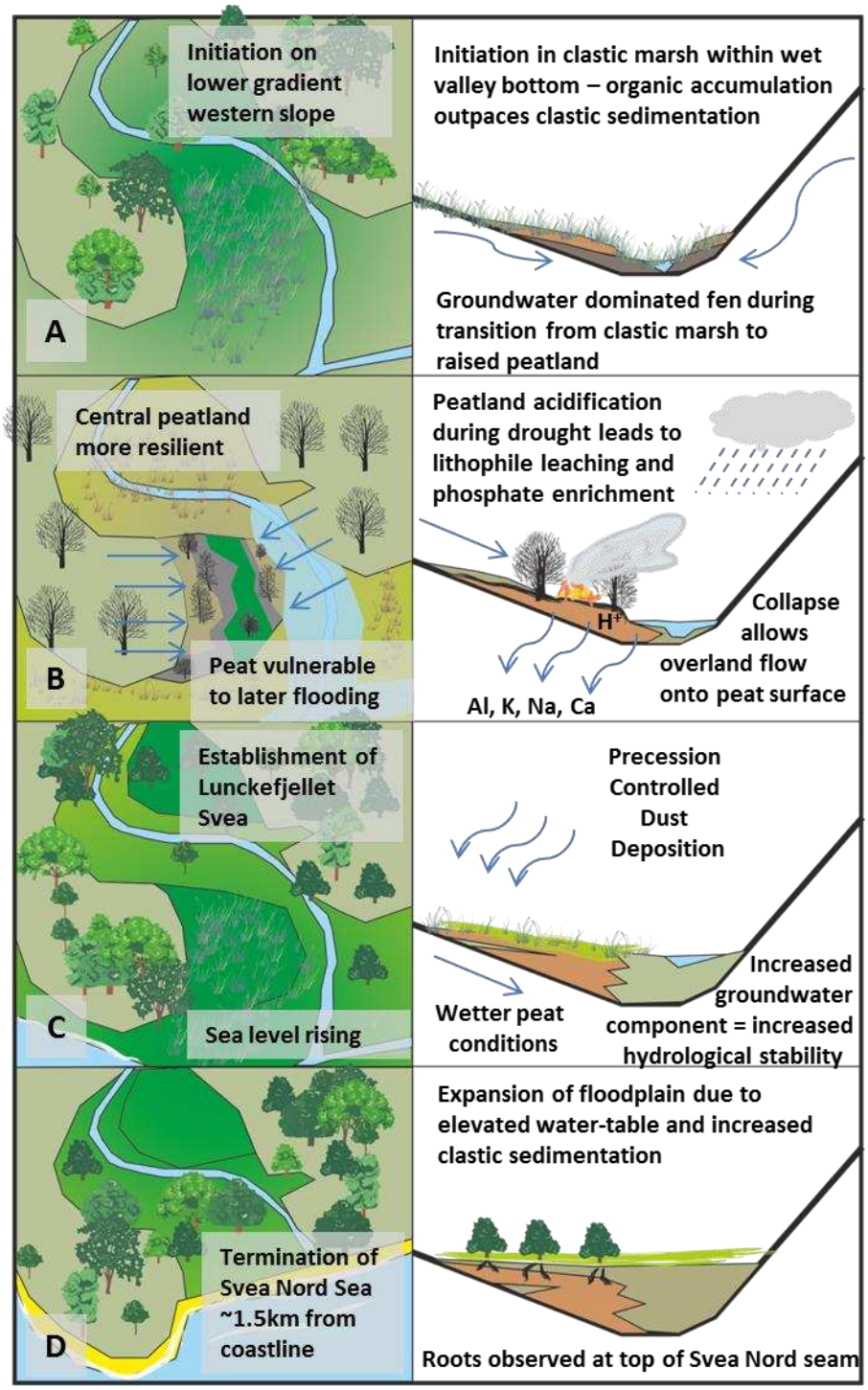

Fig. 8.2 Palaeo-environmental development of the Svea Nord Peatland from initiation to termination (A) Initiation of the peatland (B) Conditions within the Lower seam and split development (C) The upper Svea Nord Seam (D) Termination of the Svea Nord Seam

In the upper seam, the hydrological stability of the Svea seam was much greater, indicating either a wetter climate or increased groundwater supply. Sulfur increased up-seam at this location indicating increased marine influence. This also could be the cause of increased groundwater influence upon the peatland. The distribution of lithophile elements was preserved in the upper seam with ~2.5 cycles/m. The seam was followed by deposition of floodplain sediments with rootlets preserved penetrating the roof of the seam (Fig. 8.2)

Coal deposition then shifted to the north to fans, adjacent to gulleys within the Grønfjorden ridges. These fan deposits were vulnerable to clastic sedimentation during intense weather events producing high ash coals. The Svea period of deposition was then followed by deposition of marine sediments, before deposition of the transitional Todalen coal and further transgression

The next major phase of coal deposition was the Longyear seam. The Longear seam began at the basin margins (Bassen, Lunckefjellet) and expanded South West. The lower part of the seam (<80cm Mine 7) is characterised by occasional peatland fires. These occurred during globally warmer conditions when unstable air-masses from the south could penetrate further north causing lightning induced fires. This was accompanied from distal dust enriched in Cu. These fusinite rich layers also allowed extensive post depositional Fe-Ca carbonate deposition. Drier periods were

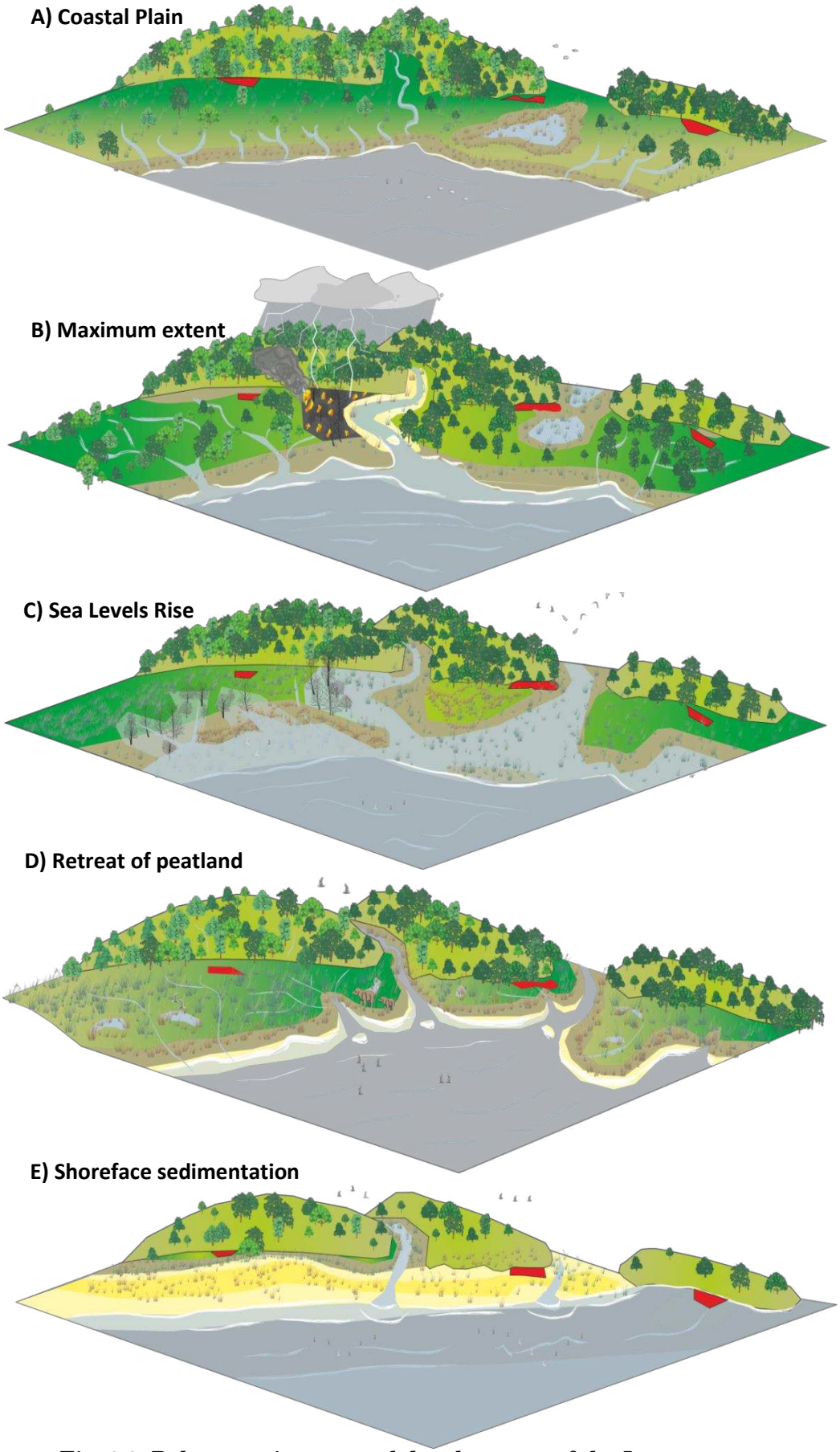

Fig. 8.3. Palaeo-environmental development of the Longyear seam, A and E based on lithology maps as defined in Section 3.4. B-D based on coal isopach maps and response to sea level shown in in Fig. 3.16

characterised by more local dust supply with similar composition to the splits within the Svea Nord seam (Fig. 8.3)

The upper part of the seam was wetter and more biodegraded representing a shift to fen conditions, this hydrological stability led to the end of the fire cycles seen within the lower seam. Increasing marine influence caused peat sulfur contents to rise and the peatland to retreat to areas of high ground, overlying the Grønfjorden highs (Fig. 8.3)

Persistent lows acted as conduits for clastic sedimentation and sulfur supply penetrating deep within the coastal plain leading to splitting and lower coal quality within adjacent peats. The last area to be inundated was in the Bassen/Operafjellet region leading to the highest coal thickness in this area. The Longyear seam was followed in most places by deposition of shore face massive sandstones containing *Ophiamorpha nodosa*.

The last stage of coal formation in the Todalen member is represented by the deposition of the minerotrophic Svarteper and Askeladden seams. Ash and Sulfur supply was dominated by clastic and marine sources. The peatlands were waterlogged allowing fine sediment to be deposited across the surface of the peatland. The thickest and highest quality coals are found in the Operafjellet region, due to its relatively protected location at the basin margins. This was then followed by Endalen member massive sandstones and

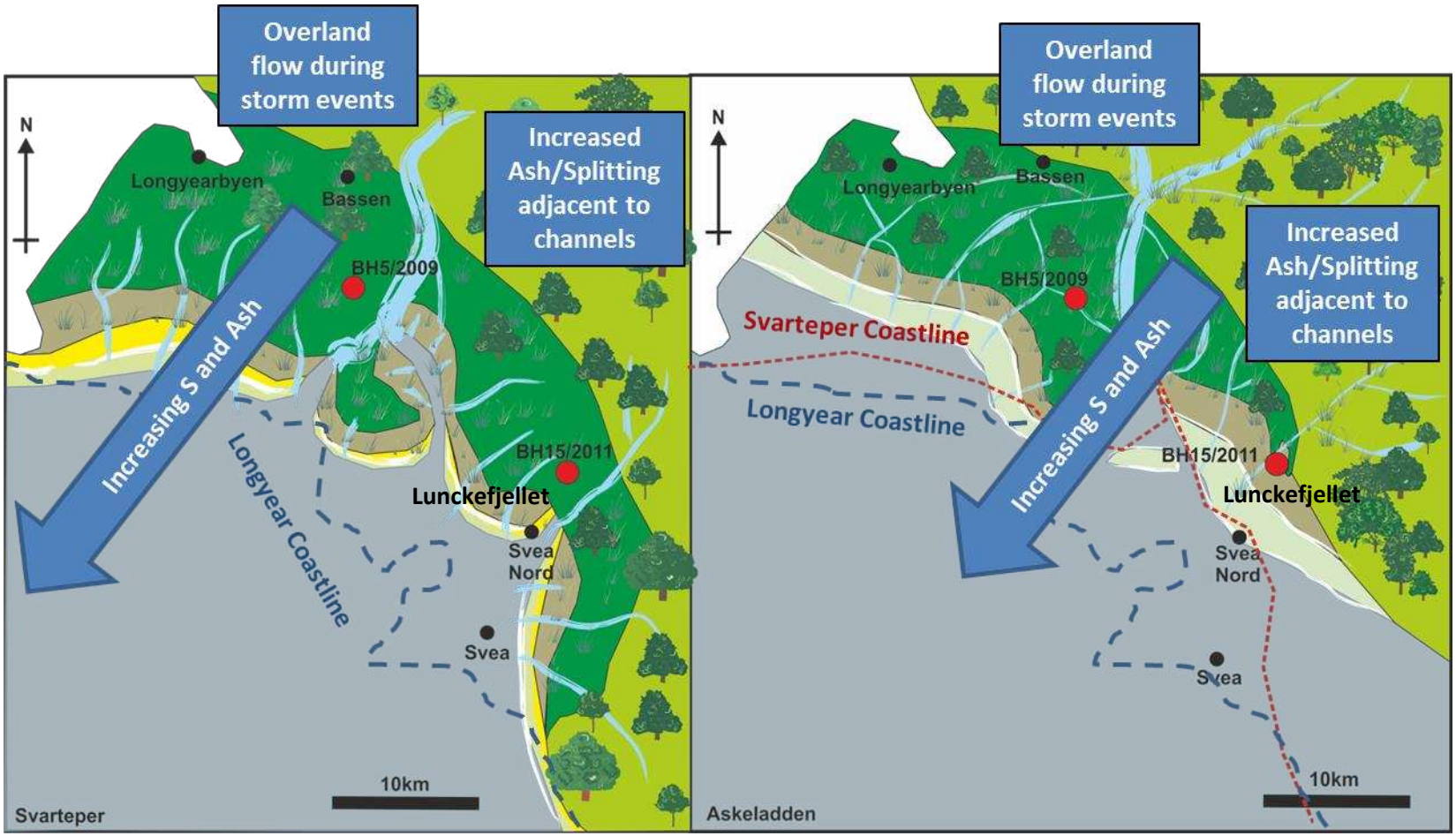

Fig. 8.4 – Summary diagram showing the main sources of Ash and sulphur from the Svarteper and Askeladden Seams alongside a demonstration of increasing marine influence from the deposition of the Longyear seam to the Svarteper/Askeladden area. The primary controls are S from seawater, Ash from marine and fluval flooding events and Fe/Ca from groundwater. Highest quality and thickest coal would be expected in the Bassen area for both seams due to its relatively sheltered position at the NE edge of the coastal plain. N.B the rapid northeasterly retreat of peatland from the Longyear to Svarteper Askeladden period represent the final infilling of the underlying palaeotopography

shore face sedimentation, except in the Operafjellet region where a thin coal seam was formed (Fig. 8.4)

The integrated approach to coal geology appears to work well within the Todalen Member, not only with respect to identifying sources of coal quality issues but also for understanding the role of hydrology, global climate and structure in controlling peatland dynamics in Palaeocene high latitude peatlands. This approach may therefore be of use when examining other coals from this period and rank

8.1.1 Hydrological Landscape Approach

The use of the hydrological landscape theory has proved to be a resilient technique for understanding the role of landscape hydrology in controlling peat thickness within a structurally simple basin, particularly when combined with a palaeo-topographic marker bed. It also shows that far from being simple systems controlled by base level changes (Bohacs and Suter, 1997), paralic systems are much more dynamic and resilient than previously thought, with areas of groundwater discharge acting as both points of initiation and refuge.

When applied within a single seam, the effect of base level changes can be modelled and peatland palaeo-hydrology inferred. When applied to a sequence of coal seams, the relative importance of various basinal controls (landscape, structure, sea-level) over time can be inferred, which could be of significant use in predicting both

the distribution and quality of coals. This is shown clearly within the Todalen member coals where a progressively diminishing landscape control is accompanied by an increasingly marine control. These changes are reflected in the character and distribution of the coals where;

- Landscape Control > Base Level Control
    - Svea Seam – Localised peatland in lenses within fans and valleys, raised peatlands, vulnerable to oxidation and collapse during dry periods, Low ash in centre of lens, high ash at peatland margins. Lithophile elements dust-supplied
- Landscape Control ~ Base Level Control
    - Longyear seam - Laterally extensive highly stable peatlands, initiate and retreat adjacent to topographic highs, channels preferentially located within underlying topographic lows. Coal quality tracks position of coastline and channels during relative sea level rises (good inland, poor at coast). Lithophile elements are primarily dust supplied.
- Landscape Control < Base Level Control
    - Svarteper and Askeladden – Minerotrophic, high sulfur peats, very wet peatland conditions, vulnerable to splitting, finely disseminated pyrite and ash throughout coal, clastic supplied

This progression is primarily achieved by the gradual infilling of topography by transgressive phase deposition between each of the coal seams. Features similar to the Svalbard coals have observed in the New Zealand, Waikato coal (Hall, 2003) using a similar technique, primarily coals thinning into topographic lows and thickening adjacent to structural highs. Other authors also describe similar coal distributions (Bohacs and Suter, 1997 and references therein).

The results from this work and reports of similar coal distributions to those shown in this study shows that the hydrological landscape technique may be of use in more complicated basins. Particularly to predict the location of the thickest coal deposits and interpret the relative controls upon peat deposition and coal character

The hydrological landscape approach shows that coal thickness and distribution may also be of use in understanding the structural development of basins. In the Todalen member, this allowed a number of swells and troughs to be identified, extending previous models of the swell system (Sokholov et al., 1968; Livšic, 1974; Harland, 1997) up to the Billefjorden fault zone and filling a conspicuous gap in the structural map of the Central Tertiary Basin.

In addition, as these features affect the distribution of the Grønfjorden bed and the coal seams indicates that the swells and troughs were already present during the Late Cretaceous hiatus.

and may reflect draping over pre-existing Carboniferous structures shown by Eiken, (1994) or the initial stages of the West Spitsbergen orogeny.

This shows that coal distribution may be of use in more structurally complex basins, allowing the relative timing of faulting to be understood as if present prior to coal formation, coal distribution should thicken towards any break in slope created. This should also be preserved even if the fault is later reactivated. Coal also appears to be useful for identifying very minor structural features that are difficult to see in the field.

8.1.3 Oil Potential of the Svalbard Coals.

The upper Svalbard coals (Longyear, Svarteper and Askeladden) are shown to have maximum oil yields in excess of 400mg/g coal with hydrous pyrolysis and Rock-Eval yields comparable to many oil shales. The coals also show significant retorting potential with yields between 175-190 mg/g similar to values achieved on a sub-economic basis in the Kings Bay region during the 1920's.

The inferred maturity gap between the Svalbard coals is due to suppression of vitrinite reflectance by enrichment in hydrogen rich oil prone material. This has implications for local and regional basin models indicating reflectance gradients in the Adventdalen region consistent with lower estimates (0.15%/km) and greater burial and subsequent uplift within the N. Barents during the Tertiary.

Oil potential is thought to be due to the incorporation of hydrogen rich plant material and bacterial lipids into humic material, followed by preservation by organo-sulfur molecule formation. This process appears aided by the unusual conditions present at high latitude during the Palaeocene, namely the temperate climate, high seasonality, high productivity and pH regulation effect of a coastal position combined to form optimum conditions for perhydrous vitrinite formation. This is consistent with previous models of high latitude oil prone coal formation (Wilkins and George, 2002; Petersen, 2005).

If replicated across the entire basin, the Todalen coals represent a significant unconventional oil/gas province whose importance can only increase as conventional oil reserves decrease.

8.2 Future Work

The Svalbard coals represent a significant oil resource, and consequently are of economic interest, particularly as the retortion process removes sulfur from the coals through the conversion of pyrite to pyrrhotite. This opens up new areas of mining to exploitation as the areas of sulfur rich coals have been previously considered sub-economic. In areas where conventional mining is not possible due to the previous mining in-situ techniques may also be appropriate.

However, further investigation with more samples from a larger variety of locations are required to confirm the models for oil prone coal formation presented in this study. This would be primarily in the form of transects inland from the inferred palaeo-coast showing oil potential up-seam at each site and observing where the raised bog-fen transition occurred. In addition, pilot scale testing of the retorting potential of the coals would be required to confirm the results from nitrogen pyrolysis. The oils produced would have to be characterised more fully to identify any quality issues and potential markets. The sub-coke produced from retorting is also a valuable resource if of sufficient quality and therefore more work is required to evaluate the coke and identify potential markets for the coal. Evaluation of suitable coal reserves within existing mines would also be required

In-situ retorting would have the advantage of allowing extraction of the Longyear, Svarteper and Askeladden seams at locations where coal thickness was unsuitable for conventional mining. If in-situ retortion was considered, the technique would need to be adapted for coals from existing oil shale techniques (Burwell et al., 1970; Qian and Wang, 2006). In addition a full economic and environmental evaluation would be required before exploitation could take place.

In addition, other coals formed at similar latitudes both on Svalbard (Cretaceous, Helvetiafjellet Formation; Tertiary Kings Bay coals, Hoel, 1925; Tertiary Barentsburg Coals; Carboniferous Pyramiden Coals; Abdullah et al., 1988) and in the wider Arctic (Middle Jurassic Kuhn Ø coals, E Greenland; Petersen and Rosenberg; Petersen et al, 2006; Jurrasic Hochstetter Foreland coals, NE Greenland, Bojesen-Koefoed et al., 1996) may also have significant oil potential making this area of great interest both due to their contribution offshore oil fields and as an unconventional resource in their own right.

The discovery of significant bacterial communities within Palaeocene peatlands may have implications for both studies of Palaeocene climate/carbon cycling and future peatland response to anthropogenic climate change. However, currently the information gained from hopane and methyl-hopane concentrations within the Longyear seam is qualitative, whereas climate models require quantitative data.

To do this bacterial hopane precursors in peats would have to be quantified at different latitudes and compared to hopane contents from coals formed in similar environments. This is difficult due to the difficulties of extracting peats for organic geochemical analysis and due to the far more numerous precursor molecules than microbial biomarkers.

In addition, Methyl-hopane precursor molecules appear to be relatively rare within biological samples (Pers. Comm. H. Talbot, 6th July 2012) but extremely common within geological samples. This mismatch requires further investigation, through examining new species/more samples or looking for missing precursor molecules. In addition, previous work has used compound specific ^{13}C isotope analysis upon hopanes to infer the size of methanogen community within coals (Pancost et al., 2007). Also the effects of differential preservation within a seam would have to be fully quantified before data could be used.

If these problems could be resolved, this would allow the extensive coal reserves across the world to form a record of terrestrial carbon fluxes at different latitudes over geological time, something which is currently very limited.

The similarities between the fire dynamics of the Canadian Arctic (McCoy and Burn, 2006) and the fire cycles observed within the Longyear seam indicates that a similar stable polar air mass existed

during the Palaeocene. To examine this further, more sections would be required from coal seams within Svalbard and the wider Arctic. If confirmed this could help confirm the minimum and maximum extent of the polar air mass during the Palaeocene as well as possibly identifying the most common routes of storm pathways moving north.

The use of $\delta^{13}C$ and n-alkane δH analysis may have great potential for reconstructing the terrestrial carbon record from this location and past terrestrial hydrological conditions.

The bulk carbon isotope record of coals has been shown previously (Briggs, 2007) to be of use in identifying orbital cyclicity within coals and for correlating coals with marine $\delta^{13}C$ records. This was attempted within this study however, variations in $CaCO_3$ content masked any changes in coal $\delta^{13}C$ values. In future work the coals would have to be pre-extracted with HCl prior to analysis to remove any inorganic carbon which could affect the carbon record from these coals.

The δD ratio of plant compounds is determined by the isotopic composition of precipitation entering the plant system which is primarily controlled by climate (Dawson et al., 2004). The ratio is also controlled by processes such as evaporation and transpiration which are also a function of temperature as isotopically light water is preferentially evaporated compared to more deuterium enriched

water (Hoef, 1987). If used in the context of this study this would be able to confirm the variations in global climate inferred from the organic petrographic and inorganic data collected in this study.

References

Abdullah, W., Murchison D., Jones, J.M., Telnaes, N., Gjelberg, J., (1988) Lower Carboniferous coal deposition environments on Spitsbergen, Svalbard. Organic geochemistry 13(4-6), 953-964.

Alexander, R., Kagi, R.I., Woodhouse, G.W., (1981) Geochemical correlation of Windalia oil and extracts of winning group (Cretaceous) potential source rocks, Barrow Subbasin, Western Australia. American Association of Petroleum Geologists Bulletin 65, 235-250.

Allen, M.R., Smith, L.A., (1996) Monte Carlo SSA: Detecting irregular oscillations in the presence of coloured noise. Journal of Climate, 9, 12, 3373-3404

Amon, J.P., Thompson, C.A., Carpenter. Q.J., Miner. J. (2002) Temperate zone fens of the glaciated Midwestern USA Wetlands 22 2 301-317

Anderson, R.S., Hallett, D.J., Berg. E. Jas, R.B., Toney, J.L., de Fontaine, C.S and DeVolder A. (2006) Holocene development of Boreal Forests and fire regimes on the Kenai Lowlands of Alaska. The Holocene, 16, 6, 791-803

Archer, D., Winguth, A., Lea D., Mahowald, N., (2000) What caused the glacial/interglaci al atmospheric pCO2 cycles? Reviews of Geophysics, 38, 2, 159-189

Aspøy, I (2011) – Sedimentological Development of the Askeladden Sequence of the Todalen Member (Paleocene) at Lunckefjellet, Svalbard. Masters Thesis in Sedimentolog/Petroleum Geology, University of Bergen/UNIS

Avramides, E.J., Christou, M., Jones, D.L., (2009). Resilience of soil microbial activity and of amino acid dynamics to the removal of plant carbon inputs during winter. Scientia Agricola 66, 132-135

Berner E.K. and Berner R. A. (1997) Global Environment: Water, Air and Geochemical Cycles. Prentice Hall, Eaglewood Cliffs: New Jersey

Bechtel, A., Gruber, W., Sachsenhofer, F., Gratzer, R., Lucke., A., Puttman, W., (2002a) Depositional environment of the Late Miocene

lignite (Alpine Foreland Basin): insights from petrography, organic geochemistry and stable carbon isotopes. International Journal of Coal Geology 54, 3, 153-180

Bectel, A., Sachsenhofer, R.F., Kolcon, I., Gratzer, R., Otto, A., Puttmann, W., (2002b) Organic Geochemistry of the Lower Miocene Oberdorf lignite (Styrian Basin, Austria):its relation to petrography, palynology and palaeoenvrionment, International Journal of Coal Geology, 50 (1): 31-57

Bechtel, A., Sachsenhofer, R.F., Markic, M., Gratzer, R., Lucke, A., Puttman, W., (2003) Paleoenvironmental implications from biomarker and stable isotope investigations on the Pliocene Velenje lignite seam (Slovenia) Organic Geochemistry, 34, 9, 1277-1298

Bechtel, A., Markic, M., Sachsenhofer, R.F., Jelen, B., Gratzer, R., Lucke, A., Puttman, W., (2004) Paleoenvironment of the the upper Oligocene Trbovlje coal seam (Slovenia) International Journal of Coal Geology 57(1) 23-48

Bechtel, A., Sachsenhofer, R.F., Zdravkov, A., Kostova, I., Gratzer, R.,(2005) Influence of floral assemblage, facies and diagenesis on petrography and organic geochemistry of the Eocene Bourgas coal and the Miocene Maritza-East lignite (Bulgaria). Organic Geochemistry, 36, 11, 1498-1522

Belyea L.R., Baird, A.J., (2006). Beyond "the limits to peat growth" cross-scale feedback in peatland development. Ecological Monographs, 76, 3, 299-322

Blythe, A.E., Kleinspehn, K.L., (1998) Tectonically versus climatically driven Cenozoic exhumation of the Eurasian plate margin, Svalbard: Fission track analyses. Tectonics, 17, 621-639

Bojeson-Koefoed, J.A., Kalkreuth, W., Petersen, H.I., Piasecki, S., (2012). A remote coal deposit revisited: Middle Jurrassic coal at Kulhøj, western Germania Land, northeast Greenland. International Journal of Coal Geology 98, 50-61

Bohacs, K., Suter, J., (1997), Sequence Stratigraphic Distribution of Coaly Rocks: Fundamental Controls and Paralic Examples, American Association of Petroleum Geologists Bulletin, 81, 1612-1639

Bopp L., Kohfeld, K.E., Le Quéré, C., Aumont, O., (2003) Dust impact on marine biota and atmospheric CO_2 during glacial periods. Paleoceanography 18 12 24-1 – 24-9

Bray, E.E., Evans, E.D., (1961). Distribution of *n*-paraffins as a clue to recognition of source beds. Geochimica et Cosmochimica Acta 22, 2-15.

Breivik, A.J., Mjelde, R., Grogan, P., Shimamura, H., Yoshio, M., Nishamura, Y., (2005) Caldonide development offshore-onshore Svalbard based on ocean bottom seismometer, conventional seismic and potential field data, Tectonophysics, 401, 1 79-117

Breivik, A.J., Inge, J., Mjelde, R., Raum, T.J., Faleide, J.I., Muai, Y., Fleuh, E., R (2010). Crustal structue beneath the Trondelag Platform and adjacent areas of the mid-Norwegian margin, as derived from wide angle seismic and potential field data. Norsk Geologisk Tidsskrift. ISSN 0029-196X. 90, 4, 141-161

Briggs J., Large, D.J., Snape C.E., Drage, T., Whittles. D., Cooper, M., Macquaker, J.H.S, Spiro, B.F., (2007) Influence of climate and hydrology on carbon in early Miocene peatland. Earth and Planetary Research Letters, 253, 445-453

Briggs J., (2007) Influence of climate and hydrology in an early Miocene peatland, PhD thesis, University of Nottingham.

Bruhn, R., Steel, R.J., (2003) High resolution sequence stratigraphy of a clastic foredeep succession (Palaeocene, Spitsbergen): An example of peripheral-bulge-controlled depositional architecture: Journal of Sedimentary Research, 73. 745-755

Bubier, J.L, Moore, T.R., Roulet, N.T., (1993) Methane Emissions from wetlands in the midboreal region of Northern Ontario, Canada. Ecology, 74, 8, 2240-2254

Burwell, E.L., Sterner, T.E., Carpenter, H.C., (1970) Shale Oil Recovery by In-situ retorting a pilot study Journal of Petroleum Technology, 22, 12

Butler I.B., Rickard, D., (2000) Framboidal pyrite formation via the oxidation of iron (II) monosulphide by hydrogen sulphide, Geochimica et Cosmochimica Acta, 64, 2665-2672

Carr, A.D., Williamson, J.E., (1990). The relationship between aromaticity, vitrinite reflectance and maceral composition of coals:

Implications for the use of vitrinite reflectance as a maturation parameter. Advances in Organic Geochemistry 16, 313-323.

Carcaillet, C, Bergeron, Y, Richard P,J,H., Fréchette, B., Gauthier, S., Prairie, T.,(2001) Change of fire frequency in the eastern Canadian boreal forests during the Holocene: does vegetation composition or climate trigger the fire regime? Journal of Ecology,89, 930-946

Casareo, F.E., George, S.C., Batts, B.D., Conaghan, P.J., (1996). The effects of varying tissue preservation on the aliphatic hydrocarbons within a high-volatile bituminous coal. Organic Geochemistry 24 8/9 785-800

Cassani, F., Gallango, O., Talukdar, S., Vallejos, C., Ehrmann, U., (1988). Methylphenanthrene maturity index of marine source rock extracts and crude oils from the Maracaibo Basin. Organic Geochemistry 13, 73-80

Claquin. T., Roelandt, C., Kohfeld, K., Harrison S., Tegen, I., Prentice, I.C., Balkanski, Y., Bergametti, G., Hansson, M., Mahowald, N., Rodhe H., Schulz,M., (2003) Radiative forcing of climate by ice-age dust, Climate Dynamics 20, 193-202

Cmiel, S.R., Fabianska, M.J., (2004) Geochemical and petrographic properties of some Spitsbergen coals and dispersed organic matter. International Journal of Coal Geology 57, 77-97.

Cranwell, P.A., Eglington, G., Robinson, N., (1987) Lipids of aquatic organisms as potential contributors to lacustrine sediments, Organic Geochemistry, 11, 513-527

Cressie, N., (1993), Statistics for special data, Wiley, New York

Cvejic, J.H., Bodrossy, L. Kovács, K.L., Rohmer, M., (2000) Bacterial triterpenoids of the hopane series from the methanotrophic bacteria *Methylocaldum* spp.: phylogenetic implications and first evidence for an unsaturated aminobacteriohopanepolyol, FEMS Microbiology Letters 182 361-365

Dalland. A., Steel, R.J., 1981, Undersøkelser av den kullførende del av Firkanten Formasjen (Tertiær) i østlige del av Nordenskiöld land, Svalbard, Geologisk Institutt Universitetet i Bergen

Dallmann, W.K., Midbøe, P., Nøttvedt, A. & Steel, R. (1999): Tertiary lithostratigraphy. In W.K. Dallmann (ed.),

Lithostratigraphic Lexicon of Svalbard. Upper Palaeozoic to Quaternary bedrock. Review and recommendations for nomenclature use. Committee on the Stratigraphy of Svalbard / Norsk Polarinstitutt. 215-263.

Dawson, D., Grice, K., Wang S.X., Alexander, R., Radke. J., (2004) Stable hydrogen isotopic composition of hydrocarbons in torbanites (late Carboniferous to Late Permian) deposited under various climatic conditions. Organic Geochemistry 35, 2, 189-197

DeCelles., P.G., Giles, K.A. (1996) Foreland basin systems Basin Research 8 105-123

Denk., T., Wanntorp, L., Manum S.B., (1999) Catalogue of the Tertiary plant fossils from Spitsbergen housed in the Swedish Museum of Natural History

Dickens, G.R., (2003) Rethinking the global carbon cycle with a large, dynamic and micribially mediated gas hydrate capacitor, Earth and Planetary Science Letters, 213, 169-183

Diessel, C.F.K., (1986). On the correlation between coal facies and depositional environments. Advances in the study of the Sydney Basin. 20 Newcastle Symposium Proceedings, 246, 19-22

Diessel, C.F.K., (1992). Coal-Bearing Depositional Systems. Springer Verlag, Berlin

Diessel, C.F.K., Gammidge, L., (1998). Isometamorphic variations in the reflectance and fluorescence of vitrinite - a key to depositional environment. International Journal of Coal Geology 36, 167-222.

Dillon, P.J.,Molot, L.A., Scheider, W.A., (1997) A note on the effect of El Niño on the recovery of acidified lakes. International Journal of Environmental Monitoring and Assessment, 46, 105-111

Falkow, S., Dworkin, M., Rosenburg, E., Stackebrandt, E., (2006) The Prokaryotes: A handbook on the Biology of Bacteria, Volume 5, Prokaryotes, 5, 266-289

Dypvik, H., Riber, L., Burca, F., Ruther, D.C., Jargvoll, D., Nagy, J., Jochmann, M., (2011) The Palaeocene-Eocene Thermal Maximum (PETM) in Svalbard – clay mineral and geochemical signals. Palaeogeography, Palaeoclimatology, Palaeoecology, 302, 3-4, 159-169

Eglington, G., Hamilton, R.J., (1967) Leaf epicuticular waxes Science 156, 1322-1335

Eiken, O, (1994) Seismic Atlas of Western Svalbard Norsk Polarinstitutt Meddelelser 130 73

Engelstaedter S., Washington, R., (2007) Temporal controls on global dust emissions: The role of surface gustiness, Geophysical Research Letters, 34, 15

Faix, O., Mozuch, M.D., Kent Kirt, T. (1985) Degradation of Gymnosperm (Guaiacyl) vs. Angiosperm (Syringyl/Guaiacyl) Lignins by Phanerchaete chrysosporium, Holzforschung, 39, 203-208

Fan, Y., Miguez-Macho, G., (2011). A simpe hydrologic framework for simulating wetlands in climate and earth system models. Climate Dynamics 37, 253-278

Farrimond, P., Talbot., H.M., Watson, D.F., Schulz, L.K., Wilhems, A., (2004) Methylhopanoids: Molecular indicators of ancient bacteria and a petroleum correlation tool, Geochimica et Cosmochimica Acta, 68, 19, 3873-3882

Ficken, K.J., Li, B., Swain, D.L., Eglinton, G., (2000). An n-alkane proxy for the sedimentary input of submerged/floating freshwater aquatic macrophytes. Organic Geochemistry 31, 745-749.

Fierer, N., Craine, J.M., McLauchlan, K., Schimel, J.P., (2005). Litter quality and the temperature sensitivity of decomposition: Ecology, v. 86, p. 320-326.

Scott, A.C., Fleet, A.J., (1994) Coal and Coal bearing strata as oil prone source rocks? London: Geological Society Special Publications, Geological Society.

Freese, E., Koster, J., Rullkotter, J., (2008). Origin and composition of organic matter in tidal flat sediments from the German Wadden Sea. Organic Geochemistry 39, 820-829.

Friend, P.F., Williams, B.P.J., Ford, M., Williams, E.A. (2000) Kinematics and dynamics of the Old Red Sandstone basins. In. Friend P.F., and Williams, B.P.J. (eds) New Perspectives on the Old Red Sandstone, Geological Society Special Publication, 180, 29-60, London

Gaiser, E.E., Taylor, B.E., Brooks, M.J., (2001). Establishment of wetlands on the southeastern Atlantic coastal plain: paleolimnological evidence of a mid-Holocene hydrologic threshold from a South Carolina pond. Journal of Paleolimnology 26, 373-391

Gee, D.G. Teben'kov, A.M., (2004). Svalbard: Caledonian fragments of the Laurentian margin. In: Gee & Pease (eds.) Timanides – Neoproterozoic Orogeny Along the Eastern Margin of Baltica. Geological Society, London, Memoirs, 30, 191-207

Ghil, M., Allen, M.R., Dettinger, M.D., Ide, K., Kondrashov. D., Mann, M.E., Robertson, A.W., Saunders, A., Tian, Y., Varadi, F., Yiou, P., (2002) Advanced spectral methods for climatic time series. Review of Geophysics 40, 1, 1-41

Gorham, E. (1991) Northern peatlands- role in the carbon-cycle and probable responses to climatic warming. Ecological Application 1, 2, 182-195

Greenwood, D.R., Basinger, J.F., Smith, R.Y., (2010). How wet was the Arctic Eocene rain forest? Estimates of precipitation from Paleogene Arctic macrofloras Geology 38, 15-18.

Gustafsson, M. E. R., Franzen, L.G., (2000). Inland transport of marine aerosols in southern Sweden: Atmospheric Environment 34, 313-325

Hanson, A.D., Ritts, B.D., Zinniker, D., Moldowan, J.M., Biffi, U., (2001). Upper Oligocene lacustrine source rocks and petroleum systems of the northern Qaidam Basin, northwest China. American Association of Petroleum Geologists Bulletin 85, 601-619

Hao, F., Chen, J.Y., (1992). The cause and mechanism of vitrinite reflectance anomalies. Journal of Petroleum Geology 15, 419-434.

Harland, W. B., Pickton, C.A.G., Wright, N.J.R., Croxton, C.A., Smith, D.G., Cutbill, J.L., Henderson, W.G., (1976). Some coalbearing strata in Svalbard. Norsk Polarinstitutt Skrifter 164, Oslo

Harland, W.B., Anderson, L.M., Manasrah, D., Butterfield, N.J., Challinor, A., Doubleday, P.A., Dowdeswell, E.K., Dowdeswell, J.A., Geddes, I., Kelly, S.R.A., Lesk, E.L., Spencer, A.M., Stephens, C.F., (1997). The Geology of Svalbard. Geological Society Memoir 17, I-XXI, 1-521.

Harkel, M.J., (1997). The effects of particle-size distribution and chloride depletion of sea-salt aerosols on estimating atmospheric deposition at a coastal site. Atmospheric Environment 31, 3, 417-427

Härtner, T., Straub, K.L., Kannenberg, E., (2005). Occurrence of hopanoid lipids in anaerobic geobacter species. Fems Microbiology Letters 243, 59-64.

Hoel, A., (1925). The coal deposits and coal mining of Svalbard (Spitsbergen and Bear Island) Norsk Polarinstitutt Skrifter 6, Oslo

Hoefs, J., (1987) Stable isotope geochemistry. 3rd edition. Springer Verlag, Berlin

Huang, W.Y., Meinshein, W.G., (1979). Sterols as ecological indicators. Geochimica et Cosmochimica Acta 43, 739-745

International Committee for Coal and Organic Petrology (ICCP), (1994a). The new vitrinite classification (ICCP System 1994). Fuel 77, 55, 349-358

International Committee for Coal and Organic Petrology (ICCP), (1994b). The new inertinite classification (ICCP System 1994). Fuel 80, 4, 459-471

Jiamo, F., Guoying S., Jiayou, X, Eglington, G., Gowar, A.P., Rongfen, J., Shanfa, F., Pingan., P. (1990) Application of biological markers in the assessment of paleoenvironments of Chinese non-marine sediments. Organic Geochemistry, 16, 769-779.

Jochmann, M., (2004), The geology of the Ispallen area, Svalbard, with emphasis on the coal bearing Firkanten Formation. Unpublished Masters Thesis, Ludwig-Maximilians-Universistät, Munchen, University Centre in Svalbard, Longyearbyen

Killops S.D., Killops, V.J., (1993) An introduction to organic geochemistry. Longman Singapore Publishers (Pte) Ltd, Singapore

Killops S. D., Woodhouse A. D., Weston., R. J., Cook, R.A., (1994). A geochemical appraisal of oil generation in the Taranaki Basin, New Zealand. American Association of Petroleum Geologists Bulletin 78, 10, 1560-1585

Killops, S.D., Gunnel, R.H., Suggate, R.P, Sykes, R., Peters, K.E., Walters, C., Woolhouse, A.D., Weston, R.J., Boudou, J.P., (1998)

Predicting generation and expulsion of paraffinic oil from vitrinite rich coals Organic Geochemistry 29, 1-3, 1-21

Laban, K. L., Atkins, B. P., (1999). The determination of minor and trace element associations in coal using a sequential microwave digestion procedure. International Journal of Coal Geology, 4, 41, 351-369

Laine, A., Wilson, D., Kiely, G., Byrne, K.A., (2007) Methane flux dynamics in an Irish lowland blanket bog, Plant Soil 299, 181-193

Lambert, J. M. Jr., Simkovich, G., Walker Jr., P. L., (1998). The kinetics and mechanism of the pyrite-to-pyrrhotite transformation. Metallurgical and Materials Transactions B 29, 2, 385-396

Large, D.J., Jones, T.F., Somerfield, C., Gorringe, M.C., Spiro, B. Macquaker, J.H., (2001). A high-resolution terrestrial record of orbital climate forcing in a Late Palaeocene coal *In:* Earth System Processes - Global Meeting

Large, D.J., Jones, T.F., Somerfield, C., Gorringe, M.C., Spiro, B., Macquaker, J.H.S., Atkin, B.P (2003) High-resolution terrestrial record of orbital climate forcing in coal Geology. 31(4), 303-306

Large, D.J., (2007) A 1.16 Ma record of carbon accumulation in western European peatland during the Oligocene from the Ballymoney lignite, Northern Ireland Journal of the Geological Society. 164(6), 1233-1240

Large, D.J., Marshall. C., Meredith, W., Snape, C.E., Spiro, B.F., (2011) Potential to Generate Oil Prone Coal Source Rocks in Arctic Environments, Search and Discovery Article #40806

Lawrence, C.R., Neff, J.C., (2009) The contempary physical and chemical flux of Aeolian dust: A synthesis of direct measurements of dust deposition Chemical Geology, 267, 46-63

Lewan, M.D., (2006). Evaluating oil-shale product yields and compositions by hydrous pyrolysis. 26th Oil Shale Symposium presentations, Colorado Energy Research Institute

Lewińska-Preis, L., Fabiańska, M.J., Ćmiel, S., Kita, A., (2009) Geochemical distribution of trace elements in Kaffioyra and Longyear coals, Spitsbergen, Norway, International Journal of Coal Geology, 80, 211-223

Livšic, Y.Y., (1974), Paleogene deposits and the platform structure of Svalbard: Norsk Polarinst. Skr. 159

Lundegard, P., Knott, J.R., (2001). Polar organics in crude oil and their potential impacts on water quality. Petroleum Hydro-carbons and Organic Chemicals in the Ground Water Conference Proceeding, 1380144 Houston, Texas NGWA/APL

Lüthje, C.J. (2008) Transgressive Development of Coal-bearing Coastal Plain to Shallow Marine Setting in a Flexural Compressional Basin, Paleocene, Svalbard, Arctic Norway PhD Thesis, University of Bergen

Lüthje, C.J., Milan, J., Hurum, J.H (2010) Paleocene Tracks of the Mammal Pantodont Genus *Titanoides* in Coal-Bearing Strata, Svalbard, Arctic Norway Journal of Vertebrate Paleontology 30, 2, 521-527

Macgregor, D.S., (1994). Coal-bearing strata as source rocks-a global overview. In: Scott, A.C., Fleet, A.J. (eds.), Coal and coal-bearing strata as oil-prone source rocks?: London, The Geological Society Special Publication 77, 107-116.

Mahowald N.M., Zender, C.S., Luo, C., Savoie, D., Torres, O., del Corral, J., (2002), Understanding the 30-year Barbados dust record, J. Geophys. Res. 107 21 4561

Mahowald, N. , G. Rivera, C. Luo, (2004) Comment on Relative importance of climate and land use in determining present and future global soil dust emission by I. Tegen et al. Geophys. Res. Lett., 31, 24

Mahowald N. M., Lamarque JF., Tie. X. X.,Wolff, E., (2006). Sea-salt aerosol response to climate change: Last Glacial Maximum, preindustrial and doubled carbon dioxide climates. Journal of Geophysical Research: Atmospheres 111,

Major, H., Nagy, J., (1972). Geology of the Adventdalen map area. Norsk Polarinst. Skrifter., 138 1-58 (with map published 1964); Oslo

Maky A. B. F., Ramadan, M. A. M., (2008). Nature of Organic Matter, Thermal Maturation and Hydrocarbon Potentiality of Khataba Formation at East Aby-gharadig Basin, North Western Desert, Egypt. Australian Journal of Basic and Applied Sciences 2, 2 194-209

Manby G, Lyberis, (2000) N, Pre-ocean opening compression of the Northwestern Atlantic margin: evidence from eastern North Greenland, Journal of the Geological Society, 157, 707-710

Manum, S., Throndsen, T., (1978). Rank of coal and dispersed organic matter and its geological bearing in the Spitsbergen Tertiary. Norsk Polarinstitutt Arbok, 159-177.

Marshall, C., Large, D.J., Meredith, W., Snape., C.E., Spiro, B.F., Jochmann, M., (2012), Warm Arctic Peatlands – Future Methane Factories? Minerological Magazine, 76, 9, 184-188

Marshall C. Large, D.J., Snape, C.E., Meredith. W., Uguna, C., Spiro, B.F., Orheim, A., Jochmann, M., Mokogwu, I., Wang, Y., Friis, B, (Under Review) Oil Potential, Origin and Maturity of Coal in the Central Tertiary Basin, Svalbard, Norwegian Arctic, Organic Geochemistry

McCann, J.A., (2000) Deformation of the Old Red Sandstone of NW Spitsbergen; links to Ellesmerian and Caleodonian orogenies, Geological Society, London, Special Publications, 180, 567-584

McCoy V.M., Burn, C.R., (2005) Potential Alteration by Climate Change of the Forest-Fire Regime in the Boreal Forest of Central Yukon Territory. Arctic, 58, 276-285

McWhae, J.R.H., (1952) The major fault zone of Vestspitsbergen, Quarterly Journal of the Geological Society, 108, 209-232

Meredith, W., Russell, C.A., Cooper, M., Snape, C.E., Love, G. D., Fabbri, D. Vane, C. H., (2004). Trapping hydropyrolysate on silica and their subsequent thermal desorption to facilitate rapid fingerprinting by GC-MS. Organic Geochemistry 35 1 73-89

Meyers, P. A., Terranes, J. L., (2001). Sediment Organic Matter. In: Last, C. M., Smol, J. P., Tracking Envirnoment Change Using Lake Sediments. Volume 2 Physical and Geo-chemical Methods, Dordrecht, Kluwer, 239-269

Moi, R., (2008), Oil- prone Carboniferous coals (Tettegras Fm.) from the Finnmark Platform: Implications for an alternative and new Petroleum System based on oil generative coals of the Billefjord Gr. in the Barents Region, Masters Thesis in Geosciences, University of Oslo, Faculty of Mathematics and Natural Sciences

Mokogwu, I., (2011), Generation and Migration of Oil from Perhydrous Longyear Coal, Unpublished MSc Thesis in Petroleum and Environmental Process Engineering, University of Nottingham

Moldowan, J. M., Fago, F.J., Carlson, R.M.K., Young, D.C., Duvne, G.A., Clardy, J., Schoell, M., Pillinger, C.T., Watt, D.S., (1991) Rearranged hopanes in sediments and petroleum. Geochimica et Cosmochimica Acta, 55, 3333-3353.

Moran, K, Backman, J., IODP Expedition 302 Science Party (2006) The Arctic Coring Expedition (ACEX) recovers A Cenozoic History of the Arctic Ocean, Oceanography, 19, 4, 162-167

Montoya, J. P., Holl, C. M. Zehr, J. P.. Hansen, A. Villareal, T Capone D.G (2004), High rates of N2-fixation by unicellular diazotrophs in the oligotrophic Pacific, Nature, 430, 1027– 1031

Neuzil, S. G. (1997) Onset and rate of peat and carbon accumulation in four domed ombrogenous peat deposits, Indonesia. In: J.O. Rieley and S.E. Page (eds) Biodiversity and Sustainability of Tropical Peatlands. Samara Publishing, Cardigan, U.K., pp. 55-72.

Neunlist, S., Rohmer, M., (1985). Novel hopanoids from the methylotrophic bacteria *Methylococcus capsulatus* and *Methylomonas methanica* (22*S*)-35-aminobacteriohopane-30,31,32,33,34-pentol and (22*S*)-35-amino-3b-methylbacteriohopane 30,31,32,33,34-pentol. Biochemical Journal 231, 635-639.

Neuzil, S.G., (1997) Onset and rate of peat and carbon accumulation in four domed ombrogenous peat deposits, Indonesia In: J.O Rieley and S.E. Page (eds) Biodiversity and Sustainability of Tropical Peatlands. Samara Publishing, Cardigan, U.K, 55-72

Noble, R. A., Alexander, R. Kagi, R. I., Knox, J. (1985) Tetracyclic deterpenoid hydrocarbons in some Australian coals, sediments and crude oils: Geochimica et Cosmochimica Acta, 49, 2141-2147

Nieminen, T.M., Ukonmaanaho, L., Shotyk, B., (2002) Enrichment of Cu, Ni, Zn, Pb and As in an ombrotrophic peat bog near a Cu-Ni smelter in Southwest Finland, Peat bog Archives of Atmospheric Metal deposition, 292, 1-2, 81-89

Nagy, J., (2005). Delta-influenced foraminiferal facies and sequence stratigraphy of Paleocene deposits in Spitsbergen. Palaeogeography Palaeoclimatology Palaeoecology 222, 161-179.

Nøttvedt, A., (1982), Characteristic and evolution of the Askeladden Deltaic Sequence (Palaeocene) on Spitsbergen-with comparisons to the Ravenscar Group Deltaic Sequences (Bajocian) of Northeast England, PhD Thesis, University of Bergen

Nøttvedt A. (1985) Askeladden Delta Sequence (Palaeocene) on Spitsbergen – sedimentation and controls on delta formation. Polar Research 3 n.s., 21-48

Nottvedt, A., Cecchi, M., Gjelberg, J.G., Kristensen, S.E., Lønoy, A., Rasmussen, A., Rasmussen, E., Skott, P.H., van Veen, P.M., (1988), Svalbard-Barents Sea correlation: a short review. NPF special publication 2, 363-375

Nøttvedt, A., Cecchi, M., Gjelberg, J.G., Kristensen, S.E., Lønøy, A., Rasmussen, A., Rasmussen, E., Skott, P.H., Van Veen, P.M. (1993). Svalbard – Barents Sea correlation: a short review. In: Vorren, T., Bergsager, E., Dahl-Stamnes, Ø.A., Holter, E., Johansen, B., Lie, E. & Lund, T.B. (eds.), Arctic Geology and Petroleum Potential, Norwegian Petroleum Society, Special publication no.2, Elsevier, 363-375.

Orheim, A., (1982). Undiscovered Tertiary coal resources of Svalbard: an assessment using Monte Carlo methods. In: Embry, A. F., Balkwill, H. R., (Eds.): Arctic geology and geophysics. Canadian Society of Petroleum Geology, 399-414

Orheim, A., Bleg, G., Brekke, T., Horseide, V., Stenvold, J., (2007). Petrography and geochemical affinities of Spitsbergen Paleocene coals, Norway. International Journal of Coal Geology 70, 116-136.

Ohta, Y., Hjelle, A,, Andresen, A., Dallmann, W. K. & Salvigsen, 0. (1992): Geological Map of Svalbard, I : 100,000. Sheet B9G Isjjorden, with description. Norsk Polarinst. Temakart 16.

Otto, A., Simoneit, B.R.T., Rember, W.C., (2005). Conifer and angiosperm biomarkers in clay sediments and fossil plants from the Miocene Clarkia Formation, Idaho, USA. Organic Geochemistry 36, 907-922.

Paech, H.J., Koch, J., (2001). Coalification in Post-Caledonian sediments on Spitsbergen. In: Tessensohn F. (Ed.), Intra-

Continental Fold Belts CASE 1: West Spitsbergen,: Stuttgart, Geologisches Jahrbuch Reihe B, Polar Issue No. 7, 505-530

Pancost, R.D., Steart D.S., Handley, L., Collinson, M.E., Hooker, J.J., Scott, A.C., Grassiineau, N.V., Glasspool, I.J., (2007), Increased terrestrial methane cycling at the Palaeocene-Eocene thermal maximum, Nature, 449, 332-335

Peters, K.E., Walters, C.C. Moldowan, J.M., (2005). The Biomarker Guide. Volume 2: Biomarkers and Isotopes in Petroleum Exploration and Earth History. Second Edition, Cambridge University Press

Petersen, H.I. (2002) A re-consideration of the 'oil window' for humic coal and kerogen type III source rocks. Journal of Petroleum Geology 25,407–432.

Petersen, H.I., (2005), Oil Generation from coal source rocks: the influence of depositional conditions and stratigraphic age, Geological Survey of Denmark and Greenland Bulletin 7, 9-12

Petersen, H.I., (2006). The petroleum generation potential and effective oil window of humic coals related to coal composition and age. International Journal of Coal Geology 67 4 221-248

Petersen, H.I., Nytoft, H.P., (2006). Oil generation capacity of coals as a function of coal age and aliphatic structure. Organic Geochemistry 37, 558-58

Petersen, H.I., Rosenberg, P., (2000), The relationship between the composition and rank of humic coals and their activation energy distributions for the generation of bulk petroleum: Petroleum Geoscience 6, 137-149.

Philp, R.P. (1994). Geochemical characteristics of oils derived predominantly from terrigenous source materials. In: Scott, Fleet, A.J. (Eds.), Coal and coal-bearing strata as oil-prone source rocks? London; Geological Society of London Special Publication 77, 71-92.

Qian, J., Wang, J., (2006) World Oil Shale Retorting Technologies, International Conference on Oil Shale 'Recent trends in oil shale' 7-9 November, 2006, Amman, Jordan.

Radke, M., Welte, D.H., Willsch, H., (1982). Geochemical study on a well in the Western Canada: Relation of the aromatic distribution pattern to maturity of organic matter. Geochimica et Cosmochimica Acta 46, 1831-1848.

Radke. M., Welte, D.H., (1983). The methylphenanthrene index (MPI). A maturity parameter based on aromatic hydrocarbons. In: Bjorøy, M., Albrecht, C., Cornford, C., (eds.) Advances in Geochemistry, New York, John Wiley and Sons, 504-512

Radke, M., Welte, D., Willsch, H., (1986). Maturity Parameters based on aromatic hydrocarbons: influence of the organic matter type. Organic Geochemistry 10, 51-63.

Radke, M. (1988) Application of aromatic compounds as maturity indicators in source rocks and crude oils. Marine and Petroleum Geology 5, 224-236

Raid, G.K., Wood, R.D. (1976) Ecology of inland waters and estuaries. D. Van Nostrand and Co., New York, p 485

Rathbone, R.F., Davis, A., (1993). The effects of depositional environment on vitrinite fluorescence intensity. Organic Geochemistry 20, 177-186.

Robert, P., (1985). Histoire géothermique et diagenèse organique. Mém. Bull. Centres Rech. Explor. Elf. Aquitaine, 8 345, Pau

Rudnick, R.L., Gao, S. (2003) The Composition of the Continental Crust, pp. 1-64. In The Crust (ed. R.L. Rudnick) Vol. 3, Treatise on Geochemistry (eds. H.D. Holland and K.K. Turekian), Elsevier-Pergamon, Oxford.

Sandison, C.M., Alexander, R., Kagi, R.I., Boreham, C.J., (2002). Sulfurisation of lipids in a marine-influenced lignite. Organic Geochemistry 33, 1053-1077.

Scotese, C.R., (2001), Atlas of Earth History, Volume 1, Paleogeography, PALEOMAP project, Arlington, Texas, 52

Scott, A.C., Fleet, A.J., (1994), Coal and coal-bearing strata as oil-prone source rocks? London; Geological Society of London Special Publication 77, 107-116

Scott., A.C., (2000), The pre-Quaternary history of fire. Palaeogeography, Palaeoclimatology, Palaeoecology, 164, 281-329

Scott, A.C.,(2002), Coal petrology and the origin of coal macerals: a way ahead? International Journal of Coal Geology 50, 119-134

Shanmugam, G., (1985). Significance of coniferous rainforests and related organic matter in generating commercial quantities of oil, Gippsland Basin, Australia. American Association of Petroleum Geologists Bulletin, 69, 1241-1254

Shotyk W. (1996) Peat bogs archives of atmospheric metal deposition: Geochemical assessment of peat profiles, natural variations in metal concentrations and metal enrichment factors. Environment Reviews 4, 149-183

Simonin, P., Tindall, B., Rohmer, M., (1994). Structure elucidation and biosynthesis of 31-methylhopanoids from Acetobacter europaeus. Studies on a new series of bacterial triterpenoids. European Journal of Biochemistry 225, 765–771.

Sinninghe Damsté, J.S.S., de Leeuw, J.W. (1990) Analysis, structure and geochemical significance of organically-bound sulfur in the geosphere - state-of the-art and future-research. Organic Geochemistry 16, 1077-1101.

Skilbrei, J.R. (1991) Interpretation of depth to the magnetic basement in the northern Barents Sea (South of Svalbard) Tectonophysics, 200, 1-3, 1270141

Sluijs, A.., 14 others, & the Expedition 302 Scientists, (2006): Subtropical Arctic Ocean temperatures during the Paleocene/Eocene thermal maximum. *Nature,* 441, 610-613.

Sloan, L.C., Barron, E.J., (1992): Eocene climate model results: Quantitative comparison to paleo-climatic evidence. Palaeogeogr., Palaeoclim., Palaeoecol., 93, 183-202.

Sloan, L.C., & Pollard, D., (1998): Polar stratospheric clouds: A high latitude warming mechanism in an ancient greenhouse world. Geophys. Res. Lett., 25, 3517–3520.

Smith, S.M., Newman, S., Garrett, P.B., Leeds., J.A., (2001) Differential Effects of Surface and peat fire on soil constituents in a degraded wetland of the Northern Florida Everglades. Journal of Environmental Quality, 30, 1998-2005

Sokolov V.N., Krasil'Scikov, A.A., Livsix. J., (1968) The main features of the tectonic structure of Spitsbergen, Geological. Magazine. 105, 2, 95-115

Sorenson, K.W., (1993), Indonesian peat swamp forests and their role as carbon sinks. Chemosphere, 27, 6, 1065-1082

Spielhagen, R.F., Tripati, A. (2009) 'Evidence from Svalbard for near-freezing temperatures and climate oscillations in the Arctic during the Paleocene and Eocene', Palaeogeography, Palaeoclimatology, Palaeoecology, 278, 1-4, 48-56

Stallard R.F., Edmond, J.M., (1981),Chemistry of the Amazon, precipitation chemistry and marine contribution to dissolved load at the time of peak discharge. Journal of Geophysical Research. 86, 9844-9858

Steel, R., Dalland, A., Kalgraff, K., Larsen V., (1981), The Central Tertiary Basin of Spitsbergen: sedimentary development of a sheared margin basin: Geology of the North Atlantic Borderland: Canadian Society of Petroleum Geologists Memoir, 7, 647-664

Steel, R.J., Gjelberg, J., Helland-Hansen, W., Kleinspehn, K., Nøttvedt, A., Rye-Larsen, M., (1985), The Tertiary strike slip basin and orogenic belt of Spitsbergen, Society for Sedimentary Geology Special Publication. 39, 339-359

Steel, R., Dalland, A. (1978). Undersøkelser av den kullførende del av Firkanten Formasjonen (Tertiær) i østlige del av Nordenskiøld land Svalbard, Geologisk Institutt Universitetet i Bergen.

Steel, R.J., Worsley, D., (1984), Svalbard's post-Caledonian strata – an atlas of sedimentological patterns and palaeogeographic evolution. *In* Spencer, A.M., ed., Habitat of hydrocarbons on the Norwegian continental margin: London, Graham and Trotman 109-135

Stephens, J.F., Meng Leow, H., Gilbert, T.D., Philp, R., (1985). Investigation of the relationship between coal maturity and aromaticity: Characteristics of sodium dichromate oxidation products of Australian vitrinite concentrates. Fuel 64, 1537-1541

Stocks, B. J., Fosberg, M.A., Lynham, T.J., Mearns, L., Wotton, B.M., Yang, Q., Jin, J.Z., Lawrence, K., Hartley, G.R., Mason, J.A., McKenney, D.W. (1998) Climate change and forest fire potential in Russian and Canadian boreal forests, Climate. Change, 38, 1– 13,

Stocks, B. J., B. M. Wotton, M. D. Flannigan, M. A. Fosberg, D. R.

Cahoon, and J. G. Goldammer, (2001) Boreal forest fire regimes and climate change, In Remote Sensing and Climate Modelling: Synergies and Limitations, M. Beniston and M. M. Verstraete (Eds), pp. 233 – 246, Kluwer Acadamy, Norwell, Mass

St. John, K. (2008) Cenozoic ice-rafting history of the central Arctic Ocean: Terrigenous sands on the Lomonosov Ridge. Paleoceanography, 23,

Summons, R. E., Jahnke, L. L., Hope, J. M., Logan, G. A.. (1999). 2-Methylhopanoids as biomarkers for cyanobacterial oxygenic photosynthesis.Nature, 400, 554-557.

Suyker, A. E., Verma, S. B., Clement, R. J. and Billesbach, D. P. (1996).Methane flux in a boreal fen: Season-long measurement by eddy correlation.J. Geophys. Res. 101, 28637–28647

Talbot HM, Rohmer M, Farrimond P. (2007), Structural characterisation of unsaturated bacterial hopanoids by atmospheric pressure chemical ionisation liquid chromatography/ion trap mass spectrometry. Rapid Communications in Mass Spectrometry 21, 10, 1613-1622.

Talbot H.M, Farrimond P., (2007),Bacterial populations recorded in diverse sedimentary biohopanoid distributions. Organic Geochemistry 38, 8, 1212-1225.

Talbot H.M, Summons R, Jahnke L, Cockell C, Rohmer M, Farrimond P., (2008), Cyanobacterial bacteriohopanepolyol signatures from cultures and natural environmental settings. Organic Geochemistry 39, 2, 232-263.

Takeno, N. (2005) Atlas of Eh-pH diagrams Intercomparison of thermodynamic databases. National Institute of Advanced Industrial Science and Technology

Tangedal, O., (2011). 3D Architecture and Hydrocarbon Potential of a Pre-uplift Billefjorden Basin. Masters Thesis in Petroleum Geology, University of Bergen

Taylor, G.H., Shiboaka, M. Liu, S., (1981) Vitrinite Macerals and Coal Utilization, In Proceedings of the 1981 International Conference on Coal Science, Dusseldorf 74-79

Tipping, E., Smith, E.J., Lawlor, A.J., Hughes, S., Stevens, P.A., (2003) Predicting the release of metals form ombrotrophic peat due to drought induced acidification, Environmental Pollution, 123, 2, 239-253

Tissot, B.P., Welte, D.H., (1984) Petroleum Formation and Occurrence (2nd Edition). Springer-Verlag, Berlin, Heidelberg

Throndsen, T., (1982). Vitrinite reflectance studies of coals and dispersed organic matter in Tertiary deposits in the Adventdalen area, Svalbard. Polar Research 2, 77-91

Todd, D.K (1980) Groundwater Hydrology, 2nd Edition, Wiley, New York, Chichester, Brisbane, Toronto

Turunen, J., Roulet, N.T., Moore, T.R., Richard, P.J.H. (2004). Nitrogen deposition and increased carbon accumulation in ombrotrophic peatlands in eastern Canada. Global Biogeochemical Cycles 18: 10.10-29

Tripati. A., Eagle, R.A., Morton, A.C., Dowdeswell, J.A., Atkinson, K.L., Bahé, Y., Dawber, C.F., Khadun, E., Shaw, R., Shorttle, O., Thanabalasunderam, L., (2008)., Evidence for glaciation in the Northern Hemisphere back to 44Ma from ice rafted debris in the Greenland Sea. Earth and Planetary Science Letters, 265, 12, 112-122

Uguna, C. N., Snape C. E., Meredith W., Carr A. D., Scotchman I. C., Davis R. C., (2012a). Retardation of hydrocarbon generation and maturation by water pressure in geologic basins: An experimental investigation, In. Peters K. E., Curry, D. J., Kacewicz, M., eds., Basin Modeling: New Horizons in Researchand Applications: AAPG Hedberg Series, no. 4, p. 19– 37.

Uguna. C.N., Carr, A.D, Snape, C.E., Meredith, W., Castro-Díaz, M, (2012b). A laboratory pyrolysis study to investigate the effect of water pressure on hydrocarbon generation and maturation of coals in geological basins. Organic Geochemistry 52, 103-113

Uhl, D., Traiser, C., Griesser, U, Denk., T., (2007) Fossil leaves as palaeoclimate proxies in the Palaeogene of Spitsbergen (Svalbard). Acta Palaeobotanica, 47, 1, 89-107

Van Koeverden, J.H, Karlsen, D.A., Schwark, L., Chpitsglouz, A., Backer-Owe, K., (2010). Oil-prone lower Carboniferous coals in the

Norwegian Barents Sea; Implications for a Palaeozoic petroleum system. Journal of Petroleum Geology 33, 2, 155-181

Van Koeverden, J. H., Karlsen, D.A., Backes-Owe, K., (2011). Carboniferous non marine source rocks from Spitsbergen and Bjørnøya; Comparison with the Western Arctic. Journal of Petroleum Geology 34, 1, 53-66

Vu Thi Anh, T.; Horsfield, B.; Sykes, R. (2008) Influence of in-situ bitumen on the generation of gas and oil in New Zealand coals. Organic Geochemistry, 39, 11, 1606-1619

Vu, T.T.A, Zink, K.-G., Mangelsdorf, K., Sykes, S., Wilkes, H., Horsfield, B., (2009). Changes in bulk properties and molecular compositions within New Zealand Coal Band solvent extracts from early diagenetic to catagenertic maturity levels. Organic Geochemistry 40, 963-977

Waller, M.P., Long, A.J., Long D., Innes J.B. (1999) Patterns and processes in the development of coastal mire vegetation: multi-site investigations from Walland Marsh, Southeast England. Quat Sci Rev 18(12):1419–1444

Wang, Y., (2011) Nitrogen pyrolysis of Coals from the Central Tertiary Basin, Svalbard Masters Thesis, University of Nottingham

Wedepohl, K.H., (1995), The composition of the continental crust. Geochim. Cosmochim. Acta, 59, 1217-1232

Weimer R.J, Land C.B.(1973) Maestrichtian deltaic and inter-deltaic sedimentation in the Rocky Mountain region of the United States In: Caldwell W.G.E (ed.) The Cretaceous System in the Western Interior of North America Proc. Int. Symp. Univ. Saskatchewan, Saskatoon, May 1973, Spec Pap. Geol. Assoc. Can. 13. 633-666

Weis, D., Shotyk, W., Rieley, J., Paige, S., Gloor, M., Reese, S., Martinez-Coritzas, A., (2002), The geochemistry of major and selected trace elements in a forested peat bog, Kalimantan SE Asia and its implications for past atmospheric dust deposition. Geochim.Cosmochim Acta, 66, 13, 2307-2323

Wilkins, R.W.T., George, S.C., (2002). Coal as a source rock for oil: a review. International Journal of Coal Geology 50, 317-361.

Williams, C.J., Lepage, B.A., Johnson, A.H., Vann, D.R., (2009). Structure, biomass, and productivity of a late paleocene arctic forest.

Proceedings of the Academy of Natural Sciences of Philadelphia 158, 107-127.

Winter, T.C., (1992), A Physiographic and Climatic Framework for Hydrological Studies of Wetlands *In:* Aquatic Ecosystems in Semi-Arid Regions: Implications for Resource Management, Robbards, D., Bothwell, M.L., Eds. The National Hydrology Research Institute Symposium Series No. 7, Environment Canada, Sakatoon, Saskatchewan, Canada, 127-148

Winter, T.C., (2000), The Vulnerability of Wetlands to Climate Change: A Hydrological Landscape Perspective. Journal of American Water Resources Association 36, 2, 305-311

Winter, T.C., (2001), The Concept of Hydrological Landscapes, Journal of the American Water Resources Association, 37, 2, 335-349

Worsley, D., Aga, O.J., Dalland, A., Elverhøi, A., Thon, A., (1986), The Geological History of Svalbard, Evolution of an Arctic Archipelago: Stavanger, Den norske states oljeselskap. A.S

Yiou, P., Baert, E., Loutre, M.F., (1996) Spectral analysis of climate data. Surveys in Geophysics, 17, 6, 619-663

Yu, Z., Cambell, I.D., Vitt, D.H., Apps, M.J., (2001) Modelling long term peatland dynamics. I. Concepts, review and proposed design. Ecological Modelling, 145 ,2-3, 197-210

Websites

China Aerial image – Google Earth